Nonlinear Photonics
of Chromophore-Doped
Nematic Liquid Crystals

Oksana Trushkevych

St John's College

A dissertation submitted for the degree of

Doctor of Philosophy

at the **University of Cambridge**.

June 2005

Oksana Trushkevych

NONLINEAR PHOTONICS OF CHROMOPHORE-DOPED NEMATIC LIQUID CRYSTALS

SUMMARY

Spatial light modulators (SLMs) are increasingly used in many applications including 3D video, projection displays, optical correlation, real-time holography, permanent holographic data storage and optical telecommunications networks. For some applications, e.g. 3D video, to create devices that would be addressed by light is of major importance. Commercially available optically addressed SLMs (OASLMs) are based on adjacent photoconductor and liquid crystal (LC) layers and their resolution is limited set by the charge spread in the photoconductor layer.

Recently discovered supra-nonlinearities in LCs doped with small amounts of dyes or fullerene are very promising alternatives to conventional OASLMs.

This research is investigating optical nonlinearities in dye-doped liquid crystals and the possibility of using these effects for device applications. The main focus is on resolution, simplicity, efficiency and speed. To engineer successful applications, it is vital to understand the processes in guest-host systems upon illumination with light. A search for novel materials is also of current importance.

On the basis of experiments, the systems and effects with the most suitable characteristics for OASLMs have been identified. A dopant that gives fast switching and high efficiency has been researched for the first time. The current work has clarified the mechanism of nonlinearity introduced by this dopant.

A highly important feature of the new dopant is that it is very stable and may be used in device applications. Moreover, detailed studies have shown no dependence of resolution and speed on device thickness, while the efficiency increases as the thickness is increased. This opens attractive opportunities for further work.

Unlike the previously reported large photorefractive effects that require either a long time (1-30 sec), the application of an electric field or high optical power (>100 mW/cm^2), in this work a regime has been achieved in which the switching times of the device have been reduced to 100-200

ms at low optical fields (50 mW/cm^2) with no electric fields applied. Achieved resolution is acceptable: 180 lp/mm, but the efficiency of the devices must be increased for applications.

Based on this study suggestions on how to improve the performance of the existing systems, what to look for when creating new materials and whether there is a potential for successful applications as OASLMs are given.

DECLARATION

This dissertation contains the results of research undertaken by the author between October 2001 and December 2004 at the Engineering Department of Cambridge University. No part of this dissertation is the result of work done in collaboration with others, expect where explicitly described or cited within the text. The contents have not been submitted, in whole or in part, for any other University degree or diploma.

Oksana Trushkevych

Cambridge, June 2005

KEYWORDS

ACKNOWLEDGEMENTS

STATEMENT OF LENGTH

This dissertation does not exceed the limits for the Engineering Degree Committee: 65 000 words and 150 figures.

The length of this dissertation, including appendices, bibliography, footnotes, tables and equations is 58 000 words. There are 97 figures in total including appendices.

CHAPTER 1

INTRODUCTION: MOTIVATION AND TARGET CHARACTERISTICS

If it were only possible to command the light to go were we want, many things would become possible. 3D holographic video, all optical computing and other wonderful applications that could trigger advances in medical imaging, engineering design, home entertainment and telecommunications to name just a few.

Many currently implemented applications, as well as the ones-to-come, including 3D video, projection displays, optical correlation, real-time holography, permanent holographic data storage and optical telecommunications networks increasingly rely on devices that can perform the function of a hologram (i.e. to modulate light), but do it dynamically. These devices are called spatial light modulators (SLMs). In general, these devices modulate the reading light spatially in a way any permanent hologram would - by diffracting or alternating the reading beam from a recorded pattern. SLMs based on liquid crystals usually act as phase holograms, where the phase is set by a refractive index profile formed inside the device.

The crucial difference that makes liquid crystals (LCs) highly attractive as the active materials for light modulators is that their refractive index can be easily controlled, for example by an external electric field. For some applications, e.g. 3D video, the creation of devices that would be addressed by light, is of major importance.

Optically addressed SLMs (OASLMs) are already commercially available (see Appendix A). These devices consist of two main components[1]: a light modulator and a photoconductor. The LC layer acts as a light modulator, while a layer of hydrogenated

amorphous silicon (a-Si:H) of a thickness ~2 μm is used as a photoconductor. An external field must be applied to this system.

The idea is that an incident two-dimensional light pattern (write beam) creates on the photoconductor a certain conductivity profile. In the areas where the conductivity is changed, the resulting field imposed on the LC layer also becomes changed, leading to a refractive index change.

Two-layer OASLMs are relatively simple, but hard to manufacture, especially when a large area device is required, and their use is limited to reflection. They also possess a problem of charge spreading in amorphous silicon that limits their resolution[*] to 50 lp/mm^{2} - 80 lp/mm[1]. In special cases when using carbon doped silicon layer, a resolution up to 200 lp/mm may be achieved[3]. Another characteristic of these devices is that the refractive index variation is not created directly by the light field inside the liquid crystal. Systems that allow for a direct variation give better flexibility.

Alongside the high sensitivity to external electric field liquid crystals are sensitive to optical field. LCs exhibit a nonlinear effect called photorefractivity – the change of the refractive index under the influence of light. Pure liquid crystals are among the best nonlinear materials. What is fascinating is that it is possible to further enhance their sensitivity and nonlinear response by many orders of magnitude by introducing certain dopants. Usually liquid crystals are doped with dyes, fullerenes or carbon nanotubes. The intriguing fact is that only certain dopants give an enhancement of nonlinearity.

Amazingly large nonlinear effects at extremely low optical powers ($< 1 \text{ mW/cm}^2$) have been observed recently in some systems. If materials can be made robust enough and the effects are uniformly reliable and repeatable to be used in device applications, it would revolutionise several areas of optics, especially dynamic holography.

Dye or fullerene-doped LC systems are highly promising materials for novel OASLMs based on photorefractive effects. Such devices would be intrinsically photorefractive without the need for special layers or circuitry. It is expected that these new optical devices would have all the benefits of existing OASLMs based on a photoconductive layer and would be photosensitive by nature, without a silicon layer and

---

[*] Resolution is defined here as the spatial frequency (in line pairs per millimetre: lp/mm) at which the modulation transfer function (MTF) of the device is 50% (efficiency decreases by the factor of two).

possibly without the need to apply voltage across the device. They could be used in transmission with low power laser light, and it is possible that the resolution of a 1-layer dye-LC device will be better than that of the 2-layer amorphous silicon OASLM.

Depending on the time characteristics, novel OASLMs could be used either for 3D displays[4] or even for optical switching in networks. In the case of applications in the field of 3D displays, high resolution and memory of approximately 50ms are beneficial, so that the devices could act as microdisplays, and information could be stored on them and then tiled on a screen[5,6].

This research focuses on the optical nonlinear effects suitable for a new generation of Optically Addressed Spatial Light Modulators. Issues such as resolution, efficiency, stability and speed are addressed. It is crucial to understand which mechanisms are responsible for the nonlinearity in the doped liquid crystals in order to create successful devices. It remains a research topic to describe what exactly happens when the optical field is incident on the dye- or fullerene- doped LC. Answering this question is vital to enabling solutions on how to improve the performance of the existing systems, what to look for when creating new materials and whether there is a potential for successful applications as OASLMs.

When assessing materials and devices, the following parameters are considered:

Desirable characteristics:

Low cost   <10USD

Resolution: >100 lp/mm

Switching: Short time to imprint image <50ms

              Fast relaxation <50ms (dynamic holography) or

              Some memory ≥50ms or bistability (microdisplay applications)

Power: Low writing optical intensity ~1mW/cm^2

              Low or no voltage applied (zero – 5 V)

              Low optical losses (normal incidence to reduce reflection, no absorption of the reading wavelength)

              High diffraction efficiency

Stability: Very good chemical stability (with time) of all materials in the device

Ability to withstand high optical powers (up to $1W/cm^2$) without damage

Unchanging operating characteristics after many cycles or with time

Safety   Materials not toxic to people/environment

Not flammable

Relatively easy to recycle/destroy

Devices electrically safe (low/zero voltages)

Laser safety (low power laser light, enclosure)

Other: Greyscale possibility (displays)

Coupling with commercially available laser diodes

At the research stage it is not crucial for the system to possess all of the above parameters. There are a number of various applications for photorefractive materials, in general, and for OASLMs in particular, and requirements are usually flexible.

To summarise, the topics addressed by this research work are:

➢ to investigate novel nonlinear LC systems as materials for single-layer photorefractive OASLMs

➢ to define mechanisms that are responsible for the nonlinearity in the specific doped LC systems

In Chapter 2 the reader can find a brief introduction to a remarkable class of materials known as liquid crystals (LCs). The chapter is aimed at describing why and in what way these materials, through their unique properties, can be useful for spatial light modulation. Then, the main attention is paid to the relatively recently discovered possibility of greatly enhancing the sensitivity to light of LCs by doping them with dyes or fullerene. The mechanisms leading to nonlinear effects in doped nematic liquid crystals are briefly reviewed and the possibilities of using these phenomena for OASLMs are analysed.

In Chapter 3, a brief overview of new achievements in the field of photorefractivity in guest-host systems is given. The selection of the doped liquid crystal systems for optically addressed light modulation application is presented, based on the requirements stated at the beginning of this work. Three dopants are selected for further

consideration, exhibiting different mechanisms of photoinduced refractive index change when dissolved in LC. They are azo dye Methyl Red (MR), previously ustudied azo-substituted anthraquinone dye DC161 and fullerene C_{60}.

The structure and fabrication process of single-layer OASLM are described.

In Chapter 4, different optical interaction geometries are examined. Experimental optical setups for dynamic holographic studies and techniques used for photovoltage, photocurrent, Freedericksz transition and spectroscopic measurements used for characterisation of the samples and of the processes that occur under the influence of light are depicted.

It is vital for creating effective and successful materials and devices to understand mechanisms leading to nonlinearity in the systems under investigation. Chapter 5 is dedicated to experimental work on these mechanisms and their identification in the chosen systems.

Through the temperature, photovoltage, photocurrent and spectroscopic measurements, optical and electric Freedericksz transition studies and dynamic holographic experiments in polarised light the mechanisms in the known C_{60} and MR doped systems are confirmed and studied in detail. The full study of the mechanisms triggered by the dye DC161 is performed for the first time. The theoretical background applied to the specific conditions of the experiment is given, and data analysis is presented.

Dopants and operating regimes are analysed from the application point of view. An experimental search for guest-host-alignment systems that do not undergo irreversible processes upon illumination with light and are thus suitable for dynamic holography is presented. Specific alignments are suggested.

The most important conclusions of this chapter are:

⇒ The nonlinearity in DC161 doped systems has trans-cis transition as an underlying mechanism. It may be enhanced by the differences in the interaction of the host with trans and cis isomers.

⇒ It is possible to emphasise a particular type of nonlinearity from a large number of possible ones in a particular system by the selection of the alignment surface, interaction geometry and external field regimes.

⇒ Permanent/persistent surface effects have not been observed in C_{60} and DC161 doped devices. Polyimide and ITO cell surfaces allow good dynamic operation of the MR systems without permanent or persistent components.

Chapter 6 focuses on the important device characteristics, namely the efficiency, resolution and switching time of the dye-doped LC systems. The measurements are conducted using time-resolved dynamic holography experimental arrangements described in Chapter 4. Based on efficiency and resolution studies it is shown that DC161 doped systems are very stable and sufficiently effective, and hence are the best candidates for the targeted applications. At this point, the research further focuses on DC161 systems. Various host materials are tested. The dynamics of nonlinearity in DC161 doped systems is analysed in detail. Proof of principle thick devices are built and tested.

The most important results described in this chapter are:

⇒ In DC161 doped systems:

  ⇒ the resolution does not depend on the sample thickness;

  ⇒ the efficiency significantly increases if the device thickness is increased up to 40μm; in thicker devices a saturation of efficiency is observed;

  ⇒ the rise time has only a small dependence on the sample thickness, and relaxation time in thick devices is still fast.

⇒ An ageing effect has been found in all three systems studied.

  ⇒ C60 and DC161 doped devices significantly improve with age.

  ⇒ MR doped devices deteriorate quickly and are not reliable for device applications.

⇒ The overshoot in the build up of the nonlinearity in DC161 and MR doped devices is explained

In Chapter 7, the conclusions are drawn and suggestions relating to further work and the ways to improve current parameters of the systems are given.

To sum up, the objective of this research has been to investigate the potential possibilities of the dye-doped LC for application as a spatial light modulator. Through

experimental work the mechanisms that lead to optical nonlinearity in the studied systems have been defined, and the operational regimes studied. Ways to optimise devices for various requirements have been suggested.

This research work has prepared the ground for the next steps towards new all-optical switching devices for telecommunications and displays. Further work may include exploiting thick devices in the Bragg regime to improve efficiency; using hosts other than nematic to achieve fast switching; improving the quality of dye dispersion in the LC host to avoid ageing effects and improve efficiency; creating more effective dye structures; studying other dopants (e.g. carbon nanotubes).

CHAPTER 2

LIQUID CRYSTALS: MATERIALS FOR SPATIAL LIGHT MODULATORS

In this chapter a brief introduction to a wonderful class of materials known as liquid crystals (LCs) is given. The chapter is aimed at describing why and in what way these materials, through their unique properties, can be useful for spatial light modulation. Then, the main attention is given to the relatively recently discovered possibility of greatly enhancing the sensitivity to light of LCs by doping them with dyes or fullerene. A brief overview of the new achievements in the field of photorefractivity in guest-host systems is given and the possibilities of using new effects for OASLMs are analysed.

2.1 Introduction to liquid crystals

The year 2004 has brought the 100 years celebration of liquid crystals (LC). Since then the technology has gone ahead in mile steps, bringing to the market a wide variety of LC-based products, the most known being of course displays and detergents.

The term "Liquid crystals" (LC) has been introduced by Lehmann in 1889 and is quite self-explanatory. Indeed, materials in this phase possess many properties of crystals (e.g. anisotropy and symmetry), but flow like liquids. This combination of properties makes them absolutely unique materials.

Of course, not all materials exhibit LC phases. The molecules of the media have to be either elongated (calamitic LC) or disc-like (discotic LC). These materials may form a LC phase or phases between solid and liquid states in a certain temperature range. Such

materials are called thermotropic LC. The shape of the molecules is the key to their properties: molecules will self-assemble just like a stack of matches or coins.

Another large class of materials, called lyotropic liquid crystals, is formed by soap-like solutions, where one part of the molecule is hydrophobic, and another is hydrophilic. The phase of such materials depends on the concentration in the solvent and the shape of the molecule. All soaps and detergents are in fact lyotropic liquid crystals.

There is also a separate field of studies for polymeric LCs, polymerised LCs, polymer dispersed LCs and aligned polymer molecules.

In this work we will concentrate on thermotropic calamitic materials, as they are the most interesting from the point of view of optical and electronic engineering.

Based on symmetry differences, calamitic LC can be divided[7]:

- nematic
- smectic
- chiral nematic also known as cholesteric and
- chiral smectic.

2.1.1 Nematics and chiral nematics

The simplest LC phase is nematic. Nematic liquid crystals (NLCs) are basically one-dimensional ordered liquids, with the local preferred direction along one axis. This direction is characterised by the unit vector **n** called director. Spatial direction **n** may be quite random, in practice it is determined by weak forces (like the aligning force at the walls of the containing cell)[*].
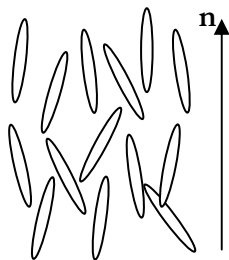
Figure 2.1 Molecules in the nematic phase.

Nematic molecules are centrosymmetric, with +**n** being the same as -**n**. Nematics are optically uniaxial systems with the optical axis parallel to **n.**

---

[*] It is possible to obtain well-aligned nematic layers by putting a droplet of nematic material between two glass slides, which have been previously lightly rubbed in one direction by a soft cloth.

The ordering of the molecules in LC phase is statistical, and the order parameter is usually defined as[8]

$$S = \frac{1}{2}\langle 3\cos^2 \theta - 1 \rangle$$

2.1

Here θ is an angle between the ordering direction (director axis) and the molecular axis. For a crystal this parameter is equal to 1, in liquids $S=0$, and in liquid crystals S may lie between 0.3 and 0.9.

As will become apparent later, the order is an extremely important parameter, as the order and microscopic properties of individual molecules together define macroscopic properties of liquid crystal phases.

The order parameter is temperature dependent. Maier-Saupe theory (for nematic phase) suggests that the order parameter is a function of reduced temperature τ and gives the following analytical approximation (within 1% error):

$$S = (1 - 0.98\tau)^{0.22}, \qquad \tau = \frac{T}{T_{NI}} \frac{V^2}{V_{NI}^2}$$

2.2

T - temperature, T_{NI} is the temperature of the transition into isotropic state, the so-called clearing temperature (materials become optically isotropic and transparent). V - molar volume at T, V_{NI} - molar volume at T_{NI}.

When molecules are *chiral* (the Greek for "handed"), a chiral nematic phase may be formed, also known as cholesteric phase (Figure 2.2). In distances comparative to the molecule length chiral nematics are the same as nematics. The chirality causes a slight, sequential change in the direction of the rod-like molecules through a section of material. This gradual change in molecular direction scribes a helix. The chiral nematic phase can be obtained also by adding a small amount of a chiral dopant to nematic LC.
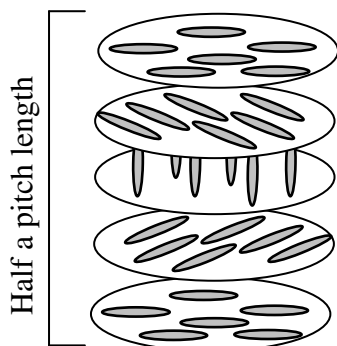

Figure 2.2 Structure of the chiral nematic phase. The views represent imaginary slices through the structure and do not imply any type of layered structure.

This helical structure has the ability to selectively reflect the light of a wavelength in a liquid crystal equal to that of the helical pitch length. Chiral nematic LCs appear therefore coloured if the pitch is of the order of the wavelength of light. The pitch length depends on the temperature and becomes shorter at higher temperatures, hence the colour of the LC is also temperature dependent. This property is commonly used for temperature detection applications.

Materials forming nematic phase are widely used for spatial light modulators and displays. The optically addressed SLMs available on the market at the moment, for example, are based on nematic liquid crystals[2].

The main features of nematic liquid crystals are low viscosity, good stability, easy to align, greyscale possibility and low cost. Relatively slow response (~20ms)[1] may sometimes be considered a major drawback.

2.1.2 Smectics and chiral smectics

The smectic mesophase is more ordered than nematic. Some positional ordering exists in addition to the orientational order of nematics. While only one nematic phase exists, the smectic phase exhibits polymorphism, i.e. there are many different types of smectic phases. The representative ones are SmA, SmC and SmC*(chiral smectic).
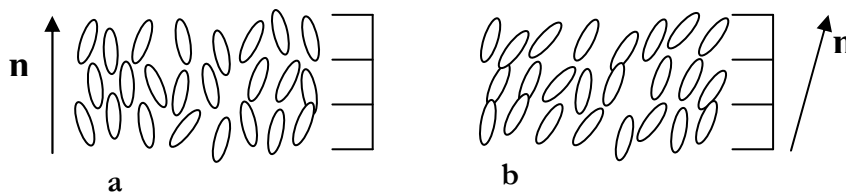
Figure 2.3 Positioning of the molecules:
a) SmA;
b)SmC

SmA liquid crystals are optically uniaxial with the **n** director perpendicular to the layers. In smectic C phases the molecular direction (and hence the **n** director) is uniformly tilted from the layer normal, leading to a small optical biaxiality. Smectic phases are very viscous. They lie between the nematic and crystalline phases in terms of order, physical parameters and temperature range.

When the molecules of the SmC phase are chiral, the phase structure is basically the same except that the molecular chirality causes a slight and gradual change in the direction of the molecular tilt (there is no change in the tilt angle with respect to the layer normal). The helix pitch in chiral smectic phases is temperature dependent, the pitch becomes longer at higher temperatures (opposite to the effect normally seen in the chiral nematic phase).

Chiral smectic C phases (*SmC**) also known as *ferroelectric* liquid crystals are very interesting, because they form a system that permits, from symmetry considerations, spontaneous electric polarisation. Permanent dipole vector **p** (Figure 2.4) represents a breakdown of a symmetry (when a stereogenic centre is introduced). It precesses around layer normal direction. Suppressing the helical structure stops the precession of the permanent dipole and causes it to align in a common direction - rendering the material ferroelectric. The helical structure is suppressed by surface alignment in thin cells, the process is called *surface stabilisation*.[9] Such structures can exhibit very fast switching and are extensively used as materials for spatial light modulators.
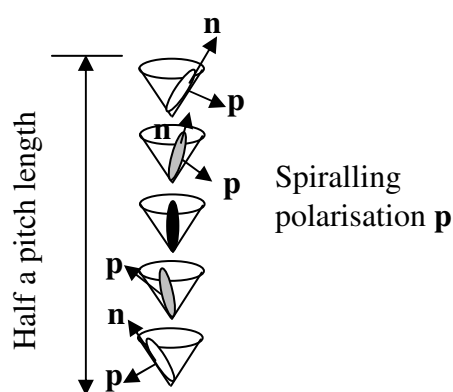
Figure 2.4 The structure of SmC* phase.

Main features: potential bistability, high speed (~1ms)[1,10,11,12]. The drawbacks of these systems are: limited to binary response, hard to align, less commercial availability.

Ferroelectric liquid crystals are very interesting for applications in OASLMs. It is anticipated to use them as materials for devices at later stages. This work, however, will mainly concentrate on nematic liquid crystals due to several main reasons. First, the strong nonlinear effects that we assess for use in OASLMs have been recently discovered mostly in nematic systems. Second, nematic systems are simpler to analyse theoretically, which is of particular importance when working on the phenomena which have not been explicitly

understood yet. And third, nematic systems best comply with the low cost and simplicity of manufacturing requirements.

2.2 Physical properties of Nematic Liquid Crystals

When looking at the bottle with LC it scatters light and appears quite opaque. This happens because when unrestricted by any boundaries, LC is formed of randomly oriented domains with the order parameter that corresponds to the given material at a given temperature. To achieve a uniform monodomain a LC has to be aligned (all domains oriented in the same direction). Alignment can be achieved by various methods: using surfactants, creating microgrooves on the surface of the cell, evaporating silicon oxide at different angles of incidence. There are two main ways to orient LC with respect to cell surface: with molecules lying parallel (planar) or perpendicular (homeotropic) to it.

The orientational order in nematic phase gives rise to the uniaxial anisotropy of its macroscopic parameters, such as for example refractive index. Anisotropy of parameters is defined in terms of the values parallel and perpendicular to the nematic director.

Special qualities of NLC are set by anisotropy in their polarisability, dielectric permittivity as well as in viscosity and elastic properties.

2.2.1 NLC in electric field: dielectric permittivity

The application of an electric field E to a material causes its polarisation P. In a material consisting of non-polar molecules, there is only an induced polarisation, which consists of two parts: electronic polarisation (which is also present at optical frequencies) and the ionic polarisation[13]. The induced polarisation is due to the deformation of electron clouds within the molecules. It does not rely on molecular motion, hence is frequency and temperature independent.

Molecules forming LC phase have permanent dipoles due to asymmetric charge distribution within the molecule. To the addition to the induced polarisation, there appears the orientation polarisation, due to the tendency of the permanent dipole moments to orient themselves parallel to the field[13]. The orientational polarisation depends on molecular motions and hence on the frequency of the applied field.

At frequencies higher than certain frequency called the frequency of dielectric relaxation f_D (frequencies much greater than molecular motions) the polarisation is

14

influenced only by electronic deformations, and its value can be an order of magnitude lower than at low frequencies, where orientational polarisation contributes considerably.

The polarisation depends linearly on the electric field, but the anisotropy of the crystal causes $\vec{P}$ and $\vec{E}$ to have in general different directions. $\vec{E}$ and $\vec{P}$ are related by tensor $\overleftrightarrow{\chi}$, called the electric susceptibility.

$$\vec{P} = \varepsilon_o \overleftrightarrow{\chi} \vec{E}$$

2.3

For nematic liquid crystals (uniaxial) there are two components of susceptibility: perpendicular and parallel to the director axis $\chi_\perp$ and $\chi_\parallel$, this can be written as

$$\begin{pmatrix} P_x \\ P_y \\ P_z \end{pmatrix} = \varepsilon_o \begin{pmatrix} \chi_\perp & 0 & 0 \\ 0 & \chi_\perp & 0 \\ 0 & 0 & \chi_\parallel \end{pmatrix} \begin{pmatrix} E_x \\ E_y \\ E_z \end{pmatrix}$$

2.4

The constant ε_o is the permittivity of free space.

The electric field and polarisation define dielectric displacement $\vec{D}$.

$$\vec{D} = \varepsilon_o \vec{E} + \vec{P}$$

2.5

The linear relationship between $\vec{E}$ and $\vec{P}$ results in a relationship between $\vec{E}$ and $\vec{D}$ given by:

$$\vec{D} = \overleftrightarrow{\varepsilon} \vec{E} \text{ , where } \overleftrightarrow{\varepsilon} = \varepsilon_o (\overleftrightarrow{1} + \overleftrightarrow{\chi}) \text{, } \overleftrightarrow{1} \text{ being a unit tensor}$$

2.6

ε is called the dielectric permittivity of the material, the anisotropy of permittivity is

$$\Delta\varepsilon = \varepsilon_\parallel - \varepsilon_\perp$$

2.7

Dielectric permittivity is probably one of the most interesting material parameters from the point of view of this research work. It defines the way the material interacts with applied electric fields, and the dielectric permittivity at optical frequencies is directly related to the refractive index of the media n:

$$\varepsilon = n^2$$

2.8

15

In the latter case (at optical frequencies, when only the induced polarisation is present) the value of the dielectric permittivity is given by a Lorenz-Lorentz equation[14]:

$$\frac{\left(n^2 - 1\right)}{\left(n^2 + 1\right)} = \frac{4\pi N}{3}\left\langle \gamma^E \right\rangle$$

2.9

where $\left\langle \gamma^E \right\rangle$ is mean polarisability, N – number of molecules per unit volume:

$$N = \frac{N_A \rho}{m}$$

2.10

where N_A is Avogadros number, ρ is density, m is molar mass (in gram molecular weight).

At low frequencies, when there is a significant contribution from the orientational polarisation, the dielectric permittivity (static) is determined by the Clausius-Mossotti equation[14]:

$$\frac{(\varepsilon - 1)}{(\varepsilon + 2)} = \frac{4\pi N}{3}\left(\left\langle \gamma^E \right\rangle + \frac{\mu^2}{3kT} \right)$$

2.11

here $\dfrac{\mu^2}{3kT}$ is the orientational component of the average static polarisability. This term is not present in the solid state and is larger than the first term.

This illustrates a very important tendency in liquid crystals - very strong dependence of parameters on the ***orientational order***.

2.3 Continuum theory of Nematic Liquid Crystals, Freedericksz transition

One of the main and most obvious properties of liquid crystals is that they are actually liquid. But of course they are not simple liquids. For example, it takes five viscosity coefficients to describe NLC[15]. However the elastic properties of liquid crystals are described by only three parameters called elastic constants. They are defined in terms of nematic director:
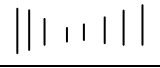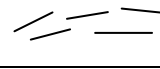
Deformation		Elastic constant	Expression
Splay	╱╱ │ ╲╲	k_{11}	div n
Twist	‖│ ‧‧ │‖	k_{22}	n rot n
Bend	╱╱ ─── ╲	k_{33}	[n rot n]

Table 2.1. Elastic constants of liquid crystals.

Volume density of free energy F resulting from elastic deformations is given by the Oseen-Frank equation (for non-chiral NLC):

$$F = \frac{1}{2}k_{11}(div\,\vec{n})^2 + \frac{1}{2}k_{22}(\vec{n}\cdot\overrightarrow{rot\,n})^2 + \frac{1}{2}k_{33}\left[\vec{n}\;\overrightarrow{rot\,n}\right]^2$$

2.12

Under the influence of the electric field, the volume density of free energy acquires a term responsible for dielectric interactions with external field (CGS units)

$$F = \frac{1}{2}k_{11}(div\,\vec{n})^2 + \frac{1}{2}k_{22}(\vec{n}\cdot\overrightarrow{rot\,n})^2 + \frac{1}{2}k_{33}\left[\vec{n}\;\overrightarrow{rot\,n}\right]^2 - \frac{1}{2}\Delta\varepsilon\left(\vec{n}\cdot\vec{E}\right)^2$$

2.13

The terms relating to the elastic energy resist deformation of the LC structure, whilst the electric field term makes it energetically more favourable to orient along ($\Delta\varepsilon > 0$) or perpendicular to the field ($\Delta\varepsilon < 0$), so that $\left(\vec{n}\cdot\vec{E}\right)$ is minimised. Such balancing of elastic and electric energy leads to a very important effect in liquid crystals under the influence of electrical field - the so-called Freedericksz transition. Basically, this is a simple electro-optical effect. The optical parameters (refractive index) of the system change when external electric field is applied.

Consider a situation when nematic director is parallel to the cell boundaries and electrodes (Figure 2.5). This is the case we would mostly deal with in this research. As the electric field applied to the electrodes is increased, a small rotation of the director occurs in the centre of the cell (at a voltage threshold). The higher voltage leads to most of the LC layer orientation switched to the state where director aligns along the field.

Let us consider that only splay deformation is involved for planar to homeotropic transition and bend deformation for homeotropic to planar transition. In these cases the threshold voltage can be calculated.
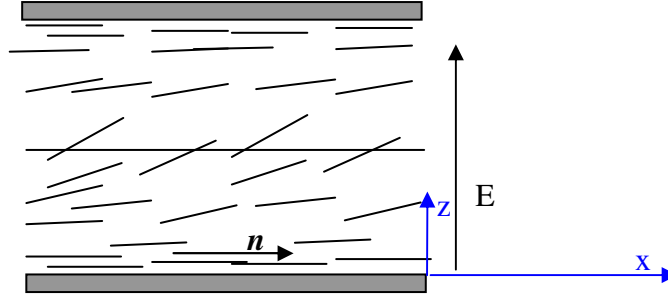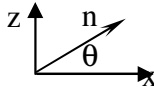
Figure 2.5.The Freedericksz transition in nematic LC under the influence of electrical field (planar to homeotropic for liquid crystal with positive dielectric anisotropy Δε>0)

In the case of planar to homeotropic transition, where

$$\vec{n} = \begin{pmatrix} \cos\theta(z) \\ 0 \\ \sin\theta(z) \end{pmatrix} \qquad\qquad \vec{E} = \begin{pmatrix} 0 \\ 0 \\ E_z \end{pmatrix}$$

$|n|=1$ and

$$\nabla\cdot\vec{n} = \frac{\partial n_z}{\partial z} = \frac{\partial \sin\theta(z)}{\partial z} = \cos\theta(z)\frac{\partial\theta}{\partial z}$$

$$\vec{n}\cdot(\nabla\times\vec{n}) = 0$$

$$\left|\vec{n}\times(\nabla\times\vec{n})\right| = \left|\left(\frac{\partial n_x}{\partial z}\right)_{x,y}\right| = \frac{\partial \cos\theta(z)}{\partial z} = \sin\theta(z)\frac{\partial\theta}{\partial z}$$

2.14

The free energy per unit volume in cgs units is given by:

$$F = \frac{1}{2}\left[k_{11}\cos^2\theta + k_{33}\sin^2\theta\right]\cdot\left(\frac{\partial\theta}{\partial z}\right)^2 - \frac{1}{2}\Delta\varepsilon E^2\sin^2\theta$$

2.15

This free energy can be minimised using the calculus of variations to give:

$$\left(k_{11}\cos^2\theta + k_{33}\sin^2\theta\right)\frac{\partial^2\theta}{\partial z^2} + \left[\left(k_{33}-k_{11}\right)\left(\frac{\partial\theta}{\partial z}\right)^2 + \Delta\varepsilon E^2\right]\sin\theta\cos\theta = 0$$

2.16

Assuming θ is small,

18

$$k_{11} \frac{\partial^2 \theta}{\partial z^2} + \Delta\varepsilon E^2 \cos\theta\sin\theta = 0.$$

2.17

In order to write equation 2.17 down in terms of dimensionless quantities, a new variable is defined:

$$\varsigma = z/d; \quad then \quad \frac{k_{11}}{d^2}\left(\frac{\partial^2\theta}{\partial\varsigma^2}\right) + \Delta\varepsilon E^2 \cos\theta\sin\theta = 0$$

2.18

ζ varies from 0 to 1. To simplify it a number of substitutions are made, where ξ is the length, and ξ_d is the dimensionless parameter:

$$\xi^2 = \frac{k_{11}}{\Delta\varepsilon E^2}; \quad \xi_d = \xi/d.$$

2.19

After substitution, the equation to be solved takes the form:

$$\xi_d^2\left(\frac{\partial^2\theta}{\partial\varsigma^2}\right) + \cos\theta\sin\theta = 0.$$

2.20

It is possible to find the solution of the above equation in terms of elliptic integrals. Both sides have to be multiplied by $d\theta/d\zeta$ making the equation easy to integrate. Let the integration constant be expressed in terms of θ_m. Then:

$$\frac{\partial\theta}{\partial\varsigma} = \frac{1}{\xi_d}\sqrt{\sin^2\theta_m - \sin^2\theta}$$

2.21

and with substitutions $m=\sin^2\theta_m$ and $t=\sin\theta/\sin\theta_m$:

$$\int_0^1 \frac{dt}{\sqrt{1-t^2}\sqrt{1-mt^2}} \equiv K(m) = \frac{1}{2\xi_d}$$

2.22

where $K(m)$ is the complete elliptic integral of the first kind. $K(m)$ equals $\pi/2$ when $m=0$ and increases to infinity as m approaches 1. Thus at threshold $\xi_d=1/\pi$, and the threshold field $E_{threshold}$ in cgs units is:

$$E_{threshold} = \frac{\pi}{d}\sqrt{\frac{k_{11}}{\Delta\varepsilon}}$$

<div align="right">**2.23**</div>

Therefore, the threshold voltage ($V_{threshold}=E_{threshold}d$) is independent of the sample thickness. It is of the order of few volts in most liquid crystal materials[8]. This means that with just a few volts one can control the LC optical properties and achieve substantial changes in retardation.

The nematic liquid crystal responds to the RMS voltage, so a strong optical field is also capable of inducing the so-called optical Freedericksz transition.

The planar to homeotropic transition is not used for the display applications, but the relation and the threshold voltage are very similar to other electro-optic switching geometries that are used for displays (e.g. twisted nematic would involve twist deformation in addition to splay and bend). Of course switching with just a few volts is a very attractive option and the reason of success of LC-based displays and non-display applications (including SLMs).

2.4 Nonlinear optics of Nematic Liquid Crystals

2.4.1 Introduction

Generally nonlinear optics deals with the phenomena, for which electric and magnetic field amplitudes of the second and higher orders play important role. The electromagnetic wave propagating through a medium exerts a force on the loosely bound electrons. Usually these forces are quite small, and in a linear medium the resulting polarisation (a dipole moment per unit volume) is proportional to the applied field:

$$\vec{P} = \varepsilon_0 \hat{\chi}\vec{E}$$

<div align="right">**2.3**</div>

At high fields, higher order terms should be considered, and the induced electric polarisation **P** can be expressed in the form:

$$\vec{P} = \varepsilon_0 \hat{\chi}^{(1)}\vec{E} + \hat{\chi}^{(2)}\vec{E}\vec{E} + \hat{\chi}^{(3)}\vec{E}\vec{E}\vec{E} + ...$$
$$or$$
$$\vec{P} = \vec{P}_L + \vec{P}_{NL}, \qquad \vec{P}_{NL} = \hat{\chi}^{(2)}\vec{E}\vec{E} + \hat{\chi}^{(3)}\vec{E}\vec{E}\vec{E} + ...$$

<div align="right">**2.24**</div>

With $\chi^{(1)}$, $\chi^{(2)}$, $\chi^{(3)}$ - linear, second and third order susceptibility tensors. P_L and P_{NL}- linear and nonlinear contributions to the total polarisation.

The relation between P and E in SI and CGS units is $P_{cgs}=3\cdot10^5 P_{SI}$, $E_{cgs}=3.3\cdot10^{-5} E_{SI}$. Therefore, the susceptibility tensors χ in CGS units and SI units would differ by the corresponding transformation coefficients.

If an optical wave of the form $E=E_o\,\sin\omega t$ (ω is frequency t is time) is incident on the medium, the polarisation will take a form:

$$\vec{P} = \varepsilon_0 \hat{\chi}^{(1)} E_0 \sin \omega t + \hat{\chi}^{(2)} E_0^{\,2} \sin^2 \omega t + \hat{\chi}^{(3)} E_0^{\,3} \sin^3 \omega t + ...$$

2.25

this may be rewritten as:

$$\vec{P} = \varepsilon_0 \hat{\chi}^{(1)} E_0 \sin \omega t + \hat{\chi}^{(2)} E_0^{\,2} (1 - \cos 2\omega t) + \hat{\chi}^{(3)} E_0^{\,3} (3\sin \omega t - \sin 3\omega t) + ...$$

2.26

In presence of these nonlinear terms, the polarisation wave generated by the harmonic optical wave in the medium does not have the harmonic profile of the incident field. This leads to a number of nonlinear effects. The terms at $E_o^{\,3}$ are responsible for an *optical Kerr effect* - the quadratic electro-optic effect leading to a change in the refractive index of a material in response to the **square** of an external electric field (in contrast to the Pockels effect where the induced index change is linearly dependent on the electric field). The Kerr effect is large in the materials with large values of $\chi^{(3)}$. On the other hand, the DC term at $E_o^{\,2}$ is responsible for the so-called optical rectification (quasi-static electric fields generation; a result of beam mixing process of the beams with the same frequency), while higher harmonics terms in 2.26 lead to the second and third order harmonic generation (generation of light with doubled or tripled frequency as a result of beam mixing process). From 2.25, the polarisation P could be written in terms of linear and nonlinear components P_L and P_{NL}:

$$\vec{P} = \vec{P}_L + \vec{P}_{NL}$$

2.27

In similar fashion, the susceptibility χ could be described by linear and nonlinear components χ_L and χ_{NL}.

The nonlinear polarisation P_{NL} involves various powers of the optical electric field and may comprise several frequency components (if $E(\omega)=E_1(\omega_1)+ E_2(\omega_2)+...$).

21

For example, consider the commonly occurring case, when the polarisation is proportional to the third power of electric field E_i: $P_{NL} = \chi_{NL} \langle E_i^2 \rangle E_i$, the brackets represent scalar multiplication of vectors.

In this case it can be shown, that an effective optical dielectric constant ε' would be given by[8]:

$$\varepsilon' = \varepsilon_i + \chi_{NL} \langle E_i^2 \rangle$$

2.28

The effective refractive index is therefore given by:

$$n^2 = n_o^2 + \frac{\chi_{NL} \langle E_i^2 \rangle}{\varepsilon_o}$$

2.29

For the typical case when the second term is much smaller than n_o, this can be approximated by:

$$n \cong n_o + n_2(E) \langle E_i^2 \rangle, \qquad n_2(E) = \frac{\chi_{NL}}{2\varepsilon_o n_o}$$

2.30

n_2 is the *nonlinearity coefficient*. Since the optical intensity I is:

$$I = \frac{\varepsilon_o nc}{2} \langle E^2 \rangle$$

2.31

Equation 2.30 may be rewritten in the form:

$$n \cong n_o + n_2(I)I, \qquad n_2(I) = n_2(E) \frac{2}{\varepsilon_o n_o c}$$

2.32

In this research under a *nonlinearity coefficient,* which is an important characteristic of the nonlinear process (see the following chapter), we mean $n_2(I)$.

2.4.1.1 Beam mixings

Since the nonlinear polarisation involves various powers of the optical electric field (2.24), then if the total electric field comprises many frequency components, there are several combinations of frequency components that will contribute to a particular frequency component for P_{NL}.

Consider a practical case when two optical waves with different frequencies w_1 and w_2 are incident on the nonlinear medium. At the output the terms with $(w_1 \pm w_2)$ will be generated. This allows amplification of weak signals (by mixing them with strong pump).

For the practically important case of photorefractivity in pure and doped liquid crystals, for two wave mixing (beams with intensities I_1 and I_2) when there is a phase shift ϕ between the optical intensity and refractive index gratings, it has been shown[8] that:

$$\frac{dI_1}{dz} = -4 g I_1 I_2 \sin \phi$$

$$\frac{dI_2}{dz} = +4 g I_1 I_2 \sin \phi$$

2.33

g is the coupling constant and is proportional to the induced refractive index change δn[16]. If $\sin \phi$ is nonvanishing, there is a flow of energy between the two beams. In some practical cases $\phi = \pi/2$, and there is a unidirectional energy flow from beam 1 to beam 2 regardless of the relative intensities of the beams.

2.4.1.2 Symmetry

The elements of the nonlinear susceptibility tensor define the nonlinear optical response of the medium. The larger they are, the stronger the response to the optical field. On the other hand, the susceptibility tensor should have certain forms of symmetry that reflect the structural symmetry of the medium[17]. This means that depending on the symmetry, certain elements of the tensor may be linearly dependent or approach zero.

The molecules forming liquid crystal phases are in general anisotropic and possess permanent dipoles. In bulk form, these molecules tend to align themselves such that their collective dipole moment vanishes. Thus, most phases including the discussed nematic phase of the LCs are characterised by a centrosymmetry[*] (**-n** and **n** directions are equivalent). In centrosymmetric crystals, the macroscopic second-order polarisability $\hat{\chi}^{(2)}$ is zero[8]. It is however nonvanishing if the nematic director **n** is distorted by an external field like an applied electric field[18].

---

[*] Nematic phase belongs to the $D_{\infty h}$ symmetry group in Shoenfliess notation or ∞/mmm in Hermann-Maugin notation.

In the situations when the dipolar contribution is vanishing, the quadrupole contribution is not necessarily vanishing and may give rise to sizeable second-order nonlinear polarisation[19].

2.4.1.3 <u>Photorefractivity</u>

The photorefractive effect has long been known in noncentrosymmetric inorganic crystals such as $LiNbO_3$. In photorefractive crystals the interference pattern produced by two intersecting coherent beams generates a nonuniform space-charge field E_{sc} by photogeneration of free carriers and subsequent carrier drift and diffusion processes[20]. As a consequence, the refractive index of the material is modulated by the interaction of the field E_{sc} with the second order (Pockels) susceptibility of the crystal (see also the equation 2.25). The refractive index grating is spatially displaced from the intensity grating, by as much as $\pi/2$ radian (nonlocality of the photorefractive effect)[20].

Optical nonlinear phenomena in Liquid Crystals are usually seen as refractive indices dependence on the optical light intensity. Although this may not necessarily involve the build up of a space-charge field, in the general sense the observed nonlinear effect can be called photorefractivity.

2.4.2 *Orientational enhancement of nonlinearity in liquid crystals*

The origin of the photorefractivity of organic composites that are isotropic in the absence of an externally applied bias field can be quite different from the nonlinear effects in crystals such as $LiNbO_3$.

A material is said to be optically nonlinear when the induced polarisation *P* is not linearly dependent on the electric component of the optical field *E*. This could happen if the optical field is very intense, or if the material's physical properties are easily perturbed by the optical field. Both of these phenomena: those associated with an intense optical field and those associated with material's susceptibility to perturbation, are found in liquid crystals[8].

The most important property of molecules forming nematic LC phases (apart from being strongly anisotropic) is their ability to reorient under very modest external fields.

A well-known nonlinear effect, the quadratic electro-optic effect (Kerr effect) in liquids, for example, relies on partial aligning of anisotropic molecules by applied field. This is similar to the nonlinearities produced in polymers. In contrast to crystalline systems,

in photorefractive polymers, for example, reorientation (of the dipolar chromophores that are responsible for the nonlinearity in these systems) is an important, sometimes even dominant, mechanism.[21]

In many respects, nematic liquid crystals are ideal for observing the orientational nonlinear (photorefractive) effect, because of the combination of their molecular anisotropy and possibility to reorient easily[22]. Molecules forming LC phase reorient in response to a field that is orders of magnitude lower than that which is required to produce an equivalent nonlinear effect in polymers simply because the reorientation in liquid crystals is easier. The result is that an applied field of only ~0.1 V/μm is required to produce a large refraction index modulation in liquid crystals (~50 V/μm is typical for polymers)[23].

2.4.3 Basics of the grating theory

Spatial light modulator can be used to produce re-writable holograms[4].

Holography is concerned with recording and reconstructing both the amplitude and the phase of an optical wave arriving from the illuminated object[24]. Recording media are sensitive only to the intensity of an optical wave. To store information about the phase, the signal beam is interfered with a coherent reference. The resulting interference pattern is recorded and can be regarded as a hologram. Reconstruction of the written information is done by a coherent reconstruction wave and is based on diffraction from the recorded pattern. In this research we record diffraction gratings as phase gratings or holograms. The terms *hologram* and *grating* will be used from time to time and have the same meaning in this text.

Consider a diffraction grating recorded on the medium and probed by the reading beam. Diffraction efficiency (*DE*) is the ratio of the intensities of the *i*-th order *diffracted* beam I_i and the *illuminating* beam I_{ill}^{*}.

$$DE = \frac{I_i}{I_{ill}}$$

2.34

---

[*] In this research we are interested in response of materials. To account for power losses due to reflections at the surfaces of the studied sample, instead of I_{ill} we use intensity of the transmitted beam before the hologram is written I_t unless stated otherwise.

The maximum diffraction efficiency, that can be obtained from thin holographic gratings, varies considerably depending on whether the grating is phase or amplitude, and on the profile of modulation.

Holograms can be divided into amplitude, polarisation and phase and distinguished by the angular selectivity and the nature of diffraction. Here we would concentrate on amplitude and phase holograms only.

Amplitude holograms block or absorb unwanted light (thus varying the amplitude of the reading light). They have low efficiency due to the associated losses. Phase holograms vary the phase of the reading light and are much more efficient. Phase holograms have also a number of other advantages including the possibility of eliminating zero order of the diffracted beam and the asymmetric diffraction which is needed for optical routing.

In holographic media based on liquid crystals the diffraction results from the modulation of refractive index. Light moves slower in the regions with high refractive index. Phase of the light that has gone through the region with higher n will fall behind the phase of the light that has gone through the region with the lower n. Changes of refractive index in the liquid-crystal based hologram are resulting in the modulated phase of the reading light. So, the holograms generated in LC films are phase holograms.

The profile of the modulation in the experiments described in this work vary from sinusoidal (obtained from the interference of two writing beams) to square (obtained by imaging an amplitude diffraction grating). For more details on the setups see Chapter 4.

Consider phase sinusoidal grating.

There are two regimes of diffraction: Raman-Nath and Bragg. There also two types of gratings: *thin* and *thick*. Angular selectivity is small in *thin* and significant in *thick* holograms. Often Raman-Nath gratings are considered *thin*, and Bragg gratings - *thick*. In this way, the terms *thin* and *thick* may be ambiguous. Distinct and meaningful definitions are possible based on either regime of diffraction or angular or wavelength selectivity.

In Raman-Nath regime the multiple diffracted orders ideally have diffraction efficiencies DE_i given by[25]

$$DE_i = J_i^2\left(\frac{2\pi d\,\delta n}{\lambda\cdot\cos\theta}\right) \equiv J_i^2(\Delta) \qquad\qquad \Delta = \frac{2\pi d\,\delta n}{\lambda\cdot\cos\theta}$$

2.35

i is the integer representing the diffracted order, Δ is optical retardance, d is the hologram thickness, λ is the reading beam wavelength, δn is the induced refractive index change and

J_i is the i-order Bessel function. The angle of incidence of the reading beam is usually small, and therefore $\cos\theta$ may be neglected. In this research we would be mainly interested in the first order of diffraction which is given by the first-order Bessel function:

$$J_1(\Delta) = \sum_{k=0}^{\infty} \frac{(-1)^k (\Delta/2)^{2k+1}}{k!(k+1)!}$$

2.36

To operate in Raman-Nath regime, the condition:

$$Q' \cdot \frac{\Delta}{2} \leq 1, \qquad Q' = \frac{2\pi\lambda d}{n\Lambda^2 \cos\theta}$$

2.37

must be satisfied. Here Λ is the *grating spacing*.

Bragg regime is described by the two-wave coupled-wave theory of Kogelnik. In this regime, the single fundamental diffracted order ideally has a diffraction efficiency given by[25]:

$$DE_1 = \sin^2\left(\frac{\Delta}{2}\right)$$

2.38

To operate in Bragg regime, the condition:

$$\frac{Q'}{\Delta} \geq 10,$$

2.39

must be satisfied. It is particularly notable, that this definition is independent of a grating thickness.

The diffraction regime defines the maximum possible diffraction efficiency obtained from the grating. In Raman-Nath regime it is:

$$DE_{max} = \max J_1^2(\Delta) = 33.8\%$$

2.40

Square gratings would have efficiency defined by taking the modulus of the Fourier transform of the amplitude of the grating wave function at $i=1$ representing the first diffracted order.

From the Mathematics data book, Fourier transform of the square wave is:

$$f(t) = \sum_{\substack{i=-\infty \\ i-odd}}^{\infty} \frac{2}{j\pi i} e^{ji\omega_o t}$$

2.41

where j is a complex number. The searched value is[*]:

$$DE_{max} = \frac{4}{\pi^2} \approx 40.5\%$$

2.42

In Bragg regime, the maximum diffraction efficiency is defined by a $\sin^2(\Delta/2)$ function and approaches 100% (see Figure 2.6). Here only a sinusoidal grating profile would be used.
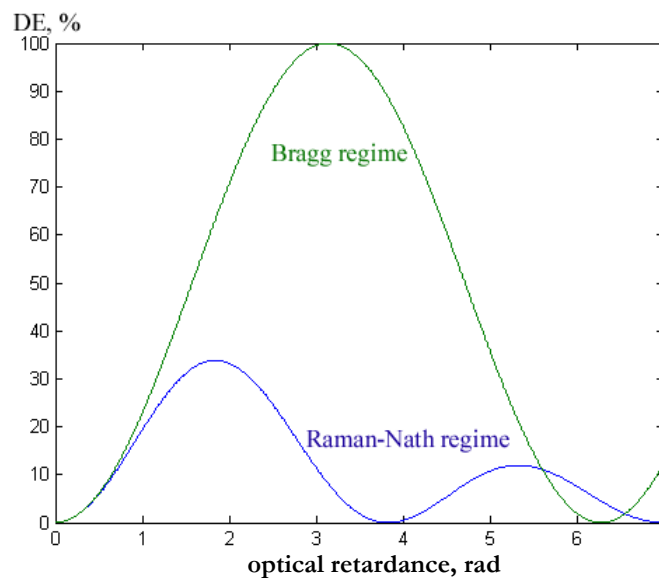

Figure 2.6. Diffraction efficiency in Raman-Nath and Bragg regimes.

For small values of the phase retardation, the diffraction efficiencies of the fundamental diffracted order converge to the same diffraction efficiency for both: thin and thick gratings.

---

[*] For an amplitude grating (modulation 0 to +1 rather than -1 to +1), the max efficiency may be shown to be $DE_{max}=1/\pi^2=10.1\%$
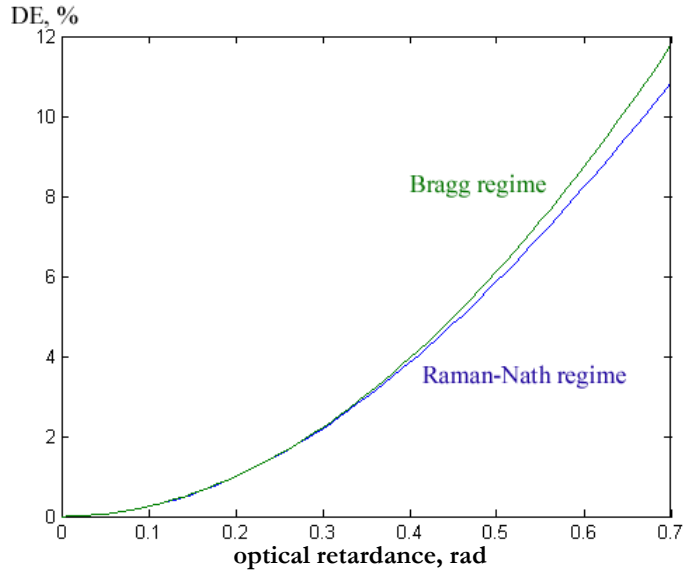
Figure 2.7 Bragg and Raman-Nath diffraction efficiency at small phase retardation.

A thin grating may be alternatively described as a grating exhibiting relatively low angular and wavelength selectivity. The angular or wavelength range for which DE decreases 2 times is defined as d/Λ. For a thin grating:

$$\frac{d}{\Lambda} < 10$$

2.43

A thick grating may be described as a grating exhibiting strong angular and wavelength selectivity. Small changes in the angle of incidence above and below the Bragg angle lead to a steep decline in the intensity of the diffracted beam. Thick grating behaviour may be considered to occur when

$$\frac{d}{\Lambda} > 10$$

2.44

Note that the definitions 2.43 and 2.44 do not accurately predict diffraction regime.

To summarise, the maximal diffraction efficiency may be different for different types of gratings, but at small phase retardation (when the efficiency is below 10-20%) this difference is negligible. The current research is concentrating mainly on Raman-Nath regime (hologram thickness of 2-25μm, λ~0.5μm, n≈1.7, grating spacing ≥10μm and Δ≤0.35 give $Q'\Delta$≤0.09). Both: sinusoidal and square grating profiles are used.

2.4.4 History of observed phenomena

In this section a brief overview of nonlinear mechanisms as well as the history of research behind them is presented.

First nonlinear optical effects in liquid crystals were found by Shen in 5CB - the 2nd harmonic generation in homeotropic samples on the surface.

In the 1970s a lot of research had been carried out with the nematic materials (usually MBBA[*]) in the isotropic phase:

- self-focusing was studied by Rao and co-workers (1971-73)[26];
- 2nd and 3rd harmonic generation - by Shelton and Shen[27] (1970) and later by Saha and Wong (1979)[28];
- non-linear Fabry-Perot action was observed by Bischofberger and Shen (1978)[29];
- degenerate four-wave mixing was reported by Fekete, Yeung and Yariv (1980)[30];
- in 1974 Wong and Shen[31] observed optical Kerr effect in 4cm thick cells with isotropic MBBA and EBBA[†] and found that Kerr constant is 100 times larger than in CS_2 – the well known nonlinear medium.

Herman and Serinko[32] (1979) suggested that a larger wave-mixing efficiency could be obtained in nematic phases if the dc field is used to bring NLC to near a Friedericksz transition. Khoo[33] extended this idea and experimentally verified it together with Zhuang in 1980[33,34].

Since 1980 researches started using to the full extent the advantages of LCs as highly correlated molecular systems by working with aligned nematic samples. In 1980 Zel'dovich, Pilipetski, Sukhov and Tabiryan[35] announced the discovery of giant optical nonlinearities (GON) in nematic LCs. By detecting a self-focusing effect, they measured nonlinear dielectric permittivity nine orders of magnitude higher than it is in a strong nonlinear liquid like CS_2. Zel'dovich theoretically predicted and described while Tabiryan and others experimentally observed the effect. They used 60μm planar aligned cell, optical powers of <50W/cm^2 and the extraordinary wave. Similar results were reported later (1981)

---

[*] MBBA - p-methoxy-benzylidene p-n-butylaniline, exhibits nematic liquid crystalline phase at room temperature, T_{NI}=42.5^{o}C (T_{NI} is the temperature of the nematic to isotropic transition). [31]

[†] EBBA - p-ethoxy-benzylidene p-butylaniline, exhibits nematic liquid crystalline phase at room temperature, T_{NI}=78.5^{o}C.[31]

Odulov, Reznikov and co-workers[36] reported in 1982 the observation of giant optical nonlinearity using low power laser beams 10^{-1} W/cm^2 which couldn't be associated with Kerr nonlinearity, for the experiments were carried out under conditions where this orientational Kerr nonlinearity shouldn't appear. They used planar aligned 60μm MBBA cell for recording dynamic holographic gratings. The strongest effect was observed in extraordinary beams. They explained these results by the change of polarisability of molecules under the action of light, and also reported that maximum effect occurred with light which is absorbed strongly. The nonlinear change in the refractive index was proportional to the number of photons absorbed.

This nonlinearity was 10^9 times larger than in a well-known nonlinear medium CS$_2$. Liquid crystals became important materials in nonlinear optics. Successful theories followed experimental advances. Multiwave mixing processes in pure NLCs have been thoroughly quantitatively analysed, and theory experimentally verified by Khoo and Liu in 1989[37].

Yet it appeared that the most dramatic effects and nonlinear materials were still to come. In 1990, Jánossy *et al.* discovered that when small amounts of absorbing dyes are added to NLCs (typically less than 1%), a much stronger nonlinearity can be observed[38]. The strength of the optical torque acting in dye-doped materials can be completely different from that of the corresponding pure transparent hosts, despite the small change observed in the dielectric anisotropy. The researchers were working with anthraquinone dyes and observed a significant increase of the optical torque, in some cases by more than two orders of magnitude (now sometimes called the Jánossy effect).

This discovery has opened a very attractive and simple way of sensitising LCs to light and making them powerful nonlinear materials. But nothing is as simple as it may seem at first sight. The strength of the additional absorption-induced torque is *highly dye specific*[39] and does not show any direct correlation with the absorption coefficient of the system. Such a correlation exists only with the same dye at different concentrations - then the induced torque is proportional to dye concentration (and correlates with absorption). For certain dyes the optical torque was found to be enhanced by more than two orders of magnitude for dye fractions below 1%[38]. For other kinds of dyes the torque was reversed in sign, so as to reorient molecules away from the electric field direction[40]. Still other dyes are ineffective, i.e., they leave the optical torque approximately unaltered[39]. These strong torque variations are reflected into equally strong variations of the optical nonlinearity. The

main challenge was and still remains to answer the question what makes a specific system work.

Another way of obtaining large nonlinearity was about to be discovered. It appears that some dopants, namely: Rhodamine 6G (R6G), Methyl Red (MR) and fullerene C_{60} lead to completely different (from the induced torque) mechanisms of nonlinearity. Rudenko & Sukhov have proved that the nonlinear effect resulted from the presence of a space-charge field[42]. Observations and theoretical groundwork of orientational photorefractivity in dye-doped nematic liquid crystals were reported in 1994 by Khoo and Liang[41] and Rudenko and Sukhov[42]. The magnitude of the space-charge field is determined by the magnitude of the photoconductivity relative to the dark conductivity and the difference in the diffusion coefficients of charges that are photogenerated in some dopants. An orientational response of molecules in LC phase to the space-charge field (in conjunction with an applied external field) was modulating the index of refraction.

This phenomenon can be called the "photorefractive effect" in a more specific sense: i.e. refractive index change through the conductivity change of the media under the influence of light in conjunction with an applied external field leading to space charge field formation and orientational effects. The effect is characterised by the very typical $\pi/2$ phase shift between the intensity grating and refractive index grating leading to wavemixing and other nonlinear phenomena.

The typical geometry of experiments for wavemixing is shown on Figure 2.8. Two unfocused, coherent laser beams (usually with $\lambda=488nm$ or $\lambda=514nm$) intersect in the LC layer and create an intensity grating. A small modification to the following setup involves a third laser beam on a different wavelength ($\lambda=633nm$) to probe the recorded interference pattern.
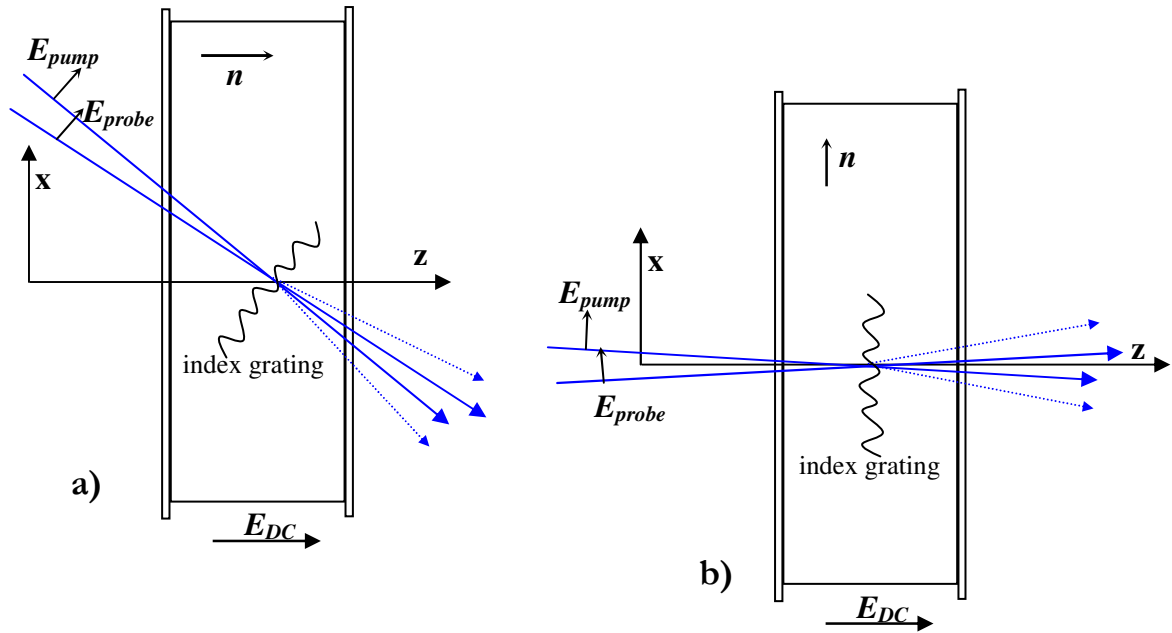
Figure 2.8 The typical geometries for wavemixing observation for
a) homeotropically and
b) planar aligned liquid crystal layers with positive dielectric anisotropy[16].

At the early stages, researchers used the liquid crystalline material p-n-butylaniline (MBBA), later 4'-pentyl-4-biphenylcarbonitrile (5CB) as the host materials. As a dopant, the laser dye Rhodamine 6G (R6G) was used at first. A small electric field (~0.1 V/μm) was applied. In R6G dye, a very small difference in the diffusion coefficients of the positive and negative ions was reported[42]. Much stronger space-charge field could be formed within the liquid crystal if cations and anions from the dopant with larger difference in diffusion coefficients were utilised[23]. The torque exerted on the molecules in the LC phase has a quadratic dependence on the field, therefore much larger photorefractive effects than in R6G doped nematic liquid crystals were actually possible.

New materials were studied by different researchers: perylene[43], Methyl Red (MR)[16] and fullerene C_{60}[44]. This led to a rapid increase in the number of observed nonlinearities, MR being may be the most exciting material nonlinear optics has ever encountered.

It has been also found that MR and C_{60} under the influence of prolonged illumination and electric field form permanent holograms (but electrically switchable by the application of a large ac field at millisecond speed). Permanent gratings were explained as dopant adsorption on the surface in the illuminated areas, modifying anchoring of the LC

layer[16]. Surface effects have been theoretically treated by the joint efforts of Italian and Ukrainian groups[45].

In 1998 Khoo and co-workers[46] have announced the discovery of what they later called Supra Optical Nonlinearity effect (SON). Intensities as low as $1mW/cm^2$ have been used. The authors have shown that it is possible to generate extremely large nonlinear refractive index change per optical field density n_2^* ($2 - 6 \ cm^2/W$) in Methyl Red and azobenzene LC – doped Liquid crystals[47]. Many processes were believed to be at work in the systems under investigation, such as photo-induced space-charge generation and flows, trans-cis isomerisation and dopant-liquid crystal molecular torque. Very large nonlinear coefficients for MR doped systems ($1cm^2/W$) were also obtained through the surface induced nonlinear effect (SINE)[48]. It occurred without a direct optical or electrical torque on the director in the bulk. The following year nonlinearities of more than $100cm^2/W$ in MR doped systems have been reported[49]. It has been found that the surfactant used for alignment is critical for obtaining extremely high sensitivity and large effects. Material was shown to be sensitive to optical fields as low as $40\mu W/cm^2$. Later even larger, almost unbelievable values of nonlinearities up to $1000cm^2/W$ in MR doped systems were theoretically predicted by Khoo et al[50], and although many researches including myself were sceptical, the prediction was supported by the experiment very soon.

In 2003 Simoni et al[51] have announced a colossal[†] optical nonlinearity in randomly oriented MR doped systems. The effect was due to alignment of adsorbed MR molecules on the sample surface under the influence of light. Nonlinear coefficients of $1000cm^2/W$ have been observed. The subject remains open and there are still research activities going on in the field.

---

[*] n_2 is the nonlinearity coefficient $[cm^2/W]$ and is often used to evaluate the material. It shows the induced change of refractive index $\Delta n_{induced}$ (not to be confused with birefringence) per unit optical density $I \ [W/cm^2]$

[†] naming nonlinearity which is 10^8 times higher than Giant optical nonlinearity, and 100 times larger than Supra optical nonlinearity is probably not an easy task.

2.5 Basic mechanisms of optical nonlinearity in NLC

2.5.1 Pure nematics

Pure liquid crystals exhibit strong optical nonlinearities due to their susceptibility. Superimposed on this, there is a much larger effect due to their orientational properties (see section 2.4.2 on page 24).

The primary processes responsible for nonlinear effects in crystalline, liquid crystalline and liquid materials are associated with electronic transitions in the molecules. To describe such process it is necessary to employ quantum mechanical theories. On the other hand, in liquid crystals many processes are essentially classical in nature[8]. The processes like thermal, density effects, flows, electrostrictive effects lead to much stronger nonlinearities.

Intense laser field may give rise to coupled thermal, orientation effects and flows. Orientational effects were studied by Eichler and McDonald in tilted homeotropic samples. The authors have shown that the reorientation of the director is due to the stresses induced by the intense laser pulse[52].

In the absorbing media thermal effects are also present. Single photon absorption bands in most LCs are in the UV region, but at high optical intensities two and three-photon absorption is possible with the larger wavelengths (visible and infrared part of the spectrum). The absorbed optical energy is transferred to heat leading to the change of all temperature dependent parameters, in particular the order parameter and the density due to thermal expansion, resulting in refractive index change of the material. Large temperature changes will inevitably lead to density modulation. Density change can propagate as an acoustic wave and will lead to the simulated Brillouin scattering[*].

In strong spatially modulated electromagnetic field (due to the fact that molecules can be polarised in the field), there will appear a force that pulls molecules into the regions with higher field - the electrostrictive force[8]. In the case of very large fields (achieved by high power laser beams) and strong gradients, flows can appear.

---

[*] light will shift in phase upon interacting with sound waves moving in the medium, this is called Brillouin scattering.

The temperature rise in illuminated areas can also lead to strong effects. When we operate in the proximity of the clearing point of liquid crystal material, all physical parameters of the LC are critically temperature dependent.

Thermal, density and flow effects were described by Khoo et al[53]. Absorption of the laser gives rise to a large build-up of pressure (from both density and temperature effects). This pressure forces the molecules to flow in a radial direction from the beam centre. The flow gives rise to director-axis reorientation. The effect is further complicated by the inevitably large overall temperature rise, which drastically changes almost all the physical parameters (which are also highly anisotropic).

All of the effects discussed above are present in pure nematic liquid crystals and are observed at comparatively high optical intensities. They are beyond the scope of this research except for the thermal effect which may be quite significant in absorbing doped systems and which is discussed in the following section.

2.5.2 Doped nematic LC systems

All of the described nonlinearities occurring in undoped liquid crystals will occur in doped LC. In addition to that, many dopant-triggered mechanisms exist. They are found at much lower light intensities, and that makes them attractive from the applications point of view. In this research we will concentrate on these low power effects.

2.5.2.1 Thermal effects

Due to the strong absorption in the doped films, even modest optical fields may lead to a temperature rise high enough to melt the liquid crystal film. In less extreme cases the illuminated areas will be heated. The refractive index change δn_T may be described by[8]:

$$\delta n_{\perp T} = \frac{\partial n_{\perp}}{\partial T} T(t); \qquad \partial n_{\parallel}/\partial T = 10^{-3} ; \quad \partial n_{\perp}/\partial T = -2*10^{-3} \text{ at } 25^{\circ}C$$

$$\delta n_{\parallel T} = \frac{\partial n_{\parallel}}{\partial T} T(t); \qquad \partial n_{\parallel}/\partial T = 10^{-2} ; \quad \partial n_{\perp}/\partial T = -10^{-2} \text{ near } T_{NI}$$

2.45

$\partial n/\partial T$ are thermal index gradients at different temperatures, T_{NI} is the nematic to isotropic transition temperature also known as clearing temperature.

In the temperature region near the transition temperature from nematic to isotropic phase (T_{NI}) refractive indices show critical behaviour, and strong nonlinearity can be observed.

Temperature effects are very fast and may be observed on 50-100 microsecond time scale. Thermal gratings decay very quickly due to thermal diffusion. Thermal diffusion time constants have been reported by Khoo[8] to be of the order of 50-100μs. As diffusion is anisotropic in liquid crystals, grating decay constants are different for the cases when the grating vector is parallel or perpendicular to the LC director.

Calculation of the temperature profile in dye-doped films is often complicated and requires certain approximations. In the general, case, the heat equation for nematic liquid crystal films has the following form:

$$k_{\perp}\left(\frac{\partial^2 T}{\partial x^2} + \frac{\partial^2 T}{\partial y^2}\right) + k_{\parallel}\frac{\partial^2 T}{\partial z^2} - \frac{\partial T}{\partial t} = -Q_{abs}(x,y,z,t,I)$$

2.46

here the z axis is chosen along the director axis, $k_{\parallel}$ and $k_{\perp}$ are thermal conductivity coefficients along and perpendicular to the director. Q_{abs} is the absorbed optical energy and in the general case depends on a lot of parameters.

When the impinging optical field I is spatially modulated, Q_{abs} will be modulated as well. In this case diffusion plays an important part in the nonlinear effect. The calculation accounting for diffusion when the periodic optical field is incident on the absorbing medium is described in Chapter 5, and the technical detail of the calculation may be found in Appendix D.

Another complication is that in the presence of photoisomerisation of the dye (see the following sections on trans-cis isomerisation), the absorption of the sample may decrease when the optical intensity is increased. In systems doped with dyes undergoing photoisomerisation absorption depends both on time and intensity.

For a Gaussian beam of a large diameter $\omega_o \gg d$, (ω_o is a beam diameter and d is the cell thickness) and infinite substrates, the stationary temperature (at thermodynamic equilibrium) has been calculated by Jánossy and Kosa[54]:

$$T_{stationary} = T_{ambient} + \frac{PA}{4\sqrt{\pi}k\omega_o}$$

2.47

here A is the sample absorptance (the fraction of absorbed energy, $A=P_{absorbed}/P_{impinging}$), $T_{stationary}$ and $T_{ambient}$ are the temperatures of the illuminated sample at thermal equilibrium and room temperature respectively. *P* is the impinging beam power, *k* is thermal conductivity (considered to be the same for the film and the substrate, and isotropic) and ω_o is the writing beam diameter.

In case of uniform illumination of the whole sample by the expanded beam used in many experiments, a one-dimensional model where the heat is dissipating in the *z* direction may be assumed (Figure 2.9).
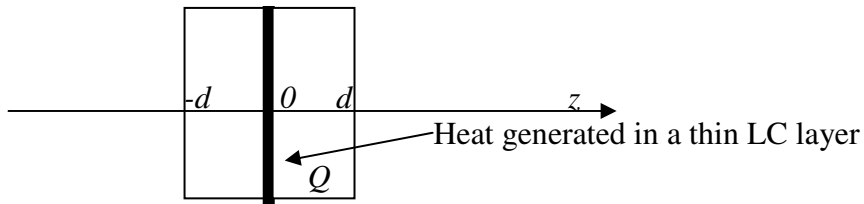

Figure 2.9 Heat conduction model of an absorbing liquid crystal film between two glass substrates.

The problem is symmetric in respect to the plane *z*=0. The heat generated in the dye-doped LC layer (approximated by δ- function) is dissipated in both, ±z directions equally: from each direction $Q_{gen}=\frac{1}{2}Q\delta(z)$. For the stationary state for the positive direction of *z* [0; +∞] we may write:

$$\frac{\partial^2 T}{\partial z^2} = -\frac{Q}{2k}\delta(z)$$

2.48

The solution for the given boundary conditions (ends thermally insulated) is:

$$T_{stationary}\Big|_{z=0} = T\Big|_{z=d} + \frac{Qd}{2k}$$

2.49

where d is glass thickness (1mm in all our samples), k - thermal conductivity of the glass, Q is the rate of generated heat flow normalised per area (mW/cm^2).

Thermal effects for holographic liquid crystal devices have been considered by some authors[55]. It has been reported, that careful temperature and writing optical pulse duration tuning are required as well as high optical powers (10W/cm^2).

We find it not efficient to rely solely on thermally induced nonlinearities, although they might be present and may enhance the performance of the studied devices. This is investigated in more detail in Chapter 5.

2.5.2.2 Induced optical torque

Under the influence of an optical field, the director in transparent nematics aligns parallel to the electric field of the light beam. This phenomenon is known as the optical Freedericksz transition and has been observed at optical powers above $7 \cdot 10^3$ W/cm^2 (see for example the work by Marucci et al[56]). The corresponding volume torque (in cgs units) can be written as[8]:

$$\Gamma^{opt} = \frac{\Delta \varepsilon}{4\pi} \left(\vec{n} \cdot \vec{E} \right) \left(\vec{n} \times \vec{E} \right)$$

2.50

where n is the director, E - electric field vector, $\Delta\varepsilon$ - dielectric anisotropy of material.

When small amounts of dye are added to the LC, it results in increase of the optical torque. The net light-induced torque in a doped LC system is a superposition of the direct optical torque and a "dye-induced" torque.

It was suggested that the torque, induced by the dye, has the same form as the time-averaged optical torque[57]:

$$\Gamma^{dye} = \frac{\xi}{\Delta \varepsilon} \left\langle \Gamma^{opt} \right\rangle$$

2.51

ξ is a dimensionless parameter proportional to the dye concentration and depends solely on the structure of the dye. It is positive for some dyes and negative for others[40]. In contrast with the transparent LC case, in many dye-doped systems, the optical field tends to align the director perpendicularly to the electric-field vector (Figure 2.10).
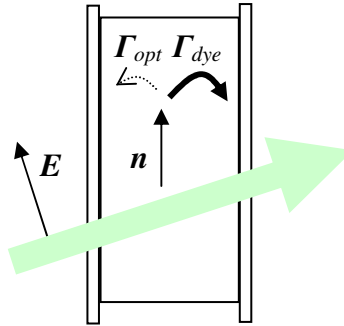
Figure 2.10 Direct optical and dye torques on the molecule for a case of negative ξ. Optical torque is present only in case of oblique incidence of light on the sample.

Jánossy[57] suggested a model to explain this behaviour. According to it, light-induced reorientation in dye-doped LC systems is due to interaction between the excited dye molecules and nematic host. The change of the dye-host interaction energy upon excitation is the source of the absorption-induced torque.

Marrucci et al[58] extensively studied induced optical torque, sometimes called the Jánossy effect. They have recently announced[59] the finding of the mechanism of this effect. The variation of the intermolecular interactions is assumed to be driven by the variation of the two molecular parameters[60]: the dye-host orientational energy u^* and the dye rotational diffusion constant $D^\dagger$. The hypothesis was formed and recently experimentally verified[59] by the authors, that the variation of the dye rotational diffusion constant is responsible for the light induced change of the interaction between the dye and the host resulting in dye-induced optical torque.

The Jánossy effect is often observed in anthraquinone dyes, sometimes requiring external DC fields or focused light beams. The optical power required to observed this effect varies from system to system being approximately in $10 - 10^2$ mW/cm^2 range. The effect depends strongly on the combination of the host and the dopant, and it still remains a research topic to predict from molecular structure, whether a large or small nonlinearity would be obtained.

---

* the average free-energy gained by a dye molecule when it is aligned to its neighbouring host molecules. Characterises equilibrium behaviour of dye molecules.

† determines the orientational Brownian motion performed by the molecule due to thermal agitation. Characterises kinetic behaviour of dye molecules.

2.5.2.3 Trans-Cis isomerisation in azo dyes

Molecules, that have a double N=N bond (an azo group) can form two stable conformations, the *trans* and *cis* isomers. One of the models of spatial configuration of the double N=N bond is shown on Figure 2.11a.
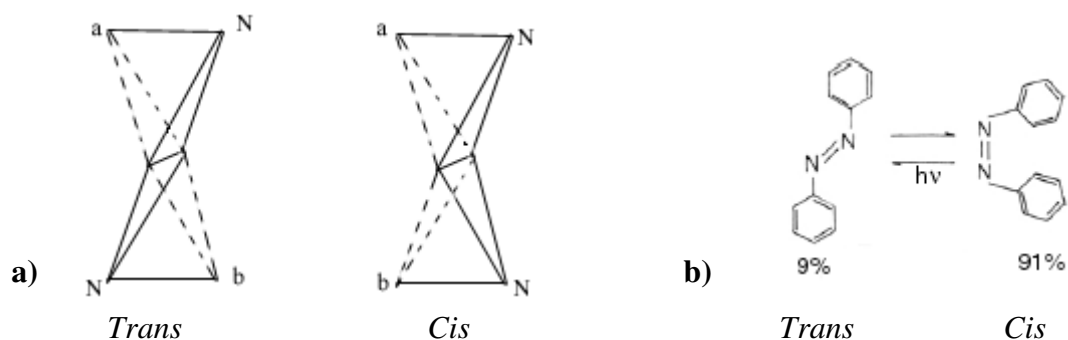

Figure 2.11 Trans-Cis isomerism:
a) the tetrahedron models of Trans and Cis conformations
b) isomerisation of azobenzene.

If we assume that the valencies of trivalent nitrogen maybe directed towards the three corners of a tetrahedron, at whose fourth corner lies the nitrogen itself, then the azo compounds appear as double tetrahedra with one edge in common[61].

Under the influence of light, molecules with azo groups may undergo transformation from one form to another. This is a form of photoisomerisation. Photoisomerisation is associated with the absorption of a photon by one of the two nitrogen electrons which do not take part in chemical bonds (the so-called lone pair). The absorption is attributed to $n \rightarrow \pi^*$ transition and for azo compounds usually lies in the near ultraviolet wavelength range. Azo compounds with different aromatic groups have the absorption maximum $n \rightarrow \pi^*$ in the visible, and can be highly coloured[62].

Photoisomerisation, in short, can be described as excitation by light to the excited state and consequent relaxation from the excited state to trans or cis ground state by radiationless decay. The state diagram of azo compounds is highly complicated[63]. To explain the nonlinearity observed in azo dye D2, a simplified diagram of dye photoexcitation has been used in reference 64, involving separate excited states for trans and cis isomers, and long lived triplet states (Figure 2.12a).
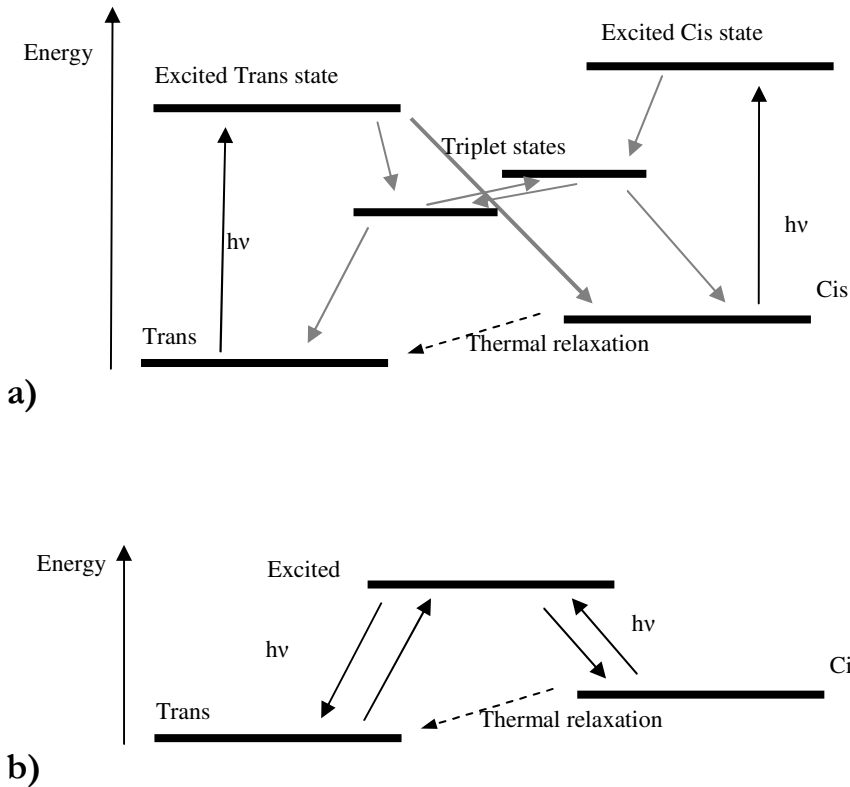
Figure 2.12. Schematic energy model of Trans-Cis photoisomerisation:
a) triplet states accounted for
b) single excited state approximation

The experimental observation to be discussed in Chapter 5 can be explained by a simpler model, using only one excited state, which was suggested by Janossy et al[65] (Figure 2.12b).

Trans isomers of dichroic dyes usually have the lowest energy. They have elongated molecular shape and much higher order parameters in LC than cis species. These isomers behave as two different dyes with different absorption spectra and different torques that they impose on the LC[65]. Change of the torque on the LC upon isomerisation of the dopant leads to orientational nonlinear effects, as described in the previous section.

Another mechanism of reorientation of host molecules is through the change of the geometrical shape of the azo compound when it undergoes the trans-cis transition (Figure 2.11) leading to a change in the geometrical order of the surrounding molecules of host material. For many systems there is approximately equal probability of forming cis- or trans- isomer. The most common situation is that when the isomer is irradiated at a particular wavelength the ratio of cis or trans compounds approaches a value that is

characteristic for this wavelength - a photostationary state. The main factor governing the final ratio of isomers is the relative probability of exciting the ground state of each of the isomers[61].

Trans-cis transition can be very fast (<10ns), and can be used for device applications. In particular, it has been suggested by T. Ikeda et al[66] to use trans-cis dopants in conjunction with ferroelectric LCs for under 1ms switching.

2.5.2.4 Space-charge field

Some dopants (Methyl Red for example) when illuminated by light generate ionic charge carriers. Some dopants (fullerenes, R6G) are excellent for increasing the photoconductivity of the liquid crystals[44]. Both photogenerated charges and photoconductivity would lead to a space-charge field build up, as will be shown below.

Consider the intensity profile obtained from the interference of two beams:

$$I_{op} = I_0 \left(1 + m\cos(qx)\right), \qquad q = \frac{2\pi}{\Lambda};$$

2.52

where q is the grating wave vector; Λ is the grating spacing, x is coordinate along the gating, m – optical intensity modulation factor.

$$E_{ph} = q \, vmk_b T \left[\frac{(\sigma - \sigma_d)}{2e\sigma}\right] \sin(qx)$$

The space-charge field due to photoinduced ionic production will be given by[16]:

2.53

where k_b – Boltzman constant, σ – illuminated conductivity, σ_d – dark conductivity, $v=(D_+ - D_-)/(D_+ + D_-)$; D_+ and D_- are the diffusion constants for the positively and negatively charged ions.

The photogenerated ions diffuse from illuminated regions with higher conductivity into non-illuminated regions. This process is in general characterised by different diffusion coefficients D_+ and D_- for ionic species of different signs. As a result, a certain spatial distribution of ions is obtained resulting in space-charge field.

E_{ph} is shifted in phase by $\pi/2$ in respect to the impinging field. Therefore, the director axis reorientation function is also shifted with respect to the optical intensity function. This phase shift will lead to wavemixing effects, that are indeed observed experimentally[41].

There are two other sources of space-charge field, the so-called Carr-Helfrich fields[67]:

$$E_{sc}^{\Delta\sigma} = -\left(\frac{\Delta\sigma\sin\theta\cos\theta}{\sigma_{\parallel}\sin^2\theta + \sigma_{\perp}\cos^2\theta}\right)E_z$$

2.54

$$E_{sc}^{\Delta\varepsilon} = -\left(\frac{\Delta\varepsilon\sin\theta\cos\theta}{\varepsilon_{\parallel}\sin^2\theta + \varepsilon_{\perp}\cos^2\theta}\right)E_z$$

2.55

they arise from the conductivity anisotropy $\Delta\sigma$ and dielectric anisotropy $\Delta\varepsilon$ under the influence of electric field E_z^*. This field can be either applied externally or generated internally due to photovoltaic effect[†] (sufficiently large in Methyl Red doped systems[46]). $\sigma_{\parallel}$, $\varepsilon_{\parallel}$ and $\sigma_{\perp}$, $\varepsilon_{\perp}$ are conductivities and dielectric permittivities along and perpendicular to nematic director. θ is the director reorientation angle relative to its initial position.

For a small induced reorientation, these space-charge fields are an increasing function of θ. After reorientation has been established, it is possible to maintain these fields only by maintaining external field, without participation of the optical field.

Space-charge fields and refractive index profiles in case of sinusoidal spatial modulation of incident optical field are summarised on Figure 2.13 below.

The incident optical field induces the change of conductivity in the illuminated areas as well as the production of ions (a). The ions diffuse and form a space-charge field (b). The molecules in LC phase reorient in this field with a characteristic phase shift of $\pi/2$ (c).

---

[*] z axis is perpendicular to the grating vector

[†] Photovoltaic effect is found in strongly absorbing photocharge- producing systems. Due to the intensity gradient (because of the absorption) a difference in the amount of charges at the front and back electrodes of the sample is created which is manifested in a voltage build up.
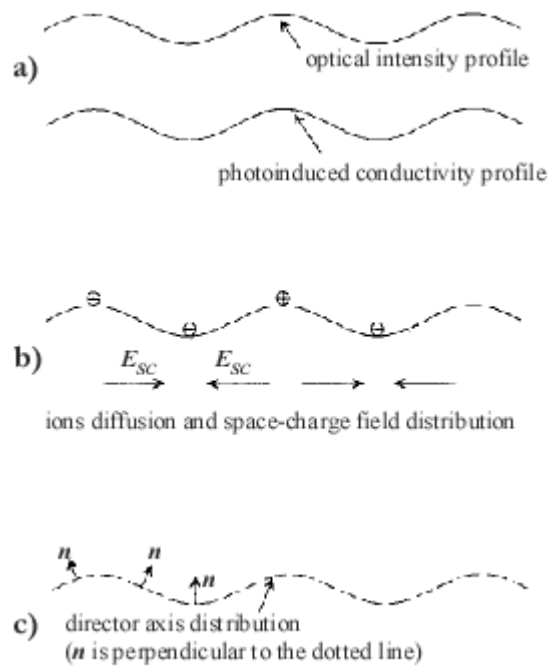
Figure 2.13 Schematic depiction of a photorefractive effect in nematic liquid crystals[16].

As suggested by Khoo[68], there are three main mechanisms of director reorientation in doped NLC involving space-charge field:

1) Photocharge production and conductivity inhomogenity due to photo-induced increase in conductivity lead to space-charge field build up and director reorientation (as on Figure 2.13).

2) Photocharge generation under the influence of the optical field and applied dc field causes the Carr-Helfrich effect, which is due to the conductivity and dielectric anisotropies of NLC. Ionic conduction and photorefractive director axis re-orientation lead to the space charge field formation through dielectric and conductivity anisotropies. The space-charge field results in further director re-orientation and refractive index change (Figure 2.13b and c).

3) In conjunction with applied dc field, a small reorientation of the director axis (caused by photorefractive effect) will produce space charge field (Figure 2.13b), which may create material flows along the direction of the field. This will cause further director re-orientation and the refractive index change (Figure 2.13c).

When the reorientation angle is small, flows (3) and Carr-Helfrich effects (2) may be neglected. The reorientation angle θ_o, induced in conjunction with an applied field in a homeotropic sample which is tilted with respect to the beams (geometry on the Figure 2.8a), was calculated by Khoo[68] to be:

$$\theta_0 = \frac{\Delta\varepsilon E_z E_{ph}^{(0)} \cos\beta}{K\left[\dfrac{\pi^2}{d^2} + q^2\right]}$$

2.56

$q=2\pi/\Lambda$ is the wave vector of the grating with a spacing Λ formed by interfering beams. E_{ph} varies as q (from 2.39), therefore

$$\theta_0 \sim \frac{q}{\left[\dfrac{\pi^2}{d^2} + q^2\right]}$$

2.57

and the maximum reorientation is obtained when $q=\pi/d$ and therefore $\Lambda=2d$.

This is an important result from the point of view of device engineering. The effects that involve space-charge field formation have strong resolution dependence on the sample thickness.

The stronger the space charge field, the larger the reorientation angle and the induced refractive index change. It may seem a good option to simply increase the applied DC field, as the space-charge field is linearly dependent on the latter. Unfortunately there are limitations on the value of DC field that can be applied to the device.

First, large DC field induces a flow in nematic liquid crystal doped with ions, resulting in the so-called dynamic scattering[67]. This effect is highly undesirable. It has been shown, that threshold for dynamic scattering in C_{60} doped liquid crystals may be increased by adding carbon nanotubes to the solution[69]. The effect is attributed to complex structures formed by nanotubes and C_{60} that inhibit dynamic scattering.

Second, DC field leads to the material deterioration through ionic processes. This problem is usually treated by applying "compensating" DC pulses of opposite sign after the "writing" pulse has been applied.

2.5.2.5 Surface induced nonlinearity

It was already mentioned in the beginning of this chapter that it is possible to induce a preferred direction in nematic liquid crystal by simply rubbing the surface. This is an example of a phenomenon, when a physical pattern on a surface defines alignment by forcing the molecules to line up in a certain direction. On the other hand, repulsion and attraction on a molecular level will define planar or homeotropic alignment or a specific pretilt of the molecules in respect to the surface.

The interaction of molecules forming LC phase with a substrate depend on the nature of both the compound and the surface. It has been shown, that the nematic LC bulk alignment is fully determined by the orientational ordering of the first LC monolayer adsorbed on the substrate[70].

Interaction of molecules forming LC phase and a surface are described by the anchoring energy. If the latter changes, reorientation may occur[71].

Some dopants, namely Methyl Red and C_{60} may be adsorbed on some surfaces. The process in MR doped nematics has been studied in detail by Ouskova et al[72]. A layer of Methyl Red is adsorbed on a surface from the LC solution. When excited by light, trans-cis isomerisation or desorption/adsorption of the dye leads to significant changes of the anchoring energy leading to strong orientational effects.

Reversible surface effects in nematics doped with MR are resulting in the strongest nonlinearities found so far[51]. Nevertheless, from the device application point of view these effects are too slow (tens of seconds) to be exploited.

When MR- and C_{60}-doped samples are subjected to prolonged illumination, especially in conjunction with external fields, the change of anchoring energy becomes persistent[*] or permanent[†68]. This is undesirable for applications where dynamic change of written information is required, including spatial light modulation. It will be shown in Chapter 5 that it is possible to avoid permanent effects by careful choice of alignment.

2.6 Summary and conclusions

The combination of strong optical anisotropy with possibility of reorientation and sensitivity to external fields makes liquid crystals very attractive for many applications.

---

[*] Lasting for days

[†] Lasting for the lifetime of the sample

It is possible to enhance sensitivity of liquid crystals to light by adding small amounts of dyes or fullerenes. When illuminated, a number of disparate effects occur in doped systems.

Heating in highly absorbing films can induce large refractive index changes. Thermal effects are very fast but temperature tuning for efficient operation is important, and high optical intensities are required. This is not convenient for applications in optically addressed spatial light modulation.

Optical torque on the liquid crystal can be significantly enhanced by dyes. Dopant-induced optical torque depends strongly on guest-host system. It leads to fast (under 100ms) reorientational processes.

Trans-cis isomerisation in azo dopants is a fast process involving conformational change in the dopant. It leads to geometrical reorientation of surrounding host molecules. Cis and trans isomers can be viewed as different dyes, and the torques that they impose on the LC may be considerably different. Both, dopant assisted optical torque and trans-cis isomerisation are good candidates as effects to be exploited in spatial light modulators.

Under spatially modulated optical field in dye- or fullerene- doped liquid crystal films space-charge fields may be generated leading to director reorientation. This effect requires externally applied electric field. In case of Methyl Red such fields may be generated internally under the influence of light. Reorientation of the director depends on the spatial frequency of the field and is maximal when it is twice as large as the cell thickness. This effect is interesting from the applications point of view. It is large and allows control with external electric field. The drawback is that the time scale of effect is of the order of seconds.

Surface effects are a very powerful tool for orienting liquid crystal film. Transient surface effects are the strongest nonlinearities ever observed. Unfortunately they are too slow for device applications (10s of seconds). Permanent and persistent surface holograms may be formed in MR and C_{60} doped samples under prolonged illumination. This effect must be avoided in spatial light modulators.

Many groups have been working in the area of dye-doped liquid crystals. Various dopants and host materials were investigated with the aim to obtain higher nonlinearity. The situation in nonlinear materials at a recent stage is described in more detail in the following chapter.

CHAPTER 3

MATERIAL PARAMETERS, DOPANT SELECTION AND SAMPLE PREPARATION

Out of a large spectrum of dyes and liquid crystals, available in the market and from research institutions, materials for the doped devices are chosen. This is an important step in the research, and will have to be iterated, as more understanding of the effects and processes in doped LC systems is gained.

3.1 Choosing materials for novel OASLMs

To make a choice of materials, an evaluation method must be chosen. We aim for high efficiency at low power light, safety, relatively low cost and good optical and time stability.

3.1.1 Evaluating nonlinear materials

There is a number of ways of studying nonlinear effects in LC materials. In addition to observing diffraction from the recorded grating, nonlinearity can be studied using methods like the so-called z-scan[76] or observing beam amplification in a wavemixing geometry. Materials evaluated using these different methods are hard to compare. Here commonly used parameters for evaluating nonlinear materials are reviewed and the most convenient parameters from the point of view of the applications (and thus this research work) suggested.

49

3.1.1.1 Diffraction efficiency

The diffraction efficiency of the material (*DE, %*) is often used as a guide when assessing various systems and materials.

As a materials comparison criteria, diffraction efficiency can be used only if the experimental conditions have been the same; otherwise such a comparison becomes useless if not misleading. For example, for a fixed grating spacing, material in a thin sample with a recorded sinusoidal-wave phase grating and an efficiency of 20% is more efficient than a material in a thick sample giving an efficiency of 30% (see Table 2.2 in the previous chapter). Thus, although diffraction efficiency is a very natural and useful parameter, it should be used with caution and together with explicit information about the experimental geometry.

3.1.1.2 Nonlinearity coefficient

To make a careful quantitative comparison of a nonlinear response, the so-called nonlinearity coefficient n_2 *[cm^2/W]* is often used (see also the previous chapter). It shows the induced change of refractive index $\delta n_{induced}$ per unit optical density *I [W/cm^2]*:

$$n_2 = \frac{\delta n_{induced}}{I}$$

3.1

This parameter can become very large at low optical fields (for materials and effects with extraordinary sensitivity). Such supra optical nonlinearities often rapidly saturate with an increase of the optical power. So, when using a writing beam power of 10 mW/cm^2, we cannot expect, for example, a thin MR doped film with n_2=1000 cm^2/W to produce a change of refractive index of *$\delta n = n_2*10^{-2} W/cm^2 = 10$*. As in the previous case, this evaluation parameter should be used with caution, and with the linear region of optical intensity dependence specified.

3.1.1.3 Photoinduced refractive index change

The most appropriate parameter for evaluating nonlinear *material* from the application point of view is the optically induced change of the refractive index $\delta n_{induced}$. This parameter is calculated from the *DE* accounting for the geometry of the experiment; it is a true material characteristic and does not depend on the sample thickness. The induced refractive index change is the key parameter responsible for the efficiency of the device, the

possible phase modulation. It is best measured at the saturation optical intensity, and used together with information about this intensity.

3.1.1.4 Maximum phase modulation

Phase modulation Δ is a key *device* characteristic. It is used when describing the response of OASLM (see Appendix A for example). It is connected with the refractive index change and diffraction efficiency through the relation:

$$\Delta = \frac{2\pi d\, \delta n_{induced}}{\lambda}$$

3.2

d is the hologram thickness, λ is the reading beam wavelength. Usually it is given in respect to π, not in radians. It is desirable to obtain a modulation of 2π from a device.

3.1.2 The state of art in nonlinear liquid crystal materials

The discovery of nonlinearities at least 10^6 times exceeding those observed in photorefractive crystals ($n_2 \sim 10^{-4}$) has led to extensive study of various materials, especially dye-doped systems. The current situation in the field is condensed in the following tables. The first row denotes the research group that has been working on the LC system. The next rows give details of the applied fields and optical power used, followed by details of material switching times, resolution and efficiency (presented in all discussed forms). Details of device thickness, alignment and plausible mechanisms, leading to nonlinearity in specific system, are also shown.

During recent years research has been focused on obtaining the highest nonlinearities possible. This has resulted in impressive achievements, as can be seen from the tables below. The first row in the Table 3.1 represents characteristics of commercially available device based on amorphous silicon (a-Si:H) photoconducting and nematic liquid crystal layers and is given for comparison.

In brief, materials have been found that are very sensitive to optical fields or do not require an external electric field. Mechanisms have been researched leading to very large nonlinearities. Fast processes exist (limited only by the response time of the LC). All these desired properties have not yet been combined in one system.

Parameter	a-Si:H OASLMs[*]	C$_{60}$	Carbon nanotubes+C$_{60}$	
Research group	Hamamatsu[2]	Khoo et al[47,71]	Khoo et al[72]	
Applied voltage	±5V 50Hz-100kHz	>1.5V$_{DC}$ (+3Vpp$_{AC}$)	4.5V (dynamic scattering at 5.2V)	20V pulse
Optical power	1 mW/cm^2 50 µW/cm^2 high sensitivity	mW/cm^2	2 mW/cm^2	160 µW/cm^2
Switching time	30/40 ms (60 ms/70 ms at high sensitivity)	15-20 min, becomes permanent at prolonged illumination, electrically switchable	seconds	100 ms
Resolution	50 lp/mm	100-200 lp/mm, max at $\Lambda=2d$[†]	-	
DE,%	30% (10 lp/mm), ~1% (50 lp/mm)	5%, dynamic scattering	8%	1%
n$_2$	-	~0.5 cm^2/W	0.8 cm^2/W	7 cm^2/W
δn	-	1.4*10^{-3}	1.6*10^{-3}	1.1*10^{-3}
Δ	π	0.11π	0.16π	0.11π
d	-	25 µm	25 µm	
Alignment	-	Homeotropic (HTAB)	Homeotropic (HTAB)	
Effect	Photo-conductivity in a-Si:H	Space-charge	Space-charge	

Continued on the next page…

Continued…

Parameter	Methyl Red doped NLC				
Research group	Simoni et al[51,77]		Khoo et al[78]	Residori, Petrosian[79]	
Applied voltage	0V		0-5V	0V	
Optical power	40 $\mu W/cm^2$	7 mJ/cm^2	4 mW/cm^2	100 $\mu W/cm^2$	20 mW/cm^2
Switching time	20s	4ns pulse, 30min signal build-up; permanent	>1s (50 ms at 20 mW/cm^2) becomes permanent easily	>100s	100ms
Resolution	-	Max 500 lp/mm	Max 500 lp/mm	-	
DE,%	26% (>50% at 1mW/cm^2)	20% at 125 lp/mm detectable at 500 lp/mm	30%	25%	7%
n_2	1000	3.4	Up to 10^3 predicted	>100	0.2
δn	$9.4*10^{-2}$	$6.7*10^{-2}$	$2.4*10^{-2}$	$1.2*10^{-2}$	$5.5*10^{-3}$
Δ	0.45π	0.32π	0.45π	0.38π	0.18π
d	1.5 μm		6 μm	10 μm	
Alignment	Homeotropic (HTAB), planar (rubbed glass)	Planar (PVC)	Homeotropic (HTAB), planar (rubbed ITO, glass, PVA)	Homeotropic (HTAB, HTAC)	
Effect	Surface	Permanent surface	Space-charge fields	Surface + trans-cis	Trans-cis

Continued…

Parameter	Anthraquinone dyes		Discotic LC	LC with conjugated acetylene groups	BMAB[*]
Group	Marrucci et al[80]	Parka et al[81]	Mcdonald et al[82]	Pagliushi, Macdonald[83]	Khoo et al[50]
Applied voltage	0V	To pre-tilt to homeotropic	DC 3V; T=60ºC	DC 9V	>5V
Optical power	Focused beam	10 mW/cm^2	4 mW/cm^2	1.4 mW/cm^2	1 mW/cm^2
Switching time	100 ms	2 ms	Not known	1-5 s	~1 s
Resolution	-	1000 lp/mm, max at $\Lambda=2d$[†]	-	-	-
DE,%	-	2% 25% at max resolution	-	19%	-
n$_2$	n$_2$=2*10^{-4} cm^2/W	0.5 cm^2/W	6 cm^2/W	17 cm^2/W at low power light	2 cm^2/W
δn	Δn/P=14 W^{-1}	5*10^{-3}	2.4*10^{-2}	3*10^{-3}	~2*10^{-3}
Δ	-	~0.2π	0.52π	0.31π	~0.08π ?
d	55 μm	5-15 μm	5 μm	25 μm	10 μm ?
Alignment	Homeotro-pic	Planar, pre-tilted to homeotropic	Planar (Polyimide)	Planar (Polyimide)	Planar (PVA), homeotropic (HTAB)
Effect	Guest-host	Space-charge	Space-charge	Space-charge	Trans-cis, guest-host

Table 3.1. The current state of art in nonlinear materials.

---

[*] Butylmethoxy azobenzene - an azobenzene LC material. Khoo et al used NLC doped with 10wt% BMAB

[†] Λ - grating spacing; d - cell thickness.

3.1.3 Materials selection

For preliminary studies materials which satisfied stability, cost and safety requirements, and gave a promise of nonlinearity at low optical powers were selected. The full list of preliminary selected dopants can be found in Appendix B.

3.1.3.1 Dopants

As can be seen from the above description, there is a good range of materials that have potential for applications in OASLMs. All of the materials mentioned have advantages and drawbacks. The first step towards a device would be to define the materials and effects that are most promising[*].

Azobenzene LCs and pure liquid crystals with conjugated acetylene groups possess very poor stability and have not been considered further. Discotic LCs require high temperatures (T=60°C) and also have a stability problem.

Methyl red[†] is one of the most promising and versatile materials. This dopant gives flexibility with the mechanism that one wishes to exploit: it can produce photocharge[71]; being an azo dye it undergoes trans-cis photoisomerisation[50]; it triggers very strong surface-induced nonlinearities[54]. Advantages of Methyl Red doped systems:

+ No applied DC field necessary
+ Voltage control possible
+ Very high efficiency possible
+ High speed may be achieved using trans-cis isomerisation in the bulk
+ High resolution
+ Low cost, produced in large quantities
+ Relatively safe to work with

Drawbacks:

− "on" and "off" times with highly efficient surface effects are unacceptably slow (over 20 s)
− switching for space-charge field mechanisms is slow

---

[*] We aim to assess existing materials. Improvement of molecular parameters is out of the scope of this research work.

[†] Methyl Red is available in three forms: MR hydrochloride, MR sodium salt and MR crystals. See Appendix B for structures. In the literature MR crystals dye is usually used.

— Resolution depends on thickness for space-charge field mechanisms

— Ionic effects may mean poor time stability

— Permanent/persistent component formation

The use of trans-cis transition in MR and other azo dyes as a mechanism of nonlinearity is attractive.

The other promising class of materials is **fullerenes (especially C_{60}) and carbon nanotubes**. C_{60} is a very effective photoconductivity enhancing agent, it also contributes to photocharge generation[71, 84]. The photorefractive effect in carbon nanotube-doped nematics is believed to be of the same nature as in C_{60} doped systems[72]. Advantages:

+ Voltage control

+ Can be switched quite fast with the field (20Hz in nematic not a problem)

+ High efficiency possible

+ Only small concentrations (0.05wt%) required to produce large nonlinearity

These materials are best suitable for applications where a small range of spatial frequencies is used, or where a grating needs to be switched on and off quickly, because:

— Resolution depends on thickness

— "on" and "off" times with optical switching are very slow

— Ionic effects may mean poor time stability

— Very low solubility

— Strong dynamic scattering (can be reduced by adding CNT to C_{60} solutions)

— Possible permanent/persistent component formation

Another very interesting class of materials is anthraquinone dyes. They are rarely ionic and exhibit very good time stability and light fastness. They are also more readily dissolved in LCs and possess high order parameters. Some anthraquinone dyes exhibit the so-called Janossy effect. Although this effect has been well researched, it is still not possible to predict what the interaction would be for the specific guest-host combination.

A selection of anthraquinone dyes and other dopants (a full list with structures and parameters is given in Appendix B) were studied as materials for optically addressed spatial light modulators. Three dopants: Methyl red crystals[*], C_{60} and 2,6 azo-substituted anthraquinone dye DC161 exhibited a strong nonlinear effect at low optical power and were selected for intensive studies.

---

[*] As preliminary studies have revealed, MR crystals dye gives the largest effect and best sensitivity.

3.1.3.2 Host materials

Orientational effects that lead to nonlinearity in liquid crystals rely on the large anisotropy of LC molecules. In materials with high birefringence even small reorientation (or disorientation) of the molecules will lead to relatively large refractive index change and resulting phase modulation of the reading light. Thus materials with high birefringence are the best candidates for spatial light modulators. Moreover, materials with high conductivity anisotropy and dielectric permittivity anisotropy are more efficient in terms of space-charge field generation through Carr-Helfrich effect[*].

To obtain fast relaxation, low viscosity and large elastic force acting on the molecules (high elastic constant) are necessary.

Other requirements include good stability, wide temperature range of operation, possibility to dissolve dopants.

For research purposes we have chosen different host materials. Full details together with what is known concerning their chemical structure can be found in Appendix B:

Host material	Refractive indices and birefringence (λ=589nm)			Dielectric anisotropy (1kHz)	Elastic constants $\cdot 10^{-12}$N		Flow viscosity (20^oC) mm^2/s	Clearing point T_{NI}
	n_e	n_o	Δn	$\Delta\varepsilon$	K_{11}	K_{33}		
5CB	1.71	1.53	0.18	20.1	5.5	6.96	34	34°C
E7	1.7462	1.5216	0.2246	13.8	11.1	17.1	39	61°C
BLO48	1.7904	1.5277	0.2627	16.8	15.5	28.0	47	100°C
ZLI2222[†]	1.6134	1.5010	0.1124	5.3	-	-	14	66.5°C

Table 3.2 Parameters of host materials.

These hosts allow the study of the influence of optical anisotropy, elastic properties and viscosity on the value and speed of the nonlinear effects. A choice of clearing temperatures allows the separation of the thermal mechanism. Various molecular structures should exhibit different behaviour when Janossy effect is involved.

---

[*] See Chapter 2, p. 29 for more details.

[†] ZLI2222 is used occasionally in preliminary studies.

3.1.3.3 <u>Aligning agents</u>

In this research we have studied various aligning agents. Molecules forming LC phase are aligned by mechanical (grooves or other surface pattern) and chemical (e.g. hydrogen bonding) interaction with the surface of the cell. Homeotropic alignment was introduced by surfactants *ZLI1134*[*] (**non-ionic**) and *HTAB*[†] (**ionic**).

Planar alignment was introduced by obliquely evaporated *SiO$_x$* (when evaporated at 60° relative to the substrate, gives planar alignment with no pre-tilt at the surface) and rubbed polymer alignments that are introduced by spinning. The water or alcohol solution of the polymer polyvinyl alcohol *PVA,* is spun on the substrate and dried. Alternatively, the solution of the monomer AM4276 for *polyimide* (*PI*) alignment is spun on the substrate and polymerised by annealing at $T = 220^o$C for 2 hours.

3.1.3.4 <u>Stability of the materials</u>

The good stability of the host liquid crystal material depends significantly on its ionic content and absorption on the writing wavelength, as the electrochemical and photochemical reactions are the main sources of material deterioration. Commercially available thermotropic liquid crystal phases have negligible absorption in the visible range and very low ionic content and therefore very low electrical conductivities.

Introducing optically absorbing dopants usually does not cause any problems to the photochemical stability of the liquid crystal host material as long as the dopant is photochemically stable itself. On the other hand, dopants that lead to significant optical nonlinear effects are often ionic. Additional ions in the material aid the space-charge field formation but decrease the electrochemical stability of the system.

It is important therefore to find systems exhibiting large nonlinear effects with small or no trade off to the stability of the material and thus the lifetime of the device.

3.2 Sample preparation

Single layer dye-doped LC devices should be quite simple to build, especially on an industrial scale, however a lot of care must be taken when making these devices in the

---

[*] Liquid crystal, **non-ionic** surfactant.

[†] Hexadexyl trimethyl ammonium bromide, **ionic** surfactant.

laboratory. Strict cleanroom conditions are necessary to ensure that there are no impurities in the samples.

Special care has to be taken to avoid contamination of materials by ions. As has already been discussed, some mechanisms leading to nonlinearity rely on ions in the system and hence are very sensitive to ionic content. It is also well known that ions shorten the lifespan of the devices and must be avoided. The quality check of most LC devices usually includes impedance measurements. Resistivity up to 10^{10} Ohm·m is usually required from the electrically switchable devices.

The dye-doped LC mixtures are prepared in the class 100[*] cleanroom. To promote dispersion of the dopant in the host material[85], the mixture is heated above the temperature of the transition to the isotropic phase T_{NI} and agitated. This operation is repeated about 10 times, until the solution is visibly uniform. Before filling the cell, the mixture is usually filtered using 0.2 µm pore filter.

3.2.1 Device structure

The structure of single layer optically addressed spatial light modulator is shown below:
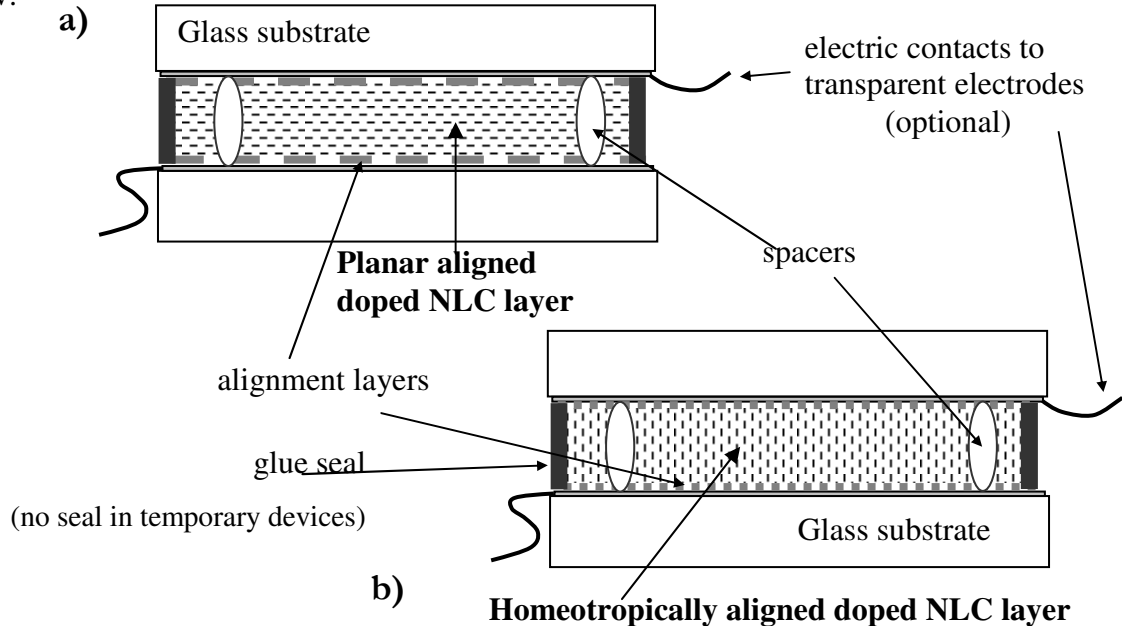
Figure 3.1. The structure of devices (often referred to as cells):
a) planar aligned (LC molecules parallel to substrate)
b) homeotropically aligned (LC molecules perpendicular to substrate)

---

[*] Less than 100 particles per 1m³.

3.2.2 Device fabrication

Two types of devices are prepared: temporary and sealed.

For preliminary tests, when the stability of device is not essential, a simplified method of sample preparation is used to obtain temporary samples. The method is fast and simple, and a large number of test samples can be quickly obtained. This technique is beneficial when it is necessary to test new material or monitor general trends before building more elaborate devices. The temporary cells are not uniform and have to be handled with care, as the edges are not properly sealed. Temporary cells deteriorate in months.

For detailed studies, sealed cells are prepared. The preparation is more complicated, and the conditions of preparation are very strict. The resulting devices are well aligned, uniform and safe to handle (no leaks of material). Due to good sealing, material in the cell does not make contact with air and moisture. As the ionic content is controlled during fabrication, there are no external sources of material deterioration with time[*]. Such devices are reliable and stable.

3.2.2.1 Temporary cells

Processing room facilities, instead of the cleanroom, are exploited. Glass substrates with deposited ITO layer are commercially available. In some cases glass without ITO layer is utilised. Glass slides are cleaned following the cleaning procedure, described in Appendix C, and blow-dried with a nitrogen gun. Alignment layers[†] (*PVA*, *HTAB* in water solution) are spun or simply poured on the substrates. Samples are blow-dried and left to finish drying for 25 minutes at room temperature. The PVA layer is lightly rubbed with a cleanroom grade tissue to achieve planar alignment.

The spacers (micro spheres in water solution or a thin film of defined thickness) are applied on the perimeter of one glass slide. If spacers in solution are used, the samples are left to dry for another 25 minutes at room temperature.

A droplet of doped LC material is applied to one prepared glass slide and covered with the other. The pressure is applied using two crocodile paper clips. They hold the

---

[*] Only material instability may lead to device deterioration.

[†] Sometimes no special layers are used, the alignment is obtained by rubbing the glass surface.

sample together and help to achieve selected and relatively uniform cell thickness. Excess LC material is cleaned away and the edges are sealed by transparent tape.

In case an electric field has to be applied, the leads are soldered to the surface of the sample. Conventional solder together with a solution of conductive polymer is used for this purpose.

3.2.2.2 <u>Sealed cells</u>

The cells are built and later filled by Dr. T. D. Wilkinson. Preparation involves cleaning of the glass substrates with their indium tin oxide (ITO) layer[*], putting on alignment layers (by spinning or evaporating), assembling two glass slides with a spacer of defined thickness, and sealing three sides with a polymerisable glue. Cells prepared in this way are filled by capillary action and sealed with the glue. Contact leads to ITO electrodes are soldered and the quality of the contact checked.
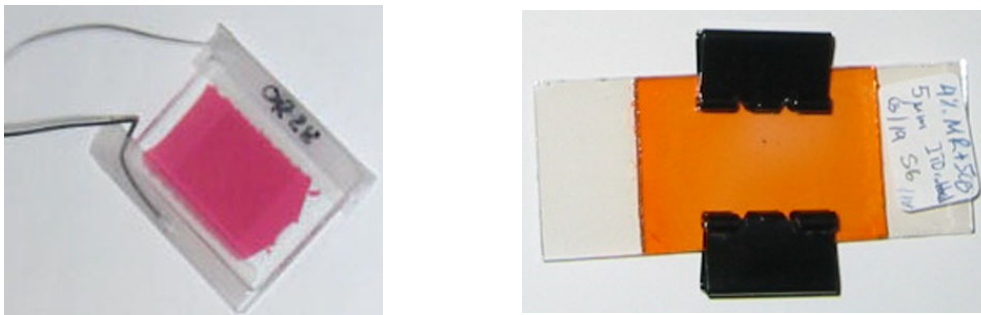
Figure 3.2. Typical devices prepared in Cambridge University Engineering Department:
a) device made by Dr. T. D. Wilkinson in Photonics and Sensors cleanroom
b) typical device prepared by the author following the simplified technique

Alignment agents used are rubbed polyimide (polymerised AM4276 which is referred to as *PI* in this work) and obliquely evaporated SiO_x for planar alignment, and *ZLI1134* for homeotropic alignment. The polyimide produces a small (1-2° degrees pre-tilt) while SiO_x promotes planar alignment with no pre-tilt.

Adherence to strict cleanroom conditions prevented us from using ionic surfactants like HTAB as aligning agents. Spacers are usually 5-20 μm.

---

[*] Acting as transparent electrode.

3.2.3 Devices prepared for studies

For further research a variety of devices doped with three dopants has been made.

Studies on Methyl red as a dopant led to preparing the following cells (mainly using the simplified technique):

⇒ various alignment layers (PVA, rubbed glass, rubbed ITO, rubbed PI, HTAB, ZLI1134),

⇒ various thickness (1 µm, 5 µm, 10 µm, 14 µm, 25 µm)

⇒ dye concentration (0.5%, 1%, 3.5% by weight)

⇒ in host materials 5CB and E7.

Studies on DC161 as a dopant led to building devices with the following characteristics:

⇒ various thickness (2 µm, 10 µm, 14 µm, 20 µm, 40 µm, 60 µm, 125 µm)

⇒ dye concentration (0.1%, 0.5%, 1% by weight)

⇒ in host materials 5CB, E7, BLO48.

Also a good selection of samples (5CB doped with 1wt% and 0.5wt% DC161, with thickness 5 µm, 9 µm and 15 µm) prepared earlier in 1987 was available for study.

Studies on C_{60} involved making the following devices:

⇒ thickness 5.5µm and 20µm

⇒ various dopant purity (99.5%, 88-98%, soot)

⇒ in host materials 5CB and BLO48.

The list of all devices with names and parameters are given in Appendix D and details of the liquid crystals and dyes are given in Appendix B.

3.3 Summary and conclusions

There is a variety of promising nonlinear dopants for liquid crystals and other nonlinear LC materials.

Three dopants have been chosen for further studies. They are to be used with different nematic LCs so that the influence of the host material can be studied.

Single layer optically addressed spatial light modulators have a simple structure. They consist of glass slides (with or without transparent electrode), alignment layers, spacers and doped liquid crystal layer.

The devices must be prepared in a cleanroom to ensure good time stability and uniformity. For preliminary studies a simplified technique for sample preparation is used.

A good selection of devices has been made available for this research.

CHAPTER 4

EXPERIMENTAL TECHNIQUES

4.1 Samples characterisation methods

4.1.1 Polarised light microscopy

After preparation, samples are viewed under the polarised light microscope to check for uniformity and find possible defects. Areas with defects should be avoided in the optical studies.

Figure 4.1. Microphotographs of samples viewed under crossed polarisers, magnification ×250. Alignment direction along one of the polarisers. Host material 5CB.
a) alignment defect in a cell with sputtered SiO_x as aligning agent;
b) uniform area in the same sample;
c) crystallised dye in MR doped cell.

If no light gets through at any sample position when the polarisers are crossed, it indicates good homeotropic alignment. A good contrast between dark and bright states

when rotating planar aligned devices on the microscope stage at crossed polarisers indicates good planar alignment.

Although mixtures are filtered prior to filling the cells, in some samples dopant re-crystallises with time, which can be seen under the microscope (Figure 4.1c). It has been found that devices with re-crystallised dye have significantly deteriorated[*].

4.1.2 Polarisation spectroscopy

Absorption is a very important parameter in the dye-doped systems. In general, the light incident on a sample is reflected, scattered, absorbed and transmitted:

$$I_o = I_{tr} + I_{sc} + I_{ref} + I_{abs} = (T + S + R + A)I_o, \qquad T + S + R + A = 1$$

4.1

I_o is the incident optical intensity, I is the transmitted optical intensity, T is transmittance, R - reflectance, A - absorptance, S - scattering losses.

Absorption process may be described by Beer's law:

$$I = I_o e^{-\alpha d} = I_o A$$

4.2

d is the sample thickness, α is absorption coefficient expressed in [cm^{-1}]. This parameter gives information about the efficiency of absorption of a medium.

When a dye with geometric anisotropy is dissolved in a LC, the dye molecules tend to arrange themselves in such a way that the long molecular axis aligns along the LC director. Dyes with geometrical anisotropy also possess anisotropy of physical properties, for example, absorption. Such dyes are called dichroic and have different spectra of absorption for light polarised along and perpendicular to long-wave electron transition oscillator (LETO) which may or may not coincide with long molecular axis of the dye[† 87].

The degree of ordering with respect to director ***n*** of a dichroic dye is one of the main criteria of the dye efficiency as an absorbing media. The order parameter *S* of the dye within a LC (not to be confused with the LC order parameter) is calculated from the

---

[*] The discussion of this can be found in Chapter 6.

[†] In our systems LETO aligns along the LC director, in other words, maximum absorption is obtained for light polarisation parallel to the direction of LC alignment.

polarisation absorption spectra of the dye solution[87] and can be higher than the LC order parameter:

$$S = \frac{(D_\parallel - D_\perp)}{(D_\parallel + 2D_\perp)}$$

<div align="right">***4.3***</div>

where $D_\parallel$ and $D_\perp$ are optical densities for light with parallel and perpendicular polarisation in respect to LC director. Optical density is connected with transmittance by relation:

$$D = \log_{10}\left(\frac{1}{T}\right)$$

<div align="right">***4.4***</div>

By taking a natural logarithm of 4.3 and differentiating the result, the error of the calculated order parameter may be derived:

$$\frac{dS}{S} = \frac{dD_\parallel}{D_\parallel - D_\perp} + \frac{dD_\perp}{D_\parallel - D_\perp} + \frac{dD_\parallel}{D_\parallel + 2D_\perp} + 2\frac{dD_\perp}{D_\parallel + 2D_\perp}$$

$$dD_\parallel = \frac{1}{\ln 10}\frac{dT_\parallel}{T_\parallel}; \qquad dD_\perp = \frac{1}{\ln 10}\frac{dT_\perp}{T_\perp}$$

<div align="right">***4.5***</div>

The dye order parameter is usually calculated at maximum absorption wavelength. Transmission spectra are measured for two light polarisations. The measurements were conducted on the automated setup from *Rees Instruments* (Figure 4. 2).
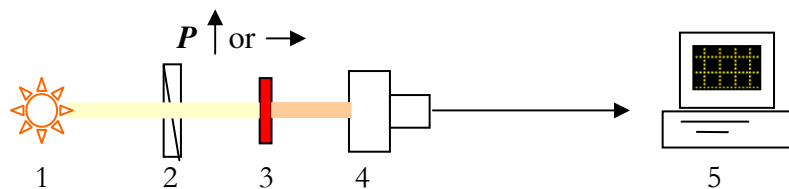
Figure 4. 2 Setup for measuring transmission/absorption in polarised light. 1 – light source, 2 – polariser, 3 – sample, 4 – photodetector, 5 – system controller and computer.

The light from the Hg lamp 1 (Rees Instruments light source model 6282, with a power supply model 6260), containing wavelengths from 350 to 850nm is collimated and polarised by a polariser 2 before impinging on the sample 3. It is then collected by a sensor 4 (model 6146), from which the data is sent to the Optical Spectrum analyser Monolight 6000, with a photomultiplier tube (PMT) unit (*Rees Instruments*, model 6118) and then to *Rees Instruments* system controller 6202 and computer 5.

First, a reference measurement is taken with an undoped LC cell of the same thickness to account for absorption in ITO electrodes and other losses for reflection and scattering. Then a sample transmission is measured and calculated, averaging over 500 measurements for each wavelength.

Transmission or absorption spectra of the samples are a valuable source of information. Firstly, the dye order parameter in the given liquid crystal can be calculated. The correlation between the order parameter, sample uniformity and performance will be discussed in Chapter 6. Secondly, it gives information for choosing appropriate wavelength ranges of operation (reading in the wavelength region with lowest absorption and writing in absorption band).
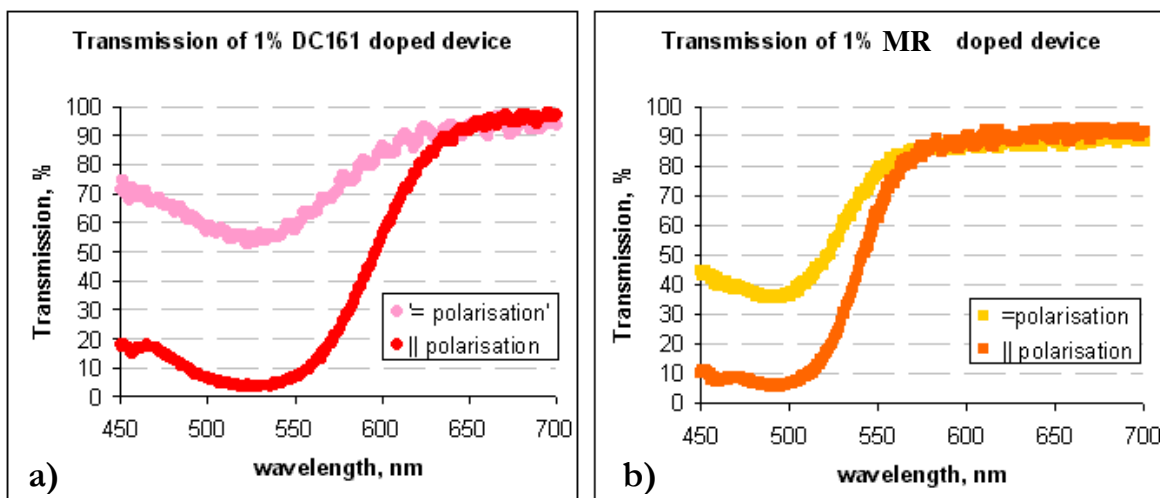
Figure 4.3 Transmission spectra of light polarised along and perpendicular to the alignment direction of the sample. a) Methyl red doped 5CB device; b) DC161 doped 5CB device.

As nonlinear phenomena rely on the absorption of photons, it can be seen, that the operating wavelength range in DC161 doped devices is 460-560nm (*Figure 4.3* a). T o operate MR doped devices, λ~450-540 nm can be used (*Figure 4.3* b). At λ>600 nm losses

for absorption are minimal in both systems, thus reading beam may be in the range 600-700 nm.

The systems used in this research have the following absorption characteristics:

Absorption coefficient α for various light polarisations at λ=514 nm				
Dopant \ concentration	0.5wt%		1wt%	
Polarisation direction	$\alpha_{||}$	$\alpha_\perp$	$\alpha_{||}$	$\alpha_\perp$
MR	1000 cm^{-1}	300 cm^{-1}	2000 cm^{-1}	800 cm^{-1}
DC161	1500 cm^{-1}	270 cm^{-1}	3000 cm^{-1}	500 cm^{-1}
C_{60}	0.01wt% concentration, α~10 cm^{-1}			

Table 4.1. Absorption coefficients of the systems under investigation.

Order parameters of the dyes in studied samples are around 0.36±0.03 for MR doped samples and 0.55÷0.61±0.03 for DC161 doped devices depending on the device[*]. Complete information with values of absorptance and order parameters for all samples doped with dichroic dyes is given in Appendix D.

4.2   Methods for studying samples in the electric field

To understand the processes happening in doped LC devices it is very important to research the behaviour of the devices when the electric field is applied. The impedance of the liquid crystal layer is important. High impedance is expected from LC devices, indicating the absence of ionic impurities and good lifetime. Freedericksz transition (reorientation from planar to homeotropic alignment under the influence of electric field) is an important phenomenon in planar aligned liquid crystal devices with liquid crystals with positive dielectric anisotropy. It is important to know the Freedericksz transition threshold voltage especially when there is a need to apply an external electric field. Although the threshold voltage for transition in the particular system can be calculated from the liquid

---

[*] The order parameter depends on the quality of alignment and dye distribution. More detail may be found in Appendix D.

crystal parameters (Equation 2.20, Chapter 2), we have found that in dye-doped samples this voltage is significantly higher than in pure LC devices.

4.2.1 I-V measurements

When the voltage is applied to the LC device, it produces a small current (usually of the order of 10^{-9}A). This current is due to ionic impurities or dopants, and charge injection from the electrodes which grows as the voltage is increased.
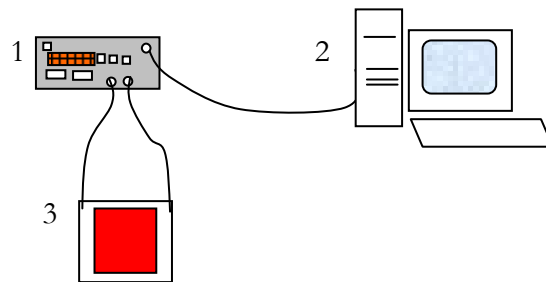

Figure 4.4 The setup for conducting I-V measurements. *1 – measuring unit, 2 – computer, 3 – sample.*

The measurements of the current are performed using a Hewlett Packard 4140B PicoAmmeter (precision 10^{-12}A) and DC source 1. The current is measured through the sample 3, as the external electric field is applied by the voltage source 1. The data are collected by computer 2.

The results obtained are used for the analysis of ionic processes in the doped devices and are discussed in Chapter 5.

4.2.2 Impedance measurements and Freedericksz transition (FT)

The setup for measuring complex impedance of the sample is used to monitor capacitance, resistance and dielectric permittivity behaviour of the samples as a function of frequency and AC voltage applied. The measurements are taken on the *Schlumberger* Impedance/gain - phase analyser SI 1260 with the aid of a Chelsea Dielectric Interface unit from *Dielectric Instrumentation*. *Solatron* Impedance Measurement Software controls the system and collects the data.

The temperature is stabilised at 22°C. The frequency response is measured at the smallest applied field in order not to disturb the molecular order in the sample (0.1V$_{rms}$ used). The voltage behaviour can be probed at different frequencies.

The complex impedance measured by the device (current through the sample "in" and "out" of phase with the applied voltage, precision of the measurement 10^{-7}A) is used to calculate the capacitance and resistance of the samples approximating the LC sample with the model of capacitor and resistor in parallel.

The real and imaginary parts of impedance are:

$$Z_{real} = \frac{R}{1+\omega^2 cR} \qquad\qquad Z_{im} = -\frac{\omega cR}{1+\omega^2 cR}$$

4.6

Here ω is angular frequency, R - resistance and c capacitance. These equations allow the values of R and c to be calculated. Resistivity ρ of the sample material can be found using the relation:

$$\rho = R\frac{A}{d}$$

4.7

where A - electrode area, d - sample thickness, R - resistance of the device.

Capacitance is connected to the dielectric permittivity of the medium:

$$\varepsilon = c\frac{1}{\varepsilon_o}\frac{d}{A}$$

4.8

where ε_o - permittivity of free space.

Impedance in LC devices is usually measured at high frequencies (1kHz), so that molecular motion does not influence the measurements. Resistivity of LC devices gives an idea of the level of the ionic purity of the LC. It is important, that LC devices have high resistivity and a low content of ionic impurities for good lifetime characteristics if external electric fields must be applied.

It is interesting to note that the impedance of a device changes if any molecular reorientation occurs (due to molecular anisotropy). Thus the curves showing dependence of resistivity and capacitance (connected to ε through equation 4.3) on applied voltage will have a non-monotonous behaviour and are a sensitive method for studying the Freedericksz transition threshold (Figure 4.5). Capacitance curves give a more straightforward

connection to the dielectric properties of the medium and, therefore, the Freedericksz transition, and are used to define the threshold.
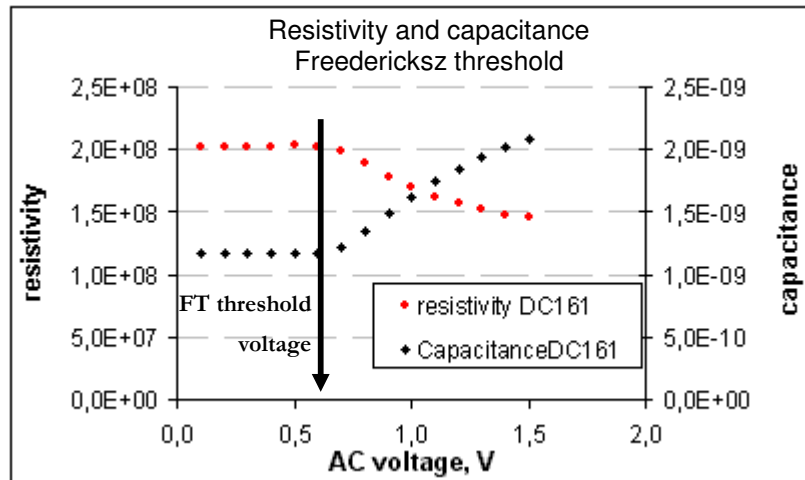

Figure 4.5. Definition of Freedericksz transition threshold from capacitance and resistivity curves. The graph represents the data collected for 10 μm 1% DC161 doped 5CB device with PI alignment (device 11, see Appendix D).

4.2.3   Freedericksz transition (optical measurements)

Another way to define the Freedericksz transition threshold relies on the effective birefringence, measured at normal incidence through the liquid crystal layer.
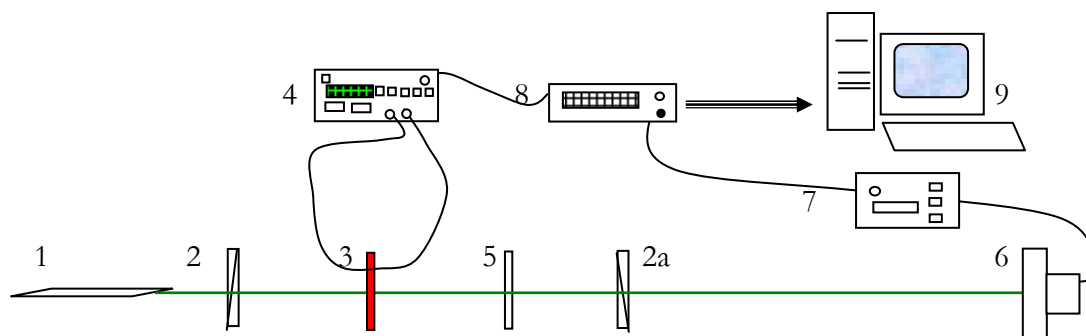
Figure 4.6 Setup for optical studies on Freedericksz transition threshold. 1 – laser, 2, 2a – polarisers, 3 – sample, 4 – waveform generator, 5 – Soleil Babinet compensator, 6 – photomultiplier, 7 – voltage generator, 8 – computer.

The sample 3 is placed between crossed polarisers 2, 2a, its optical axis at 45° to the axis of polarisers. A very weak laser beam (λ=532 nm)[*] from a highly stable source 1 is passed through the system. A Soleil Babinet compensator 5 is used to compensate for birefringence and obtain a minimal optical signal through the system. Now, if there is any change (decrease) in the refractive index of the sample, as associated with molecular reorientation and the Freedericksz transition, the compensation would be not full, and light would be able to pass through the system.

An AC electric field with variable frequency and amplitude from the *Wavetek* programmable arbitrary/function generator (model 275) 4 is then applied. As the voltage reaches the threshold value for the system (planar to homeotropic transition), the light is transmitted through the optical system and reaches the photomultiplier 6. The high voltage generator 7 supplies the power (1.1 kV) for the multiplier. The signal from the photomultiplier is amplified using a 7260 DSP lock-in amplifier from *EG&G Instruments*. The signal from the amplifier and applied voltage are registered using an Autocal digital multimeter 1065 from *Datron Electronics Limited* and stored on computer 8.

The threshold is defined from the graph representation of the collected data (Figure 4.7).
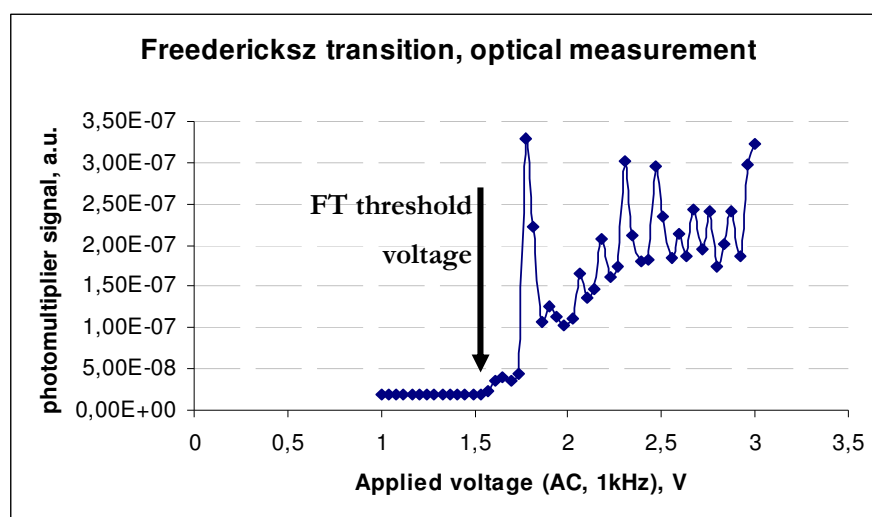
Figure 4.7 Freedericksz transition, optical measurement. The applied field is at 1kHz. The sample is 5CB doped with 1% of DC161.

---

[*] Though this wavelength is absorbed by the MR and DC161 dyes, it was ensured that the intensity of the light was 10 times weaker than the minimum intensity where nonlinear effects are observed.

Below the FT threshold voltage the optical signal remains low as the voltage is increased. At the threshold voltage the liquid crystal starts to reorient, the effective birefringence and therefore the retardation changes, and light is transmitted through the system. This is registered as an increase of the signal from the photomultiplier (Figure 4.7).

4.3 Setups for photogenerated charge studies

Under the influence of light, photocharges may be generated in the bulk of the device, or injected from the electrodes if external voltage is applied.

The measurements of the photogenerated currents and voltages give important sets of data that help in understanding the processes in the studied systems under the influence of light.
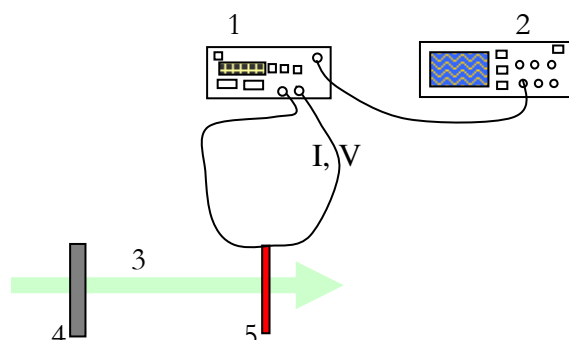
Figure 4.8. Photovoltage and photocurrent measurements. *1– a measuring unit, 2 – oscilloscope, 3 – exciting laser beam, 4 – electrically controlled shutter, 5 – sample.*

The photogenerated current and voltage in the sample (5 on Figure 4.8) are studied using a measuring unit 1: for current measurements *Hewlett Packard* 4140B PicoAmmeter (precision 10^{-12}A) is used, photovoltage in a similar manner is studied using *Keithley* 177 Microvolt DMM meter (precision 10^{-6}V). In both cases, the signal is recorded dynamically using oscilloscope 2, as the illuminating beam 3 is switched on and off with the aid of voltage controlled electronic beam shutter 4. The sample is illuminated by the expanded beam from the Ar+ ion laser using λ=514 nm. Optical intensity of illumination can be varied.

4.4   Experimental arrangement for measuring magnitude, dynamics and resolution of the optical nonlinearity

Optical nonlinearity manifests itself through the change of the refractive index in the studied system under the influence of light. The most sensitive way to study such small changes of the refractive index is to create in the studied sample a refractive index profile (a hologram) in form of a grating. The refractive index profile in form of a phase grating would diffract light with maximum possible efficiency of 33.8% for sinusoidal and 40.5% for square grating in thin samples (see Chapter 2, equations 2.38 and 2.40). Such gratings may be recorded by light at the wavelength which supports nonlinearity, and probed with a weak light beam, which is not absorbed and does not trigger any effects in the studied systems.

When studying optical nonlinearities, we are interested in several parameters, the magnitude of the effect, its dynamics and resolution.

The dynamics of the observed nonlinearities, as has been discussed already in Chapter 2, are a valuable source of information regarding the mechanism of the nonlinearity. Most of the measurements in this work have been performed dynamically, as the writing beams are switched on and off.

There are a number of ways to create intensity profiles, by imaging a pattern (an amplitude grating with a square profile) or by creating an interference pattern (sinusoidal amplitude profile) on the device. Each of these methods has its benefits and limitations. In this work these experimental methods are used to complement each other.

4.4.1   Diffraction from an imaged Ronchi[88] grating

An imaging arrangement has been developed for forming dynamic gratings in doped LC cells (Figure 4.9). The Ar$^+$ ion laser (Innova 90 from *Coherent*) is operating in a range of wavelengths in the blue and green part of visible spectrum (absorbed by the studied dopants). We mostly use the wavelengths λ=488 nm and 514 nm. The maximum laser power obtainable is up to 1 W, the beam diameter is 3 mm.
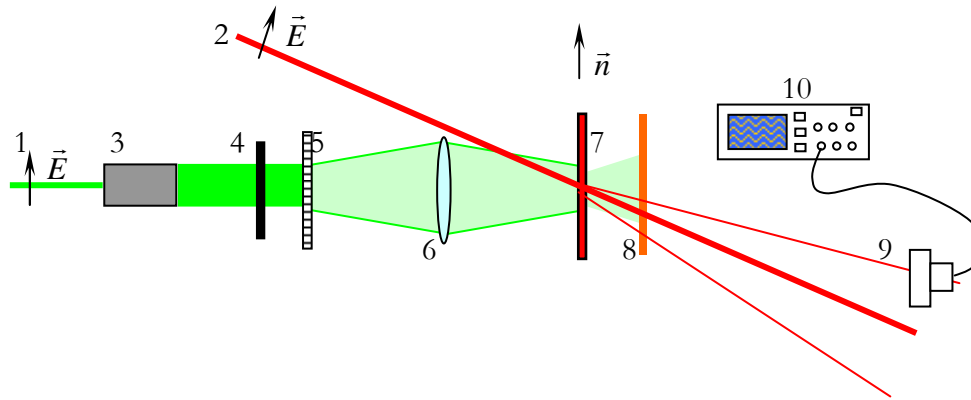
Figure 4.9 Imaging setup. *1, 2 – writing and reading laser beams, 3 – beam expanding unit, 4 – electrically controlled shutter, 5 – Ronchi grating, 6 – lens, 7 – sample, 8 – filter, 9 – photodiode, 10 – oscilloscope.*

The writing beam 1 is expanded by the collimator 3 and may be switched on and off with the aid of the electronically controlled shutter 4. The expanded beam is spatially modulated by a diffraction grating 5 (a set of square-wave amplitude gratings with spacing ranging from 15 to 120 line pairs per millimetre). The resulting intensity profile is imaged onto the sample 7 using a lens 6 (*4f* system).

The grating created in the sample is a phase grating. It is no longer square, but close to sinusoidal, because the aperture of the imaging lens acts like a low-pass filter in Fourier domain and cuts out all higher order spatial frequency components.

A He-Ne laser beam 2 (λ=633 nm, power 1 mW) is used to read the recorded information. The resulting diffraction of the reading beam can be viewed on a screen or measured by a photodiode 9 preceded by the OD7[*] filter 8 to cut out light at the writing wavelength. The signal from the photo sensor is read by the oscilloscope (TDS 2200) 10, as the writing light is switched on and off. DC and AC voltage of different frequencies and with different waveforms can be applied to the sample.

This technique is very simple and straightforward. It does not suffer from coherence problems, which is an advantage over the interference setups (described further where?). The control of the quality of an interference pattern is complicated, but with the imaging setup it is possible to account for the imperfections in the grating (e.g. scratches on the surface) we image. This is done by comparing the signal diffracted by a sample with the signal, diffracted by the grating rather than with the impinging beam. The grating 5 on

---

[*] Suppresses the signal on λ=488 and 532 by a factor of $10^{7.}$

Figure 4.9 is a square wave amplitude grating with a theoretical diffraction efficiency in the first order of about 10.1% (see Chapter 2). From these considerations, the doped LC material efficiency characteristics, which do not depend on the quality of the grating, may be obtained.

The drawback of the imaging setup is that when the cell is tilted away from the image plane, the quality of the image deteriorates; so tilted devices are difficult to study. At high spatial frequencies (100 lp/mm and higher) it becomes increasingly difficult to obtain a good focused image of the grating, and it is impossible to study the resolution of the devices.

4.4.2 Diffraction from a two-beam interference grating

To create interference fringes on the sample, two coherent laser beams are propagated through the sample, intersecting at a small angle within the sample. The interference pattern formed in this way is a sinusoidal intensity grating with a period Λ, which depends on the angle of intersection φ and wavelength of optical radiation λ[8].

$$I = I_0 \left(1 + m\cos(qx)\right) = I_0 \left(1 + m\cos\left(\frac{2\pi}{\Lambda} x\right)\right), \qquad \Lambda = \frac{\lambda}{2 n_\parallel \sin\dfrac{\varphi}{2}}$$

$$4.9$$

m is an optical intensity modulation factor and $n_\parallel$ is the refractive index seen by the writing beam (see also equation 2.38 in Chapter 2).

A measure of the quality of the interference fringes is the "visibility", defined as[89]:

$$V = \frac{(I_{max} - I_{min})}{(I_{max} + I_{min})}$$

$$4.10$$

where I_{max} is the maximum intensity and I_{min} is the minimum intensity.

If the paths traversed by the two beams are equal in length and the intensities in the two beams are equal, the fringe visibility is approximately equal to 1. If one path changes while the other remains stationary, the fringes will degrade and the visibility will decrease. The coherence length L_c is usually defined as the path length difference that corresponds to a fringe visibility of 50%.

$$L = \frac{c}{\Delta \nu}$$

4.11

where c is the speed of light, and $\Delta \nu$ is the linewidth of the laser light[90].

The normal multimode output of an Ar^+ ion laser, which is used as a writing beam source in our experiments, has a coherence length of about 100 mm. An intracavity etalon may be inserted inside the resonator to concentrate the laser power in a single mode. The width of a single mode is less than 50 MHz, and the resulting coherence length can be more than 6 meters. Thus when operating with the etalon inside the laser cavity, the coherence length does not put limits on the difference in the beam paths (and thus on the spatial frequency of the pattern which can be created).

To create interference patterns, either unexpanded Gaussian beams from an Ar^+ ion laser beam 1 (λ=488 nm or λ=514 nm) (Figure 4.10) or uniform expanded beams (Figure 4.12, Figure 4.14) are used. A doubled frequency Nd:YAG laser (λ=532 nm) is also used as writing light source in some experiments. A He-Ne laser beam 2 (λ=633 nm) is used to read recorded information.
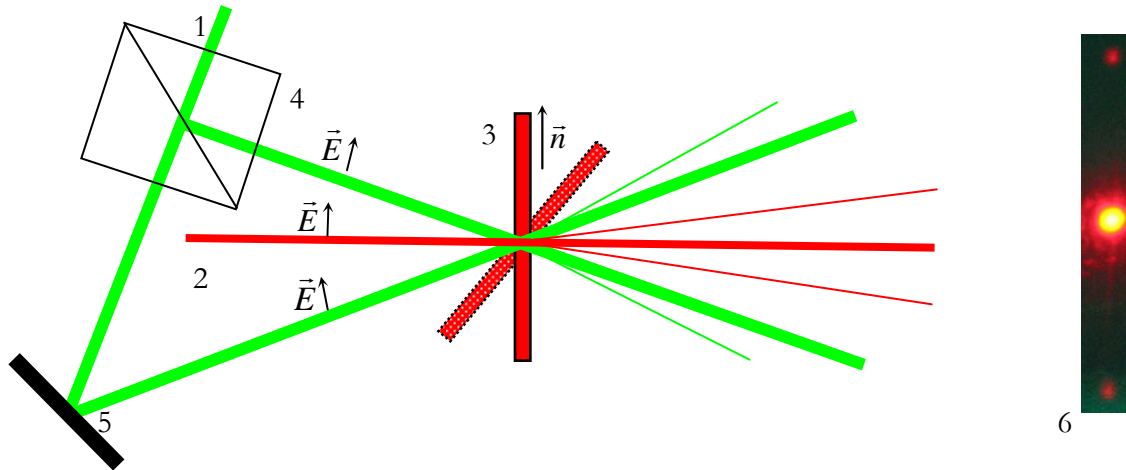
Figure 4.10 Pump-probe setup with unexpanded Gaussian beams. 1 – writing optical beam, 2 – reading beam, 3 – sample, 4 – beamsplitter, 5 – mirror, 6 – screen or photodetector.

A non-polarising beamsplitter 4 is used to obtain two coherent beams of equal intensity. These beams are overlapped on the sample 3 with the help of mirror 5. The resulting diffraction of a reading beam 6 may be either observed on the screen or recorded

dynamically (as the writing beams are switched on and off) with the aid of a photodiode and an oscilloscope (as on Figure 4.9).

To obtain maximum efficiency, all beams must be polarised parallel to the director axis of the LC layer. The sample can be rotated around all axes (x, y and z). The setup on Figure 4.10 allows the observation of the self-diffraction of writing beams (Figure 4.11).

Figure 4.11 Self diffraction of the writing beams. The second order is visible on the right. The intensity of the zero-th order is suppressed for illustration purposes.

It is easier to monitor the optical intensity of the writing beams when operating with a uniform optical intensity profile. Many studies in this thesis have been performed using the setup on Figure 4.12.
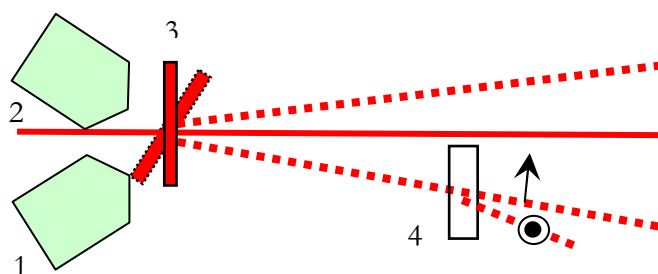
Figure 4.12 Pump-probe setup with expanded uniform beams. 1 – writing laser beams, 2 – reading laser beam, 3 – sample, 4 – Wollaston prism.

Expanded laser beams 1 form an interference pattern on a sample 3. When it is required to register diffraction of both vertically and horizontally polarised probe beams, the reading beam 2 polarisation is set to be 45° in respect to the LC director to obtain equal components in horizontal and vertical polarisation direction. The Wollaston prism 4 is used to spatially separate orthogonally polarised beams (see Figure 4.13), so that they can be registered simultaneously.
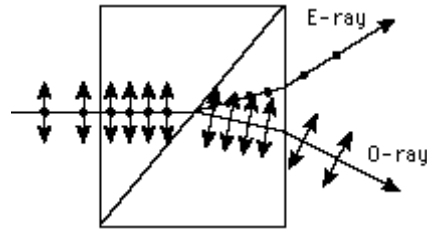
Figure 4.13. The separation of orthogonally polarised light by Wollaston prism.

For resolution studies, when the spacing of the fringes in the interference pattern has to be varied frequently from 2 μm to over 30 μm, it is very convenient to use a Michelson interferometer for creating the interference pattern.
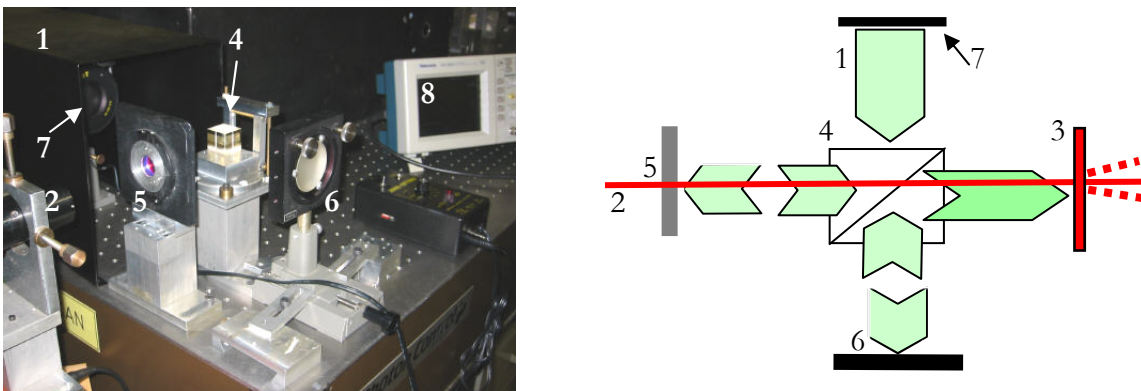

Figure 4.14 Michelson interferometer setup for resolution studies. _1_ – writing laser beams, _2_ – reading laser beam, _3_ – sample, _4_ – beamsplitter, _5_ – cold mirror, _6_ – mirror, _7_ – shutter, _8_ - oscilloscope.

The collimated expanded beam 1, controlled by the shutter 7, is divided into two beams of equal intensity at the beamsplitter 4. After reflecting from the mirrors 5 and 6, the beams are overlapped on the sample 3. The interference mirror 5 reflects short wavelengths and allows long ones to pass. The He-Ne laser beam 2 is passed through the interference mirror 5 and is diffracted from the sample when the pattern is written on it. The first diffracted order is registered by the photodiode and oscilloscope 8.

This arrangement uses space economically and allows quick changes of interference pattern spacing, but suffers from a high sensitivity to vibration, and the interference pattern has poor contrast[*], which leads to very low diffraction efficiency observed from the devices. Thus it is used only for relative studies on different devices.

---

[*] It was not possible to ensure equal writing beam intensity; the ratio of the beam intensities was 1:1.5.

The grating spacing in all experimental arrangements is controlled by the reading beam using the relation:

$$d \sin\varphi = m\lambda, \qquad \sin\varphi \approx \frac{l}{L}$$

4.12

where d is grating spacing; m - number of the diffracted order, $m=1$ is usually used; l - the distance from the zero-th order to the m-th order; L - the distance from the sample with recorded grating to the screen.

4.5 Summary and conclusions

The quality of liquid crystal cells and devices may be examined by polarised light microscopy. Impurities and defects may be observed under the microscope. Good planar alignment of liquid crystal must exhibit a strong contrast between dark and bright fields, as the sample is rotated between the crossed polarisers. The alignment of dichroic dyes in the liquid crystal hosts may be monitored by measuring the absorption of light polarised along and perpendicular to the alignment direction of the devices.

Studies of the electric response of devices to applied electric fields are important for understanding of ionic processes that occur in doped LC systems. Due to the complexity of dye and fullerene-doped liquid crystal systems, their electrochemistry is highly complicated and makes a vast research field out of the scope of this work. The most important, from the point of view of engineering properties, are addressed, such as resistivity, the Freedericksz transition threshold and photocharge generation.

Photogenerated currents may be measured dynamically for different optical powers with the precision of 10^{-11}A, photogenerated voltage may be measured as a function of time and illuminating power with the precision of 10^{-6}V.

For the studies of optical nonlinearities several complementary experimental arrangements have been used. Imaging setup is used to write images (potentially any image, not only grating) at normal incidence. It allows obtaining the doped LC material efficiency characteristics, which do not depend on the quality of the grating. The imaging setup cannot be used at high spatial frequencies (100 lp/mm and higher).

To create interference patterns, either unexpanded Gaussian or uniform expanded beams from Ar^+ ion laser are used. When operating with the etalon inside the laser cavity, the coherence length does not put limits on the difference in the beam paths and thus on the spatial frequency of the pattern which can be created. In the case of narrow beams, it is possible to observe self-diffraction of the writing beams. Optical intensity on the sample is hard to monitor when the beam profile is not uniform, so most of the studies, which research dependence on the optical power, have been performed with expanded beams. It is convenient to perform resolution studies using the Michelson interferometer setup. This setup may be used to compare different devices, but it is not suitable for absolute value diffraction efficiency studies.

CHAPTER 5

MECHANISMS OF OPTICAL NONLINEARITY

The aim of this chapter is to consider relevant mechanisms and processes that take place in the systems under investigation. The effects that are possible in our systems include thermal nonlinearities, induced optical torque, trans-cis isomerisation, space-charge field build-up and surface-induced nonlinearities. The low laser powers which we use would not trigger electronic nonlinear effects like Electrostriction (Brillouin scattering) and flow effects[8].

The mechanisms which occur in the three selected dopant systems[*] are studied. They are distinguished based on the temporal response characteristics, geometry in which the highest nonlinearity is observed, dependence on the host materials, external fields, photogenerated voltage and currents, absorption behaviour and surface interface.

5.1 Highly absorbing devices: temperature effects

One of the most obvious mechanisms leading to nonlinearity in highly absorbing Methyl Red and DC161 doped samples is thermal. Thermal effects do not require an external electric field. They would be expected to be larger in planar oriented LC layers doped with dichroic dyes, when the writing beam polarisation is parallel to the LETO of the dye, and the reading beam is polarised along the LC director.

This is exactly the geometry in which we observe strongest nonlinearity in DC161- and MR- doped devices with no external fields[†] (see Figure 6.2 in Chapter 6).

---

[*] For a detailed discussion of why these three systems have been chosen see Chapter 3.

[†] MR devices exhibit a more complex dependence on geometry when external fields are applied.

The discussed geometry will give the highest nonlinearity not only for thermal effects, but for all absorption-triggered orientational or order parameter related effects. Thus the geometry of the experiment gives some idea of what effects could be involved, but further studies must be undertaken to narrow down the possible range of phenomena leading to nonlinearity in each system.

The work below is aimed at giving a good understanding of the thermal processes that might be involved. The operating regime may then be chosen to either optimise device performance[*] or to minimise thermal influence, so that other sources of nonlinearity can be studied.

5.1.1 Time scale and dynamics

As described earlier in Chapter 2, the absorbed optical energy is transformed mainly into heat. Many parameters of the liquid crystal, including refractive indices, depend on the temperature. Hence, a spatial illumination profile will result in a spatial temperature profile, and in a refractive index profile. Another important factor is that the order parameter critically depends on the temperature near the phase transition, hence not only the refractive index, but also all the LC physical parameters will vary, including those that are related to any orientational nonlinearities.

There are two clear time scales for the thermal effects in liquid crystals. One, a very fast thermal grating formation, builds up in 30µs when using Q-switched pulsed radiation at λ=532nm and diffuses in less than 100µs[8]. We do not study fast temperature effects as they are not suitable for the applications that are considered here (due to very high optical power requirements of ~10W/cm^2).

When continuous radiation is used, some equilibrium temperature profile is reached through diffusion and heat conduction. The resulting thermal grating can lead to a large nonlinearity if the overall sample temperature is close to the phase transition. This critical thermal behaviour is connected to a general temperature rise in the sample and is very slow, 10s of seconds or even minutes.

The dynamic behaviour of the diffracted signal can be highly informative for understanding the processes taking place in the device. Here we look at the dynamics of

---

[*] For applications devices are usually required to operate in a wide temperature range (from +10 to at least +40 for the indoor devices), hence temperature control is highly undesirable.

nonlinearity at high optical powers, when the thermal effects should be more pronounced (Figure 5.1).

The two-beam interference setup described in Chapter 4, Figure 4.10, is used. Samples are normal to the reading beam, the polarisation direction of all the beams is chosen along the nematic director and the LETO direction of the dye. The host material with the lowest transition temperature is chosen (Appendix B). The writing wavelength is chosen in the region of maximum absorption of the given device, where the temperature effects should be most pronounced. DC161 doped devices are operated at λ=514nm, and MR doped samples at λ=488nm (see Figure 4.3 for absorption spectra of MR and DC161). The behaviour in DC161 and MR doped devices is very similar. The data collected from 10μm thick 1% (by weight) MR doped 5CB sample is presented below.
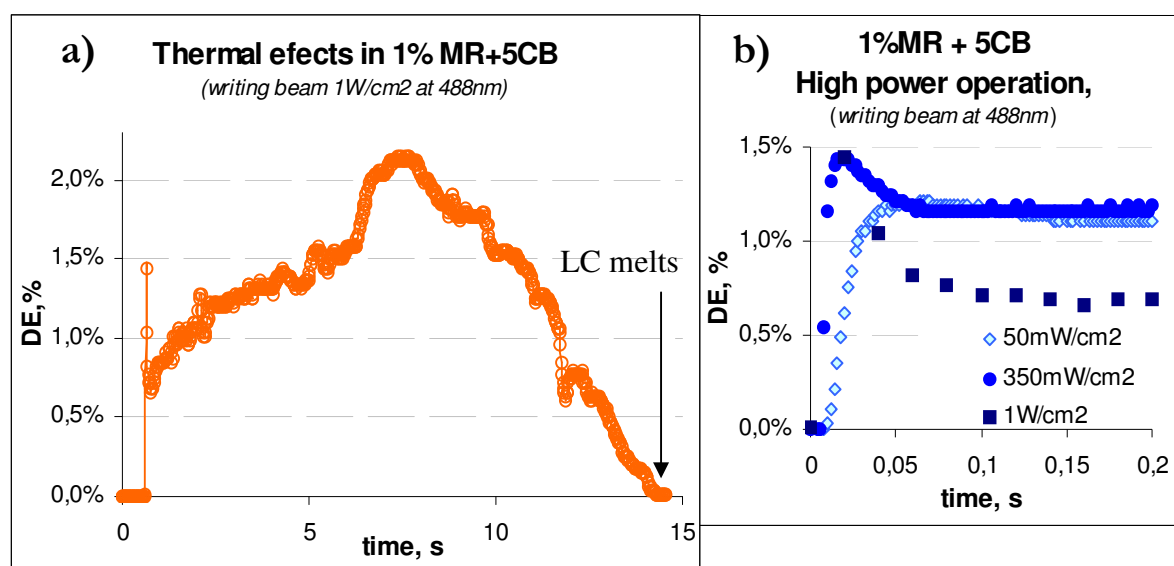
Figure 5.1 High power operation in absorbing devices, unexpanded beams[*].
Samples are normal to the reading beam, polarisation direction of all the beams is chosen along the nematic director and the LETO direction of the dye (arrangement as on Figure 4.10).
a) melting of the 10μm 1wt% MR doped 5CB film (absorptance over 90% at λ=488nm; melting temperature of 5CB 34°C)
b) operation of the film at a shorter time scale for different optical powers.

---

[*] Initial spike appears at high optical powers; the corresponding threshold power depends on the quality of the projected image or interference fringes and may be as low as 30mW/cm^2 (see Chapter 6).

The overshoot in the diffracted signal in Figure 5.1 is discussed in detail in Chapter 6 when describing the dynamics of the nonlinear effect. After the initial spike in the signal has disappeared, instead of reaching a steady value of diffraction, as it happens at lower optical powers[*], the signal grows steadily due to the overall sample temperature rise and associated rise in the $dn_{\parallel}/dT$. As the temperature in the illuminated regions reaches the melting point, the energy is used to melt LC in the illuminated areas. During this process the temperature in the illuminated regions does not change, while "dark" regions are continuously heated due to diffusion and conductivity. This results in the decrease of the diffracted signal, which reaches zero as the film melts completely. The whole process takes 14 seconds at $1W/cm^2$ and is repeatable.

5.1.2 Overall temperature rise and stationary state

When the writing optical power is low, so that the phase transition temperature is not reached in the LC layer, a stationary state will be established. The overall temperature rise can be calculated and measured, as discussed below.

For the case when two unexpanded Gaussian beams overlap on the sample, the general temperature rise at steady state in the sample may be evaluated using the equation derived by Jánossy and Kosa[56] (equation 2.45, Chapter 2). The maximum temperature rise in a 10µm 1% (by weight) DC161 sample (absorptance 91.5%) at light intensity $50mW/cm^2$, is calculated to be **5.1^o**. At ambient temperature 22^oC, it is about **6.9^o** away from the isotropic transition temperature in 5CB. In E7 and BLO48 doped samples the calculated temperature rise is respectively about 33° and 72° away from the transition to isotropic state (see also Appendix B), hence any critical behaviour cannot be expected, and thermal effects may be assumed to be negligible.

In the case of the illumination profile formed by two interfering expanded beams, used in many experiments, the steady state temperature inside the device may be calculated by solving the heat conduction differential equation 2.46 (see Chapter 2). To set appropriate boundary conditions, the temperature at the sample surface ($T_{z=d}$) must be defined.

The surface temperature can be experimentally measured using a thermocouple. A heat sink compound 340 from Dow Corning is used to improve thermal contact between the

---

[*] See for example Figure 5.12 below.

glass surface and the thermocouple. The samples are illuminated until the saturation value of the temperature is reached.
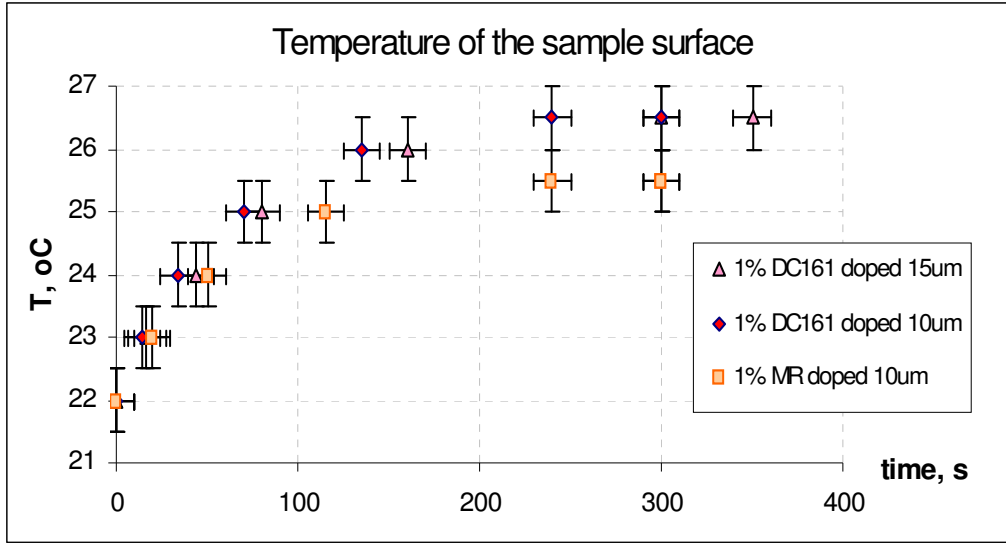

Figure 5.2. The measured temperature of the device surface upon illumination. Optical power I=50mW/cm^2. The planar devices with the highest absorptance are chosen. Light is polarised along the nematic director and LETO direction of the dye. The geometry of the interacting beam and nematic director is the same as in the previous experiment.

As can be seen from Figure 5.2, the time, required for the temperature rise, is tens of seconds. The stationary value is reached within 5 minutes for all devices. Thus it is expected that the purely thermally induced nonlinearity would reach the saturation value accordingly, i.e. in 5 minutes. We have already shown, that at high optical powers the enhancement of nonlinearity is indeed observed on a large time scale, tens of seconds (Figure 5.1).

A simple estimation of a temperature rise within the sample can be done using Equation 2.49 (Chapter 2). Under an incident light of intensity 50mW/cm^2 and wavelength λ=514nm, the averaged temperature of a LC layer $T_{z=0}$ yields the results shown on Table 5.1 below.

Absorptance is derived from the transmission (*T*) spectrum of the devices ($A_\% = 100\% - T_\%$), which is obtained following the procedure described in Chapter 4. The reflection, scattering and absorption in glass and ITO layers are accounted for by

referencing the measured transmission with the transmission of an undoped otherwise identical sample.

Device, doped 5CB (T_{NI}=34°C)	Absorptance %	$\Delta=T_{z=0}-T_{z=d}$ (calculated)	$T_{z=d}$ (measured)	$T_{z=0}$ (resulting)	$T_{NI}-T$ (resulting)
15μm 1% DC161[*]	98.4%	3.1	26.5±0.5	**29.6**±0.5	*4.4±0.5*
10μm 1% DC161[*]	91.5%	2.9	26.5±0.5	**29.4**±0.5	*4.6±0.5*
10μm 1% MR[*]	82.6%	2.6	25.5±0.5	**28.1**±0.5	*5.9±0.5*

Table 5.1. Temperature rise in dye-doped planar aligned devices for the case of uniform illumination with expanded beams. The devices with the highest absorptance are chosen. Light is polarised along the nematic director and LETO direction of the dye.

In this way, the overall temperature rise for the cases of expanded and unexpanded beams does not differ substantially (it is calculated to be slightly higher in case of expanded beams), and thus both setups should exhibit a similar effect given it has a thermal origin.

5.1.3 Temperature profile

To obtain the full picture of the temperature profile, a simulation using the software computational system MatLab has been performed. Details of the calculations, assumed model and the program script can be found in Appendix E.

Two expanded beams form a sinusoidal optical grating with 20μm spacing; optical power is 50mW/cm^2. The 10μm thick 5CB device doped with 1% DC161 by weight is modelled. Absorption and resulting temperature profile are carefully accounted for (Figure 5.3). The difference in heat conductivity of the glass and of the liquid crystal is also considered.

The calculation is done for the steady state. The initial temperature conditions are satisfying the steady state solution of the one-dimensional equation (2.48) and experimentally measured boundary conditions.

The calculated temperature profile in and around the LC layer is shown in Figure 5.4, and in more detail on a colour map in Figure 5.5.
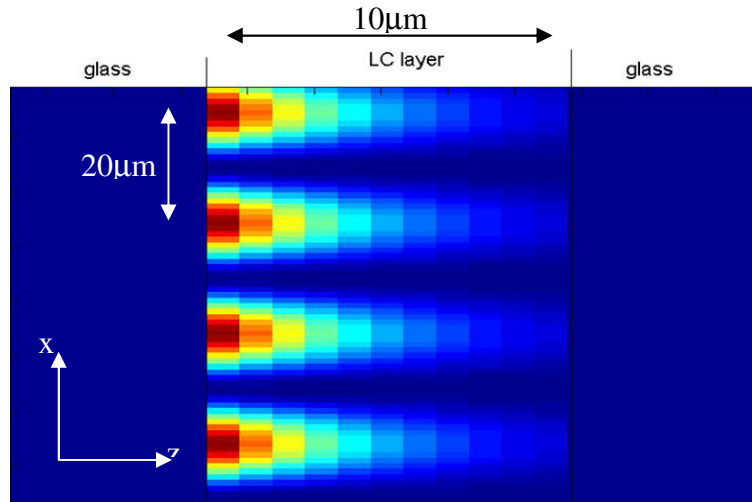
---

[*] percentage by weight

Figure 5.3. Absorbed optical energy profile in the device. The interference pattern with fringe spacing of 20μm (modulation in x direction) is projected on highly absorbing device. The decrease of the optical power as the beam is absorbed in the doped LC layer is accounted for (modulation in z direction). Note the difference in the scales of x and z axes on the figure (used here for illustration purposes only).
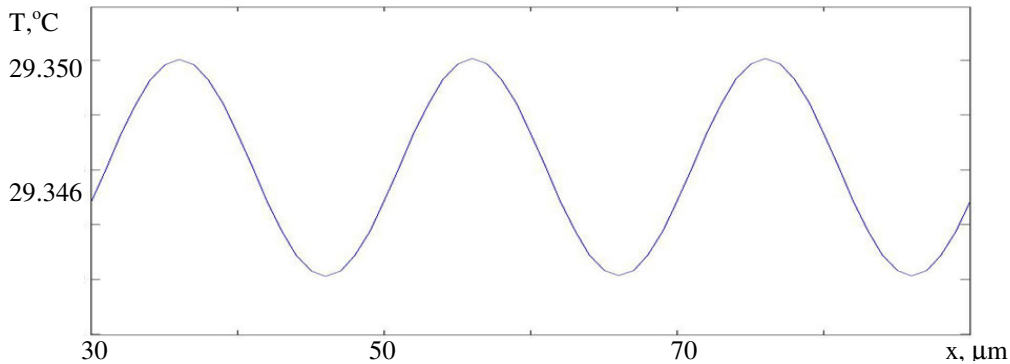

Figure 5.4 The calculated temperature profile in the LC layer[*], 20μm fringe spacing, 50mW/cm^2 illumination intensity.

The maximum temperature in the illuminated areas reaches 29.35°C, and the lowest in the dark regions 29.34°C, yielding a temperature difference of less than 0.01°C. The diffraction efficiency of such thermal grating, probed with an extraordinarily polarised laser beam at λ=633nm, is calculated from the refractive index temperature dependence for 5CB crystal at corresponding temperature. At 27°C dn_e/dT=3.8·10^{-3} for 5CB liquid crystal [8], and the corresponding diffraction efficiency is be less than 3·10^{-4}%.

---

[*] During calculation the LC layer is divided into sub-layers. The temperature profile is taken in the sub-layer with highest temperature modulation (see also Figure 5.5).
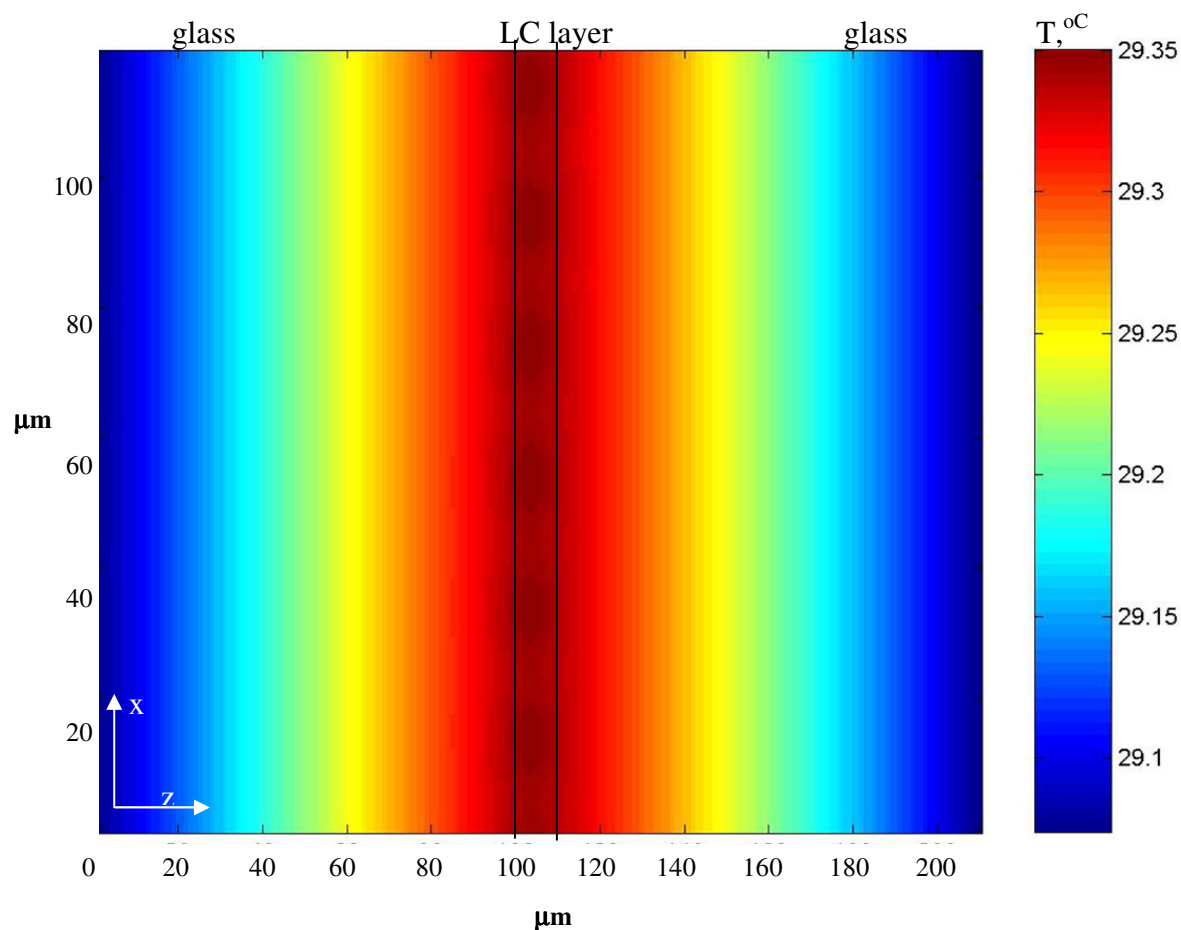
Figure 5.5 The calculated temperature profile in the device - the colour map[*]. Fringe spacing 20μm, film thickness 10μm, absorptance 91.5%; illumination intensity 50mW/cm^{2}.

In reality, the temperature difference between the bright and dark regions may be even smaller, as only heat conductivity mechanism is considered, but diffusion of the molecules, which may be large on the micron scale, is not accounted for. Also, in practice the contrast between bright and dark fringes is not perfect.

The calculation for high optical power (1W/cm^{2}) gives DE=0.66% at a temperature 1 degree away from the transition to the isotropic state. The higher efficiency observed near the phase transition (Figure 5.1) can be explained by the fact that mechanisms other than thermal are involved[†].

---

[*] The hottest points on the colour map are shifted slightly towards the side, from which the light beams come in, because more energy is absorbed at the front part of a liquid crystal layer.

[†] Not only $dn_{\parallel}/dT$ exhibit critical behaviour near the transition temperature, but the order parameter and all physical parameters associated with it.

5.1.4 Choosing an operating regime

Absorption associated temperature rise, as has been experimentally observed (Figure 5.1, Figure 5.2), is usually slow. If powers under 50mW/cm^2 and **short pulses** are used, the temperature rise and associated effects could be considered insignificant.

To verify the flexibility of use of the ambient temperature range, the studies at $T_{ambient1} = 22^{o}C$ and $T_{ambient2} = 27^{o}C$ (temperature in the room) have been performed.

The setup with expanded beams interfering on a sample, described in Chapter 4 (Figure 4.12), has been used, as the temperature rise in this geometry is slightly larger, as has been shown above. The planar sample with high absorptance[*] (95.2%), thickness of 10μm and 5CB host material has been chosen. All beams have been polarised along the director. The total optical power in both beams has been 34mW/cm^2 and the pulse length has been set to 1s. Both of these parameters are typical for the majority of the experiments in this work.

At the power 34mW/cm^2 the sample at steady state may be heated (assuming continuous irradiation) to 5.6^{o}C below the transition temperature from $T_{ambient1}$ and to 0.55^{o}C below the transition temperature from $T_{ambient2}$. From ref. , page 52, $dn/dT|_{TNI-T=5.6^{o}C}$ = 3.8·10^{-3} and $dn/dT|_{TNI-T=0.5^{o}C}$ = 9.8·10^{-3} for 5CB liquid crystal. The calculated ratio between the diffraction efficiencies $DE_{Tambient1}$ and $DE_{Tambient2}$ for the 10μm 5CB sample is presented on the figure below (**dT** is the amplitude of the induced temperature profile).

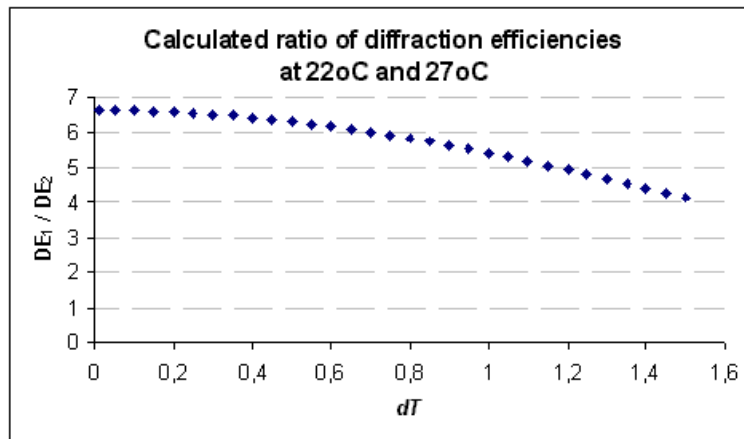**Figure 5.6 The calculated ratio of diffraction efficiencies in the 10μm doped 5CB sample for the two ambient temperatures $T_{ambient1}$ = 22°C and $T_{ambient2}$ = 27°C.** dT **is the amplitude of the induced temperature profile.**

---

[*] This value of absorptance is the highest among 9 and 10μm devices.

When the discussed steady temperature state is reached, the difference between the diffraction efficiency at the two ambient temperatures should be noticeable (Figure 5.6).

If the illuminating pulses are relatively short, the steady state is not reached. As can be seen from Figure 5.7, there is almost no difference in the resulting diffraction from the sample at different ambient temperatures. The measurements have been taken ensuring that all other parameters (optical intensity, contrast, grating spacing etc.) are not changed.
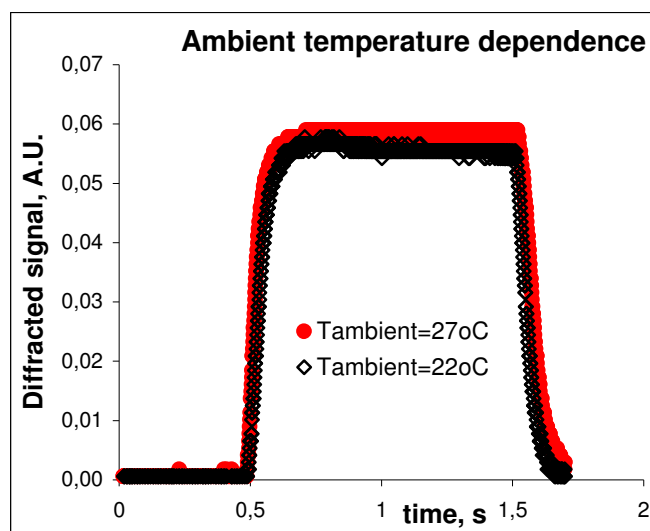
Figure 5.7 Operating at optical power 34mW/cm², short pulses, various ambient temperatures. The sample is 9μm thick 1%DC161 doped 5CB with absorptance 95.2% at λ=514nm.

Thus, there is no need for careful temperature control when studying or operating devices with comparable absorption (i.e. all the devices studied in this work), if relatively short pulses (under 1-2 seconds) are used.

In further experimental work the ambient temperature is 22-23°C.

5.2 Optical Freedericksz transition

Light induced Freedericksz transition has been reported[37] to have a threshold intensity of 155W/cm² in 5CB films. This is more than 3 orders of magnitude larger, than used in experiments in this work. Indeed, no optical nonlinearity has been observed in the undoped nematic samples in the setups used.

Moreover, at normal incidence in homeotropic nematic films possessing positive dielectric anisotropy, as is in the case with all the studied host materials (see Appendix B for host parameters), the optical Freedericksz transition does not occur (see also Chapter 2).

Therefore, it is possible to exclude the optical Freedericksz transition from the effects occurring in the studied devices.

5.3 Dopant-enhanced induced optical torque

Induced dopant-assisted optical torque, also known as the Jánossy effect (see Chapter 2), is mainly found in anthraquinone dye-doped systems. This effect has never been observed in MR or C_{60} doped LC systems despite a large number of studies by different groups. Therefore it is assumed that the Jánossy effect is not present in MR and C_{60} doped devices. On the other hand, we cannot exclude this possibility in DC161, as it is an anthraquinone dye. If the Jánossy effect were involved, a strong dependence on the host material would be expected[59]. To study the possibility of the enhancement of the optical torque as a source of nonlinearity in DC161 doped systems, devices based on 3 different host materials (see Appendix B for structural formulae), 5CB, E7 and BLO48 from Merck, were built, and their efficiency examined. See Chapter 6 for the details of the measurements and device performance.

A major ageing effect has been found in DC161 doped devices. It has been observed, that DC161 devices dramatically improve with age. The ageing effect will be discussed in more detail in Chapter 6.

We found no significant difference between the performances of freshly doped E7 and BLO48[*] (see Chapter 6). As the birefringence of BLO48 is higher than in other host materials used, it should produce the largest effect. Nevertheless, the performance of BLO48 based devices until now has been significantly lower than in 5CB based devices, and slightly lower than in E7.

As devices with different host materials have been manufactured at different times, no unambiguous conclusion about the presence of Jánossy effect in DC161 doped systems can be made.

---

[*] BLO48 doped devices have been manufactured 7 days later than E7 doped devices.

5.4 Nonlinearity due to Trans-Cis photochemical isomerism

Methyl Red is an azo dye. DC161 dye is an anthraquinone derivative possessing two azo groups. The presence of azo groups in these dopants and their symmetry suggest the possibility of trans-cis isomerisation. The geometrical change of shape of the dopant molecules upon isomerisation could be a source of nonlinearity in doped LCs.

Unlike MR and DC161, C_{60} cannot undergo trans-cis isomerisation (from symmetry and structure considerations). Thus, photoisomerisation cannot be the source of nonlinearity in C_{60} doped systems.

It is well known that MR exhibits Trans-Cis isomerism when illuminated by blue and green light, producing a nonlinear effect[89,90]. In general, DC161 may also undergo photochemical isomerisation when excited with green and blue light. Here we will first examine the compatibility of the observed nonlinearity with the trans-cis isomerisation mechanism.

The time scale of trans-cis transition is very fast[65], and the "on" response of the system will be influenced mainly by the LC dynamics. No external field is required; to the contrary, an external field above the Freedericksz transition may quench the reorientation of molecules in LC phase. As for geometry, the strongest effect should be observed – in the same way as in the case with temperature effects - in planar oriented samples for optical writing and beams co-polarised with dye LETO and LC director respectively[*]. Maximum absorption is achieved in this case as well as the most effective modulation.

The observed nonlinearity in MR[†] and DC161 doped systems is in agreement with this time scale and geometry. The application of voltage above the Freedericksz threshold quenches the nonlinear effect completely in DC161 doped devices (while in MR devices it leads to the appearance of ionic effects, and as a result, nonlinearity is not quenched, but even enhanced).

Trans-cis transition is generally accompanied by a change in absorption (trans and cis forms usually have different absorption spectra in polarised light).

---

[*] LETO of both dyes is parallel to the liquid crystal director

[†] MR exhibits behaviour that is more complicated. One of the possible regimes of operating these devices is in the discussed geometry.

The measurements of absorption change are hampered[*] by possible reorientation of dye molecules together with host material molecules upon illumination with light (when the orientational nonlinearity due to trans-cis isomerisation occurs).

The change of absorption in DC161 doped samples is indeed observed upon illumination (Table 5.2).

Geometry, nematic director $\uparrow n$		Light transmitted through the device, Impinging probe intensity I_o=0.178mW	
E_{pump}	E_{probe}	I_{pump}=0	I_{pump}=75mW/cm^2
$\uparrow$	$\uparrow$	0.018±0.004 mW	0.036±0.004 mW
$\rightarrow$	$\rightarrow$	0.128±0.004 mW	0.124±0.004 mW
$\rightarrow$	$\uparrow$	0.128±0.004 mW	0.132±0.004 mW
$\uparrow$	$\rightarrow$	0.018±0.004 mW	0.030±0.004 mW

Table 5.2. Transmission in planar DC161 doped devices without external electric fields applied. The observed change in transmission may be due to trans-cis isomerisation of the dye as well as due to the re-orientation of host and dye molecules.

In the case where the reorientation of the LC is fixed by the applied voltage (homeotropic sample, 45° incidence, as in[67]), the absorption change is very weak. Insufficient laser stability does not allow for an accurate measurement of the absorption change in this case, and also in the case of a small change of MR doped devices.

To summarise, trans-cis isomerisation is a possible mechanism of nonlinearity in MR and DC161 doped devices.

Now let us concentrate on the isomerisation of the DC161 dye molecule.

---

[*] A more precise measurement is possible when the motion of the host molecules is restricted by applied voltage. This is achievable in the case of homeotropic sample with ITO electrodes, in a planar device with lateral electrodes, or in a planar device with ITO electrodes and a host material with negative dielectric anisotropy.

5.4.1 Trans-cis isomerism in DC161

Dc161 dye has some unique features that distinguish it from other dyes that are used to enhance photorefractivity in LC. The molecule is an anthraquinone derivative possessing two azo groups (Figure 5.8). Being an anthraquinone dye it has a high order parameter when dissolved in liquid crystals S_{dye}=0.56 confirmed by dichroic measurements (see Chapter 4). The presence of azo group suggests that there are trans- and cis- isomers. With two groups and given symmetry, one can deduce the possible molecule conformations. We call them Trans, TransCis and CisCis.

The chemical molecular modelling software ChemOffice from Cambridge Soft Corporation[91] including packages for drawing ChemDrawUltra 6.0 and a modelling package Chem3D 5.0 has been used to model stable conformations of the DC161 molecule. The modelling software allows the calculation of the steric energy of the conformation as well as the minimisation of the energy (using semi-empirical methods) of the system based on the mathematical apparatus of mm2 packet[91]. The calculation is done for molecules in gas phase at absolute zero.

5.4.1.1 Trans and Cis conformations

The minimum steric energy corresponds to the trans- configuration. The molecule in this state is planar which agrees with the reported geometry for the anthraquinone molecule[63] and other anthraquinone and azo compounds[92,93,94], including the azo dye Methyl red[90] in their minimum energy configuration.

There are two similar conformational structures (Figure 5.8) both having total steric energy of 38.0 kcal/mole. There is only a slight difference in molecular shape between them: the overall length of the molecules differs by 0.61Å, width differs by 2.53Å due to the difference in the angle between the anthraquinone core and the groups in 2 and 5 position (144° and 152.8°). In general there are no obvious selection rules that would give preference to either of the conformations, so they may both be present in solution. In a LC phase when there is a degree of disorder, introduced by rotations and vibrations, as compared to the crystalline phase, this difference in structure is negligibly small. We will therefore assume there is only one ground state conformation that leads to forming of TransCis and CisCis forms upon excitation.

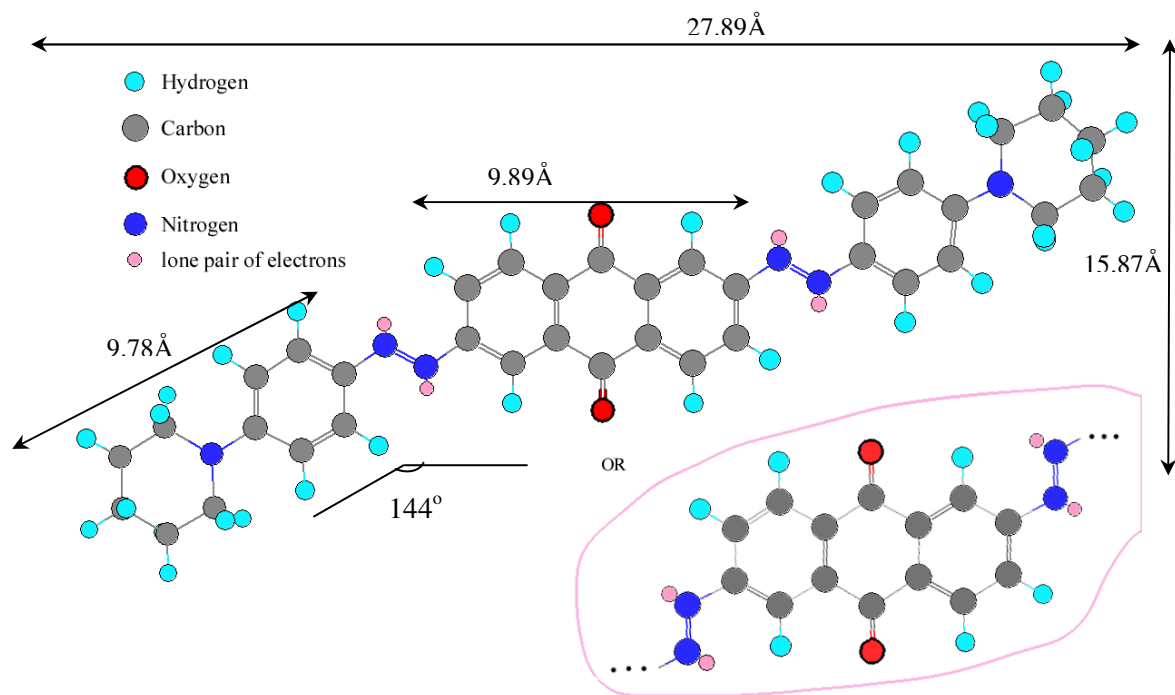The steric energy of the Trans configuration is considered the lowest energy level E_0.

Figure 5.8 Structural formula of a Trans configuration of DC161 molecule. Inset shows the second possible conformation. Both conformers are planar.

The second energetically possible configuration is TransCis. In this configuration only one of the two azo groups undergoes trans-cis isomerisation (as in Figure 2.11, Chapter 2). The planar geometry is no longer favourable (Figure 5.9). This is similar to the shape of cis-MR molecule[90].

The part of the molecule after the N=N double bond bends approximately 15 degrees out of plane and 72 degrees in plane of the anthraquinone core. These values are important in understanding the geometry of a possible orientation change of the LC influenced by the configurational change in the dye. They suggest that reorientation of surrounding host molecules, triggered by such transition in the dopant, will be in two planes (in the plane of the sample and out of the plane.) Such reorientation is indeed observed in DC161 doped devices and will be described in more detail in the next section.
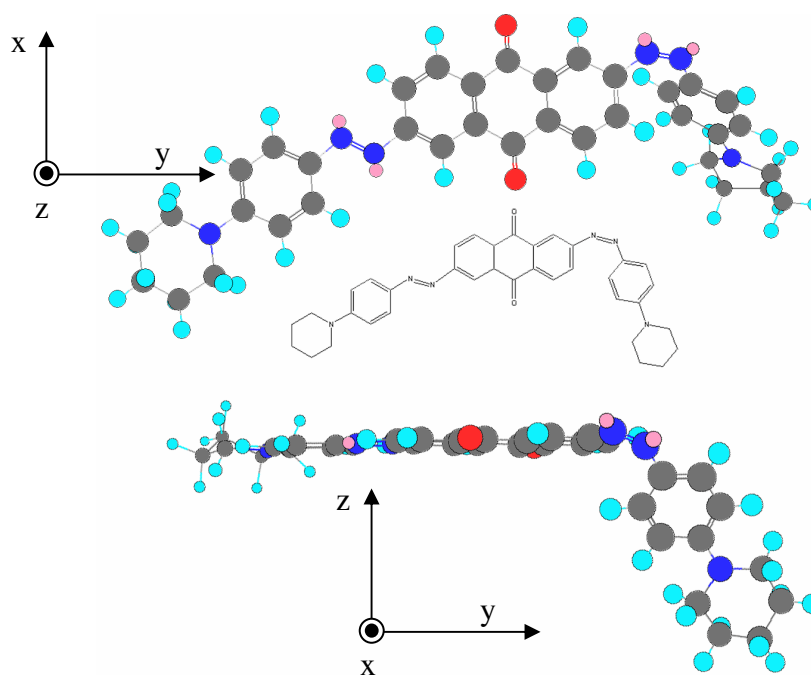
Figure 5.9. TransCis configuration of DC161: the structure is no longer planar.
a) xy plane projection
b) structural formulae
c) xz plane projection.

The next local energy minimum corresponds to the conformations CisCis boat with about 13° bend out of plane of the molecule and 73° - 76° in-plane bend; and CisCis zigzag with 25° out of plane deviation and 73° - 76° in-plane bend (Figure 5.10).
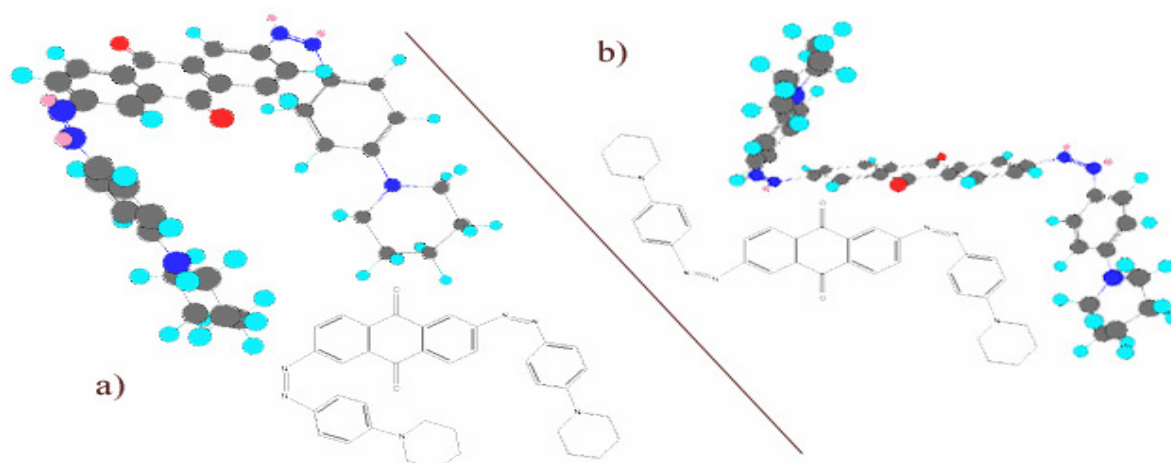

Figure 5.10. CisCis conformers of DC161 molecule.
a) boat conformational structure; b) zigzag conformational structure

5.4.1.2 Isomers: energy considerations

Using the Chem3D package it has been calculated, that the total steric energy with respect to trans form for TransCis, CisCis boat and CisCis zigzag conformations is 12.4, 24 and 24.3 kcal/mole respectively. To undergo the transition, certain potential barriers have to be overcome.

Let us estimate the approximate value of the respective barriers between Trans, TransCis and CisCis configurations. The transition is introduced in excited state in which the bond between two nitrogens becomes single and allows free rotation. The rotation is split into small steps, and the steric energy related to each configuration is calculated. As configuration changes from the equilibrium, the associated energy is increased. In the vicinity of the highest energy barrier point the minimum value of step (1°) is used for higher precision in defining the barrier.

Following this procedure, the steric energy barriers have been estimated to be of the order of 30kcal/mole for transition from trans to TransCis and about 40kcal/mole for transition from TransCis to both CisCis states.

The energy associated with one molecule in electron volt is:

$$E[eV] = \frac{1}{N_A} \frac{E[kcal]}{3.8 \cdot 10^{-23}}$$

5.1

where N_A is the Avogadro number, and $3.8 \cdot 10^{-23}$ is the corresponding unit transformation coefficient.

Using transformation 5.1 the values of the energy barriers for transitions from Trans to TransCis and from TransCis to CisCis can be calculated to be 1.3 and 1.73 eV. The energy needed to undergo transition directly from Trans to CisCis is hence 3.03eV.

Maximum light absorption of the molecule lies in the region of 530nm (corresponds to the 2.35eV gap between the ground and excited states of the molecule). The lowest energy level in the excited state, also known as the lowest vibrational level[*], corresponds to about 590nm (2.1eV). We excite the molecule using λ=514nm or λ=488nm.

---

[*] Each molecule has electronic, vibrational and rotational energy, the last being the smallest. Each electronic energy level of the molecule can be divided into sub-levels corresponding to different vibrational energy. The level with the lowest vibrational energy represents the bottom of the energy zone, which is used to calculate the bandgap. It corresponds to the red edge of absorption.

This gives energy of 2.41eV and 2.55eV per each photon absorbed and is enough to allow for the configurational transition from Trans to TransCis state[*]. This is in agreement with the fact, that trans to cis transitions in azo dyes are usually triggered by the light in the ultraviolet and visible range[64] (corresponds to photon energies 2 - 3.5eV).

Such a transition would lead to a change of optical absorption in the dye molecules as well as the change in the geometrical order of the surrounding host molecules and to a change in the order parameter in the illuminated areas, and thus to the refractive index change.

Geometrical reorientation of the liquid crystal resulting from the Trans-Cis transition or Jánossy effect can be studied by monitoring the refractive indices of the sample. The study of such reorientation in DC161 doped devices is performed and discussed in the following section.

5.4.2 Geometrical reorientation in DC161 doped systems

As has been shown above, the absorption of a photon may lead to the change in the conformation of the dopant molecule. This change of shape would lead to reorientation of surrounding host material molecules.

Here a model is suggested where the change of refractive index in DC161 doped systems is induced by reorientation of small (smaller than λ) clusters of LC that surround dye molecules[†]. Such a reorientation may have various spatial characteristics, namely it can appear macroscopically as an isotropic decrease of the order parameter (equal for vertical and horizontal probe) in the illuminated region (order-disorder transition) or more complicated dependence (anisotropic change of order parameter or reorientation). This reorientation is studied experimentally.

The setup described in Chapter 4 in Figure 4.12 is used. The writing light polarisation is parallel to director axis (Figure 5.11). The diffracted signal is monitored by

---

[*] The optical intensities used ($< 1W/cm^2$) lead to a low probability of two-photon absorption or absorption of two photons during the lifetime of the TransCis state and therefore to a low probability of transition to the CisCis state.

[†] When 1% by weight of dye is put into the LC host, is equal to about 1:234 molecules ratio for DC161 and 1:108 for MR. This means that, given that the dye is evenly distributed inside the host material, each dye molecule is virtually surrounded by about 5-7 layers of LC molecules. As molecular size is sub-nanometre, the resulting clusters are smaller than the optical wavelengths used.

both vertical and horizontal polarisations of the reading beam. The presence of diffraction in general indicates that there is a difference in refractive indices of the illuminated and non-illuminated regions of the sample.
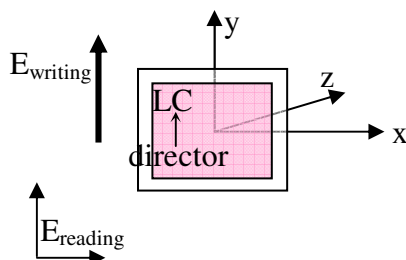

Figure 5.11. Geometry of the experiment. Writing beams are polarised along the nematic director; reading beam polarisation consists of vertical and horizontal components. No external electric fields are applied.

The diffraction efficiency of a 9μm 1%DC161 doped 5CB device is monitored for vertical and horizontal reading beam polarisations as a function of writing beam intensity. The nonlinear effect saturates at a writing beam intensity of about 30mW/cm^2.

Diffraction build-up and relaxation dynamics are indicative of time scales of the mechanisms responsible for the orientational change in a particular direction. Figure 5.12 shows a typical dynamic behaviour of the diffracted signal for both reading beam polarisations. Build-up and relaxation times are almost identical in both cases, which leads to the conclusion that the change of ordinary and extraordinary refractive indices is triggered by the effects on the same time scale or one effect only. This supports the suggested trans-cis transition as an underlying mechanism for observed nonlinearity.
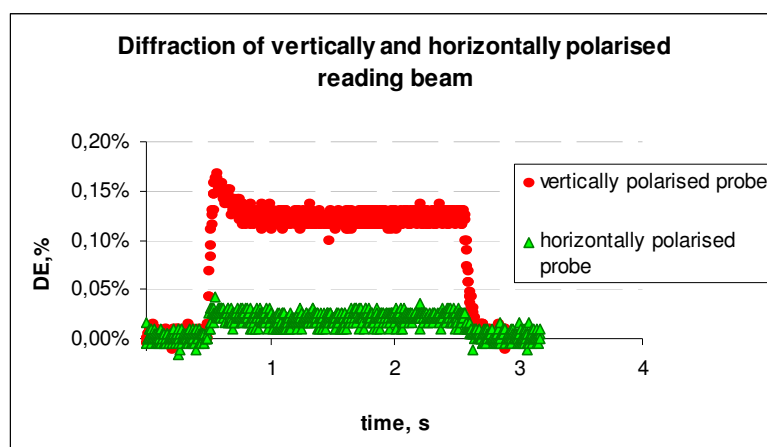

Figure 5.12. Typical dynamic behaviour of diffracted signal for both polarisations of the reading beam[*] in 9μm 1% DC161 doped sample; writing beams 50mW/cm^2.

---

[*] An overshoot at high light powers is treated in more detail in Chapter 6, where we attribute it to the imperfect contrast between bright and dark fringes.
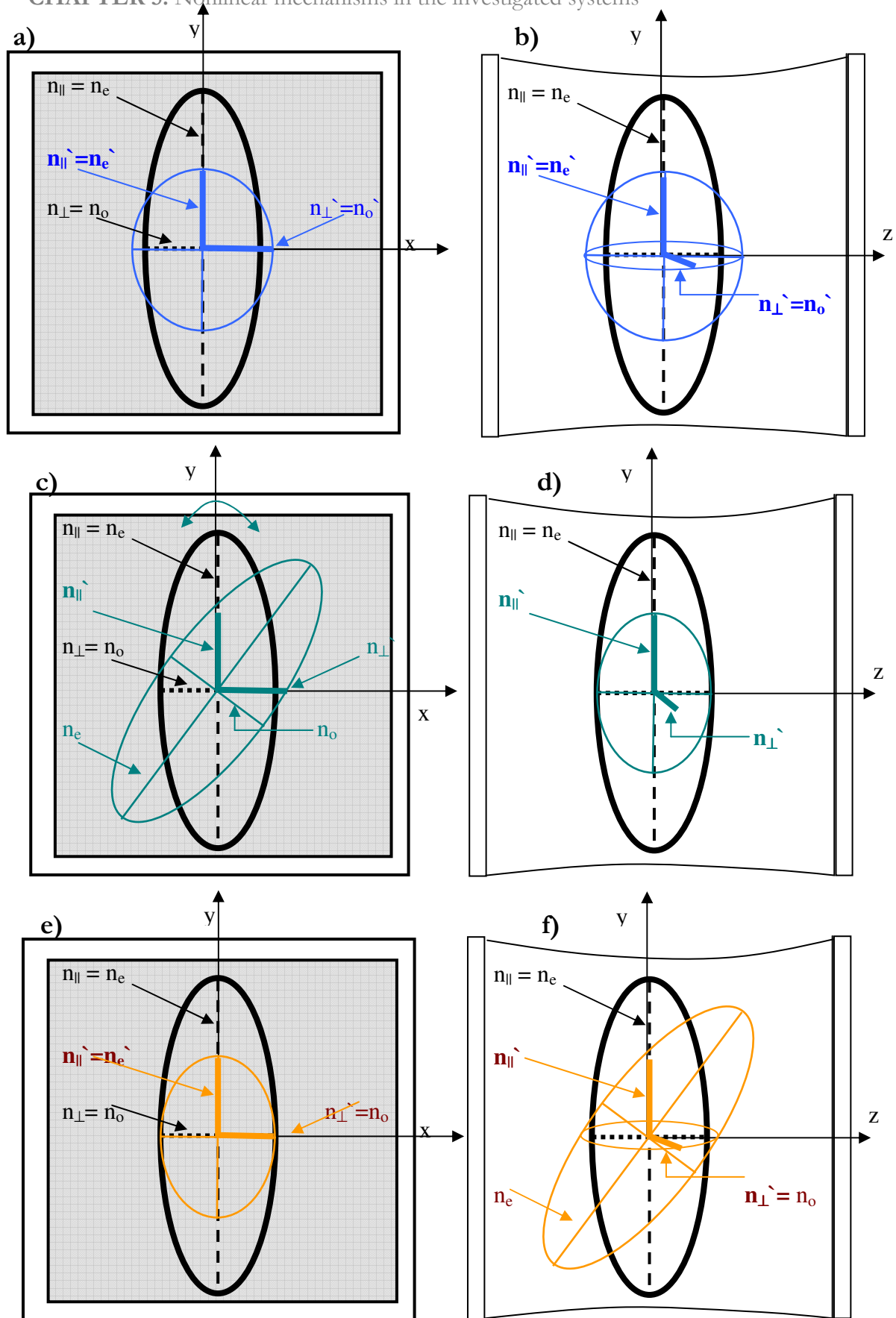
a)

$n_{\parallel} = n_e$

$\mathbf{n_{\parallel}`=n_e`}$

$n_{\perp}= n_o$

$\mathbf{n_{\perp}`=n_o`}$

y

x

b)

$n_{\parallel} = n_e$

$\mathbf{n_{\parallel}`=n_e`}$

$\mathbf{n_{\perp}`=n_o`}$

y

z

c)

$n_{\parallel} = n_e$

$\mathbf{n_{\parallel}`}$

$n_{\perp}= n_o$

$n_{\perp}`$

n_e

n_o

y

x

d)

$n_{\parallel} = n_e$

$\mathbf{n_{\parallel}`}$

$\mathbf{n_{\perp}`}$

y

z

e)

$n_{\parallel} = n_e$

$\mathbf{n_{\parallel}`=n_e`}$

$n_{\perp}= n_o$

$n_{\perp}`=n_o$

y

x

f)

$n_{\parallel} = n_e$

$\mathbf{n_{\parallel}`}$

n_e

$\mathbf{n_{\perp}`= n_o}$

y

z

Figure 5.13 Optical indicatrix: *a), b)* order parameter change; *c), d)* reorientation in *xy* plane; *e), f)* reorientation in *yz* plane.

Diffraction is registered for both: the vertically and the horizontally polarised probe (circles and triangles respectively in Figure 5.12). This indicates that there is a general change of the optical indicatrix, being either the change of the shape (Figure 5.13a, b), reorientation (Figure 5.13c-f) or both simultaneously.

The question whether we are dealing with a change of shape of the indicatrix or its reorientation basically is a question whether the nonlinear effect leads to the isotropic disorder on the macroscopic scale, or is due to the enhanced optical torque.

The change in the refractive index seen by the horizontally polarised probe from symmetry considerations cannot be induced by reorientation of the optical indicatrix (Figure 5.13c and d) when the pump beam is parallel to director axis. There is no preferred direction of rotation around z axis. Only the change of order parameter can be responsible for the observed effect in the horizontal direction, and $n_\perp$ is identical with n_o (Figure 5.13a, b).

On the other hand, the change in $n_\parallel$ in the illuminated areas can be due to the change in order parameter alone (then $n_\parallel$ will be identical to n_e) or influenced by reorientation (Figure 5.13). To separate these two cases, we study the order parameter in our system.

The diffraction efficiency is connected with the refractive index change by the following formula (see also Chapter 2, Equation 2.26):

$$DE = \left(J_1(\Delta\varphi)\right)^2; \quad \Delta\varphi = \frac{2\pi d\left(n_{dark} - n_{illu\,min}\right)}{\lambda}.$$

5.1

Where J_1 is the first order Bessel function, d is the LC layer thickness, n_{dark} and $n_{illumin}$ are refractive indices seen by the probe beam in dark and illuminated areas.

The connection between the refractive index and the macroscopic order parameter can be described using the de Jeu and Bordewijk model[8] :

$$\varepsilon_\parallel = n_e^2 = 1 + \left(\frac{N}{3\varepsilon_0}\right)\left[\alpha_l k_l(2S+1) + \alpha_t k_t(2-2S)\right]$$

$$\varepsilon_\perp = n_o^2 = 1 + \left(\frac{N}{3\varepsilon_0}\right)\left[\alpha_l k_l(1-S) + \alpha_t k_t(2+S)\right]$$

5.2

Differentiating (5), one can obtain:

$$d\varepsilon_{\parallel} = n_e dn_e = AdS$$

$$A = \frac{N}{3\varepsilon_0}(\alpha_l k_l - \alpha_t k_t)$$

$$d\varepsilon_{\perp} = n_o dn_o = -\frac{1}{2}AdS$$

5.3

The negative sign in the equation for the $d\varepsilon_{\perp}$ indicates the direction of the change. From 5.3:

$$dn_e = 2\frac{n_o}{n_e}dn_o$$

5.4

If the dependence between experimental values of dn_e and dn_o obey the equation 5.4, we can conclude that the observed effect is due to the change of the order parameter only (not of the thermal origin, as discussed in the previous sections). Otherwise reorientation is involved.

Figure 5.14 shows the calculated refractive index change (following equation 5.1) using the experimentally obtained diffraction data from the horizontally and vertically polarised reading beams.
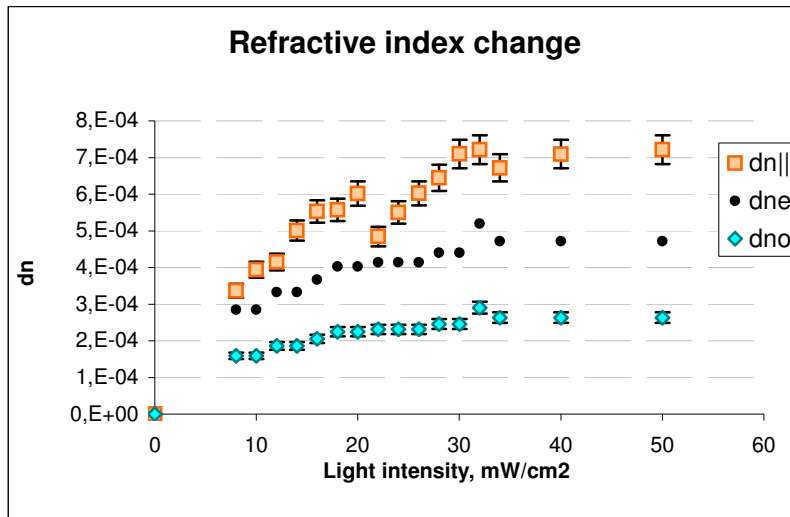
Figure 5.14. Refractive index change as a function of illuminating light intensity, for vertically and horizontally polarised probe in 9μm 1wt% DC161 doped 5CB film.

The experimental value of the refractive index change (called $dn_{\parallel}$) for the vertical probe (squares) does not coincide with the dn_e expected (equation 5.4) from change of the order parameter (small black circles). Values for dn_e and $dn_{\parallel}$ are similar at lower excitation

intensities, but with increasing writing light intensity diverge and have a difference of more than 1.5 times at saturation. Therefore, there is anisotropy in the refractive index change.

To summarise, in the studied system the superimposed order-disorder and reorientation mechanisms are present. Samples in the tilted geometry have been studied to investigate the direction of such reorientation (Figure 5.15).
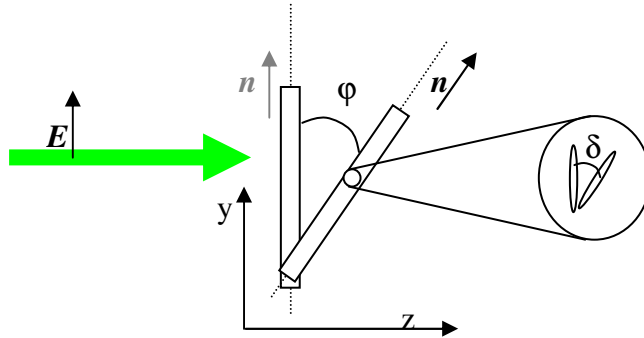

Figure 5.15 Experimental geometry in tilted samples. The angle between the writing beam polarisation direction and the director is no longer zero, as it is in the case of normal incidence.

At normal incidence (geometry in Figure 5.11) in non-illuminated areas $n_{||} = n_e$ and this is its maximum value. The appearance of diffraction from the vertically polarised probe beam indicates the formation of a phase grating and thus a difference in respective refractive indices of illuminated and dark areas. This implies that the refractive index in illuminated areas is decreased.

In the tilted samples, in general, $n_{||}$ can either decrease or increase.

If $n_{||}$ decreased, diffraction from the tilted samples will be comparable with the normal incidence case. Experiment supports this first possibility (see Figure 5.16).

The increase of $n_{||}$ in illuminated areas is not possible for a number of reasons. First, it does not comply with the fact, that there is a general change in the order parameter which is registered by the horizontally polarised probe (diamonds on Figure 5.16). The change in the order parameter leads to the overall decrease of n_e, and $n_{||}$ can never exceed n_e. Second, as has been shown above, at normal incidence the refractive index for the vertically polarised probe can only decrease. In this case there would be a discontinuity at

small tilt angles of the sample (where $\varphi < \delta^*$) leading to the dramatic decrease in diffraction efficiency at small tilt angles. We do not register this discontinuity on the experiment (Figure 5.16).

Thus, the change of refractive index seen by the vertically polarised probe is always a decrease of $n_{||}$. This observed decrease of the refractive index is due to lowering of the order parameter and reorientation. The direction of reorientation of the optical indicatrix (and molecular director) to decrease the refractive index is away from the writing beam.

DE in tilted geometry
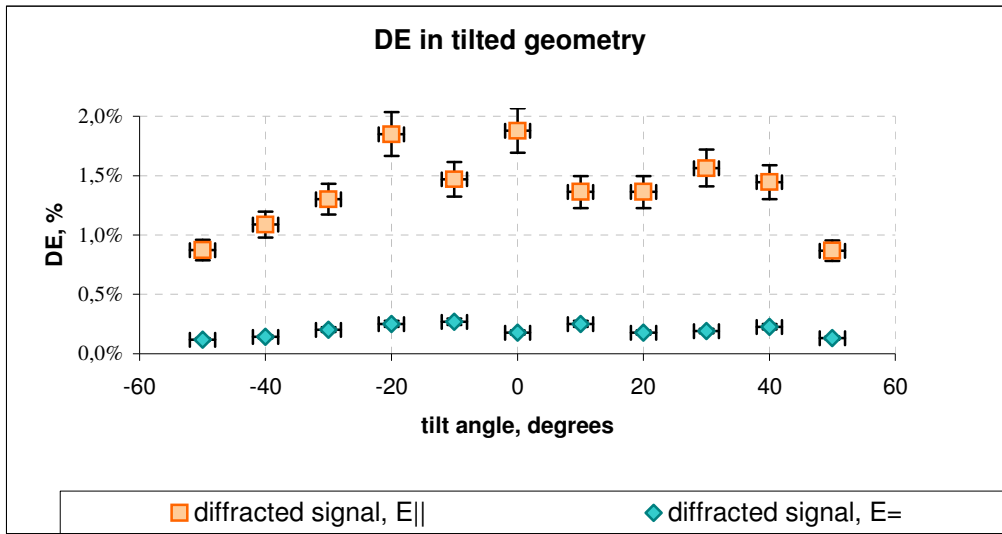
Figure 5.16 Tilted 15μm 1wt%DC161 doped 5CB sample - Diffraction Efficiency studies using vertically (squares) and horizontally (diamonds) polarised probe. Optical power of the writing beam 30mW/cm².

Indeed, the refractive index in the sample, tilted by the angle φ as seen by the vertically polarised reading beam will be:

$$n_{||}^{dark} = \frac{n_o n_e}{\sqrt{n_o^2 \cos^2 \varphi + n_e^2 \sin^2 \varphi}}$$

5.5

In illuminated areas it will be given by:

$$n_{||}^{illum} = \frac{n_o n_e}{\sqrt{n_o^2 \cos^2 <\phi> + n_e^2 \sin^2 <\phi>}}; \qquad <\phi> = <\varphi \pm \delta>$$

5.6

---

* The angle δ is small (because the resulting refractive index change is small).

Here $<\phi>$ is the spatial average of resulting angles $\varphi \Gamma \delta$. If the probability of reorientation $+\delta$ is the same as $-\delta$, the resulting $n_{||}$ will depend on φ only, and no diffraction should be detected. If reorientation occurred in the $-\delta$ direction only (towards the writing light polarisation), the effective refractive index will increase. If there is reorientation in the $+\delta$ direction (away from the beam polarisation), we will register a decrease of $n_{||}$. Thus reorientation away from the beam polarisation is the only possibility.

It is important to note that experimentally it is possible to see only the effect averaged throughout the sample thickness. The actual order and degree of molecular orientational change will vary with distance from the excited molecule. Parameters that restrict liquid crystal from orientation (surface alignment energy) will lead to the molecular reorientation changes approaching zero near the surfaces.

We have shown that the diffraction efficiency angular dependence correlates with the absorbed optical power per unit thickness[95].

Adding this information to the discussion of possible mechanisms in DC161, we suggest that the observed director motion in these systems is triggered by the dopant undergoing a trans-cis transition. This results in the anisotropic change of macroscopic order parameter. Such change involves reorientation of host material molecules away from the light polarisation and decrease of the order parameter.

Trans-cis isomerisation as a mechanism of nonlinearity was reported earlier for azo dyes like methyl red[89,90]. In anthraquinone and some azo dyes Jánossy effect has been reported (e.g. [60],[96]). In this research we have studied an azo-anthraquinone dye for the first time and have defined the mechanism responsible for nonlinearity introduced by this dye as a dopant for liquid crystals.

Here $<\phi>$ is the spatial average of resulting angles $\varphi\Gamma\delta$. If the probability of reorientation $+\delta$ is the same as $-\delta$, the resulting $n_{||}$ will depend on φ only, and no diffraction should be detected. If reorientation occurred in the $-\delta$ direction only (towards the writing light polarisation), the effective refractive index will increase. If there is reorientation in the $+\delta$ direction (away from the beam polarisation), we will register a decrease of $n_{||}$. Thus reorientation away from the beam polarisation is the only possibility.

It is important to note that experimentally it is possible to see only the effect averaged throughout the sample thickness. The actual order and degree of molecular orientational change will vary with distance from the excited molecule. Parameters that restrict LC director from orientation (surface alignment energy) will lead to the molecular reorientation changes approaching zero near the surfaces.

We have shown that the diffraction efficiency angular dependence correlates with the absorbed optical power per unit thickness[97].

Adding this information to the discussion of possible mechanisms in DC161, we suggest that the observed director motion in these systems is triggered by the dopant undergoing a trans-cis transition. This results in the anisotropic change of macroscopic order parameter. Such change involves reorientation of LC director away from the light polarisation and decrease of the order parameter.

Trans-cis isomerisation as a mechanism of nonlinearity was reported earlier for azo dyes like methyl red[89,90]. In anthraquinone and some azo dyes Jánossy effect has been reported (e.g.**Error! Bookmark not defined.**,[98]). In this research we have studied an azo-anthraquinone dye for the first time and have defined the mechanism responsible for nonlinearity introduced by this dye as a dopant for liquid crystals.

5.5 Photoinduced charge-related effects

In MR and fullerene-doped liquid crystal layers the director axis reorientation is often attributed to the optically induced space-charge fields [43, 46, 70]. Many effects can take place simultaneously in doped LC systems. The aim of this section is to verify whether the

described charge-related effects take place in the MR and C_{60} doped devices based on given host materials and alignment surfaces in the preferred geometry[*] of the experiment, and whether these effects are present and lead to nonlinearity in DC161 doped systems.

Photocharge-related nonlinearity results from reorientation of LC director in the space-charge field, which builds up in the presence of a periodic optical field and DC field in the z direction (Figure 5.17)[†]. This space-charge field may be due to generation of charges in excited fullerene or dye molecules and subsequent migration and diffusion of these charges due to dielectric and conductivity anisotropies, and the so-called Carr–Helfrich effect **Error! Bookmark not defined.**, [70] (see also Chapter 2, equations 2.52 and 2.53).

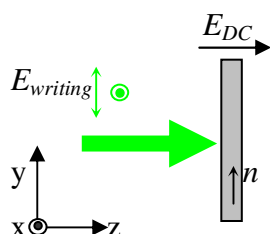DC field may be either externally applied or generated internally (as in the case of Methyl Red[48]).

Figure 5.17. Geometry of the experiment involving application of external field. The voltage is applied across the sample, in z direction.

Photogenerated charges would manifest themselves in the form of photovoltage build-up and photocurrents. Thus it is informative to observe charge behaviour as the sample is illuminated. For example, strong ionic behaviour in the material is supporting the ionic origin of the reorientation, and no strong ionic behaviour will require a different explanation for the existing reorientation like, for example, trans-cis transition etc.

---

[*] Planar aligned devices, all beams are polarised along LC director, and the beams' incidence direction is normal to the sample surface.

[†] See also Figure 2.13, Chapter 2.

5.4.3 Methods

We use the methods described in Chapter 4 to study photo-ionic behaviour of the investigated systems. These methods include current response to the externally applied electric field (*I/V* measurements), impedance measurements, Freedericksz threshold studies and photogenerated current and voltage measurements.

Photoinduced charge-related effects are based on a space-charge build up (Chapter 2). Space-charge build up upon illumination is expected to change the overall charge behaviour of the device, as the sample is illuminated. For example, a photogenerated current or voltage may appear. The photocurrent and photovoltage in devices may not directly contribute to the photorefractive effect, but they reflect the charge behaviour in the device. This concept is applied to all devices in this research.

First of all, the photogenerated charge measurements are compared with the nonlinear optical response of the devices, and conclusions are drawn for each of the dopants whether ionic effects contribute to the nonlinearity. The comparison is based on the temporal characteristics of the photogenerated voltage and optical nonlinearity.

Then, the conclusions from the I/V and impedance measurements and Freedericksz transition studies presented in Appendix D are employed to gain a more detailed insight into ionic processes that may take place in the investigated devices.

5.4.4 Pure nematic films

When undoped planar 5CB, BLO48, and planar and homeotropic E7 films are illuminated with a laser beam, the photoinduced current and voltage is smaller than the sensitivity of the measuring system (precision 10^{-12}A and 10^{-6}V). This indicates that the light intensities and wavelengths used are not capable of creating ions in pure materials. When doped films are illuminated a variety of effects are observed which can be attributed to the dopant or dopant/host system.

5.4.5 Fullerene-doped LC

Large optical nonlinearity in C_{60} doped systems had inspired a lot of studies[16, 46, 48, 70] and has been characterised as due to the space-charge build up (see

Chapter 2). The space-charge field mechanisms of the nonlinear effect would manifest themselves through a number of parameters[70]:

⇒ External electric field must be applied or generated internally for the effect to take place; there is a distinct dependence of the nonlinearity magnitude on the applied or generated field.

⇒ The time scale of the nonlinear signal build up should be slow, comparable with the speed of photo-induced ionic processes in doped LC systems (studied as photogenerated voltages and currents).

⇒ In some cases, the recorded hologram may be maintained by the external field only, even when the optical field has been switched off (Carr-Helfrich effect).

⇒ The photorefractive effect has a $\pi/2$ phase shift from the incident optical intensity profile, thus enabling beam mixing (see Chapter 2, also discussed in detail in references 16, [39] and [70]).

⇒ The largest reorientation of LC director is achieved when the grating spacing is double the sample thickness[70] (see also Chapter 2, p. 34).

5.4.5.1 Pre-history effect

Out of the six C_{60} doped devices built for this research (devices 31-36, see Appendix D) only one, device 31, BLO48 doped with C_{60}, purity 99.5%, with planar alignment introduced by a PI layer, built in May 2002, has exhibited nonlinear behaviour. It is interesting to note, that C_{60} doped 5CB material is well known for producing a photorefractive effect[16] including in the planarly aligned devices**Error! Bookmark not defined.**, so nonlinearity in our C_{60} doped devices 34-36 was expected. Furthermore, no nonlinear behaviour has been observed in device 33, which is almost identical to the previously discussed device 31, but built two years later. And finally, no nonlinear behaviour was observed in device 31 until the second half of year 2003, (see section 5.5.3.4. below).

Another interesting fact is that the optical nonlinearity behaviour in the device 31 depends strongly on the recent illumination pre-history (Figure 5.18).
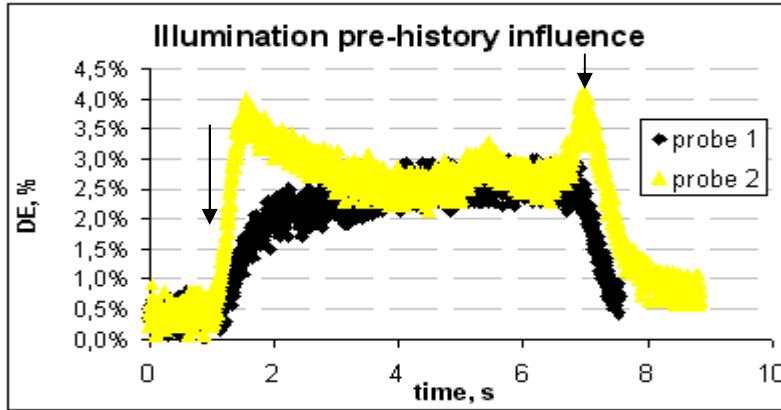
Figure 5.18. The influence of the optical pre-history. The imaging setup in Figure 4.9 is used; the optical intensity of the writing beam (λ=514nm) is only 5.5mW/cm^2. V_{DC}=5.6V is applied to the device. The device is C_{60}+BLO48 (device 31, Appendix D). The arrows indicate the moment when the optical field is switched on and off.

The first measurement (black diamonds, probe 1) is made after leaving the sample in a dark room for 5 minutes. The second measurement (light triangles, probe 2) has been preceded by 30 second illumination of the device by the expanded writing beam from the opposite side.

It is likely that the ageing effect in fresh and earlier manufactured C_{60} doped devices discussed above has a dependence on pre-history as well as an ageing. Alignment agents might be also important.

A more detailed study to research the mechanisms of nonlinearity and the reasons for the ageing effect in C_{60} doped devices has been performed on the planar aligned 20μm thick BLO48+C_{60} device (device 31) that exhibits nonlinearity.

## 5.4.5.2 Confirmation of space-charge field mechanism contribution

At the beginning of this section the conditions under which the space-charge mechanism will play the major part in the optical nonlinearity build up in the system are described. Here the experimental evidence is presented for most of these conditions to be satisfied.

$\Rightarrow$ The nonlinearity does not occur without the applied external electric field.

The field has to be chosen carefully: strong fields induce higher nonlinearity, but may also lead to light scattering through the establishment of dynamic instability (Figure 5.20). Voltages above 7V in the device 31 have lead to a decrease in the diffracted signal and ultimately to complete quenching of the nonlinear effect.

⇒ The generated photocurrent is on the same time scale with the observed nonlinearity (Figure 5.19).

In the studies by Khoo[16] C_{60} doped devices the photovoltage had been beyond the measuring system sensitivity. The system used for measurements in this work (see Chapter 4) has a higher sensitivity (3 orders of magnitude) for photovoltage measurements as
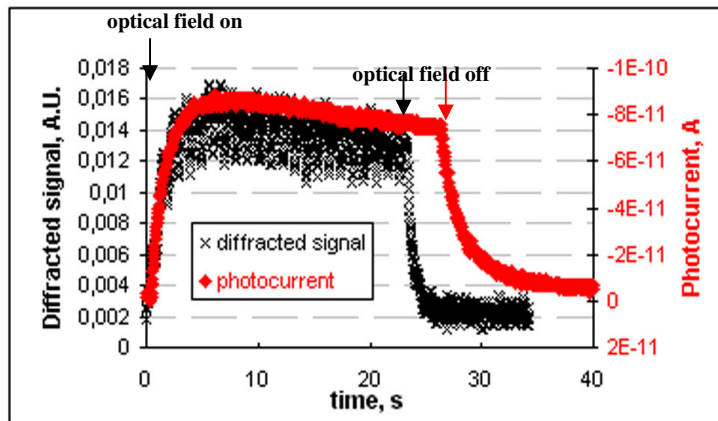

compared to the above studies by Khoo. Very small values of photocurrent (10^{-12}A) may also be registered.

Figure 5.19. Dynamics of optical nonlinearity (crosses) and photocurrent (diamonds) in planar 20μm BLO48+C_{60} device (device 31, Appendix D). The arrows indicate the moment when the optical field (λ=514nm, intensity 10mW/cm^2) is switched on and off. The DC field is 3.6V and is kept "on" during the experiment.

⇒ For the studied device the observed nonlinearity is characterised by a small reorientation (diffracted signal builds up monotonously to the value, which is lower than the maximum possible value). Out of the three main mechanisms of director reorientation in doped NLC involving space-charge field[70] (see Chapter 2), at small reorientation flows and Carr-Helfrich effects may be neglected.

Carr-Helfrich fields, once the field has been established, can be maintained by a DC field alone, without the need for an external optical field. We register the opposite - the system relaxes in less than 10s after the optical field has been switched off, although the DC field is kept on (Figure 5.19).

$\Rightarrow$ Energy transfer from one beam to another (both beams $\lambda=514nm$) (Figure 5.20) and energy interplay between +1 and -1 diffracted orders of a red probe beam (Figure 5.21) have been observed in the studied C_{60} doped device (device 31). Therefore the photorefractive effect is obtained with the phase shift with respect to the optical intensity function.
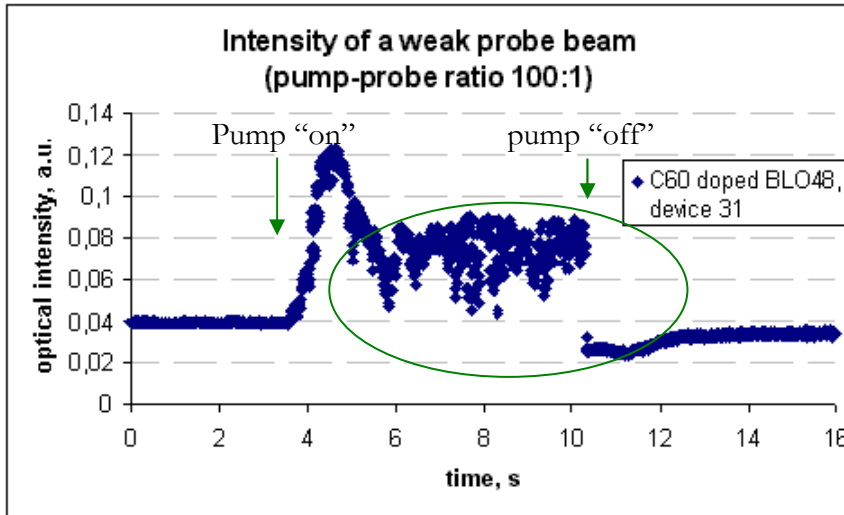
The setup in Figure 4.10 is used; the beams are impinging at normal incidence. A constant DC field ~5V is applied to the device.

Figure 5.20. Amplification of a probe beam by the pump. Pump-probe ratio 100:1; pump intensity 10mW/cm^2; the device is 20μm thick (device 31 - see Appendix D). The voltage is +5V on the front electrode. The decrease in the signal after it builds up is due to the scattering that builds up as the pump is switched on.
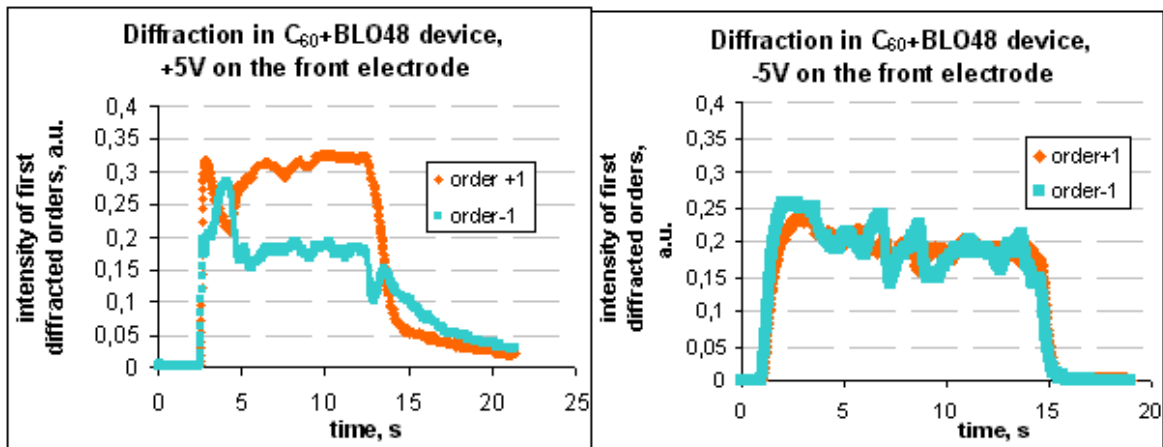

Figure 5.21. Energy interplay between ±1 diffracted orders in C_{60}+BLO48 20μm thick device (device 31, Appendix D). Optical power of the writing beams 10mW/cm^2

a) Positive voltage on the front electrode;

b) Negative voltage on the front electrode.

⇒ The resolution studies in the device in question (Chapter 6) are in agreement with the fact, that the maximum reorientation should be obtained when the grating spacing equals double the cell thickness.

Thus, the nonlinearity in the studied C_{60} doped device is due to the dopant-assisted space-charge field build up. This may also involve surface-induced processes.

5.4.5.3 <u>Asymmetry of the electrodes</u>

The adsorption of the dopant material on the surface of the device may lead to nonlinearity through surface phenomena (see the detailed discussion in the following section). For example, a photoconductive layer could have formed in the device 31 that exhibits nonlinearity. Adsorption on the surface is likely to be influenced by the optical and electric pre-history of the device and in general case would be asymmetric.

The asymmetry is indeed found in the studied device in terms of charge and nonlinear behaviour. The magnitude of the nonlinearity depends on the polarity of the applied DC field, and on the order in which the light is passing through the electrodes (let us call the electrodes the "1st" and the "2nd") in an asymmetric way (Figure 5.22).

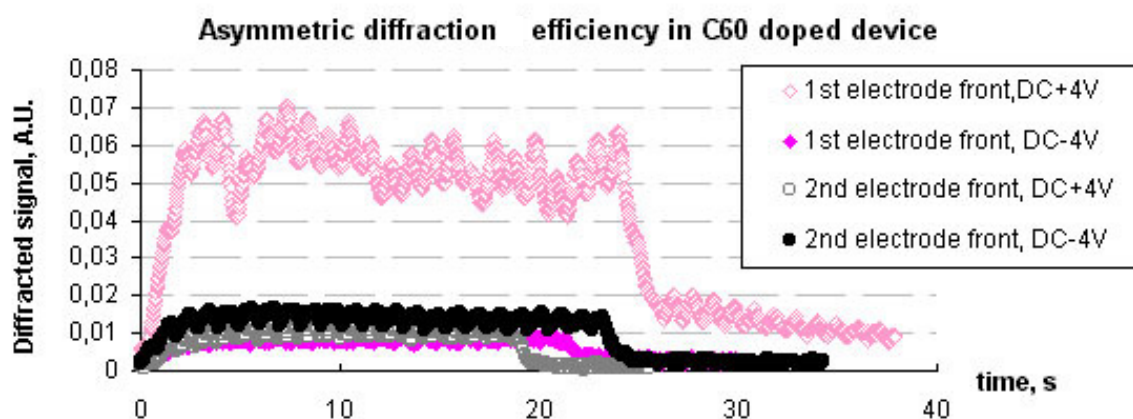*Figure 5.22 Asymmetric diffraction efficiency in planar C_{60} doped BLO48 device (device 31, Appendix D). Optical power 10mW/cm^2. Grating spacing 80 lp/mm. The imaging optical setup described in Chapter 4, Figure 4.9 is used. An external electric field is applied to the device V_{DC}=5V and V_{AC}=0.6V*.*

---

* A small AC field is applied together with DC to pre-tilt molecules and obtain a non-zero interaction angle between the incident laser electric field and the director axis necessary for the nonlinear effect to occur (AC modulation can be seen on the diffracted signal curves).

The nonlinearity is significantly higher in case where one of the electrodes is in front and has a positive polarity. If the direction of the incidence of writing beams is reversed now, the nonlinearity will be smaller, but still larger than in the case where a negative polarity is used for this electrode (Figure 5.22).

The asymmetry in the electrodes would be visible in terms of current behaviour as a response to the applied electric field. The I/V response of the C_{60} doped BLO48 device (device 31, Appendix D) is measured in dark and illuminated state for all possible geometries of illumination direction and applied field polarity (for general I/V response of the device and its comparison with undoped and other C_{60} doped samples). The setup for measurements is described in Chapter 4. The measurements are taken after the illumination has been switched on for 30 seconds in order to allow the photocurrent to stabilise (photocurrent builds up and relaxes, both in less than 10 seconds – see Figure 5.19). There are also 30 second intervals between illumination periods to reach relaxation in device.
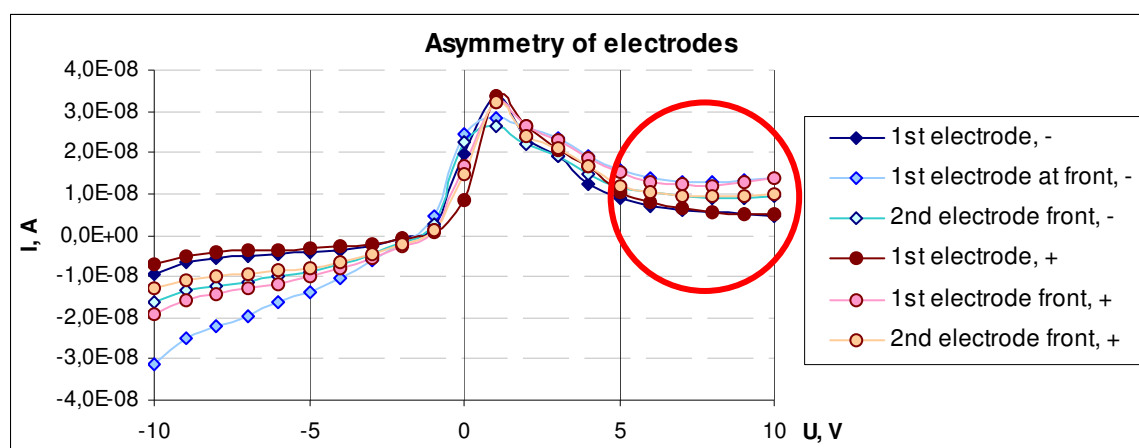

Figure 5.23. I/V behaviour of C_{60} doped BLO48 device (device 31, Appendix D) with asymmetric electrodes. "+" and "-" indicate the polarity on the 1st electrode. Dark filled circles and diamonds not marked "front" in the legend relate to the case with no illumination. Illumination at λ=514nm with the power of 10mW/cm^2 has been used.

On the I/V curves there is a difference in the current response of the sample, when it is illuminated depending on the side of illumination (Figure 5.23).

The current response of the device when it is illuminated is generally higher. In the region from +5 to +10V (area within the circle on Figure 5.23), when transient effects

connected with voltage application have disappeared (the application of voltage always starts from negative values), the current response shows a very distinct behaviour. It is lowest for the non-illuminated case, and highest for the case, when the first electrode is at the front side relative to the impinging beam. The current response in this stabilised region is independent of the voltage polarity, and depends only on the position of the electrodes relative to the impinging beam. This behaviour correlates with the behaviour of the observed nonlinearity.

The asymmetry becomes even more obvious when looking at photogenerated current and voltage (Figure 5.24).
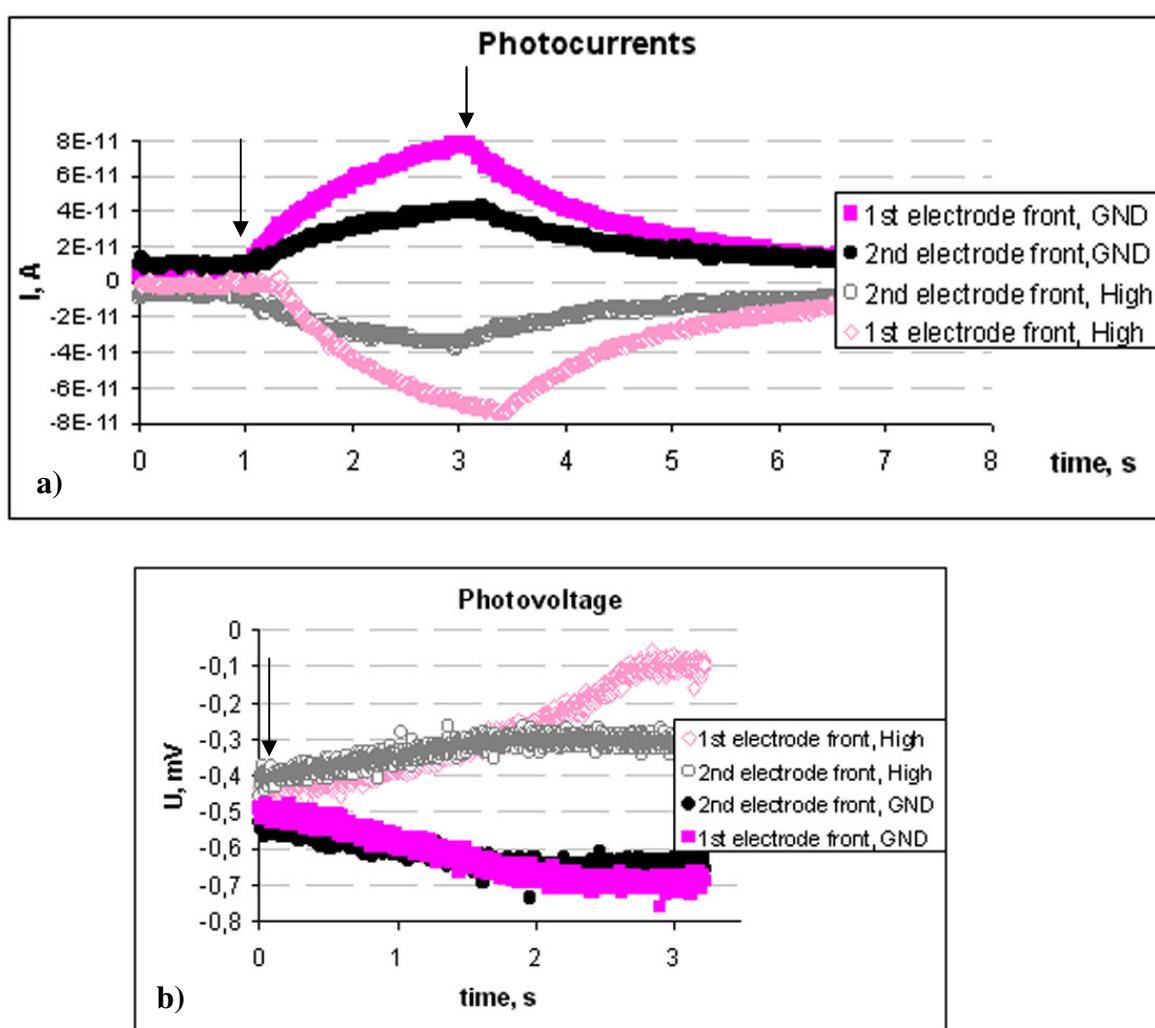

Figure 5.24   a) Photogenerated current
b) Photogenerated voltage.
High and GND indicate the polarity of the measuring system in respect to the 1st electrode. 2 s pulses of illumination at λ=514nm with optical power of 30mW/cm^2 are used. The arrows indicate the moment when the optical field is switched on and off.

The measurements for photocurrents and photovoltages (represented in Figure 5.24) are taken for both positions of the ground electrode (connected to 1st and 2nd electrode) to eliminate any possible influence of the measuring system on the sample, which may introduce small parasitic DC bias.

Independently of the optical field propagation direction and measuring unit polarity, the generated current always flows in the same direction, from the 1st to the 2nd electrode (see also Figure 5.25).

The photovoltage shows corresponding behaviour. Illumination from any direction leads to the 1st electrode having higher potential, than the 2nd (Figure 5.24). This may be explained by asymmetry due to the prehistory of the sample (e.g. dopant absorbed on one surface after prolonged illumination from this side, processes in the alignment layer due to optical/voltaic prehistory).
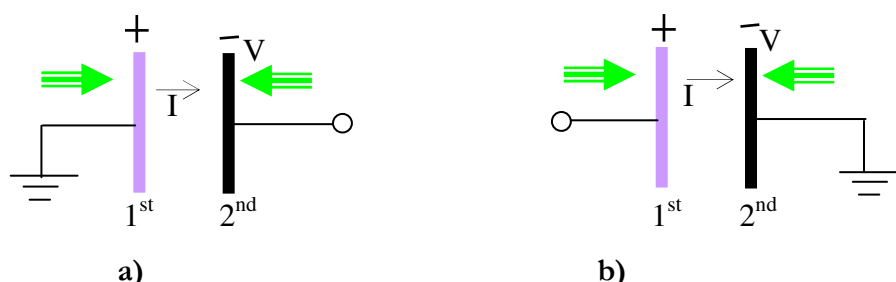

Figure 5.25. Photocurrent and photovoltage polarity in possible light propagation (arrows) geometries. a) 1st electrode (left) is grounded; b) 2nd electrode (to the right, black) is grounded.

The described photocurrent and photovoltage behaviour correlates well with the observed nonlinearity, where the highest effect is observed when the high potential is connected to the 1st electrode. Such DC bias supports and enhances the observed photocurrent further contributing to charge formation.

5.4.5.4 Differences between fresh and old C_{60} doped devices

To research the differences between the C_{60} doped devices that do and do not produce optical nonlinearity, let us concentrate on the charge characteristics of the devices. The electric and photocharge generation response of the fullerene-doped devices is

presented in Appendix D. The relevant conclusions from this section and Appendix D are reiterated below.

- The absorptance of all C_{60} devices is very low, and the devices cannot be discriminated based on absorptance measurements for a setup used in this research (Figure 4.2, Chapter 4).

It is not possible to give the any judgement on the amount of the dopant that has dispersed in the host material based on the spectroscopy studies.

- The resistivity and capacitance of freshly prepared BLO48 doped device 33 and the device 31 differ, the fresh device having higher conductivity and similar capacitance as compared to the earlier built sample.

There may be more free charge carriers in a freshly doped device. The charge mobilities are low, as the DC application for 5 minutes does not change the resistivity of the devices.

- The Freedericksz transition is the same in freshly prepared and earlier built devices based on the same host material.

Significant adsorption of C_{60} on a surface is expected to produce a very large shift in the FT threshold voltage[99]. Therefore, adsorption on the surface, if present, is too small to make a significant change to the transition (at a given precision of ±0.1V). This is a plausible assumption, taking into account nearly trace amounts of the dopant (~0.01wt%). The same can be said about charge transfer complexes influence on FT threshold.

- I/V characteristic of the earlier built device that exhibits nonlinearity is different from the characteristic obtained from the freshly built device based on the same dopant, host, alignment and preparation method.

The current from the freshly doped device grows with the voltage, indicating a presence of free charges. The current from the earlier built device is significantly lower than in both pure and fresh C_{60} doped samples suggesting the absence of free charges. The resistivity of device 31 is higher than that of the freshly prepared device 33.

- Surfaces in device 31 are asymmetric in terms of nonlinear behaviour and photovoltage generation.

Because of the strict control over the device manufacturing it is expected that the surfaces of the devices are identical. Under the influence of externally applied electrical and/or optical fields the surfaces of the earlier built device should have changed in an asymmetric

way. The nature of such change may have included asymmetric dopant adsorption at surfaces (or one surface) or formation of charge transfer complexes near the surfaces (or one surface).

The possibility of a purely surface-induced photorefractive effect in pure LC films with adjacent polymer layers doped with C_{60} has been recently reported by some authors[99,100]. This mechanism could also be responsible for the observed nonlinearity in the earlier built C_{60} doped device, as the dopant could have been adsorbed on the surfaces (Polyimide), effectively forming what would be photoconducting polymer layers.

As has been already discussed, the amount of dopant is too small to form a monolayer in the device. Moreover, we do not register the reported dramatic increase (up to 50V)[99] in the Freedericksz transition threshold in our C_{60} doped devices resulting from the charge screening by the doped polyimide layers. This screening is crucial for forming a space-charge field through photo-induced conductivity in the nematic device.

To summarise, the optical nonlinear effect in the studied C_{60} doped systems is due to the space-charge field formation through the photocharge generation and induced (small) photoconductivity.

Surface adsorption and charge transfer complexes formation are both likely to be the reason of the ageing effect in the researched C_{60} doped devices with PI alignment.

C_{60} is a very interesting dopant, and it would be highly promising to research the ways of more efficient dispersion and to study the reasons of the ageing effect reported in this work systematically.

5.4.6 Methyl red-doped NLC

Methyl Red doped systems, as has been already discussed in Chapter 2, exhibit a plethora of various mechanisms leading to nonlinearity from fast trans-cis transition to slow or permanent surface effects. MR is an ionic dopant, and ionic mechanisms play important part in MR-doped systems.

For ionic effects (as well as for surface effects) one of the most important factors that defines sample response to the light is the alignment agent. It has been reported earlier that the highest sensitivity in MR doped samples is obtained in homeotropic samples in

conjunction with ionic surfactants such as HTAB (hexadexyl-trimethyl-ammonium-bromide) and HTAC (hexadexyl-trimethyl-ammonium-chloride)[78].

We have used different alignment agents for our MR doped devices, because of incompatibility of these systems with the targeted device applications:

- HTAB may lead to permanent hologram formation
- the ions introduced to the LC from these surfactants, although increasing the sensitivity, significantly shorten the life and robustness of the devices
- HTAB and HTAC devices have been reported[78] to spontaneously realign in some regions to planar in short time (weeks).
- Planar geometry is favoured for applications, as it allows normal incidence of the writing and reading beams.

In order to understand whether ionic mechanisms are present in devices with the alignments used (PI, SiO$_x$ and ZLI3334 - see Chapter 3 for details), we have performed studies of photovoltage and photocurrent build-up and experiments in different geometries.

5.4.6.1 External field application

The first step is to check whether any ionic behaviour can be obtained with the chosen alignments. In the studied MR doped devices optical nonlinearity is observed without any external fields applied. When external voltage is applied to the studied samples, nonlinearity was found to increase (see for example Figure 5.26).
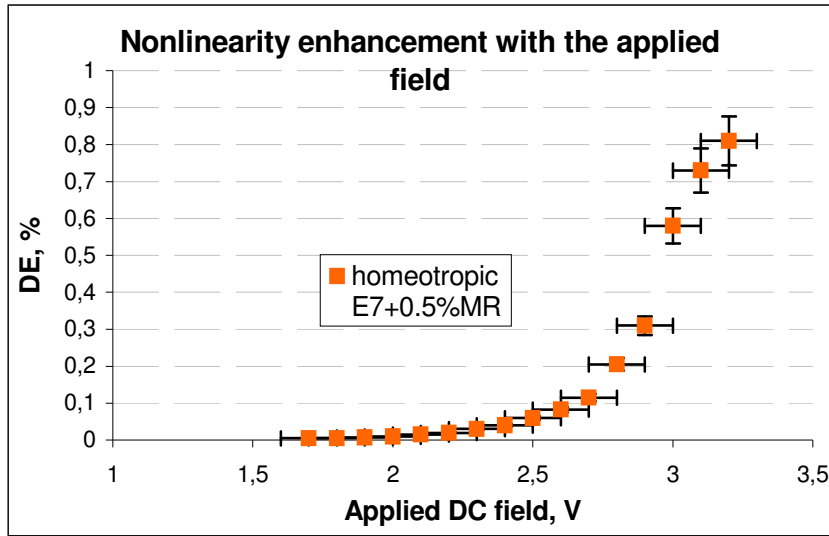
Figure 5.26. Enhancement of the nonlinearity by the applied DC field in the homeotropically aligned MR doped E7 device (device 30, Appendix D). Writing beams intensity 10mW/cm^2, λ=488nm, the imaging setup on Figure 4.9 is used. As voltages higher than 3.3V are applied, the scattering builds up very quickly. At no voltage applied, the nonlinear effect is present with small but non-vanishing diffraction efficiency.

The above enhancement of nonlinearity by external field suggests the importance of ionic mechanisms for the nonlinearity in the studied MR doped systems in the case where an external field is applied.

5.4.6.2 Internally generated field

As has been observed by Khoo et al[48], under the influence of light in HTAB aligned MR doped samples, an internally generated DC voltage along the sample axis z builds up. This generated photovoltage may be responsible for the space-charge field build up without externally applied DC field.

The reported[48] photogenerated voltage that is sufficient to produce nonlinearity through the space-charge field build up in a 1%wtMR doped 5CB film with homeotropic HTAB alignment is 6mV in 25μm device, at 1mW/cm^2 illumination (λ=488nm).

The authors in reference 48 suggest that the space-charge fields could contribute to this photovoltage build up the following way, charge migration and diffusion from the grating maximum to the minimum produces a spatially varying (grating function) space-charge field in the y direction. Due to absorption, the optical intensity varies monotonically along the z direction, and thus a (unidirectional) dc space-charge field is also established along z. The latter component is manifested in the form of a dc voltage drop across the entrance and exit indium tin oxide cell electrodes. The polarity of the observed voltage is reversed if the incident direction of the light is reversed.

Similar photovoltage behaviour is observed in our samples, that differ from the samples used in reference 48 by alignment[*]. The photogenerated voltage polarity and corresponding current direction is reversed if the light direction is reversed (Figure 5.27).
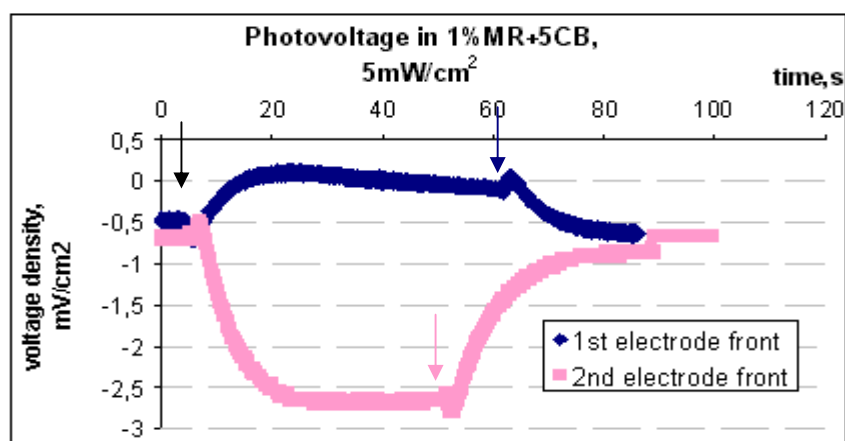

Figure 5.27. Photovoltage in 10μm 1%MR doped 5CB device with PI alignment (device 27); the setup on Figure 4.8 with illumination beam λ=488nm, I=5mW/cm² is used. The arrows indicate the moment when the optical field is switched on and off.

The voltage density is used to normalise the devices with various electrode areas. The generated voltage exhibits a distinct pre-history effect (see Table 5.3)[†].

The values of the photogenerated voltages are lower in 1% and 0.5% MR doped devices (Table 5.3 and Figure 5.27), than the reported for HTAB doped devices[48].

---

[*] See Appendix D for details on devices 26-30 used

[†] It is interesting to note, that no corresponding pre-history effect is found in terms of optical nonlinearity in the experiments with no external field applied.

Device (material, alignment)	Photovoltage, consequent measurements, illumination with λ=488; 10mW/cm^2	
	Measurement 1	**Measurement 2**
0.5wt%MR+E7, PI (device 29)	0.20 ± 0.01 mV	0.15 ± 0.01 mV
0.5wt%MR+E7, ZLI1134 (device 30)	0.32 ± 0.01 mV	0.15 ± 0.01 mV
1wt%MR+5CB, PI (device 27)	3.00 ± 0.01 mV	2.60 ± 0.01 mV
1wt%MR+5CB, SiO$_x$ (device 26)	20.0 ± 0.1 mV(overshoot)	18.6 ± 0.1 mV

Table 5.3. Pre-history dependence of photovoltage generation in MR doped devices.

The difference in the photogenerated photovoltage amplitude when the device is illuminated from different sides on Figure 5.27 may be due to the discussed illumination pre-history dependence.

Further experiments show, that, as expected, with the increased light intensity the photogenerated voltage increases.
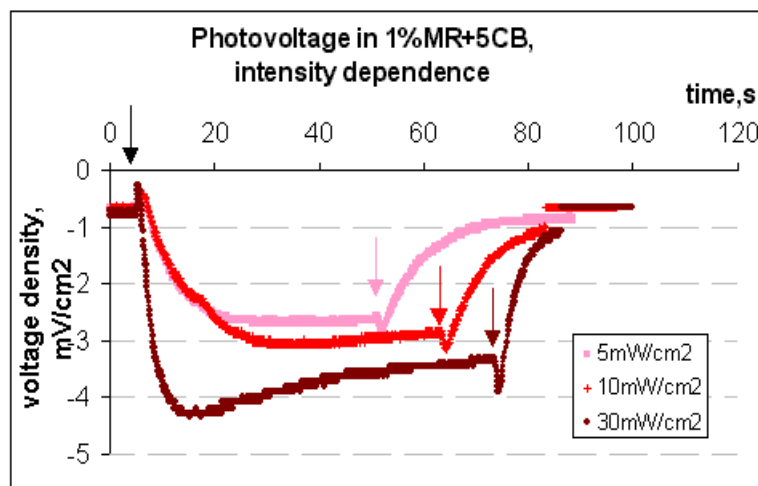

Figure 5.28. Photovoltage in 10μm 1%MR doped 5CB device with PI alignment (device 27); λ=488nm. The arrows indicate the moment when the optical field is switched on and off.

5.4.6.3 Photocharge and nonlinearity dynamics

The second step is to find out whether ionic effects are responsible for the nonlinearity when no field is applied. This is done by comparing the time scales of ionic and nonlinear effects in the chosen operating regime. The comparison between the dynamics of ionic (photovoltage build up) and optical nonlinearity effects is presented in Figure 5.29.
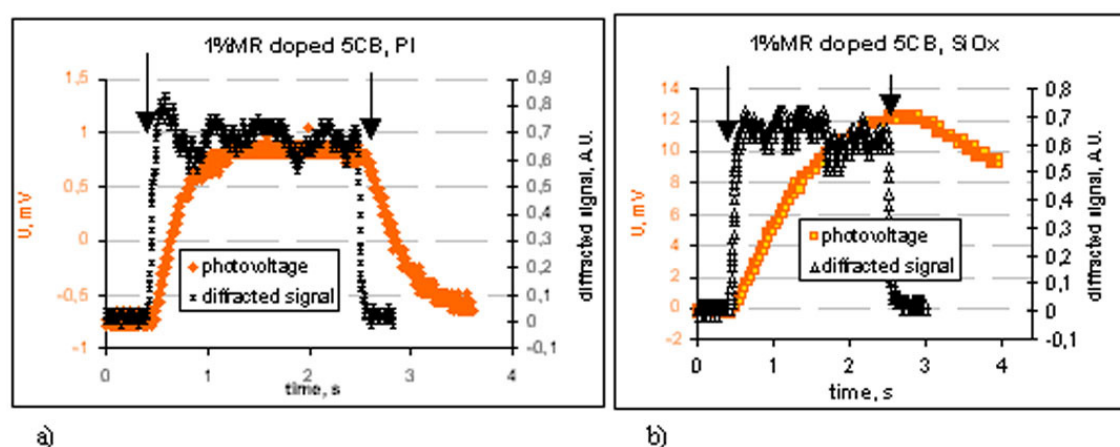

Figure 5.29 Dynamics of optical nonlinearity (black crosses (a) and open triangles(b)) and photovoltage (filled diamonds(a) and squares (b)) in planar aligned 10μm 1%MR+5CB systems with different alignments (devices 27 (a) and 26 (b)). For diffraction studies the imaging setup on Figure 4.9 is used (λ=488nm, 30mW/cm^2). For photovoltage studies the pump beam is 30mW/cm^2, λ=488nm. No external field is applied in both cases. The arrows indicate the moment when the optical field is switched on and off.

In the regime when no external field is applied (normal incidence of the writing beams is used, all beams are polarised along the director axis) the nonlinearity and photovoltage have different time scales, as can be seen from Figure 5.29.

When the external voltage is applied, the nonlinearity builds up slower (to a larger value) and correlates with the photovoltage build up, as expected for ionic mechanisms (Figure 5.30).
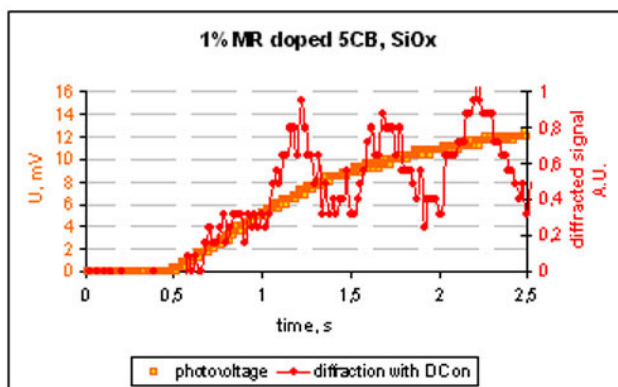
Figure 5.30 Dynamics of photovoltage and optical nonlinearity in the presence of a 1V DC field (and 0.2V AC modulation which is responsible for the oscillations in the signal) in 10μm 1%MR+5CB sample (device 26, Appendix D). For diffraction studies the imaging setup on Figure 4.9 is used (λ=488nm, 30mW/cm^2). For photovoltage studies the pump beam is 30mW/cm^2, λ=514nm, no external field is applied.

Therefore, by the choice of an operating regime it is possible to select the mechanism of nonlinearity in a MR doped system.

5.4.6.4 Alignment influence

Not only the photovoltage build-up time, but also its amplitude was found to depend on the alignment used. As the nonlinearity is expected to be higher in samples with higher photovoltages, it was interesting to study photovoltages, generated in devices of the same thickness and materials, but with different alignments, polyimide (PI) and SiO_x. It has been found that:

⇒ Devices with SiO_x alignment generate significantly higher photovoltage as compared to PI aligned devices (Figure 5.31).

⇒ The magnitude of the nonlinearity in the device with the SiO_x alignment does not differ considerably from the magnitude of the nonlinearity in PI aligned sample (Figure 5.29).

⇒ Devices with SiO_x alignment have very long stabilisation and relaxation times for the voltages (compare build up times in Figure 5.31).

⇒ Both devices exhibit same photovoltage - intensity dependence (as on Figure 5.28). The photovoltage grows as the optical power is increased and is a function of the light propagation direction (as on Figure 5.27).

⇒ Both devices exhibit very strong dependence of the photovoltage on the recent illumination pre-history (Table 5.3). This suggests that the surface-related charge effects may be involved.
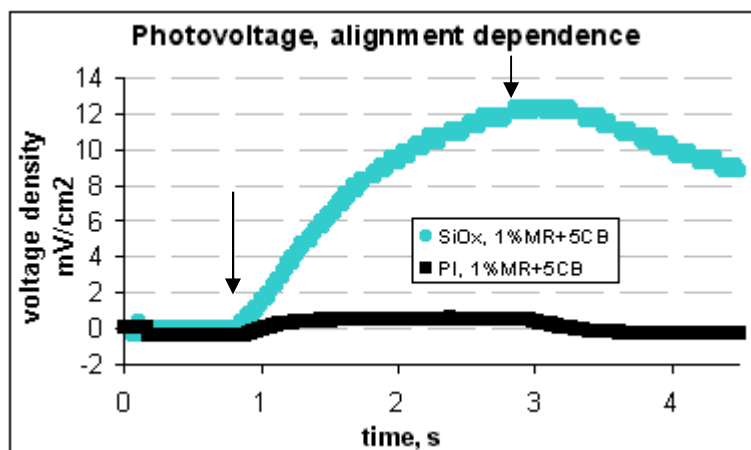

Figure 5.31. Photovoltage in 10μm 1%MR doped 5CB devices with PI and SiOₓ alignment (device 27); λ=488nm, I=30mW/cm². The arrows indicate the moment when the optical field is switched on and off.

The two devices discussed exhibit different behaviour in terms of photocurrents and photovoltages, but the optical nonlinearity in both is comparable. Therefore, ionic processes are not involved in the observed nonlinear process in the case when no external electric field is applied.

5.4.7 DC161 doped devices

There is no influence of the applied DC field on the optical nonlinearity in DC161 doped samples up to the Freedericksz threshold voltage. After the threshold voltage is reached, the nonlinearity becomes suppressed by the external field and disappears.

The measurements of photogenerated charge give small, as compared to MR doped systems, photovoltage (~0.5mV) in the studied 1% DC161+5CB 10μm and 14μm samples with PI and SiOx planar alignment (devices 9 and 11).

The photovoltage builds up slowly and takes over 60 seconds to relax. This behaviour is in contrast with the observed nonlinear effect dynamics in DC161, where switching time is counted by tens of milliseconds (Figure 5.32).
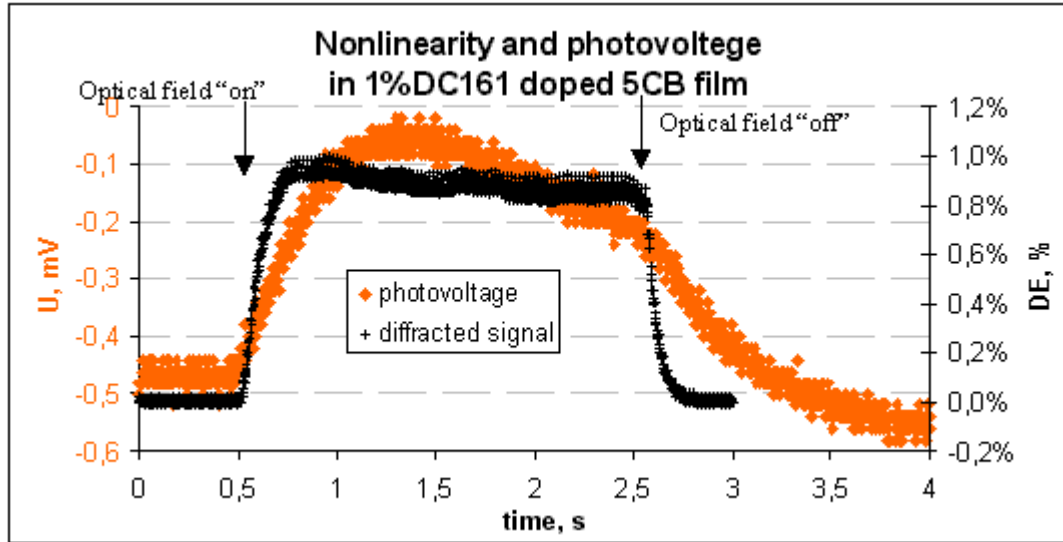
Figure 5.32. Dynamics of optical nonlinearity (black crosses) and photovoltage (diamonds). For diffraction studies the imaging setup on Figure 4.9 is used (λ=514nm, 30mW/cm^2). For photovoltage studies the pump beam is 30mW/cm^2, λ=514nm. The arrows indicate the moment when the optical field is switched on and off. The device is 10μm 1% DC161 doped 5CB with PI alignment (device 11, Appendix D).

Indifference to the applied external electric fields and different dynamic response of the charge and optical effects suggests that the nonlinear effect in DC161 doped films is not of ionic or space-charge origin.

5.5 Surface effects

Here we study the role of surface alignment in the nonlinear optical processes.

The simplest way to distinguish surface effects from other mechanisms is by their time scale. As has been discussed in Chapter 2, surface effects lead to very slow (tens of seconds) or even persistent and permanent orientational changes.

It is crucial for dynamic holography applications including OASLMs to avoid such permanent or persistent effects. The dynamic surface effects have been researched and found in MR doped unaligned samples (1% MR doped E7, ~1µm thickness), while DC161 did not exhibit any dynamic surface phenomena. On the other hand, as has been already mentioned, these effects are too slow to be exploited for the SLM applications. They are not relied upon in this work.

130

5.5.1 MR doped systems[*]

Adsorption of the excited dopant molecules on the alignment surfaces, leading to persistent and permanent reorientation and hologram formation, has been reported in MR doped LC systems in conjunction with some alignment agents[16]. This adsorption is augmented by the bonding of dye and surface molecules upon light excitation of the dye.

In the work by A. Chen and D. Brady on permanent gratings on the related dye MR Sodium Salt[†]-doped liquid crystal films, a correlation was found between diffraction efficiency of permanent holograms recorded, and surface treatments.[101] The largest permanent component was reported for the alignment agents polymethyl methacrylate (PMMA) and glass surfaces. Polyvinylcarbazole (PVC) and polyimide also showed permanent component formation but on much lower scale. Polyvinylalcohol (PVA) alignment did not allow the dopant to bond to the surface.

We have observed permanent and persistent phenomena in some of MR doped devices. To research the possibilities of avoiding this effect for applications where the dynamic change of the recorded information is required, devices with a variety of alignment agents including rubbed glass, rubbed ITO, rubbed PVA, HTAB, ZLI 1134, rubbed PI and SiO_x have been prepared and studied. To the best of our knowledge, rubbed ITO has never been studied as an alignment interface before.

This research has revealed a correlation of permanent component formation similar to the reported for MR sodium salt dye.[101] No permanent grating formation in samples with PI and ITO surfaces has been observed, though a permanent component was easily formed in cells with glass interface. PVA, SiO_x and HTAB showed intermediate characteristics (Table 5.4).

---

[*] Larger part of work, studying the influence of surface interface on permanent and persistent hologram formation, has been performed in Penn State University during the research visit to the Electro-Optics group headed by Prof. Khoo.

[†] A salt of the more commonly used MR dye, see Appendix B for chemical structure.

Alignment		Persistent grating	Permanent grating
Agent	Geometry		
Glass	Planar	~1s illumination with λ=532nm, intensity >10mW/cm^2	<50ms illumination with λ=488nm, intensity >10mW/cm^2
ITO	Planar	No, up to 50mW/cm^2	No, up to 50mW/cm^2
PVA	Planar	>5s illumination with both λ, intensity >10mW/cm^2	>5s illumination with both λ, intensity >10mW/cm^2
PI	Planar	No, up to 1W/cm^2	No, up to 1W/cm^2
SiO$_x$***	Planar	>10s illumination with both λ, intensity >50mW/cm^2	No, up to 50mW/cm^2
HTAB	Homeotropic	>10s illumination with both λ	>10s illumination with both λ, intensity >20mW/cm^2
ZLI 1134	Homeotropic	No, up to 100mW/cm^2	No, up to 100mW/cm^2

Table 5.4. Persistent and permanent grating formation in cells with different alignment surfaces.

Relaxation behaviour in dynamics of the MR doped 5CB devices of the same thickness and different alignment surfaces is shown in Figure 5.33. In cells with pure glass walls (rubbed to introduce planar alignment) illumination even for 50ms with the laser light λ=488nm with intensity over 10mW/cm^2 leads to the persistent grating formation. In cells with different alignment (same thickness, dye concentration and host material), namely ITO, prolonged illumination at comparatively high intensities (up to 50mW/cm^2) does not lead to dye adsorption on the cell surface.

---

* Persistent gratings in SiOx aligned samples have considerably faster relaxation times and may be also attributed to ionic processes, which are very slow in these systems.
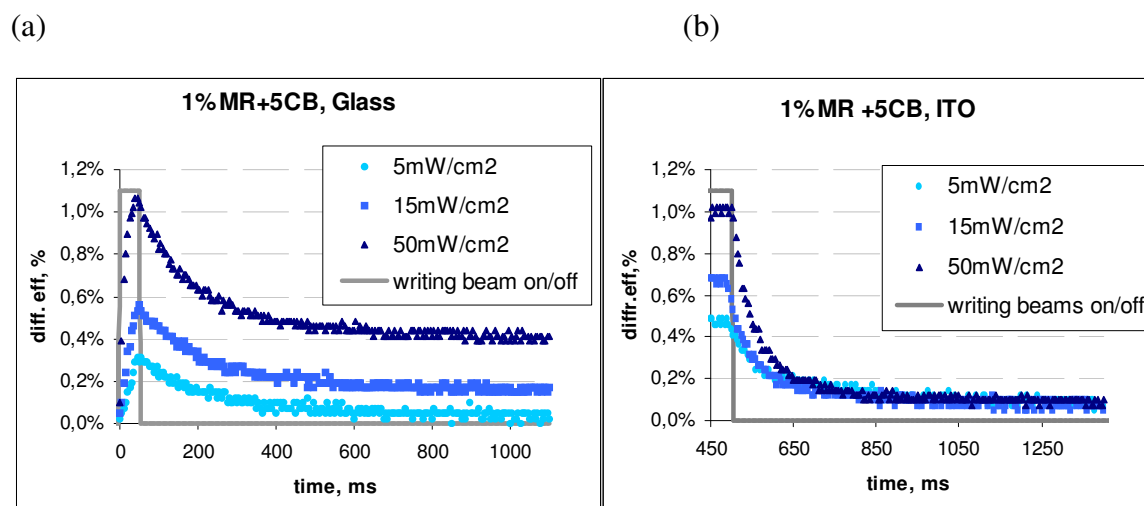
(a)   (b)

Figure 5.33 Permanent/persistent component in 2μm temporary cells, 1%MR + 5CB.
The optical setup on Figure 4.10 is used; the writing beams are at λ=488nm and
have different optical powers. The writing beams are switched on at t=0ms.
a) Glass interface after 50ms exposure to the writing beams;
b) ITO interface after 500ms exposure.

Later studies have shown that MR in conjunction with PI alignment does not form permanent or transient gratings even with very high optical powers (1W/cm^2); higher intensities lead to fast melting of the 5CB layer due to absorption and heating (**Error! Reference source not found.**).

Thus, for device applications, when dynamic change of information is required, PI, ITO and ZLI 1134 interfaces with a doped liquid crystal layer could be used.

5.5.2 *DC161 doped systems*

No formation of any permanent or persistent components in the DC161 doped samples for all interfaces used (PI, SiOx, ZLI 1134, PVA and pure glass) has been found. Light intensities up to 1W/cm^2 for prolonged periods of time (even up to the melting point of 5CB) have been used, and external fields have been applied occasionally.

Dynamic surface effect is also ruled out in DC161 doped systems, based on the disagreement of the observed holographic grating formation dynamics with the time scale of the surface effect: the former one is under 100ms (see for example Figure 5.32), and the latter is of the order of seconds**Error! Bookmark not defined.**.

5.5.3 C_{60} doped NLC devices

C_{60} doped devices with the alignments used (PI and ZLI 1134) do not exhibit permanent effects.

An argument in favour of the importance of the surface-related charge effects is that the nonlinearity strongly depends on the recent pre-illumination prehistory. Such dependence is usually associated with surface phenomena. Light may trigger some transient surface effects that may involve reversible bonding interaction between the dopant and the alignment layer. Electrode asymmetry in the C_{60} doped device that exhibits nonlinearity, discussed in the previous section, also indicates the presence of some surface phenomena.

The surface phenomena in the case of C_{60} doped devices is charge-related, and is a different effect from the surface-induced nonlinearity reported**Error! Bookmark not defined.** in MR doped systems.

5.6 Summary of the possible nonlinear mechanisms in investigated systems

We have investigated possible mechanisms in dopant-host systems based on three dopants: MR, C_{60} and DC161. MR and C_{60} doped systems have been studied by other authors before, and DC161 doped liquid crystals have been researched for the first time.

Previously a geometry with 45° incidence of the beams and homeotropic alignment of samples has mainly been used in the experiment, especially for C_{60} doped systems. In this research nearly normal incidence of the reading and writing beams, favourable in device applications, and the planar alignment have been used.

The time scale of photorefractive effects, behaviour with the external fields applied, dependence of the effects on the surface interface and host material, and changes of refractive indices are considered.

From the calculation of the temperature profile within the doped LC layer (done for the first time), it appears that the temperature difference in bright and dark fringes is

very small, less than $0.01^{\circ}C$ at $50mW/cm^2$ writing beam power. Diffusion, as a heat transfer mechanism, is not accounted for, so in reality the steady state difference of temperature may be even smaller. Large thermal nonlinearities due to the general heating of the sample close to the isotropic transition appear at optical intensities of $1W/cm^2$. They are usually slow, of the order of 10s of seconds. It has been found that the thermal effect may be considered negligible in the studied highly light absorbing devices at optical intensities under $50mW/cm^2$ when the ambient temperature does not approach phase transition temperature of the host material, or when 2 second and shorter writing pulses are used.

Another finding of this research work is that with age the efficiency of materials changes in a non-trivial fashion. C_{60} and DC161 devices improve with age. Surface adsorption and charge transfer complexes formation are both likely to be the reason of the ageing effect in the researched C_{60} doped devices with PI alignment.

The ageing effect has prevented us from more detailed research on the influence of the host, and the importance of the guest-host interaction.

Out of the range of possible mechanisms leading to nonlinear effect in C_{60} doped systems reported by different authors[16,]**Error! Bookmark not defined.**, the mechanism responsible for the optical nonlinear effect in the researched system has been specified. The nonlinearity in the C_{60} doped device is due to space-charge field formation under the influence of optical and a DC field through the generation of photocharge and induced (small) photoconductivity.

Out of six C_{60} doped devices (31-36, Appendix D) prepared for studies, only one sample (device 31) has exhibited optical nonlinearity. The devices 31 and 32-36 differ in age, also their *I/V* response is dramatically different.

The source of a space-charge field formation and ageing in device 31 has been studied in detail. The Freedericksz transition and *I/V* studies favour charge complexes formation mechanism but do not exclude adsorption of the dopant on the cell surface. We have shown that the amount of the dopant is too small to form a monolayer on at least one surface of the sample. Nonlinear optical studies indicate asymmetry of the electrodes (cell surfaces) suggesting surface influence, but do not exclude charge complex formation. Therefore, both mechanisms could be present simultaneously in the studied device.

MR doped devices have been reported to exhibit large photovoltaic effects and optical nonlinearity through space-charge effects of ionic origin (e.g. [16,70]). Our MR doped systems exhibit effects of ionic origin only when an external electric field is applied. Without the application of an external electric field in MR doped LC films the nonlinear effect is due to trans-cis isomerisation of MR molecules (similar to the findings of Chen and Brady for methyl red sodium salt dopant[89]).

A strong dependence of the ionic effects on previous illumination history suggests surface influence on the generated photovoltage (following a suggestion by Prof. Simoni). We have found that the alignment agent influences both, the magnitude and temporal characteristics of the internally generated photovoltage.

Nonlinearity in DC161 doped systems studied for the first time in this research work was found to be not of ionic or space-charge origin. The photorefractive-like effect in these systems has trans-cis isomerism as the underlying mechanism, possibly enhanced by the differences in the interaction of the host with trans and cis isomers[*].

The dynamic and permanent/persistent surface effects are attributed to particular alignment agents. They have been obtained in MR doped systems (confirming the earlier reports). It has been found for the first time that PI and ITO surfaces allow good dynamic operation of the MR systems without permanent or persistent components.

C_{60} doped NLC have been reported by other groups to exhibit permanent/persistent effects with particular alignments[16]. These long-term surface effects have not been observed in C_{60} and DC161 doped devices in conjunction with the alignment agents used in this work.

We suggest that it is feasible to exploit the particular mechanism of nonlinearity out of a large number of possible ones in particular system by the selection of alignment surface, interaction geometry and external field regimes.

---

[*] E.g. the response of 5CB doped devices is generally larger then that of E7 and BLO48 samples. This may have various reasons, one of which being that different host materials interact differently with the dopant. Such dependence is characteristic of Janossy effect. The influence of the host material is discussed in more detail in Chapter 6.

CHAPTER 6

CHROMOPHORE DOPED NLC IN DEVICE APPLICATIONS

In this chapter we focus on the specific characteristics of devices and their optimal operating regimes. The efficiency of single layer devices, their resolution and temporal characteristics of switching are studied in detail.

It is found that even very carefully prepared MR doped devices deteriorate very quickly, which is unacceptable for applications. C_{60} doped devices are interesting, but fundamentally have a strong dependence of efficiency on the spatial frequency of the hologram. We further focus on the DC161 dye-doped nematic liquid crystals and show that they are interesting materials for optically addressed spatial light modulators.

6.1 Operational characteristics: geometry, power and wavelength

Here the optimal operating regime of the devices is defined and other special considerations concerning device operation including saturation of the nonlinearity with the increasing optical power of the writing beams, its wavelength dependence and dynamic characteristics are discussed.

6.1.1 Optimal geometry

Under optimal geometry we understand the most effective relative location of the device and writing and reading beams, directions of beam polarisation and liquid crystal director axis.

6.1.1.1 Systems doped with dichroic dyes

For the optimal efficiency of reading the phase profile, which is formed in the planar aligned nematic devices, the reading beam polarisation has to be parallel to the director axis (alignment direction). This is observed experimentally (Figure 6.1).

Indeed, any change in the orientation of LC director would lead to a change in the extraordinary refractive index much larger than in the ordinary. In the case of an uncorrelated change in orientation (order parameter change), the relation between the change of the corresponding refractive indices dn_o and dn_e has been shown in Chapter 5 to be

$$dn_e = 2\frac{n_o}{n_e}dn_o$$

5.4

In the case of 5CB, where n_o=1.53 and n_e=1.71, $dn_e \approx 1.79 dn_o$. In the correlated molecular reorientation observed in DC161 doped devices the ratio between dn_e and dn_o is even larger. Thus, the extraordinarily polarised beam must be used for probing written patterns in all planar aligned devices.

The optimal result in DC161 doped systems is obtained for the case of normal incidence of light (see Figure 5.12, previous Chapter), with writing and reading beam polarisation parallel to the director axis (Figure 6.1 and Figure 6.2). This is also the dye's LETO[*] (and max absorption) direction, as has been confirmed by spectroscopy in polarised light. Maximum efficiency in systems doped with dichroic dyes undergoing trans-cis isomerisation is expected to be in this geometry, i.e., when the absorption of the writing beam is maximised.

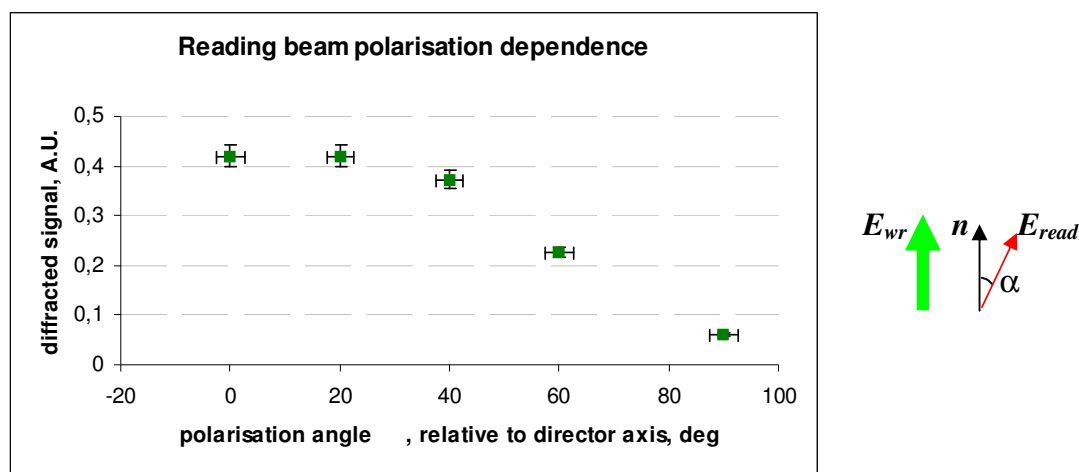[*] Long-wave electron transition oscillator.

Figure 6.1. Dependence of diffracted signal on a reading beam polarisation (angle α on the inset to the right). The device is 10μm thick 1%DC161+5CB.
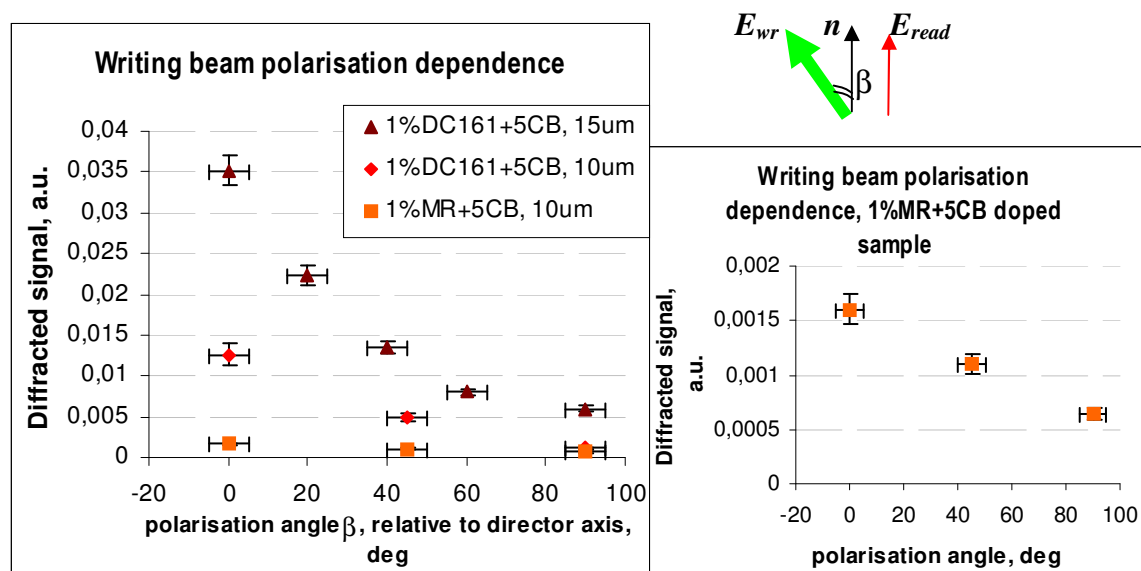

Figure 6.2. Dependence of diffracted signal on a writing beam polarisation (angle β on the inset at the top right). The graph on the right gives a better view of the performance of 1%MR doped 5CB 10μm device exhibiting a very weak signal.

As has been discussed in the previous chapter, MR doped devices exhibit various effects. Alignments (planar or homeotropic) and geometries (normal incidence or tilted device) as well as the external field regime will support a certain mechanism of nonlinearity.

For the fastest operation at no external fields, planar alignment and normal incidence are chosen to exploit trans-cis isomerisation as a mechanism leading to

nonlinearity. In this case, the highest efficiency is obtained when the writing beams are polarised along the dye's **trans** state LETO direction, which happens to be parallel to the LC director in our systems as shown by polarisation spectroscopy studies.

The dependence of efficiency on the tilt or rotation of the sample or beam polarisations is not critical in all thin* devices. We have shown, that a diffracted signal changes only slightly when the sample is tilted (by 25% with 45° tilt)[95]. One would expect a strong dependence on the tilt angle in dichroic dye-doped systems at least because the absorption of the dye decreases as the sample is tilted. Such a small difference up to a 45° tilt can be explained by the fact that the effective sample thickness as seen by the reading beam increases with tilt and compensates to some extent for the reduced absorption. Also due to the high refractive index of the LC, the actual angle of the beams in the sample is much smaller – around 30.4° when the angle in the air is 60°. Thus, positioning of the device within the optical system is not sensitive to misalignment. This is a very big advantage for applications.

The possibility of using normal incidence is another advantage of the discussed systems, imaging is simple in this geometry, and it also makes the control of reflection loss straightforward.

6.1.1.2 Fullerene-doped device

C_{60} doped systems are different from the MR and DC161 systems by being not dichroic, in other words, by having isotropic absorption in relation to light polarisation. For optimal efficiency reading beam polarisation has to be along the director axis. The optimal geometry for observing beam coupling and self-diffraction of the writing beams, the beams' polarisation has to be along the director axis. Normal incidence is usually used, as it is advantageous in applications.

The highest nonlinearity is achieved in the geometry B in the figure below (same as the geometry in Figure 2.6 b (Chapter 2) suggested by Khoo[16]). Geometry A in Figure

---

* As thin devices we would refer to devices usually 25μm and thinner, which operate in the Raman-Nath regime.

6.3 gives the best result when the sample is rotated around the y axis. See Figure 6.4 for comparison of the nonlinearity that could be achieved.
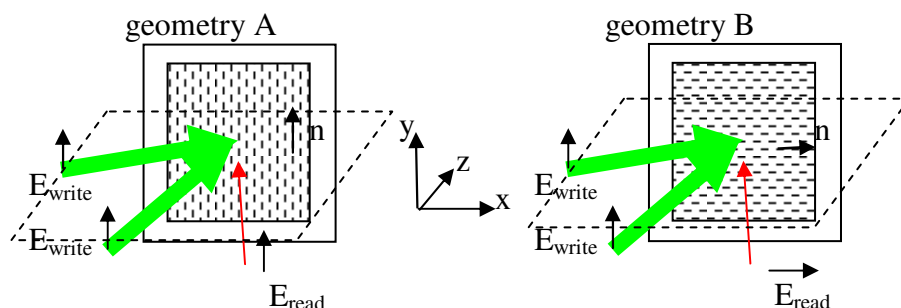

Figure 6.3 Geometries A and B of the experiment. All beams are in the xz plane (shown by the dotted line), normal to the sample. External electric field is applied along z direction.
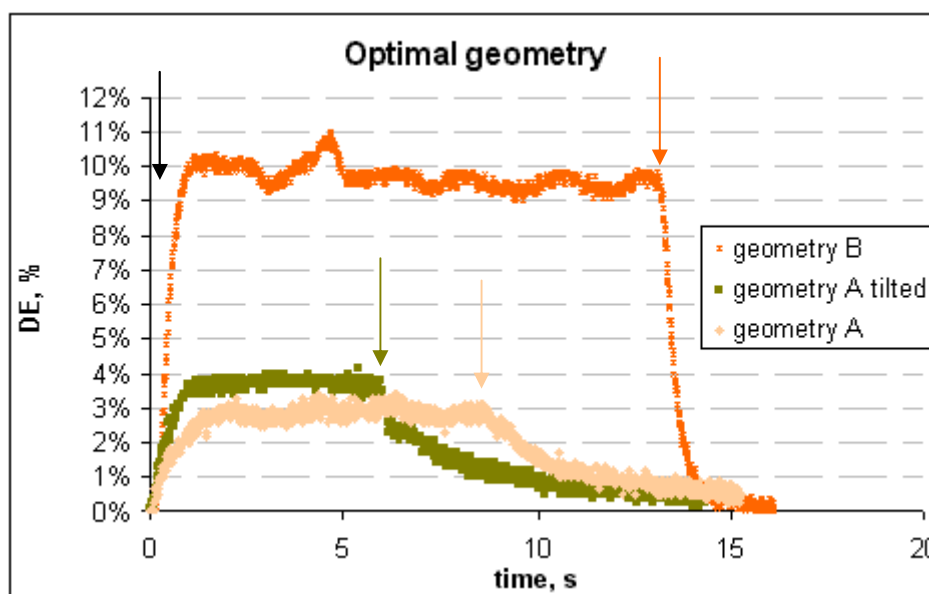
Figure 6.4. Nonlinearity in different geometries (same optical intensity (16mW/cm^2), voltage regime (5.2V$_{DC}$) and light impinging direction (1st electrode front*). The device is planar aligned 20μm C$_{60}$ doped BLO48 (device 31, see Appendix D). The arrows indicate the moments when the writing beams have been switched on and off. The DC field ~5V is constantly applied to the device during the measurement.

---

* See Chapter 5 for more details on electrode anisotropy in the studied C$_{60}$ doped device.

For optimal efficiency, reading beam polarisation has to be along the director axis. The optimal geometry for observing beam coupling and self-diffraction of the writing beams, the beams' polarisation has to be along the director axis.

Scattering of light as the voltage is applied to the sample is present at the operating voltages (Figure 6.5). The scattering hampers good performance of the devices. To minimise the noise from the scattering, the geometry where the grating vector is parallel to the alignment direction of the sample has to be used.

Figure 6.5. Scattering of the reading beam on a sample (device 31, C_{60} doped BLO48) with applied $5V_{DC}$. The device is planarly aligned, and the alignment direction is vertical. To avoid interference from the scattering, a horizontal grating should be recorded, so that the diffracted orders are above and below the main order, not on the sides.

To summarise, in all planar aligned devices studied, normal incidence could be used; the reading beam polarisation has to be along the director axis. The writing beam polarisation when parallel to the LETO of the dichroic dye gives higher efficiency. In C_{60} doped devices an external electric field must be applied. The best results are achieved when the grating vector is parallel to the director.

6.1.2 Wavelength dependence

To choose the appropriate wavelength, we have looked at the performance of the devices using the available range of wavelengths which are generated by Ar+ laser (λ=514nm; 488nm; 476.5nm; 458nm).

In DC161 devices optimal performance is achieved when the writing beam with λ=514nm is used. There is almost no change in efficiency as the wavelength is decreased from 514nm to 488nm, but the dynamics of the grating build up changes (Figure 6.6). As

the wavelength is further decreased, the build up time remains slow, as in the case of λ=488nm, but the efficiency decreases approximately two times as compared to λ=514nm and 488nm (Figure 6.6).

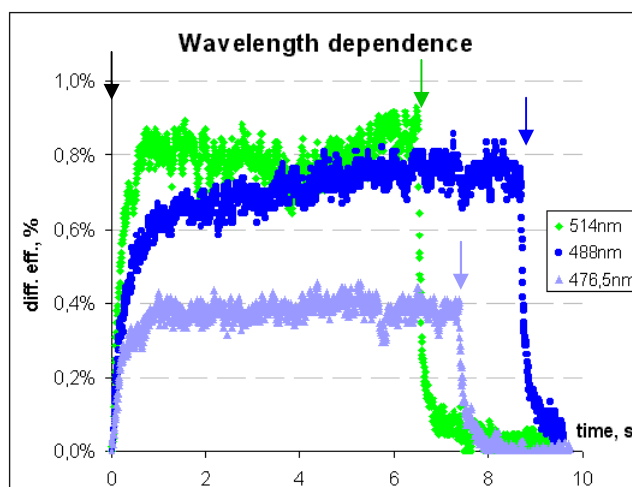*Figure 6.6 Wavelength dependence of 1%DC161 doped 5CB 9μm device (device 3, Appendix D). Arrows indicate the moments when the beams have been switched "on" and "off".*

The imaging arrangement is used (Figure 4.9), and the write intensity and grating spacing is the same for all wavelengths. The device response as the wavelength is decreased may be explained in terms of trans-cis transition as an underlying mechanism.

Photons with energy higher than the gap between the ground and excited state of the dye molecule will excite molecules to higher vibrational energy levels, and more time may be needed for them to relax to either (trans or cis) ground state. This will slow down the build up time of the nonlinearity (as on Figure 6.6), because it will take longer to reach the equilibrium ratio of trans and cis dye species.

The ratio of the number of trans and cis molecules is wavelength specific, so it is natural to expect different efficiency when exciting the system with different wavelengths. The lower magnitude of nonlinearity at λ=476.5nm can be additionally contributed by the decrease in absorptance from 91% (absorption coefficient α=2408) at 514nm to 74% (α=1347) at 476nm.

MR doped systems are more sensitive to light at 488nm, having maximal absorption at 490nm. Nevertheless, they do not show a significant decrease of nonlinearity if λ=514nm is used.

C_{60} doped devices are not expected to exhibit strong wavelength sensitivity, as the absorption spectrum of C_{60} does not exhibit any strong peaks, in contrast with the discussed dyes.

To summarise, it is important to use a corresponding wavelength for the specific dye-doped system. For DC161 doped devices λ=514nm is used, for MR doped devices λ=488nm is used, and for a C_{60} doped device both wavelengths (514nm and 488nm) may be employed.

6.1.3 Optical intensity: saturation

It has been found that diffraction efficiency of the written dynamic gratings at a fixed geometry tends to be higher for the higher writing beam intensities. More important, it saturates at high intensities.

As the optical intensity is increased, nonlinearity rises linearly at low optical intensities (under 10mW/cm^2) and saturates at about 50mW/cm^2 (Figure 6.7). The dynamics of the signal build up change as well. Very similar saturation values and behaviour is exhibited by all DC161 devices.
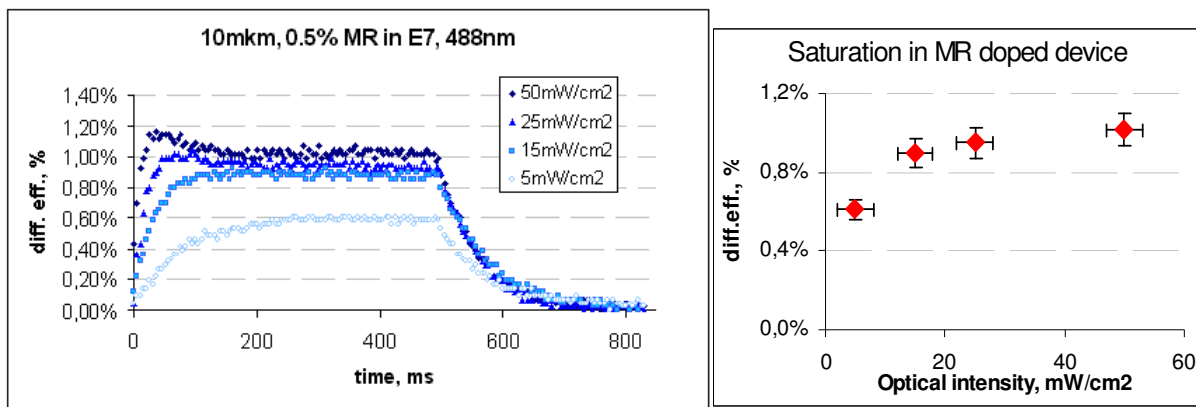
Figure 6.7. Saturation of nonlinearity in 10μm thick 0.5%MR+E7 sample (device 29, Appendix D): response of device to various optical intensities in dynamics. Inset at the right shows diffraction efficiency as a function of optical power. The wavelength used is 488nm.

C_{60} doped LC layers also exhibit higher nonlinearity in conjunction with higher optical powers. As the power of the writing beam is increased, the efficiency in general increases, but when the optical power exceeds 10-15mW/cm^2, the behaviour of the diffracted signal becomes more complicated (Figure 6.8).
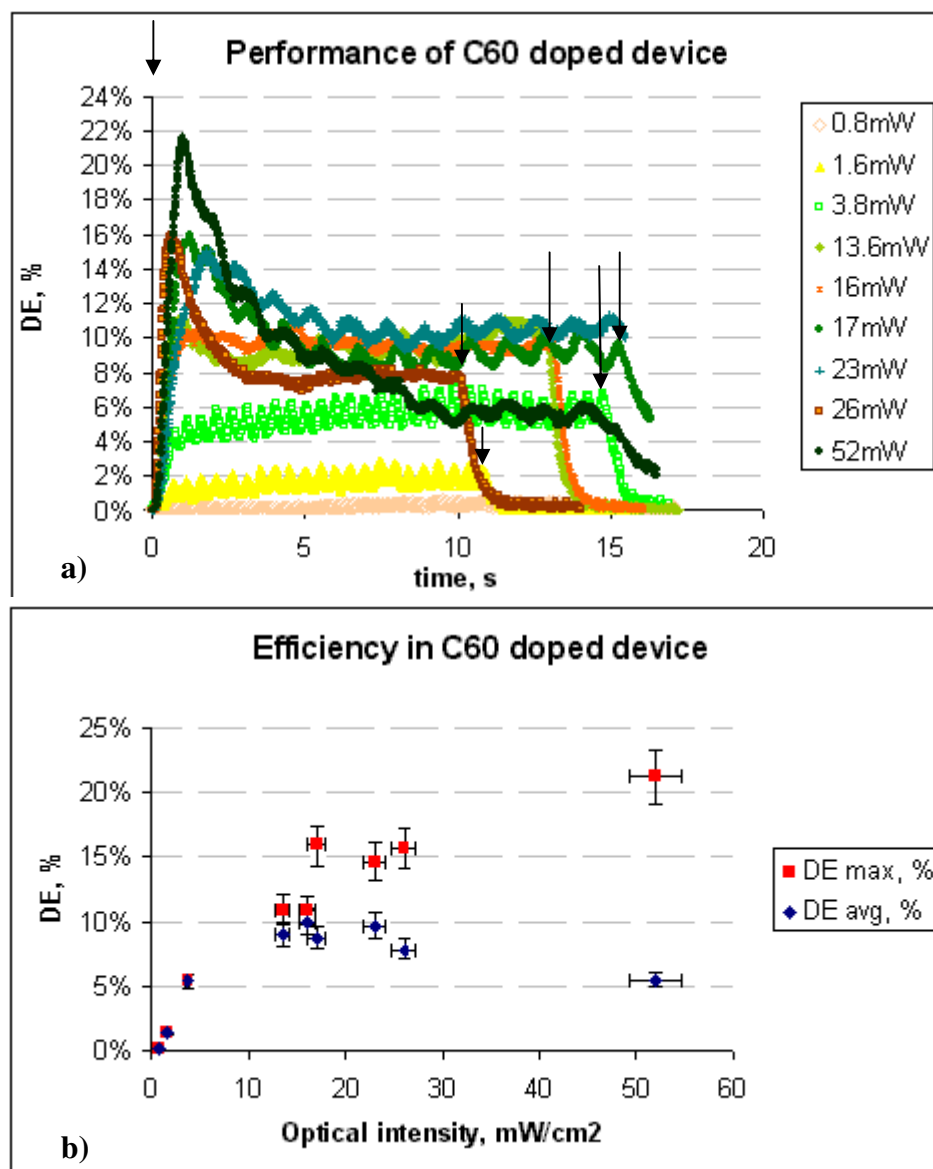
Figure 6.8 Efficiency in the 20μm C$_{60}$ doped BLO48 device (device 31, Appendix D): optical intensity behaviour. The geometry B on Figure 6.3 is employed
a) dynamics of the diffracted signal
b) summary for the overshoots and average values of diffraction efficiency.
The arrows indicate the moments when the writing beams have been switched on/off.

As a conclusion to the above, we note that it is more reliable and better from the power considerations to use an optical power of under 10mW/cm^2 for operating C$_{60}$ doped devices.

The values of diffraction efficiency obtained here are comparable to the ones cited in the literature [46, 70]. Here, for the first time, the imaging of the grating along with the traditional interference pattern creation has been utilised.

Note that all studied devices exhibit very similar saturation and overshoot behaviour. This overshoot is a feature of the experimental arrangement and is general for all devices. It will be discussed in more detail in the following section.

6.2 Dynamics

Nematic liquid crystals have response times of about 20-50ms. This speed is acceptable for a number of applications (see Appendix A). Of course, the aim is to achieve the fastest possible operation for the given system.

The dynamics of nonlinearity exhibited by dye-doped NLC films is complicated. Here we study the influence of operational characteristics like writing beam power, host material, device thickness and spatial frequency of the written hologram on the build up and relaxation times of the resulting diffracted signal in DC161 doped devices.

The chart shows a Signal versus t plot with a red exponentially decaying curve, with markers t_1 near the top at signal ≈ 0.9 and t_2 at signal ≈ 0.1, and the equation $f = e^{-t/\tau}$.
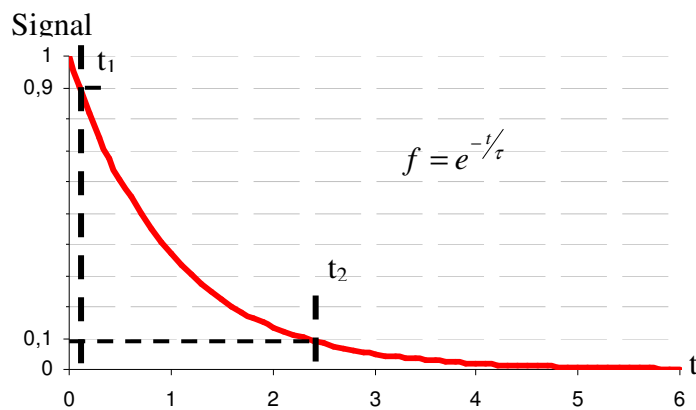
Figure 6.9. Relaxation process: decay time (t_2-t_1) and decay constant (τ) of an exponentially decaying function f.

Relaxation and build up of the written hologram can be described by the following temporal parameters:

⇒ t_{rise} / t_{decay}[*] - the rise / decay time - the time it takes for the diffracted signal to rise from 10% of its value to 90% / decay from 90% of the signal's value to 10%.

⇒ τ_{decay} - relaxation can be described by an exponential function exp($-t/\tau$), where τ is a decay constant.

Decay time and constant are connected in the following manner. Consider the relaxation process in Figure 6.9, the time it takes for the diffracted signal to decay from 90% of the signal's value to 10%, t_{decay} is t_2-t_1.

Writing down equations for both points of time,

$$\begin{cases} f_{t=t_1} = e^{-t_1/\tau} = 0.1 \\ f_{t=t_2} = e^{-t_2/\tau} = 0.9 \end{cases}$$

6.1

solving this system relative to t_2-t_1:

$$\frac{t_2 - t_1}{\tau} = -\ln\frac{1}{9} \approx 2.2$$

6.2

Hence, the nonlinearity decays in 2.2τ, where τ is the decay constant.

The max frequency at which the device can be operated is:

$$f_{max} = \frac{1}{t_{rise} + t_{decay}}$$

6.3

We measure the decay constant by approximating the appropriate parts of the graphs of diffracted signal dynamic behaviour with an exponential function of the form $e^{-t/\tau}$. In this, the statistical error due to the noise and fluctuations in the signal is minimised, as many data points are approximated at the same time. The decay time can be easily calculated from the decay constant.

---

[*] t_2-t_1 on Figure 6.9.

When comparing decay constants obtained from the diffraction efficiency measurements with theoretical values which are calculated for molecular reorientation dynamics, we must take into account the fact that the diffracted signal is proportional (in the first approximation) to the square of refractive index change. Thus if the relaxation of the refractive index change is described by the function $e^{-t/\tau}$, the diffraction efficiency relaxation would follow the $e^{-2t/\tau}$, and the resulting decay constant:

$$\tau_{DE} = \frac{\tau_{dn}}{2}$$

6.4

Similar considerations are valid for the rise times, with the addition that the build up dynamics is described by $(1-e^{-\alpha t})$, but the diffraction efficiency would be proportional to the $\sim(1-e^{-\alpha t})^2$, which cannot be described by a single exponential law.

Both cases are illustrated in Figure 6.10. Actual experimental values of diffraction efficiency and dynamics are used for the calculation of the refractive index change (following Equations 2.26 in Chapter 2).
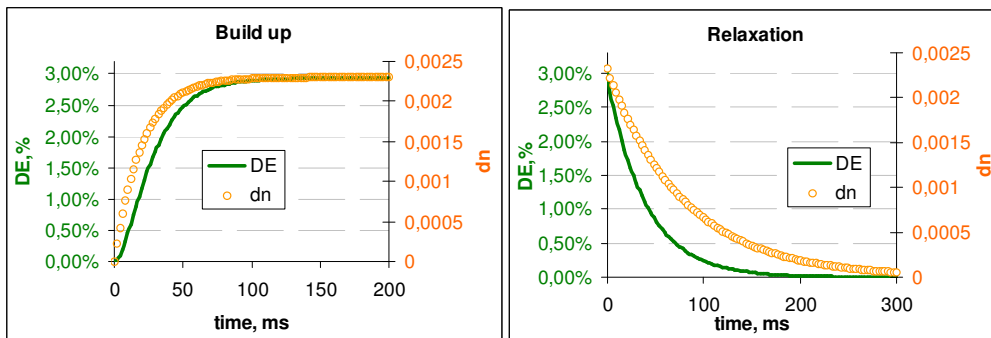
Figure 6.10 The calculated build up and relaxation dynamics of diffracted signal (solid line) and refractive index change (open circles).

Because the build up of the nonlinearity cannot be approximated with a single exponential function, the t_{rise} is calculated directly from the measurement.

The typical dynamic behaviour of a dye-doped nematic device is shown in Figure 6.11 for the example of 1%DC161 doped 5CB. The relaxation of liquid crystal has an exponential form while the build up process is more complicated.
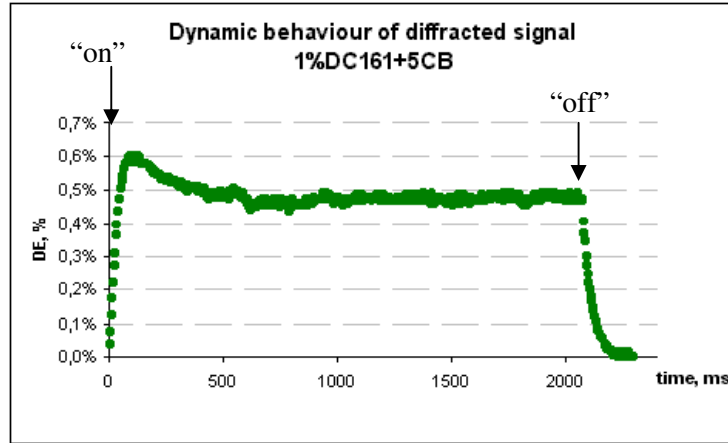
Figure 6.11. Typical dynamic behaviour of diffracted signal. The setup described on Figure 4.10 is used, λ=514nm; optical power 50mW/cm² ; sample is 1%DC161 doped 5CB, 9μm thick (device 3). The arrows indicate the time when the writing beams are switched "on" and "off".

6.2.1 Relaxation: decay times

The observed decay times from devices of various thickness (5-20μm) based on different host materials are within 40-110ms (decay constants 18-60ms) (see Table 6.1).

The decay constant from the pure thermal effect is of the order of 100μs [8], and of the orientational effects – around 10-100ms, so the time scale of the nonlinearity is defined by molecular motion.

There can be two contributions to the relaxation dynamics of orientational effects in the dye-doped systems: from the *LC* and from the *dye molecules*.

The decay constant of the liquid crystal is defined by its viscous and elastic properties and is derived from the viscous, elastic and optical torque balance equation in reference 8 (pp. 139-143). For sinusoidal optical intensity[8]:

$$\tau_{LC} = \frac{\gamma}{K\left(\dfrac{4\pi^2}{\Lambda^2} + \dfrac{\pi^2}{d^2}\right)}$$

6.5

where γ is the effective viscosity of the LC material, K is the elastic constant; d is the LC film thickness and Λ is the fringe spacing.

The decay constant for diffraction efficiency based on equation 6.4 would be:

$$\tau_{LC} = \frac{\gamma}{2K\left(\dfrac{4\pi^2}{\Lambda^2} + \dfrac{\pi^2}{d^2}\right)}$$

6.6

The observed decay times and constants are longer than the ones calculated from (6.5) (Table 6.1). There is almost no dependence of the decay time on the sample thickness even when the grating spacing is of the order of, or larger than, the thickness. Thus the relation (6.5) does not govern the relaxation in our systems. It will now be shown the dye diffusion is responsible for the temporal switching characteristics of the devices.

Name	Material	Thickness	Experimental τ_{decay}, ms	Calculated τ_{decay}, ms
1	5CB+1%DC161, old sample	15μm	55±2	10.5
2	5CB+0.5%DC161, old sample	15μm	50±2	10.5
3	5CB+1%DC161, old sample	9μm	50±2	8.5
4	5CB+0.5%DC161, old sample	9μm	50±2	8.5
5	5CB+1%DC161, old sample	5μm	49±2	5
6	5CB+0.5%DC161, old sample	5μm	40±2	5
7	5CB+1%DC161	20μm	50±2	11
8	5CB+1%DC161	20μm	60±2	11
9	5CB+1%DC161	14μm	50±2	10
10	5CB+1%DC161, purified dye	10μm	35±2	8.5
11	5CB+1%DC161	10μm	40±2	8.5

Continued…

…continued

Name	Material	Thickness	Experimental τ_{decay}, ms	Calculated τ_{decay}, ms
13	BLO48+1%DC161	14μm	20±2	5
14	BLO48+0.5%DC161	14μm	20±2	5
15	BLO48+1%DC161	10μm	18±2	4
16	BLO48+0.5%DC161	10μm	20±2	4
21	E7+1%DC161	14μm	20±2	6
22	E7+0.5%DC161	14μm	20±2	6
23	E7+1%DC161	10μm	20±2	5
24	E7+0.5%DC161, purified dye	10μm	30±2	5
25	E7+0.5%DC161	10μm	20±2	5

Table 6.1. Relaxation of devices of various thickness and based on different host materials. The optical setup in Figure 4.12 with the grating spacing 12.5µm and optical power 50mW/cm² is used. Decay time is calculated using relation 6.5 (for respective elastic constants and host materials viscosity, see Appendix B).

Let us consider the possible effect of the dye on the decay time. As suggested earlier[99], excited dye species will diffuse into non-illuminated regions, and the decay times will depend on this diffusion, the grating spacing and the lifetime of excited state.

Consider the dye molecule with two ground levels (trans and cis) (see Chapter 2). We assume that the lifetime of the excited and possible triplet states is very short compared to the lifetime of the ground states (this correlates with the calculations in Appendix F). In this case, the population of excited states may be neglected in the linear region of optical excitation, which is a good approximation for the low optical powers used.

For this case, the rate of change of the number of cis species at any moment would obey the relation (similar to the equation used by Janossy[67] for treating absorption in the presence of isomerisation):

$$\frac{\partial N_{cis}}{\partial t} = \left((N - N_{cis})\sigma_{trans}\Phi_{trans-cis} - N_{cis}\sigma_{cis}\Phi_{cis-trans}\right)\frac{I}{h\nu} - \frac{N_{cis}}{T_{cis}} + D_y\frac{\partial^2 N_{cis}}{\partial y^2}$$

6.7

where:

N is the number of dye molecules per unit volume,

N_{cis} is the number of the cis species;

σ_{trans} and σ_{cis} are the cross sections of absorption of a photon with energy $h\nu$ for trans and cis isomers;

$\Phi_{trans-cis}$ and $\Phi_{cis-trans}$ are quantum efficiencies of the respective transitions;

D_y is the diffusion coefficient in the y direction;

T_{cis} is the lifetime of the cis state;

$I=I(y)$ is a periodic optical field characterised by the grating spacing Λ.

Solution of this equation when the optical intensity is switched off can be written in the form:

$$\frac{\partial N_{cis}}{\partial t} = -\frac{N_{cis}}{T_{cis}} + D_y\frac{\partial^2 N_{cis}}{\partial y^2}$$

6.8

Since we know that at t=0

$$N_{cis} = N_{cis}^{max}\sin\left(\frac{2\pi y}{\Lambda}\right)$$

6.9

this gives a similar relation for the relaxation constant as in [99]:

$$\tau_{dye} = \frac{1}{\left(D_y\frac{4\pi^2}{\Lambda^2} + \frac{1}{T_{cis}}\right)}$$

6.10

The diffraction efficiency decay time follows the relation given by 6.4:

$$\tau_{DE} = \frac{\tau_{dye}}{2}$$

6.4

The experimentally measured relaxation times in samples of different thickness are shown in Figure 6.12. The relaxation time increases as the grating spacing is increased, and starts to saturate for spacings higher than 20µm.

The experimental data has been approximated using relation (6.10) (solid line in Figure 6.12). The following fitting parameters have been used: $D_y = 7\mu m^2/s$; $T_{cis} = 120ms$. The fact that these parameters are the same for all 5CB doped with DC161 films regardless of the dye concentration, the age of a sample and an alignment interface supports the discussed idea of dye contribution.
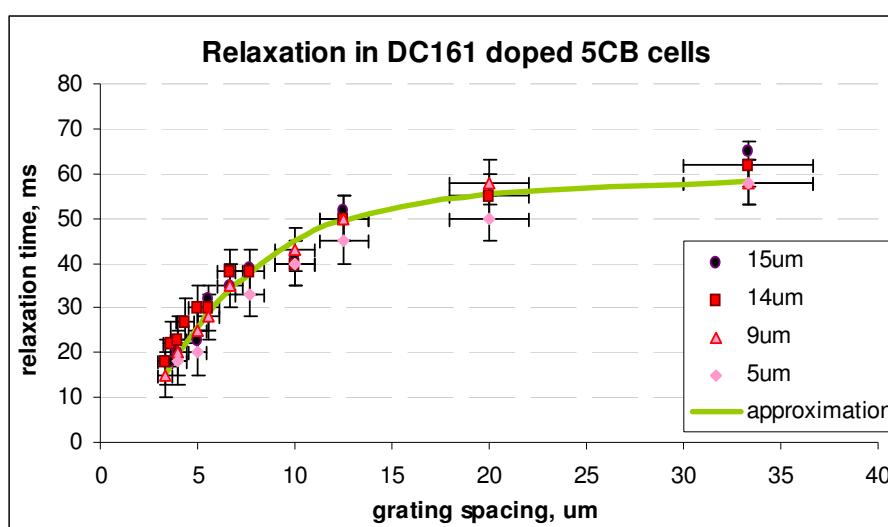
Figure 6.12. Relaxation in 5CB films doped with 1% of DC161 dye (devices 1, 9, 3, 5), dependence on the grating spacing. The Michelson interferometer arrangement in Figure 4.14 is used, the intensity of the writing beams is 50mW/cm². The solid line is a fitting curve according to the relations 6.10 and 6.4. Relaxation of 0.5% films is not shown, as they have almost the same relaxation characteristics.

At a large grating spacing in thick samples the LC relaxation time might become longer than the contribution of the dye, and the relaxation dynamics will be governed by (6.5). The calculation shows that in 5CB devices the relaxation dynamics may be governed by the elastic properties of a liquid crystal only in devices thicker than 20µm. The grating spacing threshold at which this occurs decreases from $\Lambda = 50\mu m$ for 30µm thick devices to about $\Lambda = 40\mu m$ as the device thickness is increased to over 50µm.

We observe a dependence of relaxation time on the writing light intensity (Figure 6.13).

Samples switch off faster when a higher light intensity of the writing beams has been used. For example, the decay constant τ associated with diffracted signal at writing beam intensity *30mW/cm^2* is **46ms**, while the decay constant associated with *1W/cm^2* is **33ms**. As the power of the light cannot influence the relaxation directly, we suggest that it can affect parameters that are functions of temperature, namely viscosity, elastic constants or dye diffusivity and also stimulate cis-trans thermal back relaxation.[63]
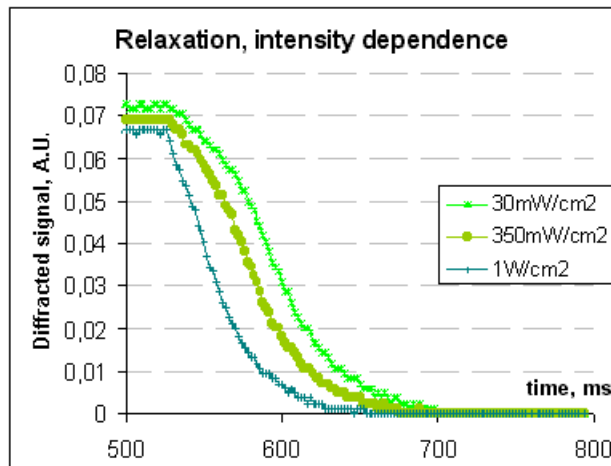
Figure 6.13. Writing beam intensity dependence of relaxation process. Optical setup in Figure 4.10 with the grating spacing 12.5µm is used. The device is 10µm thick 5CB+1%DC161 (device 11, Appendix D).

6.2.2 Build up: rise times and overshoot

The rise times of the nonlinear effect depend on many parameters, including wavelength and optical power. In DC161 doped systems the fastest operation is achieved using writing beams at λ=514nm. We study the dynamics of nonlinearity build up as a function of operating and device parameters, such as optical power, sample material and thickness, and grating spacing.

6.2.2.1 <u>Optical power:</u>

When the optical power is increased, the nonlinearity builds up faster (Figure 6.14). This is observed in MR and in DC161 devices[*]. The rise time can become as short as **6±2ms** at *1W/cm^2* (more than 10 times the difference as compared to 50 mW/cm^2).

The possibility to shorten the rise times by using high optical powers is an important result for the applications.

6.2.2.2 <u>Grating spacing:</u>

In contrast with the relaxation behaviour, the rise time has not been found to depend on grating spacing in any of the DC161 doped devices. Even more fascinating, neither has any dependence on the host material been found. Rise time in 5CB devices is the same as in E7 and BLO48 doped devices.

The observed rise time independence on the grating spacing (compare with equation 6.10 for decay time) indicates that diffusion does not play an important part in the build up process.

6.2.2.3 <u>Device thickness:</u>

Weak dependence of the rise time on the device thickness has been found (Table 6.2).

Device thickness, μm	t_{rise}
5μm (device 5)	**62ms±5ms**
10μm (device 3)	**70ms±10ms**
15μm (device 1)	**84ms±10ms**

Table 6.2. Nonlinearity rise times in 1% DC161 5CB doped devices. Optical setup on Figure 4.12 is used; the optical power of the writing beams is 50mW/cm^2. The rise constants are calculated from the rise times for the purpose of comparing with the decay dynamics.

---

[*] For example, in the 5μm thick 1% DC161 doped sample at writing wavelength 514nm the t_{rise} time decreases from approximately 70ms at writing beam optical intensity 20mW/cm^2 to about 30ms at 80mW/cm^2.

This dependence may be attributed to the strong intensity dependence of the rise time and explained by the fact that writing beam intensity significantly decreases in thick devices. Due to strong absorption, some part of the device will receive significantly less power and the resulting response of the device would be slower.

6.2.2.4 Overshoot

At high optical powers (above 30mW/cm^2), an overshoot appears (Figure 6.14). Overshoot magnitude, rise and decay times strongly depend on the writing beam intensity.
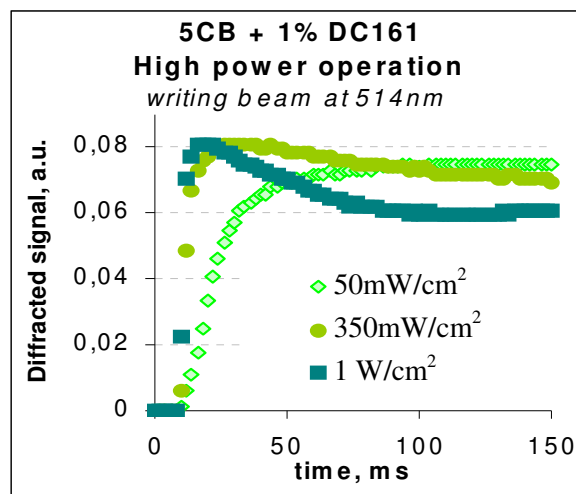
Figure 6.14. Nonlinearity build up, intensity dependence. 1%DC161 doped 5CB; thickness 10μm (device 11). The experimental arrangement in Figure 4.10 is used. The grating spacing is 12.5μm.

Overshoot has a peculiar behaviour. First of all, it is quite slow and cannot be attributed to thermal effect. The time scale suggests an orientational origin. Secondly, it is the same in various host materials with both MR and DC161 dyes as dopants, hence is not of guest-host interaction nature (also the possibility of the molecules in the excited state contributing to the overall reorientation is excluded[*] taking into consideration the time scale of the effect). Third, and most important, the overshoot is **_not always_** observed, and the form and amplitude of diffraction efficiency build up (but not its dynamics) depends on the setup used.

---

[*] Excited state lifetime in 10ms range is unlikely.

We attempt to explain this phenomenon by the imperfect contrast of the intensity profile[*] formed on the sample. The explanation is given from the point of view of trans-cis isomerisation as the main nonlinearity mechanism.

6.2.2.5 Cis species build up dynamics

The build up dynamics of cis species is theoretically treated in Appendix F. There we show that the build up can be described by:

$$N_{cis} = \frac{\beta}{\alpha}\left(1 - e^{-\alpha t}\right)$$

6.11

where

$$\alpha = N\left(\frac{1}{T_{cis}} + \frac{\sigma_{cis}\Phi_{cis-trans}I}{h\nu} + \frac{\sigma_{trans}\Phi_{trans-cis}I}{h\nu}\right) \qquad \beta = N\frac{\sigma_{trans}\Phi_{trans-cis}I}{h\nu}$$

6.12

An important conclusion is that from 6.12, $\alpha = \alpha(I)$, and therefore the build up dynamics of cis species depends on optical intensity of the writing beam. As the LC molecular motion (20-50ms) is of the same order and even faster then cis state lifetime (T_{cis}=120ms, as shown in the previous section), the molecular reorientation, refractive index change and diffracted signal will follow the behaviour of the cis population dynamics.

The dependence of diffracted signal rise time on the optical intensity of writing beams is exactly what we observe in the experiment (see for example Figure 6.14).

6.2.2.6 Influence of the intensity profile contrast

When excited by light, dye molecules undergo trans-cis isomerisation and a certain cis state population builds up, according to the wavelength and optical intensity. This process is described in Appendix F.

---

[*] In fact, the contrast is different in the setups used.

Until now we have assumed that there is no light in the "non illuminated" areas of the device. In practice this is not the case, and along with the optical field in the bright fringes of the interference pattern or bright areas imaged on the device there would be some stray light in the areas, which are supposed to be dark. This happens due to imperfect optical components, interfering beams decoherence or aberrations in the imaging system.

The presence of writing light in the dark regions would lead to cis population build up in these areas and to consequent reorientation and refractive index change. The diffracted signal relies on the difference of the refractive index in bright and dark areas, so if there were a refractive index change in dark areas as well as in bright, the resulting efficiency of the device would be lower.

Moreover, the build up of cis population dynamics depends on the optical intensity. In this case the steady state in bright regions would be reached faster then in dark regions, and the difference in the number of cis species in bright and dark areas as a function of time will have an overshoot. This behaviour of cis population in bright and dark regions would lead to the diffracted signal exhibiting an overshoot as well.

The calculation of the temporal behaviour of the diffracted signal (described in detail in Appendix F) is made for various contrasts of the intensity profile but fixed total optical power (Figure 6.15).

Here $V = \dfrac{I_{bright} - I_{dark}}{I_{bright} + I_{dark}}$ is the contrast, also known as the visibility function.
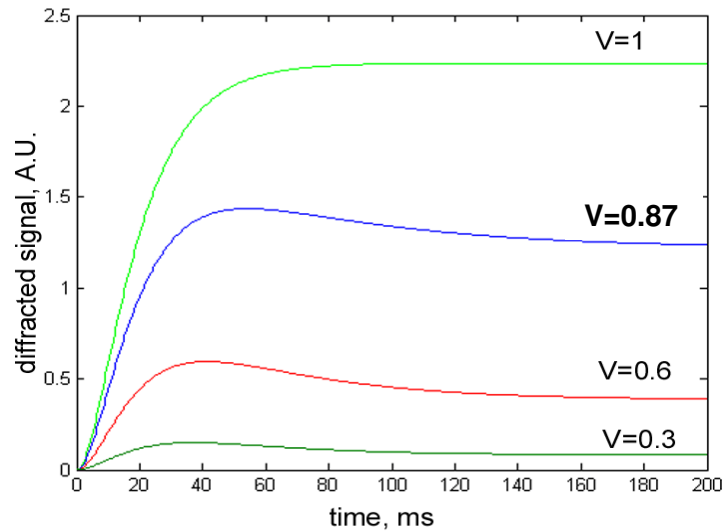

Figure 6.15 Diffracted signal calculated for the same total optical power and various values of contrast (see Appendix F).

If the contrast is approaching 1, no overshoot can be observed. As the quality of the interference pattern or projected diffraction grating decreases, the diffracted signal decreases and the overshoot is observed. When the contrast is particularly poor, the intensities in dark and bright fringes do not differ significantly and the build up dynamics of cis population is similar, hence the overshoot may be no longer observed (curve for V=0.3 in Figure 6.15).

Our observations support this proposed mechanism. In the experimental arrangements which produce a very low diffracted signal (and large noise) no overshoot is observed even at high optical powers, while in the setups which produce large diffracted signals in studied devices the overshoots become significant already at optical intensities 40-50mW/cm^2. If the optical power is further increased, the observed overshoot becomes larger, and its peak narrower, build up time decreases. At high optical powers, the stationary value of the diffracted signal becomes smaller than at lower intensities (see experimentally observed behaviour on Figure 6.17).

Calculation according to the discussed model of cis species build up and imperfect contrast for various optical intensities and fixed contrast ratio of V=0.87 gives a picture similar to results observed experimentally (Figure 6.14 and Figure 6.17)
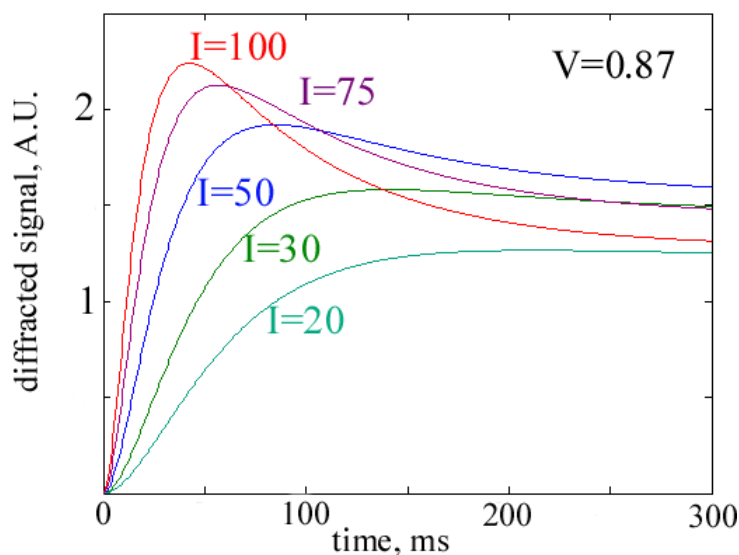

Figure 6.16 Calculated dependence of diffraction efficiency dynamic behaviour on the optical intensity (optical power is in arbitrary units).*

---

* See Appendix F.

As can be seen from Figure 6.16, our model qualitively describes the experimentally observed shortening of the rise time (Figure 6.14, Figure 6.17) and the appearance of the overshoot as well as behaviour of the stationary value of diffracted signal (growth, saturation and decrease) as the optical intensity is increased.

A more careful analysis has been made in an attempt to check the model viability and compare it with the experimental results. The diffraction efficiency of the device is calculated, assuming the linear dependence of the refractive index change on the number of cis isomers, where q is the proportionality constant and Δn is the birefringence of LC material:

$$dn = q \cdot \Delta n \cdot N_{cis}$$

6.13

The number of cis isomers N_{cis} is calculated using the described model (Equations 6.11 and 6.12). The number of dye molecules per unit volume is calculated based on the dye concentration by weight and atomic masses of the LC and dye molecules. The value of absorption cross-section is defined to be:[67]

$$N\sigma_i = \alpha_i; \qquad i = trans, cis$$

6.14

where α_{trans} and α_{cis} are the absorption coefficients of trans and cis components. Absorption coefficients of trans and cis dye species have been obtained following an experimental technique by Janossy[67], but in planar samples. In this geometry optically induced reorientation of LC director is difficult to control. The reorientation of LC may lead to reorientation of dye molecules resulting in the change of absorption. Therefore, the coefficients calculated from experimental measurements in planar cells contain a systematic error. Nevertheless, they can be a good guide when testing the model and underlying hypothesis that the observed dynamic behaviour is due to trans-cis transition and imperfect contrast of the bright and dark areas.

The calculation is made using *Matlab* software package and is described in detail in Appendix F. Here we will note some values used for the calculation and the assumptions made:

➢ The quantum efficiencies of transitions are not known and have been chosen as equal; the values of quantum efficiencies have been derived from the best fit of the experiment with the calculation ($\Phi_{trans-cis} = \Phi_{cis-trans} = 0.3$).

➢ The contrast is chosen to be *V=0.9*.

➢ Optical intensity per unit area divided by the energy of one photon, which is used in the discussed equations, yields the number of photons per unit time per unit area and is easily calculated for the given optical power and wavelength.

The model does not account for the decrease of the optical power due to absorption in the sample. In order to minimise the related error we have chosen a thin 5µm device for comparison.
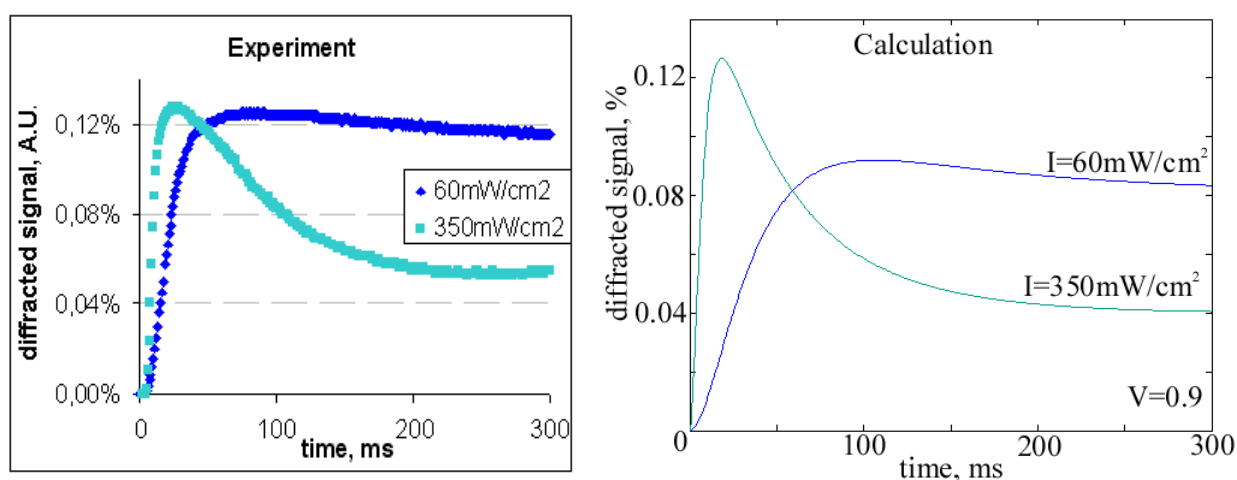
Figure 6.17 Experimentally observed and calculated (see Appendix F) overshoot at different optical intensities. 5µm 1%DC161+5CB sample; writing beam wavelength λ=488nm.

As can be seen from the above, the discussed model gives a good approximation of the complicated dynamic behaviour of dye-doped liquid crystals.

6.2.2.7 <u>Device operation</u>

The approximate frequency of the device operation can be estimated from Equation **6.3**. For 15µm DC161 doped 5CB devices the total rise and decay time at 50mW/cm^2 will be around ***200ms*** which corresponds to *f_{max}=5Hz*. This value could be increased to ***10Hz*** in thin DC161 doped BLO48 samples if using a small grating spacing (10µm). The high optical power of writing beams may be also used to further decrease rise and relaxation times.

6.3 Diffraction Efficiency

The diffraction efficiency of devices is one of the most straightforward characteristics that could be used to evaluate the nonlinear response of the materials under study. We have already used it to define the optimal wavelength, optical power, geometry and polarisation operational regimes. Here a more detailed study of dye concentration and device thickness influence is presented for the DC161 doped systems.

Diffraction efficiency is measured using 12.5µm grating spacing (80 line pairs/mm) and light intensity 50mW/cm^2. This light intensity ensures a large response from the devices. In fact, at this power, the response of 9µm and 10µm MR and DC161 devices saturates (see e.g. Figure 6.7).

6.3.1 Errors of measurements

The main errors come from the nonuniformity of the devices and occasional misalignment leading to larger reflection losses. These errors have been calculated from the measurements using the fixed geometry of the experiment, and different spots from the whole device area. These error values for each device are usually applicable to most measurements conducted in this research work. Errors vary from 5.1% to 14%, average values being around 8%-9%.

The results obtained from different experimental arrangements are usually very different, as it is very difficult to control the contrast and quality of the formed intensity profile on the device. In order to be able to compare results from different arrangements, only relative values and measurements are used. For example, optical power of saturation of efficiency, not absolute efficiency values are compared. When we need to compare absolute values, the same arrangement is used.

6.3.2 Ageing effect

The preliminary studies[*] have revealed very similar behaviour and approximately the same diffraction efficiency in freshly prepared samples filled with 5CB doped with MR

---

[*] In these preliminary studies, samples are tilted 45°, so that the plane, in which lie electrical vectors of writing beams, creates an angle with the director axis. Unexpanded Gaussian beams are used. The studies were mainly performed at Penn State University during a research visit.

and DC161 (Figure 6.18). In MR samples, efficiency could be improved by the application of DC field around 2V leading to space charge field build up (see also Chapter 5).

Freshly filled devices made following both procedures, sealed and temporary (see Chapter 3), are compared in Figure 6.18. Writing beams are switched on at t=0 ms, the duration of pulse is about 500 ms. The dynamics in all devices is very similar. The efficiency in the temporary devices (Figure 6.18, open squares and triangles for DC161 and MR doped devices respectively) is lower, probably due to the comparatively bad alignment and higher content of impurities.

At the same dopant concentration (by weight), MR devices exhibit higher nonlinearity than DC161 doped devices.
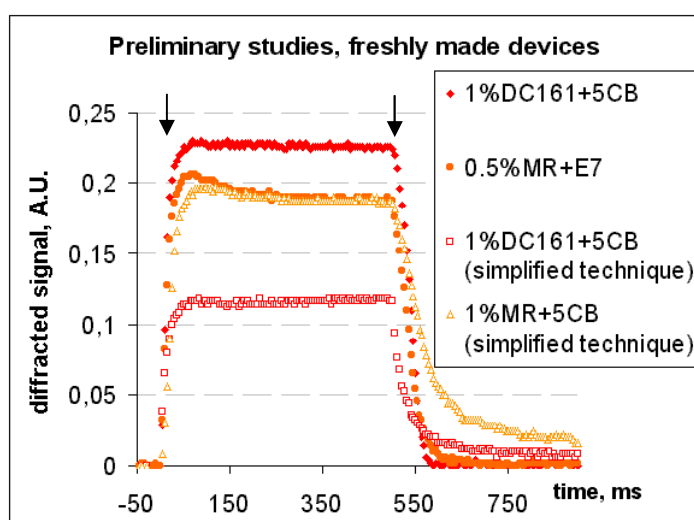
Figure 6.18. Diffraction efficiency in fresh 5CB and E7 samples doped with 0.5% MR (device 29) and 1% MR and 1% DC161 (device 11). The experimental arrangement in Figure 4.10 is used, writing beams are at λ=488 nm, grating spacing 17 μm, optical power 30 mW/cm^2. The arrows indicate writing beams' on and off moments.

MR doped devices prepared following the simplified technique deteriorate within one month. The efficiency of carefully prepared[*] MR based devices in two years' time has also significantly decreased. The diffracted signal from these devices is now barely visible, and is more than an order of magnitude smaller than in the corresponding DC161 devices.

---

[*] Following the full procedure described in Chapter 3.

Microscopy studies have revealed a network of defects in the deteriorated samples (Figure 6. 19). These defects are almost certainly the clusters of a crystallised dye. They are likely to be the cause of the very low sample efficiency at present.
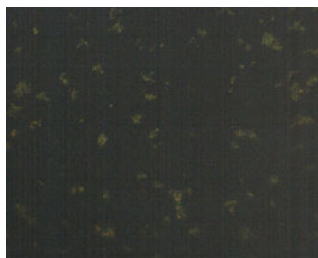
Figure 6. 19. Microphotograph of crystallised dye in 1%MR+5CB sample (device 27).

Such quick deterioration of even very carefully prepared MR doped devices is unacceptable for applications.

On the other hand, C_{60} doped systems, as has already been mentioned, have very controversial behaviour and require certain electrical and/or illumination prehistory to exhibit nonlinearity.

DC161 doped devices are also subject to what we call an ageing effect, but here the performance gradually improves with time. DC161 devices are very stable and robust. As this is one of the crucial requirements for applications, we further focus on the DC161 dye-doped nematic liquid crystals, studying their efficiency, resolution and switching times.

Graphs in Figure 6.20 represent the efficiencies of devices at the current moment. The readings were taken in 9 different spots of each device in order to monitor sample uniformity and derive statistical errors. We compare DC161 devices built in 1987, MR and DC161 doped 5CB devices built recently and freshly filled samples with other hosts.

The performance of C_{60} doped BLO48 device for comparison at the same grating spacing at optimal external field conditions (DC=5.6V, AC=5V_{pp}) is about 2.58% or 1.45% for the DC field 5.6V only. It should also be noted that C_{60} doped samples introduce strong scattering in conjunction with the applied fields.
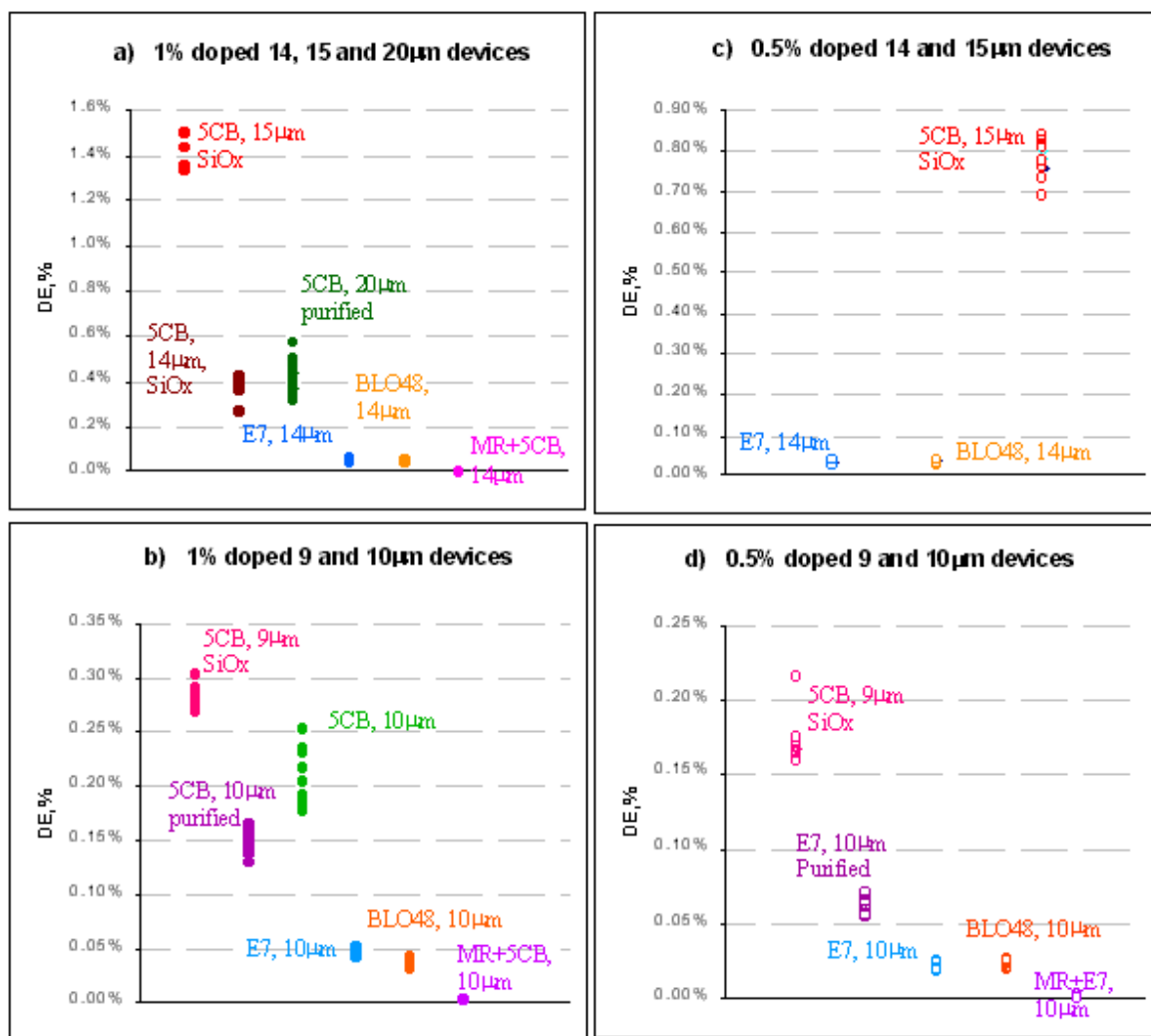
Figure 6.20. Diffraction efficiency of the devices
a) 1wt% doping level, 14 μm, 15 μm and 20 μm thickness (devices 1, 9, 7&8, 13);
b) 1wt% doping level, 9 μm and 10 μm thickness (devices 3, 10, 11, 23, 15, 27);
c) 0.5wt% doping level, 14 μm and 15 μm thickness (devices 22, 14, 2);
d) 0.5wt% doping level, 9 μm and 10 μm thickness (devices 4, 24, 25, 16, 29).
The setup in Figure 4.12 is used, grating spacing 12.5 μm, λ=514 nm, optical power
50 mW/cm^2. Alignment is polyimide (PI) and the dopant is DC161 unless otherwise
stated.

Let us discuss the performance of DC161 doped devices of the same thickness and
doping level. There is a large variation of the diffraction efficiency obtained from the
samples even with the same host material and alignment (Figure 6.20).

At a first glance, the older samples have a better performance. Indeed, in 1% doped
14 and 15 μm devices the highest efficiency is obtained from the sample manufactured in

1987 (marked 5CB, 15μm SiO_x, Figure 6.20 a). A sample with the same host, dopant and alignment produced in 2003 shows less than one-third of the efficiency (5CB, 14μm SiO_x, Figure 6.20 a). Among 9 and 10μm 1% doped devices the best performance again is shown by the oldest sample (5CB, 9μm SiO_x, Figure 6.20 b), whilst devices with the same materials have lower efficiencies.

Purification of the dye is expected to improve the performance of the device (ions in DC161 samples are not involved in the main mechanism of nonlinearity, they promote sample deterioration and can prolong relaxation times as registered during preliminary studies on samples with introduced impurities and ions). It is also likely that the dye powder has been exposed to more negative factors since 1987 than the sealed samples. Nevertheless, the influence of the dye purity was not found to be crucial. Out of two devices with identical parameters, an older device doped with unpurified dye (5CB, 10μm, Figure 6.20 b) shows better performance then the one made with a freshly prepared solution of purified dye (5CB, 10μm, purified, Figure 6.20 b). When comparing devices filled with freshly prepared solutions, the one with the purified dye (E7, 10μm, purified, Figure 6.20 d) shows higher efficiency than the device based on unpurified dye (E7, 10 μm Figure 6.20 d).

The described measurement was repeated after six months to monitor the influence of the age on the devices.

Samples built in 1987 are assumed not to have changed and have been used as reference (devices 1 and 2 in Figure 6.21), so that results from different experiments could be compared. The optical power and grating spacing are the same as in the previous measurements. Almost all the devices have exhibited an increase in diffraction efficiency.

It is worth mentioning that we do not register any sizeable changes with time in absorption in the visible light and dye order parameter in the studied devices.

It is interesting to note that devices 7 and 8 in Figure 6.21 should be identical, with the same thickness, alignment and coming from the same batch of devices. Nevertheless, they not only differ in efficiency, but this difference becomes larger with age. As the control over the device fabrication process is good, only the LC-dye solution quality could have influenced the resulting device performance. Unless this parameter can be explicitly controlled, dye-doped LC devices cannot be produced commercially.
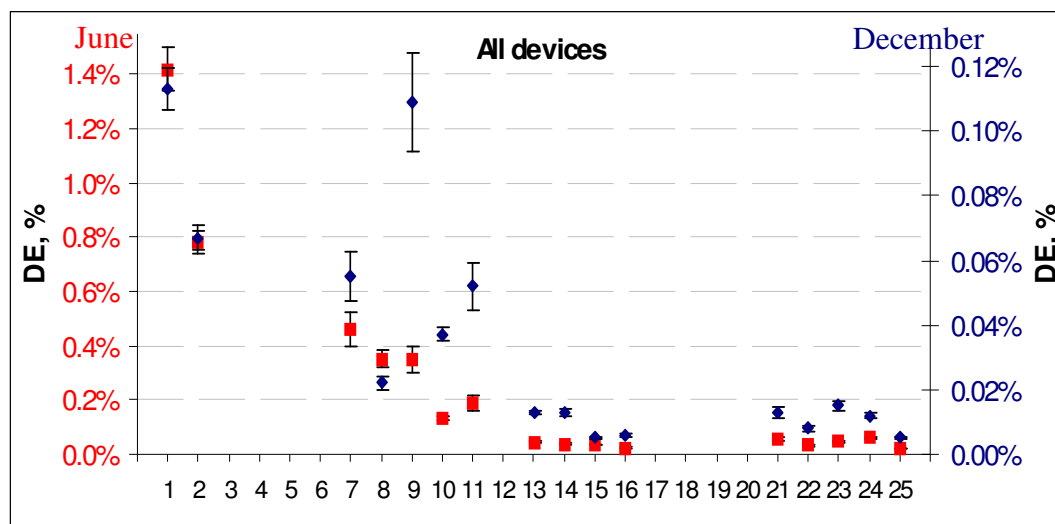
Figure 6.21 Effect of ageing on the diffraction efficiency of devices. The legend to the graph is given in Table 6.3 below.

Name	Host material	Dye concentration by weight, %	Thickness, μm
1 (reference)	5CB	1%	15
2 (reference)	5CB	0.5%	15
7	5CB	1%	20
8	5CB	1%	20
9	5CB	1%	14
10	5CB	1%, purified	10
11	5CB	1%	10
13	BLO48	1%	14
14	BLO48	0.5%	14
15	BLO48	1%	10
16	BLO48	0.5%	10
21	E7	1%	14
22	E7	0.5%	14
23	E7	1%	10
24	E7	0.5%, purified	10
25	E7	0.5%	10

Table 6.3. Devices in Figure 6.21. For more information on the devices, see Appendix D.

The observed strong dependence on age in DC161 systems (Figure 6.21) might be due to the different quality of solvation of the dye. Note that we are working with the concentrations close to saturation. With time the dispersion of the dye might improve either through some chemical processes or through diffusion and other stochastic molecular motions.

Another reason may be that the dye forms hydrogen bonds with the host material resulting in more efficient interactions between the two. Such bonding may exhibit some dependence on the host material.

It is hard to state what the influence of the host material is on the overall device performance due to the variance in solution quality, as different hosts have different capabilities of dissolving the dye DC161. At the moment we register little difference between the performance of fresh doped E7 and BLO48 (compare devices 21-13, 22-14, 23-15 and 25-16), the 5CB devices tend to give higher efficiency, especially in conjunction with SiO_x alignment.

We have already shown that the surface effects are not present in DC161 doped devices (based on their long time scale). Here the alignment may influence the anchoring, the ionic content of the device (e.g. SiO_x is known to adsorb ions from the solution) or assist in hydrogen bonds formation.

By studying samples of similar uniformity and age, it may be possible to obtain an answer to the question about the host material influence.

The main conclusion is that a lot of care should be taken to ensure a very high quality of dye-host solution and even distribution of the dopant molecules as well as good alignment with the host material. This is crucial for a good performance from the devices based on trans-cis isomerisation of the dopant as the main nonlinear mechanism.

6.3.3 Device thickness and dopant concentration

The performance of the earlier built DC161 doped 5CB samples has been investigated in more detail, and efficiencies of the devices with different thickness and dye concentration have been compared.

Doubling the dye concentration leads to a two-fold increase in the efficiency (compare 15 μm and 9 μm devices in Figure 6.22). This is expected, as the amount of

molecules that perturb geometrical order of the host is increased. Also, the increase in absorption means that the writing light is used more efficiently.
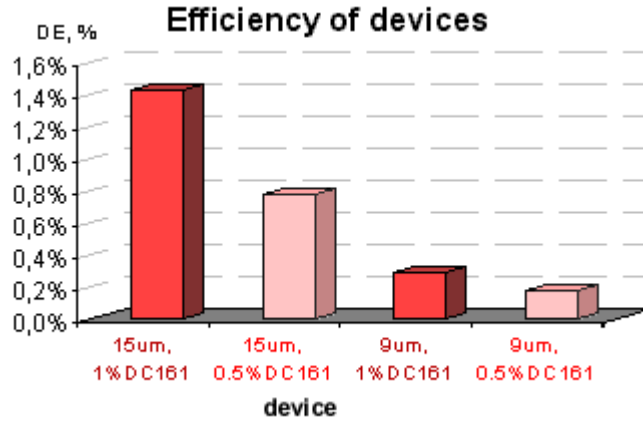

Figure 6.22. Efficiency of the earlier built DC161 devices (devices 1-4). Thickness and dye concentration dependence. The setup in Figure 4.12 is used, grating spacing 12.5 μm, λ=514 nm, optical power 50 mW/cm^2.

Diffraction efficiency of samples with both dye concentrations (0.5% and 1%) increases about 5 times as the sample thickness d is increased from 9 to 15 μm (data of the same colour in Figure 6.22). Indeed, the diffraction efficiency at small phase differences for bulk effects should be proportional to d^2:

$$\eta = J_1^2(\Delta\phi) \approx \left(\frac{\pi\Delta nd}{\lambda}\right)^2$$

6.15

(15μm)^2/(9μm)^2=2.8, while we observe about a 5-fold increase in efficiency, which does not exactly follow the relation 6.15. One of the possible explanations of such behaviour is the decrease δ of effective device thickness d_{eff} through the restriction of molecular motion probably near the surface of the device. The proportion then becomes:

$$\frac{\left(d_{eff1}\right)^2}{\left(d_{eff2}\right)^2} = \frac{(15\mu m - \delta)^2}{(9\mu m - \delta)^2} = \frac{\eta_{eff1}}{\eta_{eff2}} = 5$$

6.16

6.16 leads to the quadratic equation in respect to δ with two roots: δ_1=12 and δ_2=3; the first root does not have sense, as the effective sample thickness cannot be negative, and therefore δ=3.

169

Thus the dependence of diffraction efficiency on the thickness might be explained by molecular motion being restricted in 1.5 μm layers near the device surfaces.

6.4 Resolution

Resolution is one of the crucial parameters for OASLMs. It can be limited by many physical phenomena. In two-layer optically addressed spatial light modulators the three main limiting factors of the resolution are the fringing field effect[*], the diffusion of charges in the photoconductor bulk, and the charge spreading in the interface of the photoconductor and the liquid crystal layer[100]. The achievable resolution of two-layer devices has been reported to be usually around 50 line pairs per millimetre (lp/mm)[1, 9, 11,12].

The studies of single layer dye-doped liquid crystal films suggest that very high resolution, over 100 lp/mm may be achieved. For example, in C_{60} doped nematic devices the resolution of 100-200 lp/mm has been reported.[46] Methyl red doped nematic devices have also been reported to give extremely high resolution of about 500 lp/mm for both: nonlinearity associated with the space charge field build up[77] and surface-induced nonlinearity.[76] Resolution of up to 1000 lp/mm has been claimed for photorefractive effects involving space charge build up in NLCs doped with anthraquinone dyes.[80]

In cases when ionic effects are involved, resolution depends on the sample thickness and peaks when the grating spacing is approximately double the sample thickness.[70] The resolution in this case would be limited by the charge diffusion and the field fringing effect. Nonlinearities that rely on the response of the liquid crystal director to the change in the dopant conformation upon excitation with light in bulk (guest-host and trans-cis photoisomerisation) would be mainly limited by the dopant diffusion. The resolution of surface effect based devices would depend on the fringing field effect and the diffusion or migration of the adsorbed dye molecules.

In this section we study the practical resolution limit in the devices under investigation. The experimental arrangement described in Chapter 4 (Figure 4.12) is used. To minimise error due to fluctuations, many experimental data points during long illumination periods are collected and averaged. It is difficult to obtain a large grating spacing when writing interference pattern, as the angle of the overlapping of two interfering

---

[*] At high spatial frequencies the field in any point of the liquid crystal layer in the device would depend not only on the voltage applied across the specific pixel, but also on the voltage on the neighbouring pixels.

beams should be very small. The reading also becomes increasingly difficult, for the diffracted beam is deflected at the respectively smaller angle. The studies are performed up to 33 μm spacing (30 line pairs/mm).

To compare DC161 with C_{60} doped systems, the results of the same study are shown for the C_{60} doped 20μm thick device (Figure 6.23 e). Efficiency continuously grows as the grating spacing is increased from 3 to 33 μm. This is in agreement with the expectation of the maximum efficiency for the system to be reached at the grating spacing of 40μm.

From the resolution studies in DC161 devices (Figure 6.23 a-d) we find that efficiency remains the same when the larger grating spacing (10-33 μm) is used, and starts to decrease when the spacing becomes smaller than 8-10 μm. It almost vanishes for gratings finer than 2.5 μm (400 line pairs/mm).

Such uniform behaviour of resolution at gratings larger than 8-10 μm is very important for applications. An image with different details of various sizes will be written, and efficiency should remain the same for all spatial frequencies. What is even more important is that the resolution is virtually independent of the dye concentration and the sample thickness (Figure 6.23 a-d). Keeping in mind from the previous section that efficiency strongly increases with an increase in the sample thickness, a simple way of improving the efficiency of DC161 doped devices could be to build thick devices. The studies on thick devices are summarised in the following section.
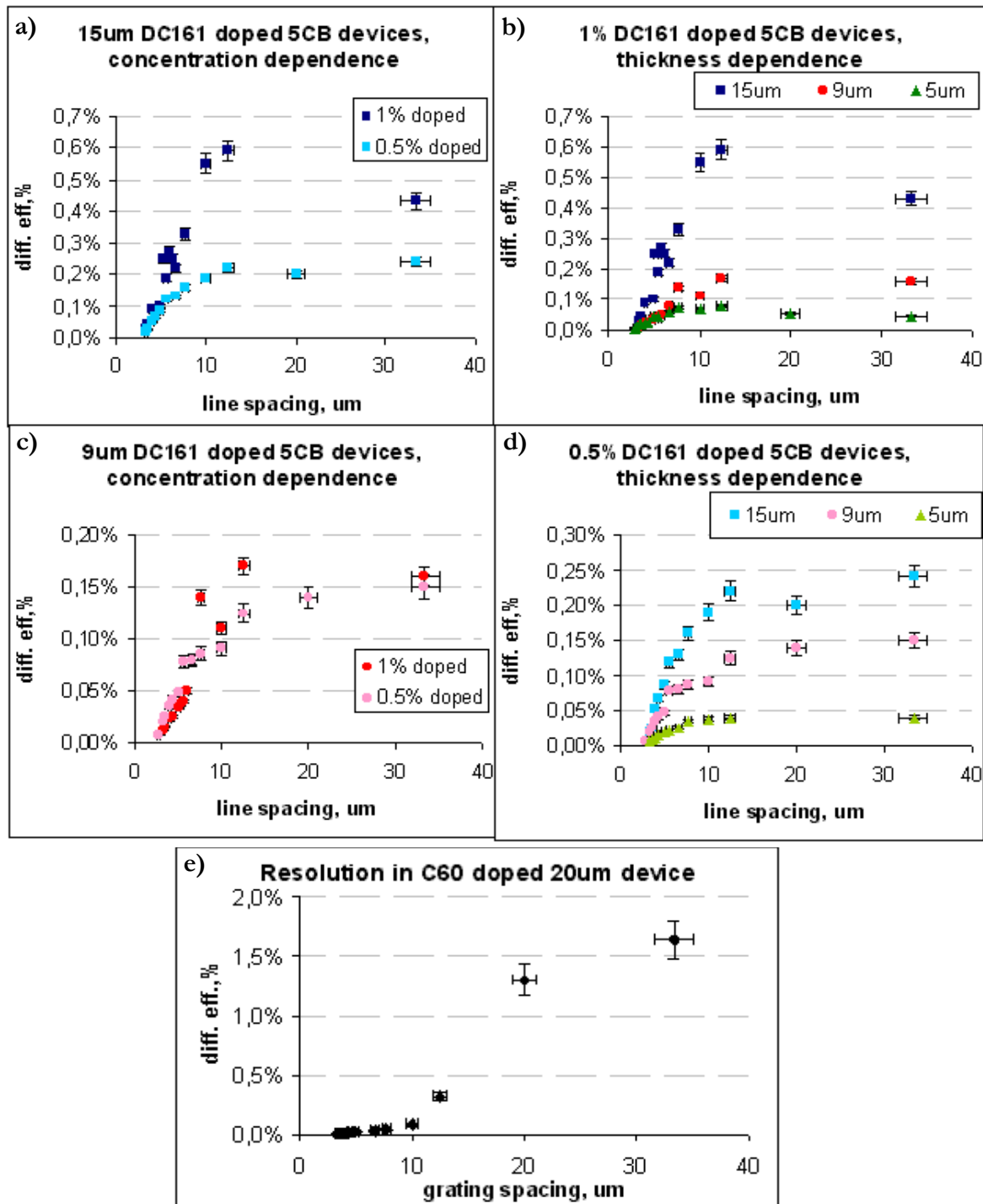
Figure 6.23. Resolution:

a), b) DC161 doped devices, dependence on dye concentration [a)-devices 1, 2; b) devices 3,4]

c), d) DC161 devices, dependence on sample thickness [c) devices 1, 3, 5; d) devices 2, 4, 6]

e) Resolution in C_{60} doped sample (device 31), 5V DC and 0.6V AC fields applied. maximum resolution expected at 40 μm

6.5 Thick devices

Experiments in thick 0.5%DC161 doped E7 devices (40, 60 and 125 μm) have been conducted using the Raman-Nath regime. The thickness parameter Q, given by **2.27,** is less than unity for 40 and 60μm devices and $Q < 3$ for 125 μm devices; also the Bragg angle condition (**2.28**) is not satisfied.

It has been shown in Chapter 2 that at small induced retardation and low diffraction efficiency Bragg matched and Raman-Nath diffraction regimes do not differ significantly (Figure 2.7). As the induced retardation approaches 2π, the difference in these two regimes becomes significant. While the efficiency of the devices is low (smaller than 10%), no difference in Bragg matched or non-matched regimes would be observed.
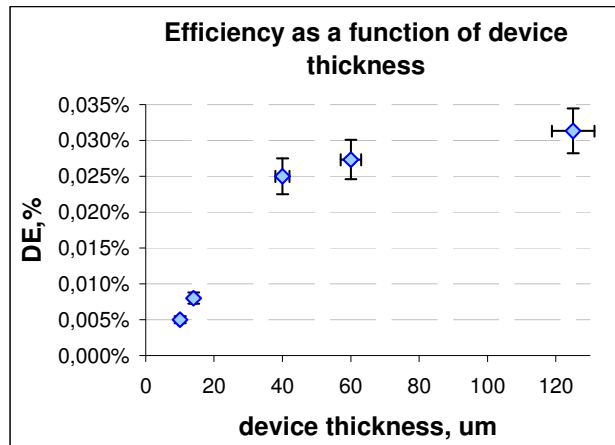
Figure 6.24 Efficiency in thick devices: saturation. The experiment is in the Raman-Nath regime (see Chapter 2), the experimental arrangement in Figure 4.12 is used, grating spacing 12.5 μm, λ=514 nm, optical power 50 mW/cm². The samples are 0.5wt% DC161 doped E7 (devices 24, 22, 20, 19, 17).

The measurements have shown, that:

⇒ the resolution allows observing nonlinearity using grating spacing ***down to 3 μm;***

⇒ the efficiency grows, but due to the strong absorption making only the front part of device active, it starts to saturate if the thickness is increased above 40 μm. (Figure 6.24);

⇒ the relaxation is still governed by dye diffusion process, and the decay time at grating spacing of 12.5 μm (80 lp/mm) is the same as in thin devices, $t_{decay}^{0.1-0.9}=88\pm5\ ms$;

⇒ the rise time in 125 μm sample is slightly larger than in thin devices, $t_{rise}^{0.1-0.9}=110\pm10\ ms$;

⇒ diffraction efficiency in 0.1% doped 125 μm device showed low diffraction efficiency, about 4 times lower than in 0.5% doped device of the same thickness and material

High resolution and almost unchanged switching characteristics as compared with thin (≤ 25μm) doped liquid crystal systems makes thick devices based on DC161 doped liquid crystals good option for improving the efficiency.

If a large optical retardation could be achieved in these devices, it may be possible to benefit from the Bragg regime. In this case, for the 125 μm device the associated grating spacing should not exceed 5μm, and the corresponding Bragg angle $\varphi=7.3^{o}$. For larger grating spacing, thicker devices should be used. To achieve uniform light intensity distribution throughout the whole thickness of the device, low dye concentrations (0.1wt%) may be introduced.

6.6 Conclusions

The 2,5 azo-substituted anthraquinone dye DC161 is an interesting alternative to MR and C_{60} as a dopant for LC as materials for OASLMs. The diffraction efficiency in DC161 due to trans-cis isomerisation is of the same magnitude as space-charge field induced nonlinearity of C_{60} and trans-cis isomerisation mechanism in MR. The process in DC161 doped systems is reversible, stable and repeatable.

Switching time in DC161 doped systems is fast (≤ 200 ms "on" and "off" cycle). The rise time may be significantly shortened with the use of higher optical powers. Relaxation is governed by dye or LC contribution, whichever is greater. We have introduced a model based on the diffusion of cis molecules and cis-trans back isomerisation to describe the observed relaxation time behaviour. This model is extended to encompass

the imperfect contrast of the written optical pattern and therefore explain the observed overshoot in the nonlinearity build up.

With age, the efficiency of the three types of guest-host systems studied changes in a non-trivial fashion. MR doped samples, as expected from ionic materials, tend to give a dramatic decrease in efficiency while C_{60} and DC161 devices improve with age. This improvement for DC161 doped systems presumably is due to changes in the chemistry or in the state of dispersion of the systems. In case of C_{60} the possible reasons of the positive effect the ageing has are adsorption on the surface or/and charge complexes formation.

Efficiency in all DC161 doped devices remains unchanged for gratings with the period larger than 8-10 μm. This resolution threshold has not been found to be dependent either on the device thickness, or on the dye concentration within the 0.5wt% - 1wt% range.

Experiments on thick devices have confirmed that the resolution is independent of the sample thickness. The dynamics in 125 μm thick devices is almost the same as in thin (≤ 25 μm) samples. The efficiency of the thin devices increases when the thickness is increased, but in samples thicker than 40 μm efficiency starts saturating, probably due to the high absorption in the devices.

Using thick DC161 doped nematic devices in the Bragg diffraction regime may compensate for the relatively low efficiency as compared with earlier reported efficiencies for ionic[48,77] and surface effects[53] in MR doped 5CB ($\geq 20\%$).

CHAPTER 7

CONCLUSIONS

Spatial light modulators are needed in a range of increasingly important applications, including 3D video, projection displays, optical correlation, real-time holography, permanent holographic data storage, optical telecommunications and manipulating the phase of the optical beam.

This research has focused on the ability of liquid crystals to exhibit photorefractivity in a way similar to nonlinear crystals. Liquid crystals can change their refractive index under the influence of light. While relatively high optical powers are required to control pure liquid crystals, the situation improves dramatically when some sensitising dopants (usually dyes or fullerenes) are introduced to liquid crystals. Dye-doped LC systems are highly promising materials for novel optically addressed spatial light modulators (OASLMs) based on photorefractive effects. Such devices are intrinsically photorefractive without the need of special layers or circuitry.

The aim of this work has been to assess the possibility of using novel photorefractive LC-based materials to create new optically addressed spatial light modulators. The following characteristics are desirable: high resolution, fast switching, low writing optical intensity, low or no voltage applied, low optical losses, high efficiency, stability.

Another main objective of this work has been to define the mechanisms responsible for the optical nonlinearity in the studied dye-doped systems. Answering this question is vital to enable solutions to the question of how to improve the performance of the existing systems, what to look for when creating new materials, and whether there is a potential for successful applications as OASLMs.

Accomplished research

On the basis of extensive experiments, the systems and effects with the most suitable characteristics for OASLMs have been identified. Very simple and robust devices have been built consisting of one layer of doped liquid crystal confined between two glass plates.

The chosen sensitising dopants are an azo dye Methyl Red, a fullerene C_{60} and an azo substituted anthraquinone dye DC161. The first two have previously been studied by many groups [46, 50, 51] and considered the most promising nonlinear dopants for liquid crystals. The DC161 dye has been studied for the first time.

A highly important feature of the new dopant is that it is stable and reliable for use in device applications. Moreover, detailed studies have shown almost no dependence of resolution and speed on the device thickness. These are important conclusions for device engineering. The efficiency of the DC161 systems increases as the thickness is increased and saturates for the thickness over 40 μm (at 50 mW/cm^2) due to the strong absorption in the device.

Unlike the previously reported large photorefractive effects that require either a long time (1-30 sec), application of the electric field, or high optical power (100-1000 mW/cm^2), a regime has been achieved in MR and DC161 doped devices where the switching times of a device have been reduced to 100 ms at low optical fields (50 mW/cm^2) with no electric fields applied.

The mechanism of nonlinearity introduced by the DC161 dye as a dopant for LCs has been elucidated and the study of the mechanisms present in MR and C_{60} doped systems has been carried out.

It has been found that it is possible to exploit the particular mechanism of nonlinearity out of a large number of possible ones in particular system by the selection of alignment surface, interaction geometry and external field regimes. Nonlinearities due to temperature and surface effects are best avoided at a recent stage for device applications. Temperature control is inconvenient, and surface effects are slow and not controllable at present. Ionic effects could be used in C_{60} doped systems when the build up time of several seconds and spatial frequency response are acceptable, and external electric control desired.

For a fast operation we suggest the use of trans-cis transition as nonlinearity mechanism. It is present in the studied MR and DC161 dyes.

Ageing effects have been observed in the systems researched. This has important implications for device engineering. MR doped devices deteriorate quickly, probably due to the ionic nature of the dopant. Despite the high promise and large popularity of Methyl Red, it is not possible to use this dye as a dopant for liquid crystals in device applications before its stability is improved. Unlike Methyl Red doped systems, C_{60} and DC161 doped devices considerably improve with age, possibly due to the guest-host systems undergoing some slow chemical transformations or the dopants to disperse through the LC medium (DC161 and C_{60}) or form charge complexes (C_{60}). It is important to avoid this effect for device applications (for example by using advanced methods of dissolving dopants) and to ensure good performance in freshly made devices.

Another important achievement has been the explanation of the peculiar dynamic behaviour (an overshoot in diffracted signal) of DC161 and MR doped systems based on a trans-cis transition mechanism model.

Studies of surface phenomena and selecting specific surface interfaces has eliminated permanent effects in Methyl Red LC systems, which have been an impediment for dynamic holography.

One of the conclusions of this research work is that azo-substituted anthraquinone dyes are a highly promising class of dopants for LC as materials for OASLMs. The diffraction efficiency in DC161 doped devices due to trans-cis isomerisation is of the same magnitude as the space-charge field induced nonlinearity of C_{60} and the nonlinearity due to the trans-cis isomerisation mechanism in Methyl Red doped systems (see also Table 7.1). The process in DC161 doped systems is reversible, stable and repeatable.

A summary of the main results for both device engineering and physics is given below. The achieved performance characteristics of the researched doped nematic liquid crystal systems as materials for optically addressed spatial light modulators are presented in the Table 7.1.

Summary of the research results

Main conclusions concerning the mechanisms of the observed phenomena

➢ Nonlinearity in DC161 doped systems has the trans-cis transition as an underlying mechanism. It may be enhanced by the differences in the interaction of the host with trans and cis isomers.

➢ The overshoot in the build up of the nonlinearity in DC161 and MR doped devices is caused by cis species build up in dark areas, as well as in bright ones, because of imperfect contrast and the difference in build up times at different optical intensities.

➢ It is possible to exploit the particular mechanism of nonlinearity out of a large number of possible ones in a particular system by the selection of alignment surface, interaction geometry and external field regimes.

Main conclusions relating to device engineering:

➢ The resolution in DC161 doped samples does not depend on the sample thickness.

➢ Relaxation time in DC161 doped devices does not depend on the sample thickness, only on the grating spacing, and is governed by dye diffusion.

➢ Build up in DC161 doped devices does not depend on the grating spacing and has a minor dependence on the sample thickness. There is a strong dependence on the optical power.

➢ The ageing effect has been found in all three studied systems.

    ➢ C_{60} and DC161 doped devices sizeably improve with age probably due to the dopant dispersing in the LC medium (DC161) or forming charge complexes (C_{60}).

    ➢ MR doped devices deteriorate quickly.

➢ Permanent/persistent surface effects have not been observed in C60 and DC161 doped devices. PI and ITO allow good dynamic operation of the MR systems without permanent or persistent components.

Summary of the achieved device characteristics

	a-Si:H OASLM, Hamamatsu[2]	C_{60} doped NLC	Methyl Red doped NLC	DC161 doped NLC
Applied voltage	Γ5V 50Hz-100kHz	$1.5\text{-}2V_{DC}$ $(+2Vpp_{AC})$	0V	0V
Optical power	1 mW/cm^2 50 μW/cm^2 high sensitivity	~10 mW/cm^2	1–50 mW/cm^2	10-50 mW/cm^2
Switching time ("on"-"off" cycle)	30/40 ms (60 ms/70 ms at high sensitivity)	<10 s electrically switchable up to 5Hz	100-200 ms permanent component eliminated	100-200 ms
Resolution	50 lp/mm	60 lp/mm	300 lp/mm	180 lp/mm
DE,%	30% (10 lp/mm), ~1% (50 lp/mm)	10% (80 lp/mm, 16 mW/cm^2)	1% (80 lp/mm, 50 mW/cm^2) may be increased by applied DC (~2.5V)	3% (80 lp/mm 50 mW/cm^2)
n_2	-	0.34 cm^2/W	0.02 cm^2/W	0.05 cm^2/W
Δn	-	$3.2*10^{-3}$	$0.8*10^{-3}$	$2.4*10^{-3}$
Δ	π	0.21π	0.06π	0.11π
d	no data	20 μm	25 μm	15 μm
Effect	**Photo-conductivity in a-Si:H**	Carr-Helfrich **Space-charge**	Carr-Helfrich Space-charge **Trans-cis** Thermal Surface	**Trans-cis Janossy** Thermal
Geometry, alignment	no data	Normal incidence; planar, PI	Normal incidence; planar, PI	Normal incidence; planar, PI
stable	yes	Improves with age	Deteriorates in months	Improves with age

Table 7.1. The best achieved performance from the three dopant systems for device applications. Parameters for commercially available nematic liquid crystal device based on amorphous silica layer from Hamamatsu are given for comparison.

Further work

In continuing this line of research, it would be important to tackle the problem of the speed and efficiency characteristics of the described systems as well as the ageing effect.

An important step is to ensure uniform dispersion of the dopant by improving dopant solubility and creating dopants readily dissolved in LCs. Our studies, as well as research by other groups, have shown that higher dopant concentration yields better efficiency. Liquid crystals are very poor solvents and it is very hard to get the dopant into solution, especially in case of fullerenes. Poor dispersion also might be one of the causes of the ageing effect where the devices need time to start exhibiting large nonlinearities.

We have shown that there is no limit on the resolution when increasing device thickness in DC161 doped systems; also the dynamics in thick devices remains almost unchanged. Using thick DC161 doped nematic devices in Bragg diffraction regime may compensate for the relatively low efficiency[*]. Devices with lower dye concentrations may have to be used to obtain smaller extinguishing of the writing beam and acceptable optical intensity in the "back" layers of the device.

It may be possible to incorporate the new dopant introduced in this research in other phases of liquid crystals as host materials. Ferroelectric liquid crystals are known to give a large phase modulation and fast bistable switching by electric fields. It has been shown[57], that in ferroelectric liquid crystals doped with azo dyes fast dopant-assisted switching by optical field through trans-cis isomerisation is achievable. Bistability is theoretically possible in these systems and will depend on the dopant relaxation to the trans state. Switching off the device by stimulating the dye to relax back to the trans state is also a very interesting option.

It is also promising to research C_{60} doped LC systems for the device applications. To achieve a more efficient charge generation higher absorption by the dopant should be

---

[*] As compared with earlier reported efficiencies of 20% and higher for ionic and surface effects in MR doped 5CB.

achieved. This could be done through tailoring dopant properties and the absorption spectrum, improving the dopant solubility and choosing appropriate operating regimes. Dynamic scattering is setting a serious limit on the efficiency and performance of the C_{60}-doped devices. It has been shown[60] that addition of carbon nanotubes (CNT) raises the voltage threshold for this undesirable phenomenon, also the nonlinearity has been reported to increase. Nevertheless, the effect is not well understood and finding ways to control dynamic scattering in doped single layer devices remains a research topic.

To summarise, my research was successful in investigating optical nonlinearities in dye-doped liquid crystals and the possibility of using these effects for device applications.

My current work encompassed one of the steps towards simplicity and efficiency in technology, and there are many more to make in future. If successful, further research would have a revolutionary impact in displays and telecommunications, medicine, and open new fields in technology.

LITERATURE CITED

[1] S. Mias, N. Collings, T.D. Wilkinson and W.A. Crossland, "Technology and performance of A-Si:H OASLMs", Recent res. Devel. Optics, **3**, pp 125-144, 2003

[2] www.hamamatsu.com; Hamamatsu, technical exhibition, SPIE annual meeting, Denver, 2004

[3] D.V. Wick, T. Martinez, M.V. Wood, J.M. Wilkes, M.T. Gruneisen, V.A. Berenberg, M.V. Vasil'ev, A.P. Onokhov and L.A. Beresnev, "Deformed-helix ferroelectric liquid-crystal spatial light modulator that demonstrates high diffraction efficiency and 370-line pairs/mm resolution", *Appl. Opt.*, **38**, 17, pp. 3798-3803 (1999)

[4] Solon Mias, PhD Thesis, Cambridge, 2003

[5] M. Stanley, P. B. Convay, S. Coomber, J.C. Jones, D.C. Scattergood, C. W. Slinger, B. W. Bannister, C. V. Brown, W.A. Crossland, A.R.L. Travis, "A novel electro-optic modulator system for the production of dynamic images from Giga-pixel computer generated holograms", *Proceedings of SPIE*, **3956**, pp.13-20 (2000)

[6] S.D. Coomber, C.D. Cameron, J.R. Hughes, D.T. Sheerin, C.W. Slinger, M.A.G. Smith, and M. Stanley, "Optically addressed spatial light modulators for replaying computer-generated holograms", Proceedings of SPIE, **4457,** pp. 9-19 (2001)

[7] P. J. Collings and M. Hird "Introduction to liquid crystals chemistry and physics", Taylor and Francis Ltd, 1997

[8] I.C. Khoo "Liquid crystals: physical properties and nonlinear optical phenomena", J.Wiley & Sons, Inc., 1995

[9] N.A. Clark and S.T. Lagerwall, "Submicrosecond bistable electro-optic switching in liquid crystals", *Appl. Phys. Lett.* **36**, pp. 899-901 (1980)

[10] G. B. Cohen, R. Pogreb, K. Vinokur, and D. Davidov, ""Spatial light modulator based on deformed-helix ferroelectric liquid crystal and a thin a-Si:H amorphous photoconductor" Appl. Opt., **36**, 2 (1997)

[11] D Williams, S G Latham, C M J Powles, M A Powell, R C Chittick, A P Sparks and N Collings, "An amorphous silicon/chiral spatial light modulator"*, J. Phys. D: Appl. Phys*. **21,** pp**.** s156-s159, (1988).

[12] F. Perennes and Z. Y. Wu, "Resolution and response-time dependence of ferroelectric liquid-crystal optically addressed spatial light modulators on grating profiles" *Applied Optics*, **36**, 17, pp.3825-3834, (1997)

[13] W.H. De Jeu, "Physical properties of liquid crystalline materials", Gordon and Breach Science Publishers Inc., 1980

[14] L.M. Blinov, V.G. Chigrinov, "Electrooptic Effects in Liquid Crystal Materials", Springer, 1993

[15] F.M. Leslie "Some constitutive equations for anisotropic fluids", *Quart. Journ. Mech. And Applied Math.,* 19, pp.357-369 (1966)

[16] I. C. Khoo, Min-Yi Shih, M. V. Wood, B.D. Guenther, P. Chen, F. Simoni, S. Slussarenko, O. Francescangeli, L. Lucchetti, "Dye-Doped Photorefractive Liquid Crystals for Dynamic and Storage

Holographic Grating Formation and Spatial Light Modulation" *Proceedings of the IEEE*, **87**, 11, pp.1897-1911 (1999)

[17] Y. R. Shen, "The principles of Nonlinear Optics", J. Wiley & Sons, Inc., 1984

[18] Z.–C Ou–Yang, Y.-Z. Xie, "Theory of second-harmonic generation in nematic liquid crystals", *Phys. Rev. A*, **32**, pp. 1189-1200 (1985)

[19] J.E. Bjorkholm, A.E. Siegman "Accurate cw Measurements of Optical Second-Harmonic Generation in Ammonium Dihydrogen Phosphate and Calcite", *Phys. Rev*, **154**, pp. 851-860 (1967)

[20] R. Wortmann, C. Poga, R.J. Twieg, C. Geletneky, C.R. Moylan, P.M. Lundquist, R.G. DeVoe, P.M. Cotts, H. Horn, J.E. Rice, and D.M. Burland, "Design of optimized photorefractive polymers: A novel class of chromophores", *J. Chem. Phys*. **105,** 23, pp.10637-10647 (1996)

[21] W. E. Moerner, S. M. Silence, F. Hache, and G. C. Bjorklund, "Orientationally enhanced photorefractive effect in polymers " *J. Opt. Soc. Am. B,* **11**, pp.320-330 (1994)

[22] F Simoni and O Francescangeli,"Effects of light on molecular orientation of liquid crystals" *J. Phys.: Condens. Matter* **11** (1999);

[23] G. P. Wiederrecht, "Photorefractive liquid crystals" *Annu. Rev. Mater. Res*., **31** (2001)

[24] J.W. Goodman, "Introduction to Fourier Optics", *McGraw-Hill Book Co.,* 1996, Chapter 9

[25] T.K. Gaylord, M.G. Moharam, "Thin and thick gratings: terminology clarification", *Applied Optics*, **20**, 19, pp. 3271-3273 (1981)

[26] J. W. Shelton and Y. R. Shen, "Phase-Matched Third-Harmonic Generation in Cholesteric Liquid Crystals", *Phys. Rev. Lett*. **25**, 23–26 (1970)

[27] S.K. Saha, G.K. Wong, "Investigation of nematic ordering using electric-field-induced second-harmonic generation", *Applied Physics Letters*, **34**, pp. 423-425 (1979)

[28] T. Bischofberger and Y. R. Shen, "Transient behaviour of a non-linear Fabry-Perot", *Applied Physics Letters*, **32**, pp. 156-158 (1978)

[29] Fekete, D.; AuYeung, J.; Yariv, A., "Phase-conjugate reflection by degenerate four-wave mixing in a nematic liquid crystal in the isotropic phase", *Optics Letters,* **5**, pp. 51-53 (1980)

[30] G. K. L. Wong and Y.R. Shen, Phys. "Study of pretransitional behaviour of laser-field-induced molecular alignment in isotropic nematic substances" *Phys Rev A*, **10**, 4 (1974)

[31] R. M. Herman and R. J. Serinko, "Nonlinear-optical processes in nematic liquid crystals near Freedericks transitions", *Phys. Rev. A,* **19**, pp. 1757–1769 (1979)

[32] I. C. Khoo, "Optically induced molecular reorientation and third-order nonlinear optical processes in nematic liquid crystals" *Phys. Rev. A,* **23**, 4 (1981)

[33] I. C. Khoo, S.-L. Zhuang, "Nonlinear optical amplification in a nematic liquid crystal above the Frederiks transition", *Appl. Phys. Lett*., **37**, 1 (1980)

[34] B. Ya. Zel'dovich, N. F. Pilipetskii, A. V. Sukhov, and N. V. Tabiryan, "Giant optical nonlinearity in the mesophase of a nematic liquid crystal (NLC)", *JETP Lett*., **31**, 5 (1980)

[35] I. C. Khoo, S.-L. Zhuang, and S. Shepard, "Self-focusing of a low power cw laser beam via optically induced birefringence in a nematic liquid-crystal film" *Appl. Phys. Lett*., 39, 12 (1981)

[36] A. S. Zolot'ko, V. F. Kitaeva, N. Kroo, N. N. Sobolev, A. P. Sukhorukov, V. A. Troshkin, and L. Czillag, "Undamped oscillations of NLC director in the field of an ordinary light wave", *Soviet Physics - JETP*, **60**, 3, pp. 488-490 (1984)

[37] Durbin S D, Arakelian S M and Shen Y R, "Optical-Field-Induced Birefringence and Freedericksz Transition in a Nematic Liquid Crystal", *Phys. Rev. Lett.*, **47,** pp.1411-1414 (1981)

[38] S. G. Odulov, Yu. A. Reznikov, M. S. Soskin, and A. I. Khizhnyak, "Polarization recording of dynamic holographic gratings in the mesophase of the liquid crystal MBBA" *Sov. Phys. Dokl.*, **27**, 3 (1982)

[39] I.C. Khoo and T. H. Liu, "Theory and experiments on multiwave-mixing-mediated probe-beam amplification", Phys. Rev. A **39**, pp.4036-4044 (1989)

[40] I. Jánossy, A. D. Lloyd, and B. S. Wherrett, "Anomalous optical Freedericksz transition in an absorbing liquid crystal" *Mol. Cryst. Liq. Cryst.* **179**, 1 (1990)

[41] L. Marrucci, D. Paparo, M. R. Vetrano, M. Colicchio, and E. Santamato G. Viscardi "Role of dye structure in photoinduced reorientation of dye-doped liquid crystals", *Journal Of Chemical Physics*, **113**, 22, pp.10361-10366 (2000)

[42] I. Jánossy and T. Kósa, "Influence of anthraquinone dyes on optical reorientation of nematic liquid crystals", *Opt. Lett*. **17**, pp. 1183 (1992)

[43] I.C. Khoo, H. Li, Y. Liang, "Observation of orientational photorefractive effects in nematic liquid crystals", *Opt. Lett.,***19**, pp.1723–1725 (1994)

[44] E.V. Rudenko, A.V. Sukhov, "Photoinduced electrical conductivity and photorefraction in a nematic liquid crystal", *J. Exp.Theor. Phys. Lett*. **59**, pp.142–146 (1994)

[45] G.P. Wiederrecht; B.A. Yoon; M.R. Wasielewski, "High Photorefractive Gain in Nematic Liquid Crystals Doped with Electron Donor and Acceptor Molecules", *Science*, New Series, **270**, 5243, pp. 1794-1797 (1995).

[46] I.C. Khoo, "Holographic grating formation in dye- and fullerene C60-doped nematic liquid-crystal film " *Optics Lett*, **20**, 20, pp2137-2139 (1995)

[47] O. Francescangeli, S. Slussarenko, F. Simoni, D. Andrienko, V. Reshetnyak, Y. Reznikov, "Light-induced surface sliding of the nematic director in liquid crystals", *Phys. Rev. Lett.,* **82**, 9, pp.1855-1858 (1999)

[48] I.C. Khoo, S. Slussarenko, B. D. Guenther, Min-Yi Shih, P. Chen, W. V. Wood, "Optically induced space-charge fields, dc voltage, and extraordinarily large nonlinearity in dye-doped nematic liquid crystals", *Optics Letters*, **23**, 4, pp.253-255 (1998)

[49] I. C. Khoo, Min-Yi Shih, A. Shishido, P. Chen and M. V. Wood, "Liquid Crystal Photorefractivity - towards Supra-optical Nonlinearity", *Opt. Materials,* **18**, pp.85-90 (2001).

[50] F. Simoni, L. Lucchetti, D. Lucchetta, and O. Francescangeli, "On the origin of the huge nonlinear response of dye-doped liquid crystals" *Opt. Express* **9**, 2, pp.85-90 (2001)

[51] A. Petrosian, S. Residori "Surfactant enhanced reorientation in dye-doped nematic liquid crystals", *Europhys. Lett*., **60**, 1, pp. 79-85 (2002)

[52] I.C. Khoo, A. Diaz, J. Ding, K. Chen & Y. Zhang, "Collective and Individual Molecular Nonlinear Photonics of Liquid Crystals" *Journal of N. Opt. Phys. And Mat.*, **12**, 2 (2003)

[53] L. Lucchetti, M. Di Fabrizio, O. Francescangeli, F. Simoni "Colossal optical nonlinearity in dye-doped liquid crystals", *Optics Communications*, **233**, pp.417-424 (2004)

[54] H. J. Eichler and R. Macdonald, "Flow-alignment and inertial effects in picosecond laser-induced reorientation phenomena of nematic liquid crystals", Phys Rev Lett. **67**, 19, pp. 2666–2669, (1991)

[55] I. C. Khoo, R. G. Lindquist, R. R. Michael, R. J. Mansfield, and P. LoPresti, "Dynamics of picosecond laser-induced density, temperature, and flow-reorientation effects in the mesophases of liquid crystals", J. Appl. Phys., **69**, 7, pp. 3853-3859 (1991)

[56] I. Jánossy and T. Kósa, "Laser-induced effects in dye-doped nematics" *Mol. Cryst. Liq. Cryst.*, **207,** pp. 189-197 (1991)

[57] A.S. Kuzhelev, A.E. Dudelzak, "Thermally induced holographic gratings in liquid crystals at telecommunications wavelengths", *J. Opt. A: Pure and Appl. Opt.* **5**, pp.L5-L8 (2003)

[58] I. Janossy, "Molecular interpretation of the absorption-induced optical reorientation of nematic liquid crystals", *Phys. Rev. E*, **47**, 4 (1994)

[59] L Marrucci, B Piccirillo, F Vetrano and E Santamato, "Longitudinal extra torque in liquid crystals due to the optical beam shape", *J. Opt. A: Pure Appl. Opt.*, **2,** pp. 294–298 (2000)

[60] L. Marucci, D. Paparo, P. Maddalena, E. Massera, E. Prudnikova, E. Santamato, "Role of guest-host intermolecular forces in photoinduced reorientation of dyed liquid crystals", *J. Chem. Phys.*, **107**, 23, pp.9783-9793 (1997)

[61] M. Kreuzer, E. Benkler, D. Paparo, G. Casillo, and L. Marrucci, "Molecular reorientation by photoinduced modulation of rotational mobility" *Physical Review E,* **68**, pp.011701(1-5) (2003)

[62] L. Marrucci and D. Paparo, "Photoinduced molecular reorientation of absorbing liquid crystals", *Phys. Rev. E,* **56**, pp.1765–1772 (1997)

[63] R. C. Weast, ed., *CRC Handbook of Chemistry and Physics*, 64th ed. CRC, Boca Raton, (1983)

[64] J.D. Coyle, *Introduction to Organic Photochemistry*, J. Wiley&Sons Inc. (1986)

[65] J. P. Simons, *Photochemistry and spectroscopy*, Wiley-Interscience, (1971)

[66] T. V. Galstyan, B. Saad, M. M. Denariez-Roberge, "Excitation transfer from azo dye to nematic host during photoisomerization", *J. Chem. Phys.*, **107**, 22, pp. 9319-9325 (1997)

[67] I. Jánossy and L. Szabados, "Photoisomerisation of azo dyes in nematic liquid crystals" *Journal of N. Opt. Phys. And Mat.*, **7**, 4, pp. 539-551 (1998)

[68] T. Ikeda, T. Sasaki, K. Ichimura, "Photochemical switching of polarisation in ferroelectric liquid-crystal films", *Nature*, 361, 4, pp. 428-430 (1993)

[69] W. Helfrich, "Conduction induced alignment of nematic liquid crystals: basic model and stability considerations", *Phys. Rev.*, **51**, pp. 4092-4105 (1969)

[70] I.C. Khoo, "Orientational photorefractive effects in nematic liquid crystal films", *IEEE J. Quantum Electron.*, **32**, pp. 525-534 (1996)

[71] I. C. Khoo, J. Ding, Y. Zhang, K. Chen, and A. Diaz, "Supra-nonlinear photorefractive response of single-walled carbon nanotube- and C60-doped nematic liquid crystal" *Appl. Phys. Lett*, **82**,21, pp.3587-3589 (2003)

[72] W. Chen, M. B. Feller, and Y. R. Shen, "Investigation of anisotropic molecular orientational distribution of liquid-crystal monolayers by optical second-harmonic generation" *Phys. Rev. Lett.* **63**, pp.2665-2669 (1989)

[73] D. Andrienko, Yu. Kurioz, Yu. Reznikov, V. Reshetnyak, "Surface driven transition in a nematic liquid crystal cell", *JETP*, **85**, 6, pp. 1119-1124 (1997)

[74] E. Ouskova, A. Iljin, Yu. Reznikov, "Light-induced anchoring of dye-doped liquid crystal on ITO and polyvinyl-cinnamate aligning surfaces", *Proceedings of SPIE*, **4418**, pp.65-71 (2001)

[75] M Sheik-Bahae, A.A Said, T.-H. Wei, D.J Hagan, E.W Van Stryland, "Sensitive measurement of optical nonlinearities using a single beam", *IEEE Journal of Quantum Electronics*, **26**, 4, pp.760 - 769 (1990)

[76] L. Lucchetti, F. Simoni, Y. Reznikov, "Fast optical recording in dye-doped liquid crystals" *Optics Lett.*, **24**, 15, pp.1062-1064 (1999)

[77] I.C. Khoo, B.D. Guentner and S. Slussarenko, "Photo-induced space-charge fields, photo-voltaic, photorefractivity, and optical wave mixing in nematic liquid crystals", *Mol. Cryst. Liq, Cryst.*, **321**, pp. 419-438 (1998)

[78] S. Residori, A. Petrosian, "Light Induced Reorientation in Azo-Dye-Doped Liquid Crystals; the Relative Role of Surface and Bulk Effects" *Mol. Cryst. Liq. Cryst.* **398**, 1, pp. 137-156 (2003)

[79] L. Marucci, D. Paparo, M.R. Vertano, M. Coliccio, E. Santamato, "Role of guest-host intermolecular forces in photoinduced reorientation of dyed liquid crystals" *J. Chem. Phys.*, **113**, 22 (2000)

[80] J.Parka, "Photorefractivity of the dye-doped NLC layers and possibility of their application*" Opto-electronics review* **10**, 1, pp.83-87 (2002)

[81] R. Macdonald, P. Meindl, G. Chilaya, D. Sikharulidze, "Reorientation of a nematic liquid crystal of discotic molecules by photoinduced space charge fields" *Mol. Cryst. Liq. Cryst.*, **320** (1998)

[82] P. Pagliushi, R. Macdonald, S. Busch, G. Cipparone, M. Kreuzer, "Nonlocal dynamic gratings and energy transfer by optical two-beam coupling in a nematic liquid crystal owing to highly sensitive photoelectric reorientation", *J. Opt. Soc. Am.*, **18**, 11 (2001)

[83] Y. Wang, "Photoconductivity of fullerene-doped polymers", *Nature*, **356**, pp. 585-587 (1992)

[84] Dr. D. Coates, private communication.

[85] A.V. Ivashcheenko, "Dichroic dyes for liquid crystal displays"

[86] M. Mansuripur, "Classical optics and its applications", Cambridge University Press, 2002

[87] E. Hecht, "Optics", Chapter 12, 3rd edition, Addison Wesley Longman, Inc., 1998.

[88] G. R. Fowles, "Introduction to modern optics", 2nd edition, Dover Publications, Inc., New York, 1975.

[89] A. Chen, D. Brady, "Real-time holography in azo-dye-doped liquid crystals" *Opt. Lett.*, **17**, 17 pp.1231-1233 (1992)

[90] H.S. Park, K.S. Oh, K.S. Kim, T. Chang, D.R. Spiegel "Change of internal hydrogen bonding of Methyl Red upon photoisomerization monitored by forced rayleigh scattering", *J. Phys. Chem. B,***103**, pp.2355-2360 (1999)

[91] www.camsoft.com; Cambridge Soft Corporation MA, USA

[92] I. Yoon, K. M. Park, S. S. Lee, G. Choi, J.S. Lee "Crystal structure of an anthraquinone dye, C.I. Disperse Violet 27" *Analytical Sciences*, **17**, pp.1355-1356 (2001)

[93] C. Sasaki, S. Kitoh, K. Yamada, K.K. Kunimoto, S. Maeda, A. Kuwae, K. Hanai "Crystal structure of 2-trifluoromethyl - 4'-dimethylaminoazobenzene" *Analytical Sciences*, **19**, pp.x1-x2 (2003)

[94] N. Biswas and S. Umapathy "Structures, Vibrational Frequencies, and Normal Modes of Substituted Azo Dyes: Infrared, Raman, and Density Functional Calculations", *J. Phys. Chem. A* **104**, pp 2734 - 2745 (2000)

[95] O.Ruzak, N.Collings, W.A. Crossland, T.D. Wilkinson, A.B. Davey "Optical Studies On Dye-Doped Liquid Crystal Systems", accepted for publication in Molecular Crystals Liquid Crystals Journal.

[96] M. Kaczmarek, A. Dyadyusha, S. Slussarenko, I. C. Khoo, "The role of surface charge field in two-beam coupling in liquid crystal cells with photoconducting polymer layers", *Journal of Appl. Phys*., **96**, 5, pp 2616-2623 (2004)

[97] P. Pagliusi, G. Cipparrone, "Optical two-beam coupling for a surface-induced photorefractive effect in undoped liquid crystals", *Opt. Lett.*, **28**, 23, pp. 2369-2371 (2003).

[98] A.G.-S. Chen, D.J. Brady, "Surface-stabilized holography in an azo-dye-doped liquid crystal", *Opt. Lett*., **17**, pp. 1231-1233 (1992)

[99] B. Saad, M.M. Denariez-Roberge, and T.V. Galstyan, "Diffusion of photoexcited azo dye in a liquid-crystal host", *Opt. Lett*, **23**, 9 p727-729 (1998)

[100] G. Moddel, L. Wang, "Resolution limits from charge transport in optically addressed spatial light modulators", *Journal of Applied Physics,* **78,** 12 pp. 6923-6935 (1995)

APPENDIX A

OASLMS IN THE MARKET

Spatial light modulators (SLMs) are increasingly used in many applications including 3D video, projection displays, optical correlation, real-time holography, permanent holographic data storage and optical telecommunications networks. For example, Holographic 3D displays based on SLMs are important for various applications including medical imaging, engineering design, and home entertainment. The amount of data required for such a display of video quality is extremely large (>1 Gigabit/s). Conventional electrically addressed SLMs will not be able to cope with such large amounts of information for many years to come. A solution was proposed by Cambridge University to partition information among several SLMs and to reassemble the optical image onto a separate device. A suitable device for such an operation is the Optically Addressed Spatial Light Modulator (OASLM).

Optically Addressed SLMs can be used in many non-display applications as well. These include optical correlators[i], image and wavelength converters[i], optical interconnects[i], optical phase-conjugation[i], optical logic gates[i], optical neural networks[i], tuneable dielectric distributed Bragg reflectors for distributed feedback (DFB) lasing[ii], permanent holography[iii], beam forming[i] and optical tweezers[i].

Characteristics of commercially available OASLM devices (Hamamatsu and Jenoptik) are shown below.

Hamamatsu[iv]: PAL-SLM x7665

Used in reflection

Readout λ:	633 or 680 nm
Writing λ:	600 to 800 nm
Resolution:	50 lp/mm
Phase modulation	2π or more

Input sensitivity (per 2π rad):	1 mW/cm^2, normal mode
	50 μW/cm^2, high sensitivity mode
Effective area	20x20 mm
Response speed (rise/fall times)	30 ms / 40 ms
	60 ms / 70 ms in high sensitivity mode

Price: ~10^{6}GBP

Jenoptik[v]: Slm 74.2 0897

Used in reflection

Write light spectral sensitivity	550-700 nm
Read-out wavelength	450-630 nm
Driving voltage, r.m.s.	2-10 V
Driving frequency	50 Hz-20 kHz
Maximum phase shift	varies from 0.25π to over 2π and depends on write light intensity and driving voltage.

Dependence on the write light intensity for some cases of driving voltages is presented on Figure A1:
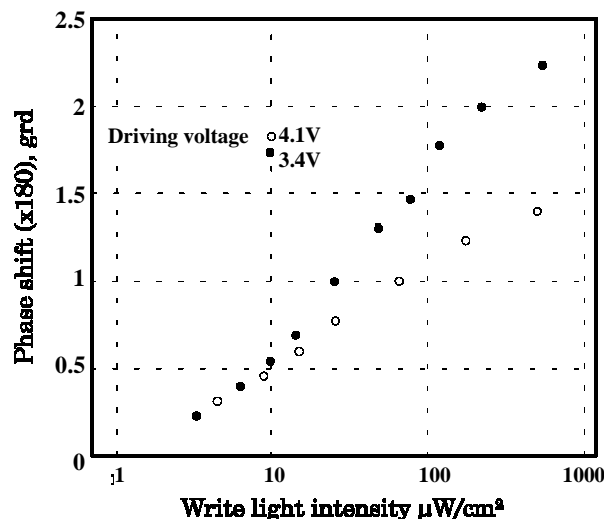

Figure A1. Phase shift as a function of writing light intensity for different voltages quoted by Jenoptik. Write light λ=630 nm; read-out λ= 550 nm, driving frequency 50 Hz.

The above devices are designed for the use in the following applications:

- Real-time holography
- Digital Holography
- Image Projection
- Pattern Projection
- Video Projection
- Phase Shifting
- Diffractive Optics
- Laser Beam Shaping
- Coherent Wavefront Modulation
- Dynamic optical tweezers
- Optical Filtering
- Image Filtering
- Pattern Recognition

---

[i] S. Mias, N. Collings, T.D. Wilkinson and W.A. Crossland, "Technology and performance of A-Si:H OASLMs", Recent res. Devel. Optics, **3**, pp 125-144, 2003

[ii] T.Matsui, M.Ozaki, K. Yoshino, "Tunable laser action in a dye-doped nematic liquid crystal waveguide under holographic excitation based on electric-field-induced TM guided-mode modulation", J. Opt. Soc. Am. B, **21**, 9, pp. 1651-1658, 2004

[iii] I.C. Khoo, B.D. Guentner and S. Slussarenko, "Photo-induced space-charge fields, photo-voltaic, photorefractivity, and optical wave mixing in nematic liquid crystals", *Mol. Cryst. Liq, Cryst*., **321**, pp. 419-438 (1998)

[iv] www.hamamatsu.com; Hamamatsu, technical exhibition, SPIE annual meeting, Denver, 2004

[v] Liquid Crystal Light Modulator Datasheet, courtesy of Kerstin Seufert of Jenoptik

APPENDIX B

CHEMICAL STRUCRURES OF THE MATERIALS USED

B.1 Host materials

B.1.1 5CB

Also known under the commercial name **K15**.

Chemical name: 4-*n*-pentyl-4-cyano-biphenyl.

Transition temperatures: solid-nematic T_{SN}=24ºC, easily supercolled to -10ºC; nematic-isotropic T_{NI}=34ºC.

Thermal conductivities[*]: $k_{\parallel}$=0.26 W/m·K; $k_{\perp}$=0.11 W/m·K.

Elastic constants (20ºC): K_{11}=5.5·10^{-12} N; K_{33}=6.96·10^{-12} N.

Flow viscosity (20ºC): η=34 mm^2/s.

Dielectric anisotropy (1kHz, 20ºC): $\Delta\varepsilon$=20.1.

Refractive indices (λ=589 nm): n_e=1.71; n_o=1.53; Δn=0.18.
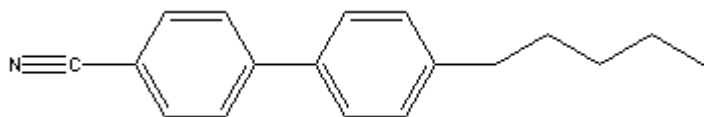

Figure B.1 The chemical structure of 5CB liquid crystal.

---

[*] H.Ono, K. Shibata, *J.Phys. D: Appl. Phys.*, **33**, pp.L137-L140 (2000)

B.1.2 E7

Chemical name: a mixture of alkile-cyano-biphenyls, alkile-cyano-tryphenyl and alkoxy-cyano-biphenyl.

Transition temperatures: solid-nematic T_{SN}= -10ºC, supercooled to <-20ºC; nematic-isotropic T_{NI}=61ºC.

Elastic constants (20ºC): K_{11}=11.1·10^{-12} N; K_{33}=17.1·10^{-12} N.

Flow viscosity (20ºC): η=39 mm²/s.

Dielectric constants (1kHz, 20ºC): $\varepsilon_{\parallel}$=19.0; $\varepsilon_{\perp}$=5.2; $\Delta\varepsilon$=13.8.

Refractive indices (λ=589 nm): n_e=1.7462; n_o=1.5216; Δn=0.2246.
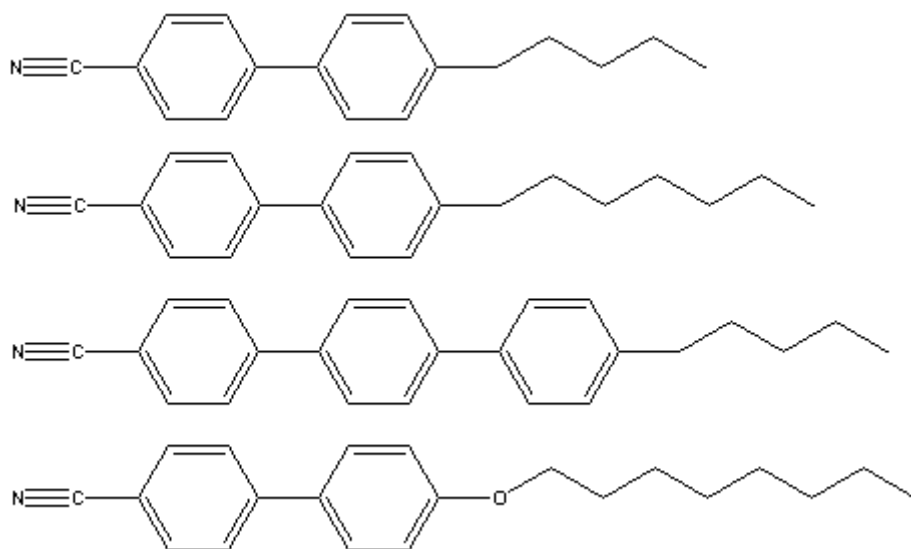

Figure B.2 The chemical structure of E7 liquid crystal.

B.1.3 BLO48

Chemical name and structure are commercial information.

Transition temperatures: solid-nematic T_{SN}= -6ºC; nematic-isotropic T_{NI}=100ºC.

Elastic constants (20ºC): K_{11}=15.5·10^{-12} N; K_{33}=28.0·10^{-12} N.

Flow viscosity (20ºC): η=47 mm²/s.

Dielectric constants (1kHz, 20ºC): $\varepsilon_{\parallel}$=22.0; $\varepsilon_{\perp}$=5.2; $\Delta\varepsilon$=16.8.

Refractive indices (λ=589 nm): n_e=1.7904; n_o=1.5277; Δn=0.2627.

B.1.4 ZLI2222

Chemical name: a mixture of phenyl-cyclohexyl, biphenyl-cyclohexyl, cyclohexyl-biphenyl-cyclohexyl. The chemical structure is commercial information.

Transition temperatures: solid-nematic T_{SN}= <-40°C; nematic-isotropic T_{NI}=66.5°C.

Flow viscosity (20°C): η=14 mm^2/s.

Dielectric constants (1kHz, 20°C): $\varepsilon_{\parallel}$=8.9; $\varepsilon_{\perp}$=3.6; $\Delta\varepsilon$=5.3.

Refractive indices (λ=589 nm): n_e=1.6134; n_o=1.5010; Δn=0.1124.

B.2 Structures of the dopants investigated

B.2.1 DC161

Chemical name: 2,5 azo-substituted anthraquinone. Dichroic. Order parameter in NLC matrix up to 0.69[i]. Max absorption wavelength λ_{max}=527 nm. Absorption coefficients of 1% solution: $\alpha_{\parallel}$=3000 cm^{-1} and $\alpha_{\perp}$=500 cm^{-1}.
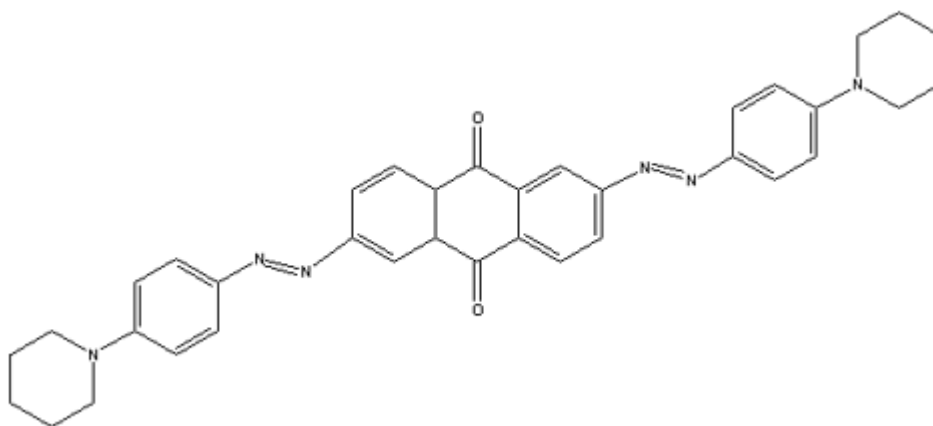

Figure B.3 The chemical structure of DC161 dye[i].

Comments: good solubility, ~1% in 5CB, E7 and BLO48 host materials.

B.2.2 DC162b

Chemical name: 1-amino, 2-ester, 4-NO$_2$-anthraquinone. Dichroic. Order parameter in NLC matrix up to 0.66. Max absorption wavelength λ_{max}=494 nm[i].
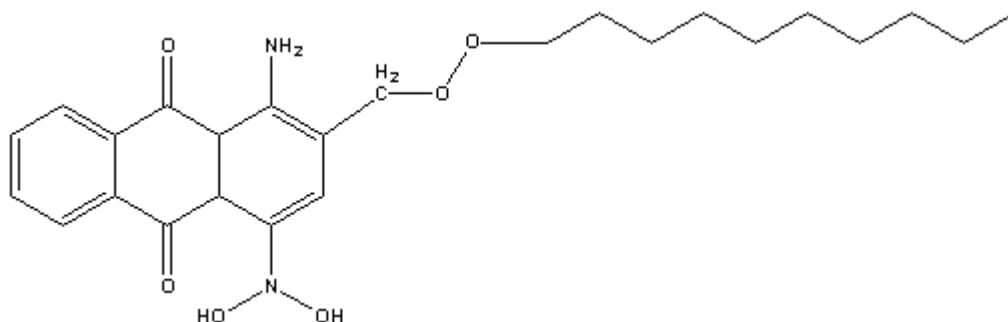

Figure B.4 The chemical structure of DC162b dye[i].

Comments: solubility less than 1% in ZLI2222 host.

B.2.3 DC168

1,2-substituted anthraquinone dye. Dichroic. Order parameter in NLC matrix up to 0.56. Max absorption wavelength λ_{max}=487 nm[i].
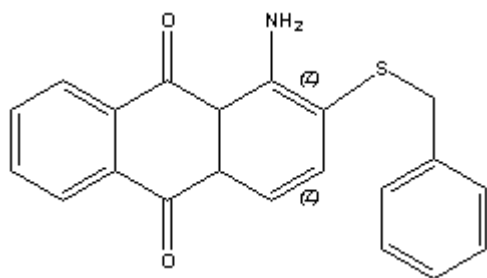

Figure B.5 The chemical structure of DC168 dye[i].

Comments: solubility less than 1% in ZLI2222 host.

B.2.4 DC179

4-substituted anthraquinone dye. Dichroic. Order parameter in NLC matrix up to 0.66. Max absorption wavelength λ_{max}=515 nm[i].
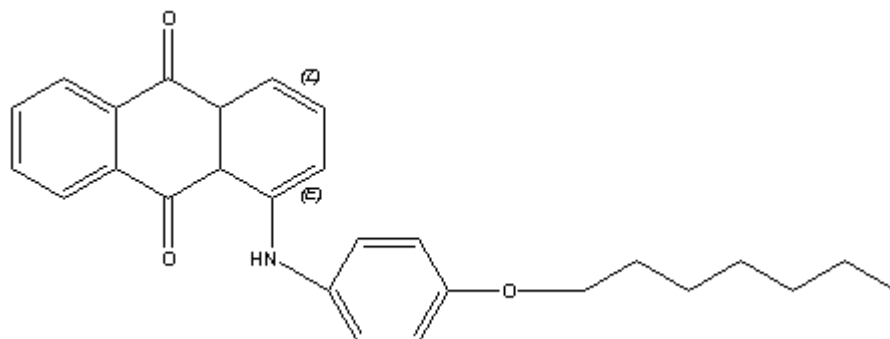

Figure B.6 The chemical structure of DC179 dye[i].

Comments: good solubility, over 2% in ZLI2222 and E7 host.

B.2.5 DC185

1,4-substituted anthraquinone dye. Dichroic. Order parameter in NLC matrix up to 0.63. Max absorption wavelength λ_{max}=470 nm[i].
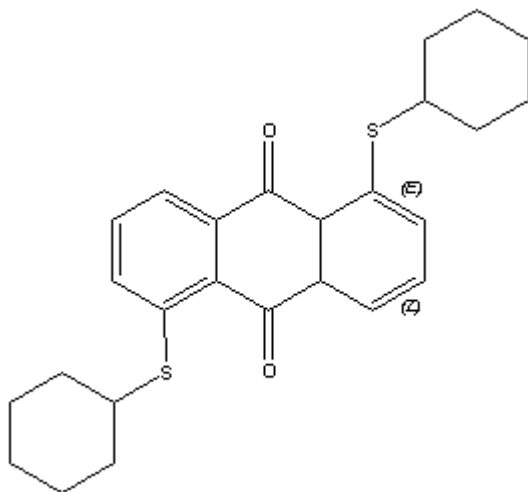
Figure B.7 The chemical structure of DC185 dye[i].

Comments: solubility less than 1% in ZLI2222 host.

B.2.6 Buckminster fullerene C$_{60}$

Aldrich Cat. No.: 37, 964-6 (99.5% purity)

Figure B.8 The chemical structure of C$_{60}$.

Comments: especially poor solubility, less than 0.02% in 5CB and BLO48 hosts.

B.2.7 Methyl Orange

Aldrich Cat. No.: 23, 410-9

Also known as acid orange. Purity ~85+%. Max absorption wavelength λ_{max}=470 nm[ii].
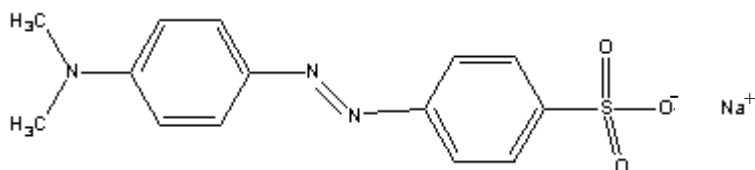
Figure B.9 The chemical structure of Methyl Orange dye.

Comments: poor solubility, less than 0.5% in ZLI2222 host.

B.2.8 Methyl Red sodium salt

Aldrich Cat. No. 11, 450-2.

Purity ~95%. Dichroic. Max absorption wavelength λ_{max}=437 nm[ii]. Absorption depends on a solvent: pH 4.2 (pink) to pH 6.2 (yellow).

Figure B.10 The chemical structure of MR sodium salt dye.

Comments: very poor solubility in general and in LC in particular: less than 0.1% in ZLI2222 host.

B.2.9 Methyl red hydrochloride

Aldrich Cat. No.: 86, 123-5

Dichroic. Max absorption wavelength λ_{max}=493 nm[ii]. Absorption depends on a solvent: pH 4.2 (pink) to pH 6.2 (yellow).
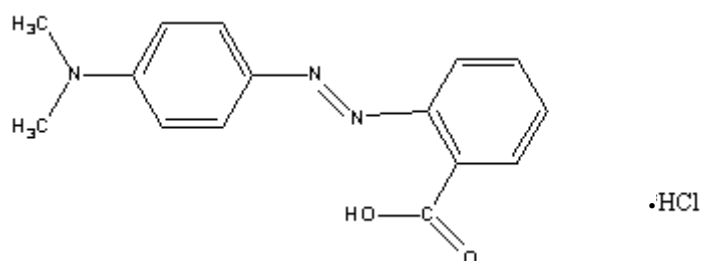
Figure B.11 The chemical structure of methyl red hydrochloride dye.

Comments: poor solubility, less than 0.2% in ZLI2222 host.

B.2.10 Methyl red, crystals (acid form)

Aldrich Cat. No.:25,019-8

Chemical name: [2-[4-(dimethylamino)phenyl-azo]benzoic acid]. Dichroic. Order parameter in NLC matrix ~0.37[†]. Max absorption wavelength is cited to be λ_{max}=410 nm[ii]. Absorption depends on a solvent: pH 4.2 (pink) to pH 6.2 (yellow).In nematic LCs 5CB and E7 λ_{max}=490 nm[†] (orange).
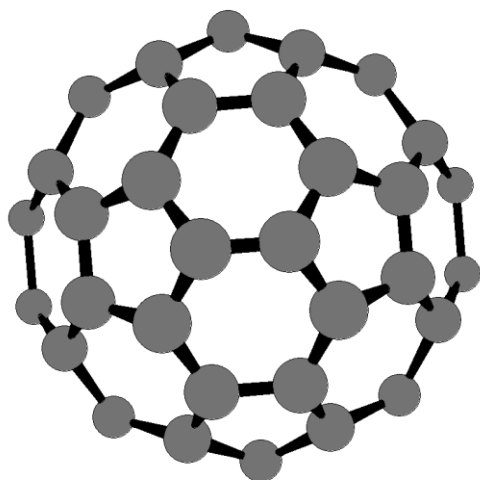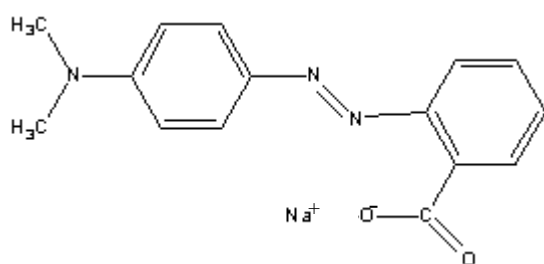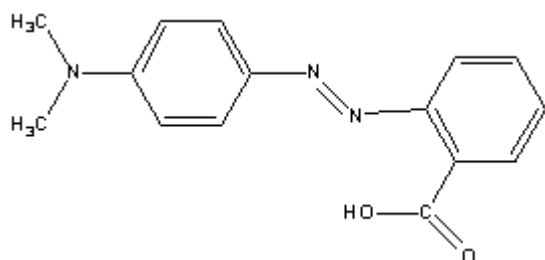

Figure B.12 The chemical structure of methyl red crystals dye.

Comments: good solubility, over 3.5% in 5CB host.

B.2.11 Rhodamine B

Aldrich Cat. No.: 25, 242-5

Laser dye. Purity ~90%. λ_{max}=543 nm.
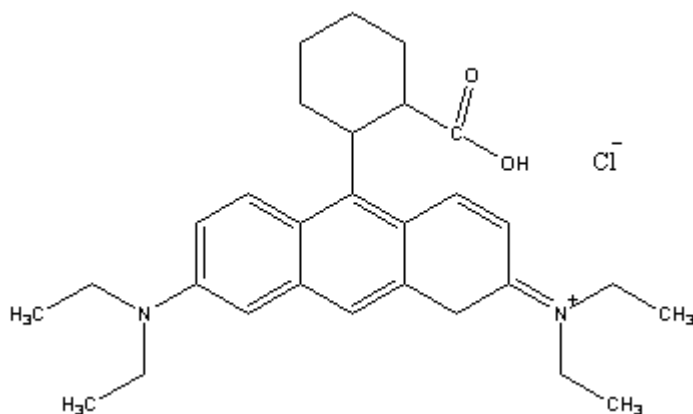
Figure B.13 The chemical structure of Rhodamine B laser dye.

Comments: solubility less than 1% in BLO48 host.

[†] Confirmed by absorption measurements in this research work - see Chapter 4 and Appendix D.

B.2.12 Cobalt complexes[‡]

a)   b)   c)
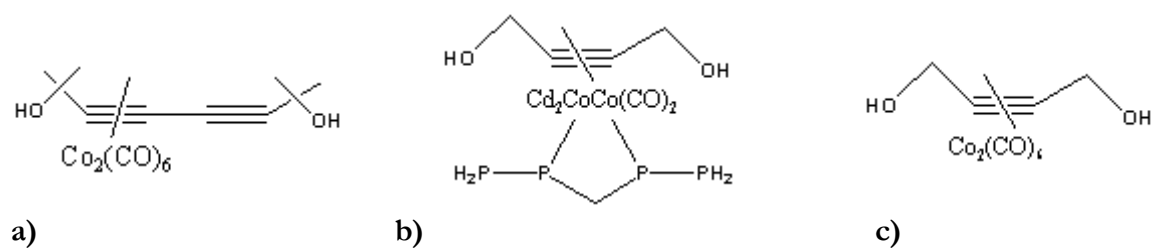
Figure B.14 The chemical structures of dyes on cobalt complexes:
a) VG1; b) VG2; c) VG3.

B.2.13 JG32 LC material[§]
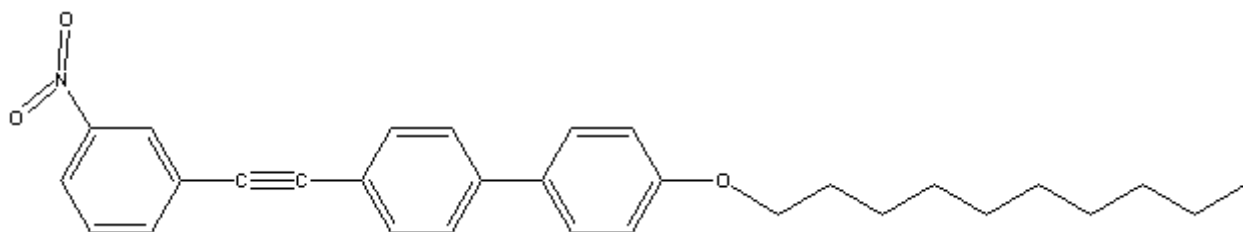
Figure B.15 The chemical structure of JG32 LC material.

B.2.14 SJ54 dye[§]
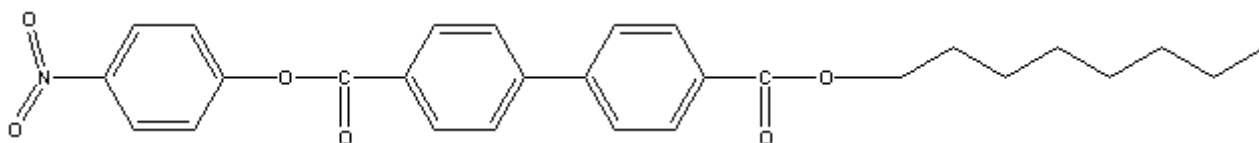
Figure B.16 The chemical structure of SJ54 dye.

[‡] Kindly offered for research by Dr. V. Golovko, Chemistry Department, University of Cambridge

[§] Kindly offered for research by Prof. J. Goodby of Hull University

B.3 Structures of the dyes researched by other groups

Marrucci et al. [iii]
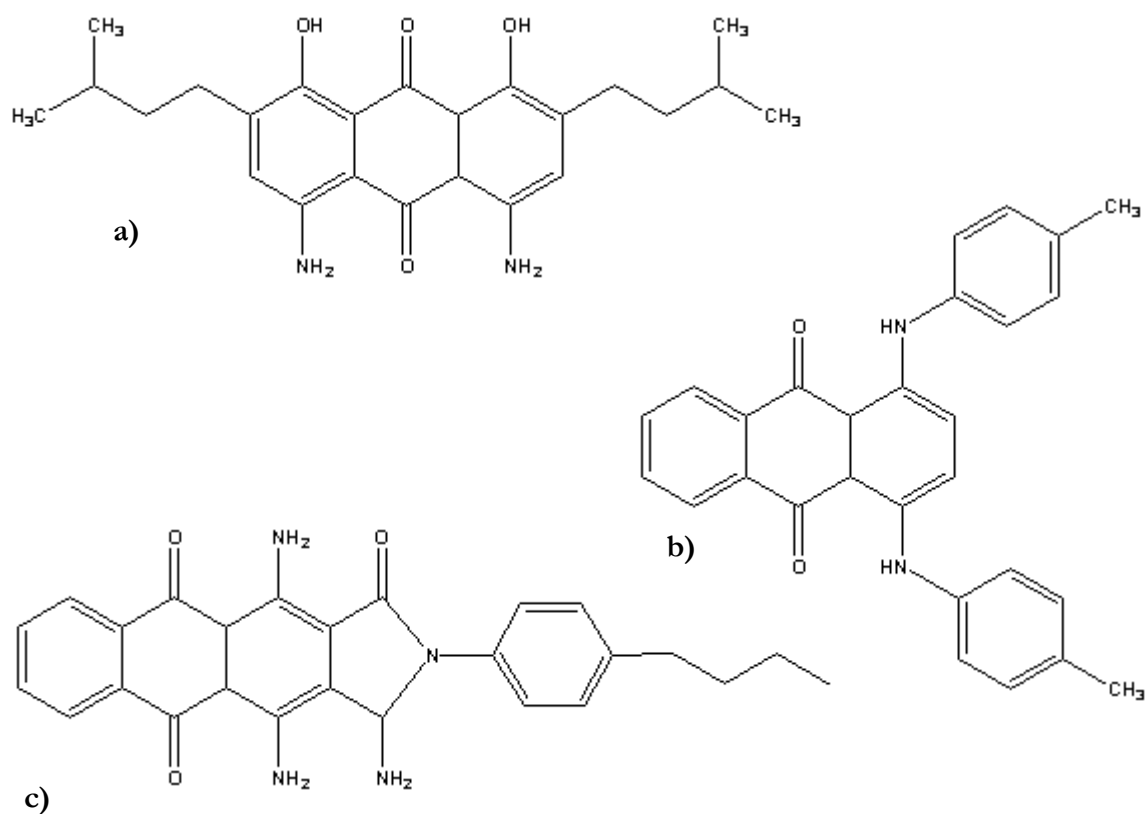
Figure B.17 The chemical structure of dyes used by Marrucci et al.
a) AD1; b)AD3; c)AD2.

All dyes are dichroic.

Parka et al. [iv]
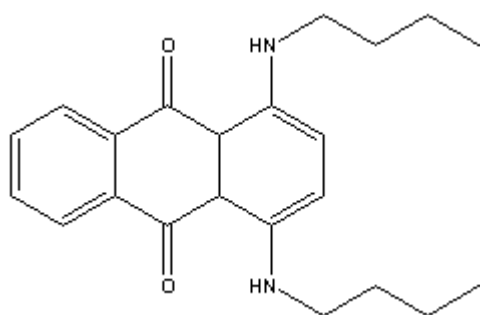
Figure B.18 The chemical structure of an anthraquinone dye used by Parka.

M. Okutan et al[v]
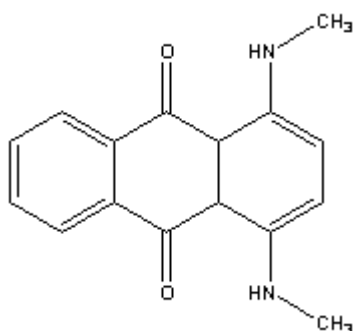
Figure B.19 The chemical structure of an anthraquinone dye used by Okutan et al.

---

[i] Dave Coates, The datasheets on the synthesised dyes.

[ii] Aldrich handbook of fine chemicals and laboratory equipment, Unighted Kingdom, 2003-2004

[iii] L. Marucci, D. Paparo, P. Maddalena, E. Massera, E. Prudnikova, E. Santamato, "Role of guest-host intermolecular forces in photoinduced reorientation of dyed liquid crystals", *J. Chem. Phys.*, **107**, 23, pp.9783-9793 (1997)

[iv] J. Parka, A. Miniewicz, A. Januszko, Y. reznikov, R. Dabrowski, Z. Stolarz "Influence of nematic liquid crystal with dye and cell construction parameters on dynamic holographic grating formation", *Proceedings of SPIE*, **4147**, pp. 335-339 (2000)

[v] M. Okutan, O. Köysal and S. E. San "Effect of laser illumination on the electro optical characters of dye doped nematic liquid crystals", *Displays*, 24, 2, pp. 81-84 (2003)

APPENDIX C

THE STANDARD CLEANING PROCEDURE

Safety:

- Wear safety spectacles.
- Use fume cupboard.
- Wear gloves.

Cleaning:

1. Immerse in 5% to 10% solution of Decon 90 with high purity water for 5 min to remove general grease.
2. Immerse in Methanol for 5 min.
3. Immerse in high purity water for 5 min.
4. Weir flush with running high purity water.
5. Blow dry with nitrogen.

APPENDIX D

INVESTIGATED DEVICES

The list of investigated devices: names and specifications

The table below shows the basic parameters of the devices used in current studies.

Name	Host	Dopant and concentration (by weight)	Alignment	Thickness	Date built
1	5CB	1% DC161	Planar, SiO$_x$	15μm	1987
2	5CB	0.5% DC161	Planar, SiO$_x$	15μm	1987
3	5CB	1% DC161	Planar, SiO$_x$	9μm	1987
4	5CB	0.5% DC161	Planar, SiO$_x$	9μm	1987
5	5CB	1% DC161	Planar, SiO$_x$	5μm	1987
6	5CB	0.5% DC161	Planar, SiO$_x$	5μm	1987
7	5CB	1% DC161, purified	Planar, 2° tilt, PI	20μm	20.05.2004
8	5CB	1% DC161, purified	Planar, 2° tilt, PI	20μm	20.05.2004
9	5CB	1% DC161	Planar, SiO$_x$	14μm	10.11.2003
10	5CB	1% DC161, purified	Planar, 2° tilt, PI	10μm	20.05.2004
11	5CB	1% DC161	Planar, 2° tilt, PI	10μm	27.01.2003
12	5CB	1% DC161	Homeotropic, ZLI1134	10μm	27.01.2003

Continued…

…continued

Name	Host	Dopant and concentration (by weight)	Alignment	Thick-ness	Date built
13	BLO48	1% DC161	Planar, 2° tilt, PI	14μm	16.06.2004
14	BLO48	0.5% DC161	Planar, 2° tilt, PI	14μm	16.06.2004
15	BLO48	1% DC161	Planar, 2° tilt, PI	10μm	16.06.2004
16	BLO48	0.5% DC161	Planar, 2° tilt, PI	10μm	16.06.2004
17	E7	0.5% DC161	Planar, 2° tilt, PI	125μm	8.09.2004
18	E7	0.1% DC161	Planar, 2° tilt, PI	125μm	6.10.2004
19	E7	0.5% DC161	Planar, 2° tilt, PI	60μm	22.11.2004
20	E7	0.5% DC161	Planar, 2° tilt, PI	40μm	22.11.2004
21	E7	1% DC161	Planar, 2° tilt, PI	14μm	10.06.2004
22	E7	0.5% DC161	Planar, 2° tilt, PI	14μm	10.06.2004
23	E7	1% DC161	Planar, 2° tilt, PI	10μm	10.06.2004
24	E7	0.5% DC161, purified	Planar, 2° tilt, PI	10μm	31.05.2004
25	E7	0.5% DC161	Planar, 2° tilt, PI	10μm	10.06.2004
26	5CB	1% MR	Planar, SiO_x	10μm	10.11.2003
27	5CB	1% MR	Planar, 2° tilt, PI	10μm	14.07.2003
28	5CB	1% MR	Planar, 2° tilt, PI	5μm	14.07.2003
29	E7	0.5% MR	Planar, 2° tilt, PI	10μm	27.01.2003
30	E7	0.5% MR	Homeotropic, ZLI1134	10μm	27.01.2003
31	BLO48	0.01% C_{60}, 99.5% purity	Planar, 2° tilt, PI	20μm	9.05.2002
32	BLO48	0.01% C_{60}, 99.5% purity	Homeotropic, ZLI1134	20μm	9.05.2002
33	BLO48	0.01% C_{60}, 99.5% purity	Planar, 2° tilt, PI	20μm	31.05.2004
34	5CB	0.01% C_{60}, 99.5% purity	Planar, 2° tilt, PI	20μm	28.04.2004
35	5CB	0.01% C_{60}, 72% purity	Planar, 2° tilt, PI	20μm	28.04.2004
36	5CB	0.01% C_{60}, soot	Planar, 2° tilt, PI	20μm	28.04.2004

Continued…

…continued

Name	Host	Dopant and concentration (by weight)	Alignment	Thick-ness	Date built
37	5CB	undoped	Planar, 2° tilt, PI	10μm	2003
38	E7	undoped	Planar, 2° tilt, PI	10μm	27.01.2003
39	BLO48	undoped	Planar, 2° tilt, PI	2μm	2001

Table D. 1. Names and parameters of the devices used in the current work.

Absorption and order parameters of devices doped with dichroic dyes

Details on the absorptance and order parameters of the samples that were doped by DC161 and MR dyes are shown in the Table D.2 below. Two values of absorptance represent absorption data for two light polarisations: $E_{//}$ and $E_\perp$ - parallel and perpendicular to the director axis respectively.

Absorptance A is calculated from the transmittance T measurements: $A=1–T^*$. The transmittance measurements are described in Chapter 4 in detail.

Dye order parameter is calculated at maximum absorption wavelength λ_{max}. For DC161 $\lambda_{max}=527$ nm; for MR $\lambda_{max}=490$ nm. The order parameter is calculated using the equations 4.3-4.5 described in Chapter 4.

Name	Host	Dopant and concentration (by weight)	Thick-ness	Absorptance, $\lambda=\lambda_{max}$		Order parameter S	Error, $\Delta S/S$
				$E_{//}$	E_v		
1	5CB	1% DC161	15μm	99.5%	67.3%	0.55	3.6%
2	5CB	0.5% DC161	15μm	97.75%	55.5%	0.55	6.9%
3	5CB	1% DC161	9μm	93.9%	47.5%	0.53	11.9%
4	5CB	0.5% DC161	9μm	82%	36.7%	0.48	28.0%

continued…

---

[*] Reflection and scattering losses are accounted for in the measurement - see Chapter 4 for details.

…continued

Name	Host	Dopant and concentration (by weight)	Thick-ness	Absorptance, $\lambda=\lambda_{max}$		Order parameter S	Error, $\Delta S/S$
				$E_{\parallel}$	E_{υ}		
5	5CB	1% DC161	5μm	78%	30.9%	0.51	38.5%
6	5CB	0.5% DC161	5μm	64.1%	23.2%	0.49	80.5%
7	5CB	1% DC161	20μm	99.7%	61.7%	0.63	3.7%
8	5CB	1% DC161	20μm	99.63%	63%	0.61	3.7%
9	5CB	1% DC161	14μm	98.1%	66%	0.47	5.1%
10	5CB	1% DC161, purified	10μm	94.2%	43.5%	0.57	12.9%
11	5CB	1% DC161	10μm	96%	43%	0.61	11.5%
13	BLO48	1% DC161	14μm	-	-	-	-
14	BLO48	0.5% DC161	14μm	64%	34.5%	0.32	59.1%
15	BLO48	1% DC161	10μm	-	-	-	-
16	BLO48	0.5% DC161	10μm	85.2%	30.2%	0.59	30.4%
17	E7	0.5% DC161	125μm	-	-	-	-
18	E7	0.1% DC161	125μm	99.25%	48.9%-	0.68	6.2
19	E7	0.5% DC161	60μm	-	-	-	-
20	E7	0.5% DC161	40μm	-	-	-	-
21	E7	1% DC161	14μm	-	-	-	-
22	E7	0.5% DC161	14μm	83%	31%	0.56	32.1%
23	E7	1% DC161	10μm	98.1%	42%	0.68	9.5%
24	E7	0.5% DC161, purified	10μm	92.3%	36%	0.61	18.1%
25	E7	0.5% DC161	10μm	76.8%	30%	0.51	41.4%

continued…

…continued

Name	Host	Dopant and concentration (by weight)	Thick-ness	Absorptance, $\lambda=\lambda_{max}$		Order parameter S	Error, $\Delta S/S$
				$E_{\parallel}$	E_v		
26	5CB	1% MR	10μm	94.2%	65%	0.36	8.1%
27	5CB	1% MR	10μm	94.4%	64.5%	0.37	8.0%
28	5CB	1% MR	5μm	73.6%	40.6%	0.34	35.8%
29	E7	0.5% MR	10μm	70.6%	35.5%	0.37	44.5%

Table D.2. Absorptance and order parameters of the investigated planar aligned devices, that were doped with dichroic dyes. The measurements and calculations are performed following the procedure described in Chapter 4.
Homeotropic devices do not exhibit dichroism (from geometry considerations), therefore the order parameter in the homeotropic devices has not been studied.
In the case of very strong absorption, beyond the sensitivity of the measuring setup (>99.7%), transmittance could not be measured, and the corresponding absorptance is not specified in the table.

Very large errors of the calculated order parameter indicate that at given absorption values of the device it is not possible to define the order parameter with high confidence. Note that the error of the calculated order parameter (equation 4.5) depends on the value of difference in the optical densities for two light polarisations of the sample. Therefore, when optical densities are low and their difference is small, which is often the case in weakly absorbing samples, the error becomes very large, and other devices have to be used for the order parameter definition.

Electric parameters of the studied devices

Resistivity

The resistivity of the studied devices is comparatively low (Table D.3). Introducing dopants further decreases the resistivity and increases capacitance. Even undoped LC samples exhibit resistivity up to two magnitudes lower than usually expected from a good,

purified, material. Nevertheless, the optical nonlinearity does not require high resistance or a high purity of the liquid crystalline material. In fact, ions (from dopants or impurities) play an essential part in some nonlinear photorefractive processes (see Chapter 2).

It is characteristic of the resistivity that it rises after a prolonged application of DC field due to impurity ions plating out at the electrodes, and therefore the medium becoming depleted of charges (Table D.3). As for the minor decrease in the capacitance, the depletion from charges is also a plausible explanation of this phenomenon.

Name	Host, dopant and concentration (by weight)	Resistivity $\cdot 10^6$ $\Omega \cdot$m	Capacitance, nF	After 5min application of $3V_{DC}$	
				Resistivity, $\cdot 10^6$ $\Omega \cdot$m	Capacitance, nF
37	5CB	54.7	0.68	135	0.62
11	5CB+1wt%DC161	5.89	0.99	5.45	0.95
27	5CB+1wt%MR	1.26	1.3	1.59	1.1
34	5CB+0.01wt%C_{60}	3.3	0.87	2.98	0.96
35	5CB+0.01wt%C_{60-72}	3.85	0.74	4.75	0.60
36	5CB+0.01wt%C_{60} soot	3.81	0.76	3.81	0.76
38	E7	76.4	0.68	-	-
29	E7 + 0.5wt%MR	5.64	0.78	-	-
39	BLO48 (2μm cell!)	37.8	0.38	47.9	0.34
31	BLO48+0.01%C_{60} (old)	7.79	0.6	7.79	0.6
33	BLO48+0.01%C_{60} (new)	5.05	0.56	5.04	0.56

Table D.3 The resistivity and the capacitance of the investigated devices.

The table above gives several interesting insights. First of all, it could be seen that all dopants significantly lower the resistance of the system either through associated impurities or because they are ionic themselves (it is not possible to distinguish these two effects by these measurements). This also applies to the increase of the capacitance. The more charge can be stored in the device (by charge carriers with low mobilities), the higher the capacitance.

Out of the three dopants used, MR gives the most dramatic change in resistance and capacitance. Methyl Red is indeed an ionic dopant, and the resistance lowering/capacitance

increase in the case when using this dopant is the greatest. Ions, introduced by MR are large (see Appendix B for structural formulae of MR crystals dye), and therefore likely to possess low mobilities.

Secondly, it is interesting to note that after the prolonged application of a DC field there has been almost no change in resistance in all doped systems, while in undoped liquid crystals resistivity has increased. This behaviour observed in the doped devices may be explained by several mechanisms, the most likely of which are the following:

- The ions that contribute to lowering the resistivity possess very poor mobility and do not plate out on the electrodes during 5 minute DC application time.
  - For example, it has been suggested that charge complexes are formed in conjunction with C_{60} in polymers[1] and may be responsible for the observed behaviour in LC systems.
  - Methyl red molecules are very large and they are a possible source of charge in the LC systems.
  - DC161 molecules are not ionic and are unlikely to form charge complexes, so the resistivity may be influenced by some other impurity that may have poor mobility or form low mobility charge complexes with the LC host.
- The process of adsorption/desorption of the ions on the surfaces is prohibited due to the dopant influence. For example, the adsorbed dopant layer may hinder the adsorption of the ions on the electrodes.
  - C_{60} may be adsorbed at the surface under the influence of light (resulting in permanent/persistent gratings).[2] Normal illumination conditions (ambient light) probably do not trigger such adsorption, but the pre-history of the samples and dark adsorption could lead to the formation of the discussed barrier layer.
  - It has been suggested that light-induced adsorption of the dye molecules in MR doped systems is the explanation for permanent grating formation[3] and for the strong surface-induced nonlinearity[4], while the dark adsorption of the dye has been also discussed in MR doped LC systems.[5] Thus the adsorption of the MR dye may be responsible for the observed ionic effect.

- Surface induced nonlinearity has not been registered in DC161 devices (see Chapter 5), nevertheless the adsorption of the molecules or impurities on the device surface may not be considered as non-existent.

● The applied field triggers processes leading to free charge generation.

  - C_{60} and MR are known[6] to generate a space-charge field under the influence of light and an external DC field, but it is unlikely that the ambient light was enough to generate a large number of charges (see also Chapter 5 on photocharge generation for all three dopants). This process is not yet defined.

All of these mechanisms may take place simultaneously. In fact, they may also be responsible for the observed capacitance behaviour. To define what exactly happens in the complex dopant-host-impurities system under the application of a DC field is a large research subject, which is outside the scope of this research work.

Freedericksz transition in dye and fullerene-doped devices

Studying a variety of dopant-LC systems, a strong dependence of the FT threshold voltage at low frequencies for certain dopants has been found. The measurements were made using the two independent techniques described above - the optical and impedance methods[*]. Freedericksz transition values for dye-doped and pure samples that were directly taken from resistance and/or capacitance curves correlate with both the experimentally optically measured results and the theoretical values (Table D.4). The theoretical values are calculated using equation 2.22 (Chapter 2). The parameters used for calculation (elastic constants and dielectric anisotropy values) for various LC materials can be found in Table 3.2, Chapter 3 and in Appendix B.

The measurements are performed utilising electric fields at different frequencies, namely 1 kHz, 100 Hz and 1 Hz. High frequency measurements (>10 Hz - above typical molecular motion frequencies) show the Freedericksz transition threshold and are identical for 1 kHz and 100 Hz.

---

[*] In cases where the dopant increases conductivity of the sample, it can trigger a dynamic instability resulting in scattering, which has nothing to do with the Freedericksz transition, but will lead to the same results when registering transmitted light through the extinguished polarisers.

Low frequency measurements are in general not meaningful in terms of the Freedericksz transition in low conductivity systems. These measurements have been performed to study the behaviour of devices at DC fields that are sometimes used for aiding optical nonlinearity. The behaviour of the doped systems in the low-frequencies/DC region is discussed below.

Name	Material, alignment	Impedance measurements		Optical measurements	
		V_{th}, V (1Hz)	V_{th}, V (1KHz*)	V_{th}, V (1Hz)	V_{th}, V (1KHz†)
37	5CB, PI theoretical value 0.55V	0.6±0.1	0.6±0.1	1.5±0.1	1.5±0.1
9	5CB+1wt%DC161, SiO$_x$	-	-	3.35±0.1	1.55±0.1
11	5CB+1wt%DC161, PI	-	0.6±0.1	2.35±0.1	1.55±0.1
26	5CB+1wt%MR, SiO$_x$	-	-	3.35±0.1	1.7±0.1
27	5CB+1wt%MR, PI	-	0.7±0.1	2.4±0.1	1.25±0.1
34	5CB+0.01wt%C$_{60}$, PI	-	0.7±0.1	-	-
35	5CB+0.01wt%C$_{60}$, PI	-	0.7±0.1	-	-
36	5CB+0.01wt%C$_{60}$, PI	-	0.7±0.1	-	-
38	E7 pure, PI† theoretical value 0.95V	1±0.1	0.85±0.1	1.4±0.1	1.25±0.1
29	E7+0.5wt%MR, PI	1.6±0.1	0.85±0.1	2.2±0.1	1.4±0.1
39	BLO48 pure, PI theoretical value 1V	1±0.1	1±0.1	1.8±0.1	1.8±0.1
31	BLO48+0.01wt%C$_{60}$, PI	0.7±0.1	0.7±0.1	1.2±0.1	1.2±0.1
33	BLO48+0.01wt%C$_{60}$, PI, new	-	0.5±0.1 ‡	-	-

Table D.4 Freedericksz transition threshold voltage in doped samples (measured by optical and impedance methods). As the impedance measurements correlate well with the optical measurements, they have not been repeated for all samples.

---

* The measurements taken at 100 Hz are almost identical with the 1 kHz case and are not displayed in the table.

† PI alignment gives small (1-2º) pretilt to the devices, while SiOx alignment produces strictly planar alignment. Pre-tilt may result in lowering of the Freedericksz transition threshold.

‡ Very gradual transition.

First, it can clearly be seen from Table D.4 that optical measurement produces higher values for the Freedericksz transition threshold voltage than is the case with dielectric measurements, and both produce values higher than the theoretical ones. This is because the threshold value in theory is defined at the indefinitely small reorientation of liquid crystal director (see Chapter 2) while the change in parameters (birefringence and impedance) may be observed only at a certain value of reorientation. It also can be seen that the impedance measurement of the Freedericksz transition is a more sensitive technique.

High frequencies and Freedericksz transition

In dye-doped devices the threshold is almost unchanged and shows a weak dependence on the alignment layers. The lowering of the threshold in the polyimide-aligned films may be understood if the pre-tilt introduced by this alignment is taken into account. The pre-tilt lowers the threshold voltage, due to a larger torque from the electric field acting on the tilted molecules as compared to the non-tilted (see Chapter 2, equations 2.11 and 2.14) for the same values of applied fields.

It is very interesting to observe that in C_{60} doped BLO48 devices the Freedericksz transition threshold is decreased, while in 5CB doped with the same dopant there is no change in the transition.

There can be a number of effects leading to the change in the threshold voltage in the systems described. Several effects may take place simultaneously in the given system:

❑ Dopant adsorption on the cell surface may lead to a change in the anchoring energy and/or change in the pre-tilt of the planar alignment. Both effects should promote homeotropic alignment and effectively lower the transition threshold.
   ▪ Such surface effect will have no dependence on the frequency of the applied field.
     Indeed, no frequency dependence has been observed in the frequency range from 1 Hz to 1 kHz.
   ▪ Dopant adsorption should not depend on the host material directly.
     The observed dependence (Table D.4) may be explained by the fact that dopant adsorption on a device surface may depend on the strength of interaction with the host compared with the strength of interaction with the alignment layer.
   ▪ Adsorption on the surface would be different for different planar aligning agents.

Having devices with only one planar aligning agent prevented verifying this idea.
Dopant adsorption on the surface has been reported to significantly increase the FT threshold in C_{60} doped devices[7]. The change of anchoring conditions due to the adsorption of the dopant may be responsible for the effect in C_{60} doped BLO48 systems, although with a smaller effect and the opposite sign of a change.

❑ If the dopant possesses a very large dielectric constant (as in the case of C_{60}), the field imposed on the host molecules on the microscopic level will be increased, thus varying the dielectric properties of the media on the macroscopic level (and lowering the actual threshold).

  ▪ This effect will have no strong dependence on the frequency of the applied field, as in the previous case.

  ▪ Trace amounts of C_{60} (0.01% concentration by weight) are used.
    Such material quantities are unlikely to be sufficient to cause a sizeable change in dielectric properties of the system.

The change of dielectric constant is not likely to be involved in the discussed lowering of the FT threshold.

❑ If charge complexes are formed in the dopant-LC system, this will vary the local field in the system and lead to the lowering of the threshold voltage.

  ▪ This effect should not have a strong dependence on the frequency of the applied field.
    This is observed on the experiment (Table D.4).

  ▪ There should be a dependence of the resulting threshold voltage, as charge complexes formation depends strongly on the materials involved.
    This is observed on the experiment (Table D.4).

  ▪ Alignment layers should not influence the formation of charge complexes, unless they are ionic or introduce impurities.
    This has not been confirmed by an experiment.

Thus, the formation of charge complexes is another likely reason for the lowering of the Freedericksz transition threshold in C_{60} doped BLO48 systems.

Low frequencies (may be extended to DC field case)

At very low electric field frequencies doped systems show peculiar behaviour with a very strong increase in the observed FT threshold voltage, especially in DC161 doped devices (~2 times increase in threshold voltage at 1 Hz as compared with 1 kHz and 100 Hz). No increase is observed in pure LCs and C_{60} doped systems.

It should be stressed that low frequency measurements do not, strictly speaking, indicate the Freedericksz transition. What they show is likely to be purely ionic behaviour of the device.

A so-called Helmholtz double layer[8] formation may be one of the mechanisms that rise the FT threshold at low frequencies. At DC and low frequency fields, the charges (ionic impurities or ions introduced by dopants, as observed in resistivity studies described above) may form a double layer, effectively screening the LC bulk from the electric field[*]. In this case, the field needed to cause the orientational changes in LC is higher than for high frequency cases, where the screening layer is not formed.

Another important piece of information derived from the measurements at low frequencies is that a large part of the applied DC field, needed for nonlinear effects associated with a space-charge field formation, when applied to MR-doped and DC161-doped samples is possibly screened. If the aim is to operate above the Freedericksz transition in the device, appropriate adjustments to the operating electric field regime should be made and higher DC fields chosen.

Although it is not possible to answer all questions about processes in the studied devices under the application of electric fields due to a complexity of LC-dopant-undefined impurities systems, the above studies give a lot of valuable information regarding operating electric field regimes, quality of the devices in terms of ionic content and possibilities of surface or charge formation in the systems.

---

[*] The capacitance measurement may be able to confirm this assumption indirectly, as the capacitance associated with the double layer is very large, tens of μF. Such measurement at low frequencies is not possible with the equipment used. An increase of capacitance up to two orders of magnitude at low frequencies is indeed observed, but this may be an effect of the measuring system, as verified by measurements on the standard resistor-capacitor model.

IV response

Cyclic voltammetry of undoped liquid crystals exhibits hysteresis (Figure D. 1). As the voltage is swept from -10V to 0V, the current formed of impurity charges flows as expected. As the voltage approaches zero, the charge carriers do not reach the electrode any longer, but collect near this electrode.

Now, when the polarity of the voltage is changed as the voltage is increased to +10V, these charges are attracted to the opposite electrode resulting in current spike. When all the charges reach the electrode, regular behaviour is expected. As the electrodes are reversed, exactly the same picture is observed.
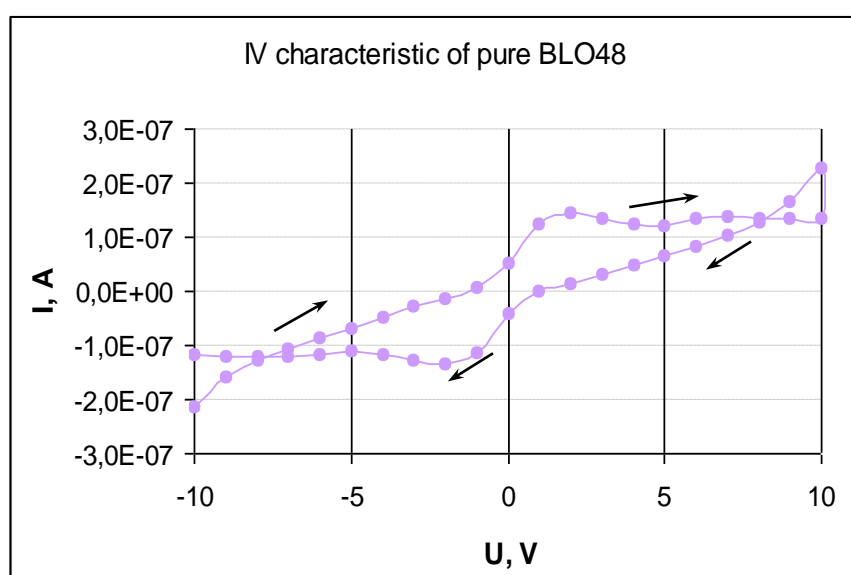

Figure D. 1 IV characteristic of pure BLO48 sample (device 39). Voltage change direction is shown with the arrows. Such current behaviour is expected from a medium with low charge density. The increase in the current after the polarity of the voltage has been changed indicates that charge carriers, that were attracted to one of the electrodes, all move to another electrode. As the medium is deprived of charges in this process, the current decreases.
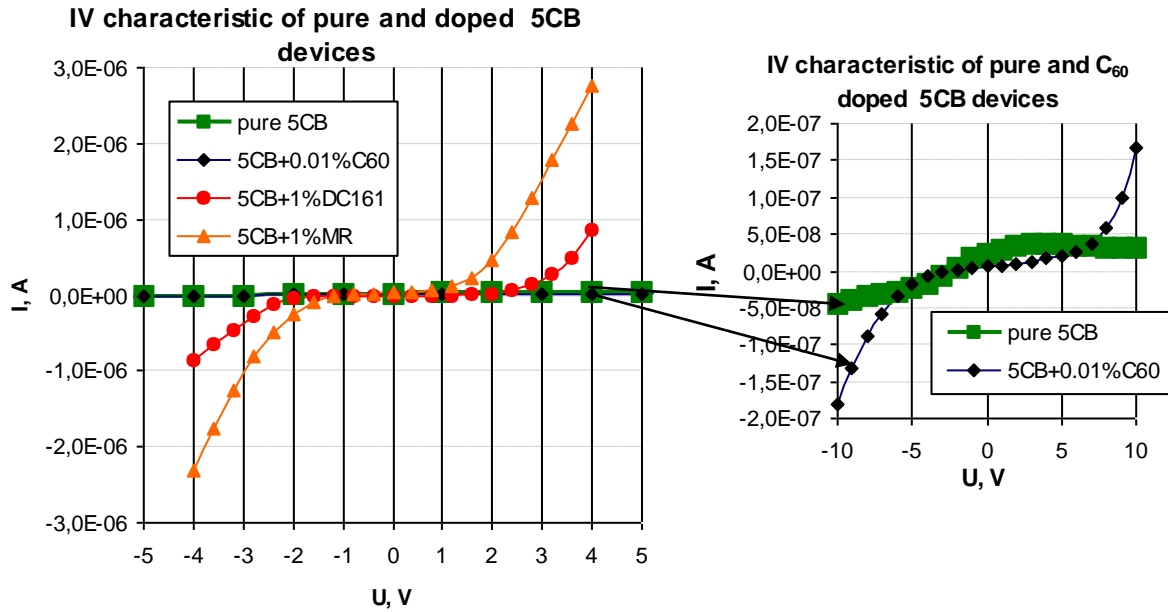
Figure D.2. IV characteristic of doped and pure 5CB devices (devices 37, 34, 11 and 27) with same thickness (10 μm) and alignment (PI). Dopants, especially MR, greatly enhance the current response and shift the IV response to the one expected from the ohmic systems (with free charge carriers). The inset shows a response of a C$_{60}$ doped 5CB device.

Inset at the top right of Figure D.2 shows a closer look at C$_{60}$ doped device characteristics, the difference between pure and doped devices becomes visible at high voltages (above 5V).

Doped LC devices also exhibit small hysteresis (see for example hysteresis in DC161 doped device on Figure 5.3).
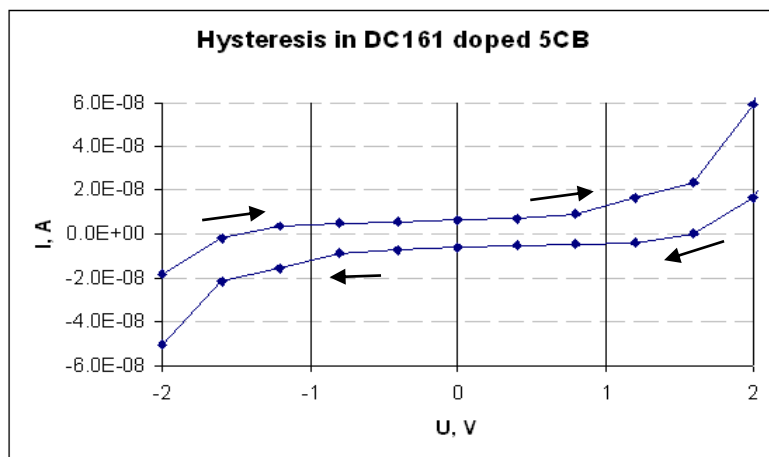

Figure 5.3 Hysteresis in IV response of DC161 doped LC device (device 11).

The current response is enhanced slightly if the device is illuminated by light. The device is C_{60} doped 5CB, illumination power 30 mW/cm^2 (Figure D.4). The enhancement of the IV response under the influence of light is in agreement with observed photocurrent generation and studies by other groups[9].
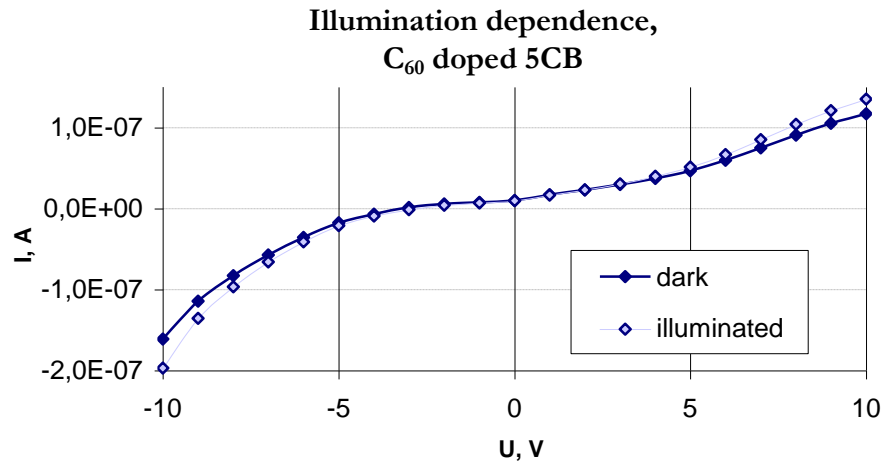
Illumination dependence,
C_{60} doped 5CB

Figure D.4. Enhancement of the current response of the C_{60} doped 5CB sample (device 34).

Let us now compare the IV characteristics of the otherwise identical C_{60} doped BLO48 devices 31 and 33, the first one exhibiting optical nonlinearity (see Chapter 5), and the second one not exhibiting nonlinear behaviour at any conditions.

The current response of the earlier built device 31 that exhibits nonlinearity is different from the characteristic obtained from the freshly built device based on the same dopant, host, alignment and preparation method (Figure D.5). The current from the freshly doped device grows with the voltage, indicating a presence of free charges. The current from the earlier built device is significantly lower than in both: pure and fresh C_{60} doped samples.
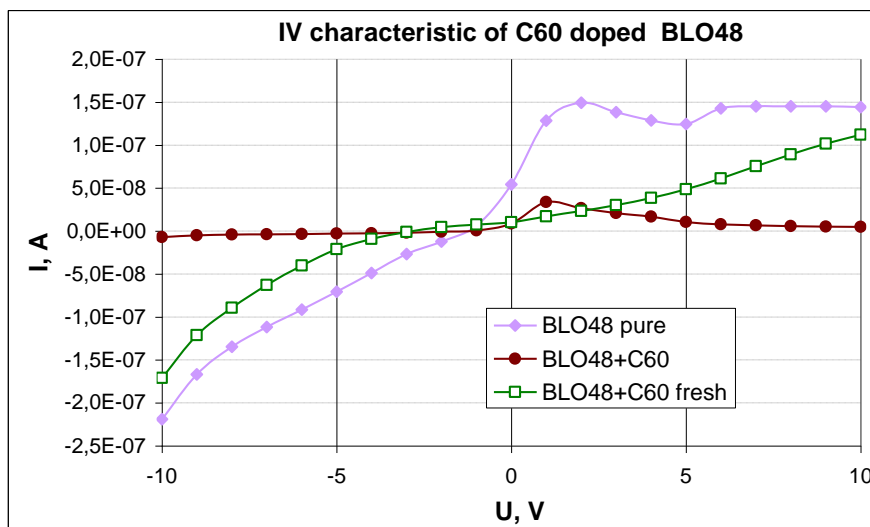
Figure D.5 IV characteristics of C_{60} doped BLO48 devices 31(old) and 33 (fresh) and a comparison with pure BLO48 sample

Such IV behaviour of the device 31 indicates the absence of the free or mobile charges. The charges could have been adsorbed at the device surface, or charge complexes may have been formed.

To summarise, the dopants, when introduced into LC host material introduce charges. MR is the most active charge producing agent. At low frequencies the Freedericksz transition threshold voltage is significantly increased in MR and DC161 doped devices possibly because of the introduced charges forming a Helmholtz double layer and screening the applied electric field.

The ageing, necessary for the nonlinearity rise in C_{60} doped devices may be accompanied by charges or dopant adsorption on one of the surfaces and/or by the formation of charge complexes with the dopant.

---

[1] Y. Wang, "Photoconductivity of fullerene-doped polymers", *Nature*, **356**, pp. 585-587 (1992)

[2] I.C. Khoo, "Holographic grating formation in dye- and fullerene C60-doped nematic liquid-crystal film " *Optics Lett*, **20**, 20, pp2137-2139 (1995)

[3] I.C. Khoo, B.D. Guentner and S. Slussarenko, "Photo-induced space-charge fields, photo-voltaic, photorefractivity, and optical wave mixing in nematic liquid crystals", *Mol. Cryst. Liq, Cryst.*, **321**, pp. 419-438 (1998)

[4] F. Simoni, L. Lucchetti, D. Lucchetta, and O. Francescangeli, "On the origin of the huge nonlinear response of dye-doped liquid crystals" *Opt. Express* **9**, 2, pp.85-90 (2001)

[5] E. Ouskova, A. Iljin, Yu. Reznikov, "Light-induced anchoring of dye-doped liquid crystal on ITO and polyvinyl-cinnamate aligning surfaces", *Proceedings of SPIE*, **4418**, pp.65-71 (2001)

[6] I.C. Khoo, "Orientational photorefractive effects in nematic liquid crystal films", *IEEE J. Quantum Electron.*, **32**, pp. 525-534 (1996)

[7] M. Kaczmarek, A. Dyadyusha, S. Slussarenko, I. C. Khoo, "The role of surface charge field in two-beam coupling in liquid crystal cells with photoconducting polymer layers", *Journal of Appl. Phys.*, **96**, 5, pp 2616-2623 (2004)

[8] C.M.A. Brett, A.M.O. Brett, "Electrochemistry. Principles, methods and applications", Oxford Univeristy Press. pp. 45-46 (1993).

[9] G.Indebetouw, P. Klysubun, "Correlation between photorefractivity, photoconductivity and dark conductivity in dye-doped, low molecular mass nematic liquid crystal cells", *Opt. Mat.*, **27**, pp. 221-233 (2004)

APPENDIX E

CALCULATION OF TEMPERATURE PROFILE

The model

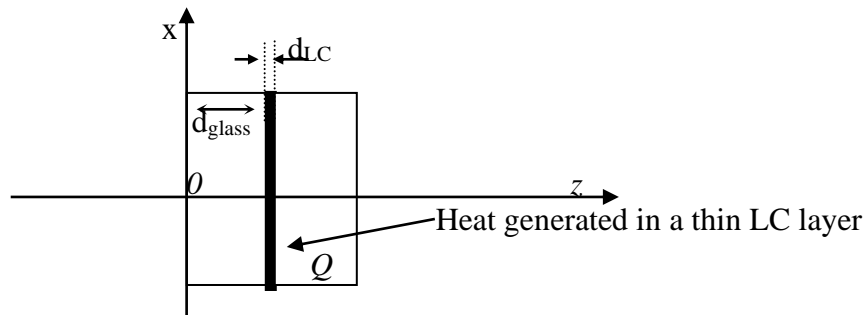The temperature profile in the LC layer confined between two glass slides

Figure E.1 Heat conduction model

 is described by equation:

$$k_x \frac{\partial^2 T}{\partial x^2} + k_z \frac{\partial^2 T}{\partial z^2} = -Q_{abs}(x,z)$$

E.1

k_x and k_z are thermal conductivity coefficients along x and z direction. In case when the grating vector is perpendicular to the director (optical intensity is modulated in x dimension, and director is along y), the k_x and k_z are the same. Q_{abs} is the absorbed optical energy, which depends on the incident optical field and absorption.

Two uniform expanded laser beams create interference pattern

$$I = \frac{1}{2} I_a (1 + \sin \frac{2\pi x}{\Lambda})$$

E.2

The intensity in the max regions is connected with the averaged optical intensity (which is measured at the experiment):

$$\bar{I} = \frac{1}{A}\int_A I dx dy = \frac{I_a}{2A}\int_A (1+\sin\frac{2\pi x}{\Lambda})dx dy = \frac{I_a}{2};$$

$$I_a = 2\bar{I}.$$

E.3

In z direction intensity will decrease, as the light is absorbed by the doped LC layer following the Labmert law:

$$I = I_o e^{-kz}$$

E.4

Where k is absorption coefficient of the media. The absorbed energy is the difference of the optical energy in the k and $k+1$ layer of absorbing media.

The initial temperature conditions are obtained by solving one-dimensional equation (z only). This gives the difference of the temperature in the plane, which is heated, and the boundary:

$$\Delta T = \frac{Qd}{2Ak}$$

E.5

The temperature at the boundary, i.e. at the surface of the sample is known from the experimental measurements.

Using derivative approximation by finite differences, the equation A.1 can be rewritten as:

$$\frac{k_x}{\Delta x^2}(T_{-1,0} - 2T_{0,0} + T_{+1,0}) + \frac{k_z}{\Delta z^2}(T_{0,-1} - 2T_{0,0} + T_{0,+1}) = -Q_{opt}$$

E.6

Solving this equation in respect to $T_{0,0}$ and making a number of iterations will give us the temperature profile in the sample. As we are interested in the difference in the temperatures between the "bright" and "dark" fringes, the convergence parameter is chosen accordingly: when the increment in the difference between the *max* and *min* temperatures in the LC layer with maximum temperature modulation becomes smaller then 10^{-8}, the calculation is stopped.

The script

This script has been written in collaboration with Andreas Georgiou, Photonics and Sensors Group, Cambridge University Engineering Department.

```
Dlc=10; % LC layer thickness, microns
Dglass=100; % glass slide thickness, μm (here we use Dglass 10 times smaller then real to
make calculations faster);
period=20; % fringe spacing, μm
n=6; % number of periods of the optical field in the cell
Xlength=n*period; % sample width, microns

Dx=1; % step in x
Xmax=round(Xlength/Dx); % a number of elements in matrix, x dimension

x=0:Dx:Xlength-Dx;
x=x';

Dz=Dx; % step in z
Zmax=round((Dglass*2+Dlc)/Dz); % a number of elements in matrix, z dimension

% to define area, where the LC is
FirstLClayer=round(Dglass/Dz+1);
LastLClayer=round(FirstLClayer+Dlc/Dz);

Intensity=50e-8; % optical intensity in mW/μm²
absorption=0.915; % sample absorption at a given optical power
absorptioncoeff=-1/Dlc*log(1-absorption);

% thermal conductivity in x and z direction (conductivity of glass) in mW/μm·K
K=0.8e-4*ones(Xmax,Zmax);
% thermal conductivity in x and z direction in LC (perpendicular to molecular axis)in
mW/μm·K
K(:,FirstLClayer:LastLClayer)=1.1e-4*ones(Xmax,-FirstLClayer+LastLClayer+1);

za=0:Dz:Dlc;
% illumination profile in z and z+1 layers
IntensityProfile=Intensity*(1+sin(2*pi*x/period))*exp(-absorptioncoeff*za);
IntensityProfile2=Intensity*(1+sin(2*pi*x/period))*exp(-absorptioncoeff*(za+1));

% absorbed optical power in glass =0
```

```
Qopt=zeros(Xmax,Zmax);
```
% absorbed optical power in LC, mW/µm³
```
Qopt(:,FirstLClayer:LastLClayer)=IntensityProfile-IntensityProfile2;
```

% setting initial temperature conditions
```
Tsurf=26.5;
TO=ones(Xmax,Zmax);
TLC=Tsurf+Intensity*0.915/0.8e-4*(10*Dglass)/2;
Ts=TLC-Intensity*0.915/0.8e-4*(Dglass)/2;
TO(:,FirstLClayer:LastLClayer)=TLC;
z1=1:Dz:Dglass;
TO(:,1:FirstLClayer-1)=Ts*ones(Xmax,FirstLClayer-1)+(TLC-
Ts)/Dglass*(ones(Xmax,1)*z1);
z2=(Dglass+Dlc+2*Dz):Dz:(Dglass*2+Dlc);
TO(:,LastLClayer:Zmax)=TLC*ones(Xmax,(1-LastLClayer+Zmax))-(TLC-
Ts)/Dglass*(ones(Xmax,1)*z1);
T=TO; % temperature matrix is set to initial value

t=0;
 delta=-1;
 THigh=0;
```

%calculation of the temperature field
```
while delta < -1e-8
```

   %boundary conditions in x direction
```
   T(1,:)=T(round(2*period/Dx),:);
   T(Xmax,:)=T(round(2*period/Dx),:);
```

%solving differential equation
```
   A=2*2*K(2:Xmax-1,2:Zmax-1)/(Dx*Dx);
   B=(K(2:Xmax-1,2:Zmax-1)/(Dx*Dx)) .* ( T(1:Xmax-2,2:Zmax-1) +
T(3:Xmax,2:Zmax-1)  );
```

```
C=(K(2:Xmax-1,2:Zmax-1)/(Dz*Dz)) .* ( T(2:Xmax-1,1:Zmax-2) + T(2:Xmax-1,3:Zmax)  );

T(2:Xmax-1,2:Zmax-1)=(Qopt(2:Xmax-1,2:Zmax-1)+B+C)./A;

% finding the  temperature difference between fringes at iterations 1 and 2, every 100
iterations
  t=t+1;
  i=rem(t,100);
  if i==1
    THigh=T(Xmax/2,108)
    TLow=T(Xmax/2,108);
      for i=10:1:Xmax-10;
        TT=T(i,108);
          if THigh<TT
             THigh=TT;end
          if TLow>TT
             TLow=TT;end
      end
    delta1=THigh-TLow;
  end
  if i==2
    THigh=T(Xmax/2,108);
    TLow=T(Xmax/2,108);
      for i=10:1:Xmax-10;
        TT=T(i,108);
          if THigh<TT
             THigh=TT;end
          if TLow>TT
             TLow=TT;end
      end
    delta2=THigh-TLow;

% the increment in temperature difference between fringes; exit cycle when it is less
then 1e-8.
```

```
        delta=delta1-delta2
    end


end


TLow
THigh
Thigh-TLow


wavelength=0.633; % the reading beam wavelength
dn=3.8e-3; % dn/dT at 27ºC


% calculation of expected diffraction efficiency
phase=2*pi*Dlc*dn*(THigh-TLow)/wavelength;
diffeff=besselj(1,phase)^2*100
```

APPENDIX F

CALCULATION OF BUILD UP DYNAMICS

The model

Let us consider the 3 level system of Figure **2.9b**. The equations describing the dynamics of trans and cis species in such system may be written as[*]:

$$\begin{cases} \dfrac{dN_{trans}}{dt} = -AN_{trans} + \dfrac{1}{2}\dfrac{N_e}{\tau_e} + \dfrac{N_{cis}}{T_{cis}} \\[2mm] \dfrac{dN_{cis}}{dt} = -A'N_{cis} + \dfrac{1}{2}\dfrac{N_e}{\tau_e} - \dfrac{N_{cis}}{T_{cis}} \\[2mm] N_e = N - N_{trans} - N_{cis} \end{cases}$$

F.1

here A and A' are corresponding Einstein coefficients that describe the loss from the ground levels to excited state due to absorption of a photon, and are connected with the absorption cross section σ of a photon with energy $h\nu$ and quantum efficiencies Φ of the respective transitions from trans and cis ground states to excited state. τ_e and T_{cis} are corresponding lifetimes of the excited and cis states.

$$A = \sigma_{trans}\Phi_{trans-e}\frac{I}{h\nu}; \qquad A' = \sigma_{cis}\Phi_{cis-e}\frac{I}{h\nu}$$

F.2

The cross section of absorption is connected with macroscopic parameter of absorptance A_b through the simple relation $A_b = \sigma_{cis}N$, where N is the number of molecules per unit volume.

---

[*] As we have already shown in Chapter 6, diffusion does not play an important role in the build up process.

$$X = e^{Mt} \cdot \left(X_0 + M^{-1}B\right) - M^{-1}B$$

$$\begin{cases} \dfrac{dN_{trans}}{dt} = N_{trans}\left(-A - \dfrac{1}{2\tau_e}\right) + N_{cis}\left(-\dfrac{1}{2\tau_e} + \dfrac{1}{T_{cis}}\right) + \dfrac{N}{2\tau_e} \\[3mm] \dfrac{dN_{cis}}{dt} = -\dfrac{N_{trans}}{2\tau_e} + N_{cis}\left(-A' + \dfrac{1}{2\tau_e} - \dfrac{1}{T_{cis}}\right) + \dfrac{N}{2\tau_e} \end{cases}$$

The system F.1 can be rewritten as

F.3

Equation F.3 may be rewritten in the matrix form:

$$\dot{X} = MX + B,$$

$$X = \begin{pmatrix} N_{trans} \\ N_{cis} \end{pmatrix}; \qquad M = \begin{pmatrix} -A - \dfrac{1}{2\tau_e} & -\dfrac{1}{2\tau_e} + \dfrac{1}{T_{cis}} \\[3mm] -\dfrac{1}{2\tau_e} & -A' + \dfrac{1}{2\tau_e} - \dfrac{1}{T_{cis}} \end{pmatrix}; \qquad B = \begin{pmatrix} \dfrac{N}{2\tau_e} \\[3mm] \dfrac{N}{2\tau_e} \end{pmatrix}$$

F.4

The software package *Matlab* allows matrix operations, in particular to raise exponential in the power of matrix. Thus we are interested in the solution of F.4 in matrix form:

$$\dot{X} = M\left(X + M^{-1}B\right)$$

$$\frac{dX}{X + M^{-1}B} = Mdt$$

$$X = e^{Mt} \cdot C - M^{-1}B$$

C is the integrating constant. From initial conditions[*] $t=0$: $N_{cis}=0$ and $N_{trans}=N$

$$X_{t=0} = C - M^{-1}B = X_0 = \begin{pmatrix} N \\ 0 \end{pmatrix}$$

$$C = X_0 + M^{-1}B$$

And the final expression for the solution is

F.5

This solution is used to calculate the dynamics of cis species build up.

The parameters that are not known and have to be guessed are:

- Quantum efficiencies of the transitions to excited state $\Phi_{trans\text{-}e}$ and $\Phi_{cis\text{-}e}$
- Lifetime of excited state τ_e

From the simulation it has been found that the lifetime of excited state should be very short as compared to the lifetime of cis state to obtain correlation with the experimental data.

In the case when the excited state lifetime is very short, and thus the number of the molecules on the excited state is negligibly small, a more simple and transparent mathematical model (suggested by Janossy) may be implemented (see also equation **6.7**):

$$\frac{dN_{cis}}{dt} = \left((N - N_{cis})\sigma_{trans}\Phi_{trans-cis} - N_{cis}\sigma_{cis}\Phi_{cis-trans} \right)\frac{I}{h\nu} - \frac{N_{cis}}{T_{cis}}$$

F.6

This is an equation of the type

$$\dot{x} = \alpha x + \beta,$$

$$x = N_{cis} \qquad \alpha = N\left(\frac{1}{T_{cis}} + \frac{\sigma_{cis}\Phi_{cis-trans}I}{h\nu} + \frac{\sigma_{trans}\Phi_{trans-cis}I}{h\nu} \right) \qquad \beta = N\frac{\sigma_{trans}\Phi_{trans-cis}I}{h\nu}$$

F.7

And the solution of equation F.6 is

$$N_{cis} = \frac{\beta}{\alpha}\left(1 - e^{-\alpha t}\right)$$

F.8

This simplified model is much easier to understand and analyse. We use it for analysis in Chapter 6.

---

[*] As there is a substantial potential barrier between trans and cis state, and the probability of the molecules to be on the cis level is approaching zero, we assume initial conditions $N_{cis}=0$.

The script

%*trans-cis transition dynamics in 3 level system (T-E-C)*

QefficiencyTE=0.3; %*quantum efficiency of transition from trans to excited state*

QefficiencyCE=0.3; %*quantum efficiency of transition from cis to excited state*

absorptionT=2291; %*cm-1 %absorption of trans species on the given wavelength*

absorptionC=1279; %*cm-1 %absorption of cis species on the given wavelength*

d nmax=0.18; % *birefringence of the material* $\Delta n=n_e-n_o$

Dlc=5e-4; % *LC layer thickness, cm*

wavelength=0.633e-4; % *cm, reading beam wavelength*

k=Dlc/10e-4;

mW=24.5e11; %*number of photons per millisecond at 514 nm writing wavelength*

power=350*mW;

Contrast=0.9;

N=1.03e19*k; % *in 1cm^3 number of molecules. Ncis and Ntrans - the population of the respective levels would be in percent.*

q=0.016; % *scales diffraction efficiency*

tauE=0.001; % *lifetime of excited state **(variable)***

tauC=120; % *lifetime of cis state (experimental value)*

Tmax=300;

dt=1;

% *intensity in bright and dark fringes;*

IntensityBright= power*(1+Contrast);

IntensityDark= 2*power-IntensityBright;

% *solution of the system of differential equations for bright fringes*

At=absorptionT/N*QefficiencyTE*IntensityBright;

Ac=absorptionC/N*QefficiencyCE*IntensityBright;

a=-At-1/2/tauE;

b=1/tauC-1/2/tauE;

```matlab
c=-1/2/tauE;
d=-Ac-1/tauC-1/2/tauE;


% define matrix A from equation Ax+B=dx/dt
A=zeros(2,2);
A(1,:)=[a b];
A(2,:)=[c d];
Ainv=inv(A);


B=N/2/tauE*[1;1];
AB=Ainv*B;
Y0=[N;0]+AB;


loop=0;


T=0:dt:Tmax; %1*tauC;
X=zeros(2,length(T));
      for t=0:dt:Tmax
              % solve the differential equation
              loop=loop+1;
              X(:,loop)=expm(A*t)*Y0-AB;
      end
% end of solution for bright fringes


% for dark fringes
AtD=absorptionT/N*QefficiencyTE*IntensityDark;
AcD=absorptionC/N*QefficiencyCE*IntensityDark;


aD=-AtD-1/2/tauE;
bD=1/tauC-1/2/tauE;
cD=-1/2/tauE;
dD=-AcD-1/tauC-1/2/tauE;


% define matrix A_{dark} from equation Ax+B=dx/dt
```

```
AD(1,:)=[aD bD];
AD(2,:)=[cD dD];
ADinv=inv(AD);


ABD=ADinv*B;
Y0D=[N;0]+ABD;


loop=0;
XD=zeros(2,length(T));
        for t=0:dt:Tmax
                % solve the differential equation
                loop=loop+1;
                XD(:,loop)=expm(AD*t)*Y0D-ABD;
        end
% end of solution for dark regions


l=length(T);
Vector=ones(1,length(T));


Dif=(X(2,:)-XD(2,:))/N*q; % the  difference in the number of cis species in dark and bright
regions


% calculation of the expected diffraction efficiency


phase=2*pi*Dlc*Dif*d nmax/wavelength;
diffeff=(besselj(1,phase)).^2*100;
plot( T, diffeff);
```
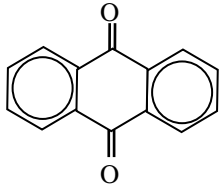
GLOSSARY

Term	Definition
3D	three dimensional;
5CB	nematic liquid crystal also known under the commercial name *K15*; chemical name: 4-*n*-pentyl-4-cyano-biphenyl; transition temperatures: solid-nematic T_{SN}=24ºC, easily supercooled to -10ºC; nematic-isotropic T_{NI}=34ºC;
absorptance A	the fraction of absorbed energy accounting for scattering and reflection, [%], $A=P_{absorbed}/P_{impinging}$; is a sample rather than a medium characteristic;
absorption coefficient α	expressed in [cm^{-1}], used in *Beer's law*; is a thickness independent parameter describing the medium;
absorption cross section σ	expressed in [cm^2/molecule], sometimes used in *Beer's law*; a thickness and concentration independent parameter describing the absorption in the medium;
ageing effect	the change of device performance either for the better or the worse with time;
alignment layer	a layer used to impose a preffered direction of the molecules in a liquid crystal film;
amplitude hologram	blocks or absorbs unwanted light thus varying the amplitude of the reading light; has therefore high losses;
anthraquinone	a chemical molecule or group of the form:
a-Si:H	amorphous silicon;

azo group	a chemical group comprising a double bond between two nitrogen atoms N=N. The molecules containing an *azo* group are asymmetric and can be in two forms: *trans* N=N and *cis* N=N. Upon excitation the isomers can change their form from one to another. This process is called *trans-cis isomerisation*.
Beer's law	$$\frac{I_{absorbed}}{I_{impinging}} = e^{-\alpha d} = e^{-\sigma c d}$$ where α is *absorption coefficient* and σ - *absorption cross section*, **c** - concentration of the absorbing molecules per unit volume;
bistability	a feature of having two stable states;
BLO48	nematic liquid crystal; transition temperatures: solid-nematic T_{SN}= -6°C; nematic-isotropic T_{NI}=100°C
Boltzman constant k_B	1.38·10^{-23} [m^2 kg s^{-2} K^{-1}]
Bragg regime	this regime is described by the two-wave coupled-wave theory of Kogelnik; the single fundamental diffracted order ideally has a diffraction efficiency given by sin^2 function;
Brillouin scattering	scattering of light from acoustic modes
calamitic LC	liquid crystals composed of elongated molecules;
carbon nanotubes	carbon macromolecules in a shape of tubes with very large diameter to length ratio. Nanotubes possess amazing mechanical, electronic and optical qualities due to very strong anisotropy of all properties.
Carr-Helfrich effect	in a nematic LC cell with applied voltage above some critical electric field strength space charge field is set up leading to convection rolls normal to the initial director alignment, with wavelength about twice the cell gap;
cell	also called a sample or a device: liquid crystal film between two glass slides;
CGS – electrostatic unit system	an acronym for **c**entimetre-**g**ram-**s**econd; a system of physical units co-exists with the standard *SI* system*;* electromagnetic formulas are simpler in *cgs* units;

chiral	from the Greek for "handed" – lacking rotational symmetry;
cholesteric LC	*chiral nematic* liquid crystal;
chromophore	molecule or group absorbing light, usually used to discuss visible range, sometimes expanded to the ultraviolet and infrared regions;
cleanroom	premises with controlled powder (dust) content in the air for device fabrication; *class 1000* – less than 1000 particles per $1m^3$; *class 100* – less than 100 particles/m^3;
clearing temperature: T_{NI}	the temperature of the transition from nematic into isotropic phase;
coherence length L_c	the path length difference of two coherent beams that corresponds to a *fringe visibility* of 50%;
colossal optical nonlinearity[i]	recently discovered surface induced effect observed in randomly oriented MR doped systems; 10^8 times larger than *giant optical nonlinearity* in pure NLCs; *nonlinear coefficient n_2* = 1000cm^2/W;
DC161	2,5 azo-substituted anthraquinone dye, dichroic; max absorption wavelength of mixture in LC matrix λ_{max}=527nm (red);
dichroism	different *absorption* in different direction - a property of anisotropically absorbing ordered media (LC, crystals);
dielectric permittivity ε	a medium characteristic (scalar for isotropic and tensor for anisotropic); expressed in [F/m]=[C^2/Nm^2]; connects *electric* and *electric displacement fields*; is connected to the *electric susceptibility* χ $\overleftrightarrow{\varepsilon} = \varepsilon_o (\overleftrightarrow{1} + \overleftrightarrow{\chi})$ (1 is a unit tensor); ε_o is the *dielectric permittivity* of free space; ε_o=8.85·10^{-12} [F/m]
dielectric relaxation frequency f_D	frequency much greater than molecular motions when the polarisation is influenced only by electronic deformations;
diffraction efficiency (DE)	the ratio of the intensities of the *i*-th order **diffracted** beam and the **illuminating** beam; measured in %;
diffraction grating	is an array of fine, parallel, equally spaced grooves
discotic LC	liquid crystals composed of disc-shaped molecules;
dynamic holography	as opposed to permanent holography, the holographic process that can be repeated – the hologram on the same media rewritten;

dynamic scattering	scattering in the LC film due to a flow in nematic liquid crystal doped with ions, induced by a large DC field;
E7	nematic liquid crystal, a mixture of alkyl-cyano-biphenyls, alkyl-cyano-tryphenyl and alkoxy-cyano-biphenyl; transition temperatures: solid-nematic T_{SN}= -10°C, supercooled to <-20°C; nematic-isotropic T_{NI}=61°C;
EASLM	electrically addressed spatial light modulator;
Einstein coefficients A and A'	describe the loss from the ground levels of the atomic system to excited state due to absorption of a photon;
electric displacement field D	a vector-valued field, appears in Maxwell's equations, generalises the electric field, expressed in [C/m^2] (Coulombs/meter^2); in most ordinary materials may be calculated as $D=\varepsilon E$ where ε is the *permittivity* of the material;
electric field E	a vector describing the electric field; expressed in [V/m^2];
electric susceptibility χ	defines the *polarisation P* response of the material to the applied *electric field E*: ε_o is the *dielectric permittivity* of free space;
electrostriction	a mechanical deformation, under the application of an electric field;
ferroelectric LC	*chiral smectic* liquid crystal phase; may form a system that permits, from symmetry considerations, spontaneous electric polarisation;
fringe visibility V	the measure of the quality of the interference fringes;
FT	*Freedericksz transition*: an orientational transition in liquid crystal films under the influence of external field (electrical, magnetic or optical); here we would refer mainly to reorientation from planar to homeotropic alignment under the influence of electric field;
fullerene	a complex carbon molecule C_n, n≥60; usually this name is attributed to C_{60};
GON[ii]	giant optical nonlinearity; discovered in 1980 in pure nematic liquid crystals; dielectric permittivity was found to be 10^9 times higher than it is in a strong nonlinear liquid like CS_2; *nonlinear coefficient* n_2=10^{-4}W/cm^2
grating	an array of equally spaced parallel lines; here this term is used in a sense of *diffraction grating* that is recorded onto devices as a

	hologram; the terms *grating* and *hologram* are used as synonyms in this work;
grating spacing Λ	a spacing between the lines of the *grating*;
greyscale	multilevel bright/dark state;
hologram	a recorded pattern containing the information about the amplitude and the phase of the optical wave from the recorded object; contains all the information about the 3D image of the object, such image can be reproduced;
holographic data storage, holographic memory	a very effective way of storing data – using three dimensions rather than two; usually *holographic memory* is permanent (not rewritable);
holography	the process/method of recording amplitude and phase of the signal wave on a media. The recorded result on the media is called a *hologram*;
homeotropic alignment	in a liquid crystal film, alignment where the long molecular axes are perpendicular to the film surface/interface with a cell wall;
HTAB	hexadexyl-trimethyl-ammonium-bromide, ionic surfactant, used as an alignment agent; introduces homeotropic alignment when spun on the glass slide;
HTAC	hexadexyl-trimethyl-ammonium-chloride, ionic surfactant, used as an alignment agent; introduces homeotropic alignment when spun on the glass slide;
ITO	indium tin oxide; a thin coating of the material is often used as a transparent electrode (~10% optical loss);
Janossy effect[iii]	enhancement of the optical torque on the LC director by the dopant upon excitation;
Kerr effect	a quadratic (nonlinear) electro-optic effect in which the refractive index change of the media depends quadratically on the applied electric field; the **optical Kerr effect** is the special case in which the external electric field is from light itself;
LC	liquid crystal;
LETO	long-wave electron transition oscillator;

lifetime of the state T_{state}	in systems with a decreasing number of particles in some state, the number of particles in this state for most physical processes (e.g. radiation) can be described by an exponential function exp($-t/T_{state}$);
lyotropic LC	liquid crystal the phase of which depends on the concentration in the solvent;
microdisplay	a small display for projection purposes;
MR	methyl red, chemical name: [2-[4-(dimethylamino)phenyl-azo]benzoic acid], dichroic azo dye; absorption depends on a solvent: pH 4.2 (pink) to pH 6.2 (yellow), in nematic LCs λ_{max}=490nm[1] (orange);
Avogadro's number N_A	N_A=6.022*10^{23} [mol^{-1}]
nematic LC	one-dimensional ordered liquids, with the preferred direction along one axis;
nonlinearity coefficient n_2	here defines the optical intensity-dependent part of refractive index [cm^2/W]: $$n \cong n_o + n_2(I)I$$ I [W/cm^2] is the optical intensity per unit area, n_o is the initial refractive index (at I=0); shows the induced change of refractive index $\delta n_{induced}$ per unit optical intensity I $$n_2 = \frac{\delta n_{induced}}{I}$$ in general, is also defined through the electric field vector: $$n \cong n_o + n_2(E)\langle E_i^2 \rangle \qquad n_2(I) = n_2(E)\frac{2}{\varepsilon_o n_o c}$$ ε_o is the *dielectric permittivity* of free space, c - a speed of light; $\langle E_i^2 \rangle$ is the mean square of electric field;
OASLM	optically addressed spatial light modulator;
optical density D	a logarithm of inverse *transmittance T*;
optical indicatrix	ellipsoid, the main axes of which equal the refractive indices in the corresponding directions in the medium;

---

[1] See Figure 4.3, Chapter 4.

optical logic gate *optical switch*	devices in which the intensity of one light beam input controls how well another light beam is either reflected or transmitted;
optical phase-conjugation	a generic term for a multitude of nonlinear optical processes capable of reversing both the direction of propagation and the phase factor for each plane wave component of an arbitrary incoming beam of light; e.g. a phase-conjugate mirror reflects all incoming rays back to their origin;
optical rectification	a nonlinear optical phenomenon of quasi-static electric field generation; a result of the beam mixing process of the beams with the same frequency $S = \frac{1}{2}\langle 3\cos^2\theta - 1 \rangle$
optical switching	the re-direction of light beams onto which information has been encoded. A main objective in optical communication systems;
optical tweezers	the application of a laser beam to physically move very small translucent objects.
order parameter	is defined as: θ is an angle between the ordering direction and molecular axis. For crystal this parameter is equal to 1, in liquids $S=0$, and in liquid crystals S may lie between 0.3 and 0.9.
order parameter of the dye in LC S_{dye}	calculated from the polarisation absorption spectra of the dye solution and can be higher than the LC order parameter;
permanent	lasting for the lifetime of the device;
persistent	lasting for hours, days or weeks;
phase hologram	modulates the phase of the reading light, very powerful and efficient;
photoconductivity	the enhanced conductivity of the medium under the influence of light;
photocurrent	a current that is generated under the influence of light;
photoisomerisation	a transformation from one molecular form (*isomer*) to another under the influence of light;
photorefractivity	the change of the refractive index under the influence of light; e.g. as in *Kerr* and *Pockels* effects;

photovoltage	a voltage that is generated under the influence of light;
PI	polyimide, used as an alignment agent; introduces planar alignment when spun on the glass slide, polymerised and rubbed;
planar alignment	in a liquid crystal film, alignment where the long molecular axes are parallel to the film surface/interface with a cell wall;
PMMA	polymethyl methacrylate, used as an alignment agent; introduces planar alignment when spun on the glass slide and rubbed;
Pockels effect	an electro-optic effect of the production of birefringence in an optical medium induced by a slowly-varying electric field where the refractive index change of the media depends **linearly** on the applied electric field (while in the *Kerr effect* the dependence is quadratic); occurs only in systems that lack inversion symmetry;
polarisation (electrostatic): ionic (orientational)	in media composed of the molecules with permanent dipole moment: polarisation due to the tendency of the permanent dipole moments to orient themselves parallel to the field; frequency and temperature dependent, not present at optical frequencies;
polarisation (electrostatic): electronic (induced)	polarisation due to the deformation of electron clouds within the molecules; frequency and temperature independent;
polarisation P (electrostatic)	response of material to external electric fields; polarisation vector P is defined as the dipole moment per unit volume;
pre-history effect	dependence of parameters on recent pre-history of the tested sample;
projection display	a display relying on the image being projected on a screen (e.g. digital projector used for presentations);
PVA	polyvinylalcohol, used as an alignment agent; introduces planar alignment when spun on the glass slide and rubbed;
PVC	polyvinylcarbazole, used as an alignment agent; introduces planar alignment when spun on the glass slide and rubbed;
quantum efficiency Φ	the ratio of the number of occurrences of the desired effect (here transition to *cis* or *trans* state) to the number of photons absorbed;

Raman-Nath regime	in this regime the multiple diffracted orders ideally have diffraction efficiencies given by Bessel functions;
refractive index n	material characteristic: the factor by which electromagnetic radiation is slowed down (relative to vacuum) when it travels inside the material;
relaxation time	the time needed for the responce signal from the device to decay from 10% to 90% of it's value;
resistance R	a sample characteristic describing the flow of current through the sample as an external voltage is applied $R=V/I;$ [Ohm] can be described in terms of its bulk *resistivity*; $R=\rho\, d/A$ (where d is the sample length, A is the sample area);
resistivity ρ	material characteristic; a measure indicating how strongly a material opposes the flow of electric current; [Ohm·m]
resolution	the spatial frequency (in line pairs per millimetre: lp/mm) at which the modulation transfer function (*MTF*) of the device is 50% (efficiency decreases by the factor of two);
rise time	the time needed for the responce signal from the device to rise from 10% to 90% of it's value;
rise/decay constant τ	build up and relaxation of a signal can be described by an exponential function $1-\exp(-t/\tau)$ and $\exp(-t/\tau)$ correspondingly, where τ is a rise/decay constant;
Ronchi grating	a *diffraction grating* with opaque and clear lines on it;
sealed samples	prepared in very strict conditions; with sealed edges; well aligned; the ionic content is controlled during fabrication, there are no external sources of material deterioration with time; reliable and stable;
SI unit system	a standard universal system using metres, kilograms, seconds as base units;
SINE[iv]	surface induced nonlinear effect; *nonlinear coefficient n_2* = 1 cm^2/W; occurs without a direct optical or electrical torque on the director in the bulk;

sinusoidal/square grating	a grating with sinusoidal/square phase or transmission profile (change of phase for phase gratings and transmission for amplitude gratings);
SiO$_x$	alignment agent, may be sputtered at different angles to the substrate introducing different pre-tilt angles of the liquid crystal film molecules at the surface; when sputtered at 60° oblique incidence, gives planar alignment with no pre-tilt;
SLM	spatial light modulator;
smectic LC	a positional ordering exists in addition to direction correlation. There are many different types of smectic phases;
SON^v	supra-optical nonlinearity; *nonlinear coefficient n_2 = 2 – 6 cm^2/W*; observed in Methyl Red and azobenzene LC – doped liquid crystals; attributed to photo-induced space-charge generation and flows, or/and to trans-cis isomerisation, dopant-liquid crystal molecular torque.
space-charge field E$_{sc}$	a charge field that is formed in the medium (here under the influence of optical and electric fields); it leads to the *photorefractive* effect;
steric energy	the energy of steric chemical bonding; used to derive the optimal geometrical shape of the molecule;
switching time	the time it takes for the device to undergo an "on"-"off" cycle;
temporary samples	devices prepared for preliminary studies following a very simple technique; they are not uniform, their edges are not properly sealed; deteriorate in months;
thermotropic LC	liquid crystal the phase of which depends on the temperature;
thick device	in this research the term *thick* would be attributed to devices with thickness over 25μm;
thick hologram	a grating exhibiting high angular and wavelength selectivity; often attributed to operation in *Bragg* regime;
thin hologram	a grating exhibiting relatively low angular and wavelength selectivity; often attributed to operation in *Raman-Nath* regime;
trans-cis isomerisation	See *azo group;*

transmittance T	the fraction of transmitted energy accounting for scattering and reflection, %, $A=P_{transmitted}/P_{impinging}$; is a sample rather than a medium characteristic;
twisted nematic (TN)	geometry, where a nematic film with alignment on the surfaces at 90° to each other in the film plane, so that the director performs a gradual twist through the cell/film thickness;
wavemixing	a nonlinear phenomenon involving the interaction of two or more coherent waves;
Wollaston prism	an optical element used for spatially separating light of different polarisation;
ZLI 1134	liquid crystal, surfactant, used as an alignment agent; introduces homeotropic alignment when spun on the glass slide;
ZLI 2222	nematic liquid crystal, a mixture of phenyl-cyclohexyl, biphenyl-cyclohexyl, cyclohexyl-biphenyl-cyclohexyl; transition temperatures: solid-nematic $T_{SN}=<-40^oC$; nematic-isotropic $T_{NI}=66.5^oC$;
z-scan	a method of registering nonlinear response (self-focusing or self-defocusing) where the sample is placed in the focused beam and moved along the optical axis of the focusing system (z axis); the resulting beam diameter is then monitored;

[i] L. Lucchetti, M. Di Fabrizio, O. Francescangeli, F. Simoni "Colossal optical nonlinearity in dye-doped liquid crystals", *Optics Communications*, **233**, pp.417-424 (2004)

[ii] B. Ya. Zel'dovich, N. F. Pilipetskii, A. V. Sukhov, and N. V. Tabiryan, "Giant optical nonlinearity in the mesophase of a nematic liquid crystal (NLC)", *JETP Lett*., **31**, 5 (1980)

[iii] I. Jánossy, A. D. Lloyd, and B. S. Wherrett, "Anomalous optical Freedericksz transition in an absorbing liquid crystal" *Mol. Cryst. Liq. Cryst*. **179**, 1 (1990)

[iv] F. Simoni, L. Lucchetti, D. Lucchetta, and O. Francescangeli, "On the origin of the huge nonlinear response of dye-doped liquid crystals" *Opt. Express* **9**, 2, pp.85-90 (2001)

[v] I. C. Khoo, Min-Yi Shih, A. Shishido, P. Chen and M. V. Wood, "Liquid Crystal Photorefractivity - towards Supra-optical Nonlinearity", *Opt. Materials,* **18**, pp.85-90 (2001).